Experimental and Analytical Study of the Shear Transfer in Composite Shallow Cellular Floor Beams

by

Bingyu HUO

Dissertation submitted in fulfilment of the requirement for the award of

PhD

in

Structural Engineering

City University London

School of Engineering and Mathematical Sciences

November 2012

Table of contents

Chapter 3 Push-out test series-I

Chapter 4 Push-out test series-II

Chapter 5 Analytical study and Finite Element Analysis of the shear connection

Chapter 6 Flexural test of composite shallow cellular floor beams

Chapter 7 Analysis of the flexural tests

Chapter 8 Conclusions and recommendations

Acknowledgements

Declaration

I grant powers of discretion to the University Library to allow this thesis to be copied in full or in part without further reference to me. This permission covers only single copies made for study purpose, subject to normal conditions of acknowledgements.

Abstract

This research investigated the longitudinal shear transfer mechanism in composite shallow cellular floor beams. The shear transfer mechanism is different with the headed shear studs used in composite construction. The shear resisting properties and behaviour of the shear transfer mechanism has not been studied previously. Experimental and analytical studies were carried out with the aims of improving and optimizing the design details, and advancing the method of shear connection in shallow floor beam construction.

The composite shallow cellular floor beam investigated in this research is a new type of beam fabricated by welding two highly asymmetric cellular tees along the web. The shear connections of this type of composite beam are formed by the web openings, which transfer longitudinal shear force. Four types of these shear connections were studied: concrete-infill-only, tie-bar, ducting and web-welded-stud shear connections.

In total, 24 push-out tests were performed in two test series to investigate the load-slip behaviour and shear resistance of the shear connections under direct shear force. The failure mechanisms of the two forms of shear connections were extensively studied, which lead to the development of a design method for the composite action.

The concrete infill element passing through the web opening is subject to a complex three-dimensional stress state, and it is difficult to analyse it using the mathematical model rather than empirical formula. Finite Element Analysis of the concrete-infill-only shear connection was performed with a parametric study to further verify the design method that has been developed.

Two flexural tests were carried out on a full-scale composite shallow cellular floor beam with a solid slab. The shear connections investigated in the flexural tests were: concrete-infill-only and tie-bar shear connections passed through the web. The behaviour and performance of the shear connections in the flexural tests were compared with those in the push-out tests.

The degree of shear connection of the two flexural tests was determined in the back analysis using plastic theory with measured material properties. Based on the findings of the push-out tests and flexural tests, two design methods of deflection check and moment resistance were developed for composite shallow cellular floor beams at the serviceability limit state and the ultimate limit state respectively. The deflection check design method is based on the uncracked section properties of the composite beam. The moment resistance design method developed in this thesis is compatible with the design methods of BS5950 and Eurocode 4 (EC4).

Notations

A_c area of the concrete infill element in compression

A_t area of the concrete infill element in tensile splitting

B_e effective width of the concrete slab

D depth of the P.N.A; diameter of the web opening

D_d diameter of ducting

D_{tb} diameter of the tie-bar

d diameter of the shank of the stud; depth of concrete in compression

E Young's Modulus of steel

E_{cm} mean secant modulus of the elasticity of concrete

F a function of the principle stress state (σ_{xp}, σ_{yp}, σ_{zp},)

f_1 ultimate compressive strength for a state of biaxial compression superimposed on $\sigma_h{}^a$

f_2 ultimate compressive strength for a state of uniaxial compression superimposed on $\sigma_h{}^a$

f_c uniaxial crushing or compressive strength (used in FEA)

f_{cb} ultimate biaxial compressive strength (used in FEA)

f_{ck} characteristic cylinder compressive strength of concrete

f_{ct} concrete tensile splitting strength

f_{cu} concrete compressive cube strength

f_t ultimate uniaxial tensile strength

f_u strength of material of the stud but not greater than 500N/mm^2

f_y yield strength of the tie-bar

h_{sc} overall nominal height of the stud

I the second moment of area

K stiffness of the shear connections; degree of shear connection

M_c moment resistance of composite section in partial shear connection

M_{comp} additional moment resistance due to the composite action

M_{pc} moment resistance of composite section in full shear connection

$M_{pl,a,Rd}$ plastic moment resistance of the steel section

$M_{pl,Rd}$ design moment resistance of composite section in full shear connection

M_{Rd}	design moment resistance of composite section in partial shear connection
M_s	moment resistance of the steel section
P_{Rd}	design shear resistance of the shear stud
P_u	ultimate shear capacity of the shear connection
P_c	shear resistance of the shear connection
P_{uc}	design shear resistance of the shear connection
R_{add}	shear resistance of the additional elements (i.e. tie-bar or shear studs)
R_c	compressive resistance of the concrete slabs in full shear connection
R_{ce}	shear resistance of the concrete infill element
R_q	longitudinal shear resistance of the shear connections in composite section
R_{tb}	tensile resistance of the tie-bar
S	is the failure surface expressed in terms of principle stresses and five parameters (f_t, f_c, f_{cb}, f_1 and f_2)
t	thickness of the web

Greek symbols

α_c	shear performance of the shear connection in composite beam
β_c	shear transfer coefficient for a close crack
β_t	shear transfer coefficient for an open crack
δ_c	deflection of the composite beam with full shear connection
$\delta_c{}'$	deflection of the composite beam with partial shear connection
δ_s	deflection of the steel beam acting alone
δ_u	slip capacity of the shear connections
η	degrees of shear connection
ε_c	concrete compressive strain
ε_{c1}	concrete compressive strain at the peak stress
γ_v	partial factor
μ_s	stiffness multiplier for cracked tensile condition (default=0.6)
υ	Poisson's ratio
σ_c	concrete compressive stress
$\sigma_{c,Rd}$	design concrete compressive stress
$\sigma_h{}^a$	ambient hydrostatic stress state

τ equivalent shear stress

τ_{max} maximum equivalent shear stress

Abbreviations

ASB   Asymmetric Slimflor Beam

BS   British Standard

EC   Eurocode

FEA   Finite Element Analysis

ULS   Ultimate Limit State

SLS   Serviceability Limit State

ATS   Automatic Time Stepping

P.N.A   Plastic Neutral Axis

e.n.a   elastic neutral axis

Chapter 1 Introduction

The properties of shear connection are fundamentally important for the behaviour and strength of the composite structure, as it transfers longitudinal shear force along the interface of the concrete and steel elements. This thesis presents investigations of unique shear transferring mechanism of composite shallow cellular floor beams. The shear transferring mechanism is different with the conventional shear studs and has not been investigated previously. Experimental and analytical studies were carried out with the aims of advancing the method of shear connection in shallow floor beam construction. The shear transferring mechanism and methodologies of the investigations will be discussed in this chapter.

1.1 Background of composite shallow cellular floor beams

In recent years, the increasing demands on shallow floor beam had led to the development of the Slimflor and Asymmetric Slimflor Beam (ASB). However, the thickness and width of the top flange increases with increase of the span; this often results in the steel sections being heavier than required. Composite shallow cellular floor beam is a new type of beam commercially developed by Westok Limited, under the trade mark of Ultra Shallow Floor Beam. The composite shallow cellular floor beam is fabricated by welding two highly asymmetric cellular tees together along the web. Regularly spaced openings are formed on the web post. The top and bottom tees are cut from different parent sections. Generally, the top tee is cut from the universal column (UC) or universal beam (UB); and the bottom tee is cut from the UC. The weight of the steel section is reduced by having a smaller top tee. The precast floor units or profiled steel decking sit on the bottom flange, creating a shallow floor construction system (Huo et al 2010), as illustrated in Figure 1.1.

The composite shallow cellular floor beam is a construction system that fits in the range of flat slab beam used in steel building technologies. The composite shallow cellular floor beam is similar to the Slimflor beam and ASB. The common feature of these beams is the flat slab structure which minimises the overall floor depth. However

the manufacturing process and the web opening feature of the composite shallow cellular floor beam gives three key advantages when compared with the Slimflor and ASB. The first one is the flexibility owing to the manufacture process, so the depth of this beam section is not fixed and can be designed according to the required floor depth. The second advantage is the service integration which provided by the unique feature of web openings. The third advantage is the enhanced composite action due to the concrete plug passing through the web opening transfers longitudinal shear force.

The composite shallow cellular floor beam creates a profile of encased section with only the bottom flange is being exposed. Typical proportion of this composite beam is 190mm to 350mm for a span of 6m to 12m (Westok Ltd). There is no fixed depth for a span as the beam section is fabricated from two different parent sections. The section depth and arrangement of the web openings are dependent on the specifications of the construction. The manufacturing process of the beam sections are explained in Section 1.1.1. Apart from the three advantages mentioned in the above paragraph, the other benefits of using the composite shallow cellular floor beams are: flat and shallow floor structure, flexibility of floor layout and fast construction time.

A flat and shallow floor structure is achieved by the asymmetric section allowing either pre-cast units or metal decks to sit on the bottom flange. The construction details are depicted in Figure 1.2. The composite shallow cellular floor beam has regularly spaced cells in the web to permit the passage of reinforcement tie bars. The web openings can also be used for the passage of building services if it is required. This further minimises the overall floor depth and eliminates unwanted floor depth needed to accommodate the building services passing underneath the beam structures.

The composite shallow cellular floor beams create a flat floor structure to enable the layout of the floor to be designed with flexibility. This floor beam further improves the application of the flat slab beams in the steel building constructions. The speed of the construction time is also improved as the beam can be used with pre-cast units and metal deck floors. This method of construction eliminates the time spent for concrete hardening in the traditional downstand composite beam constructions. Hence, concreting is no longer on the critical paths.
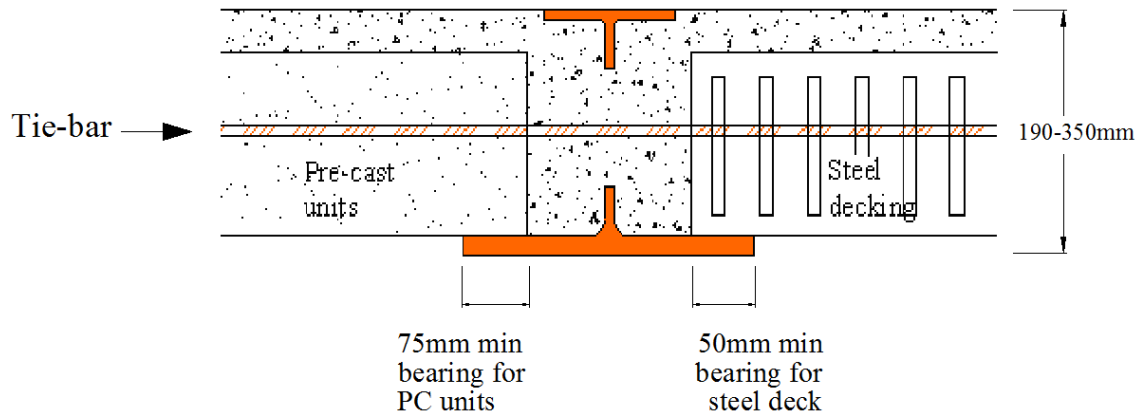
Figure 1.1 Schematic drawing of the composite shallow cellular floor beam

(a)   (b)
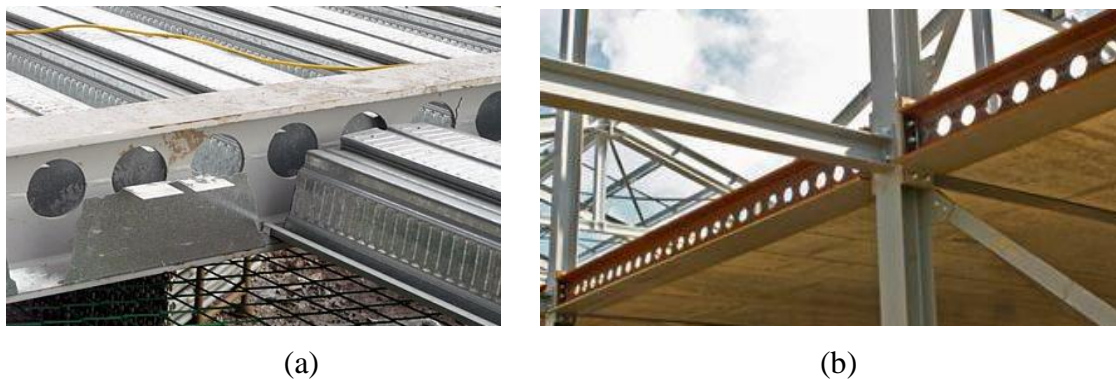
Figure 1.2 Shallow cellular floor beam used with (a) profiled steel decking (b) precast floor units (courtesy of Westok Limited)

The web openings of the composite shallow cellular floor beams provide the passage for the reinforcing tie-bars, building services and ducting through the structural depth, minimising the overall floor depth. Full service integration can be achieved when the deep profile decking is employed for the ducting passing between the ribs of the decking. The in-situ concrete fills the web openings when the floors are being cast. The concrete infill passing through the web openings, with or without tie-bars, interacts with the web openings transferring the longitudinal shear force. The objectives of this research are to investigate the unique shear transferring mechanism.

1.1.1 Manufacturing process

The composite shallow cellular floor beams do not have a standard section. The depth of the beams can be designed according to the required floor depth. The bespoke design of the section depth is benefited from the manufacturing process, as the beam section is formed by welding two asymmetric cellular tees, which are cut from different parent sections. Oxycutting technology is used in cutting the parent sections into the cellular

tees, as shown in Figure 1.3. The schematic for the manufacturing process of the beam sections is illustrated in Figure 1.4.

The profile cutting (or ribbon cutting) is the technology used to fabricate the cellular steel beams, as illustrated in Figure 1.3. The ribbon cutting can maximise the depth of the cellular tees from a parent section. The cellular tees are cut and re-welded along the web to create the cellular beams with increased depth when compared with the parent sections. The asymmetric tees of the shallow cellular floor beams are ribbon cut from different parent sections, i.e. UB for the top tees and UC for the bottom tees. The required depth of the beam sections is achieved in the design process for the asymmetric tees, as the depths of the top and bottom tees comprise the total depth for the beam sections. The depths of the tees are also bonded with the loading specifications for the composite sections. The ribbon cutting technology allows the cellular tees to be cut with the desired depth. Hence, the required beam depth can be obtained from the two parent sections.

The design of the asymmetric tees first is to select the parent sections to enable the tees to have the required depths, and the diameter and spacing of the web openings. Each parent section produces two identical cellular tees. The top and bottom tees are designed to share the same diameter and spacing of the web openings. The cutting process for the cellular tees ensures the regular spaced web openings are formed when the asymmetric tees are welded together. The re-welding process takes place once the asymmetric tees are cut, as illustrated in Figure 1.4.

Overall, the manufacturing process provides many advantages for the shallow cellular floor beams. It reduces the weight of the beam sections, and also enhances the design flexibilities of the composite beams, e.g. the depth and strength of the beam sections. The beam sections with greater capacity can be designed by selecting the stronger parent sections.
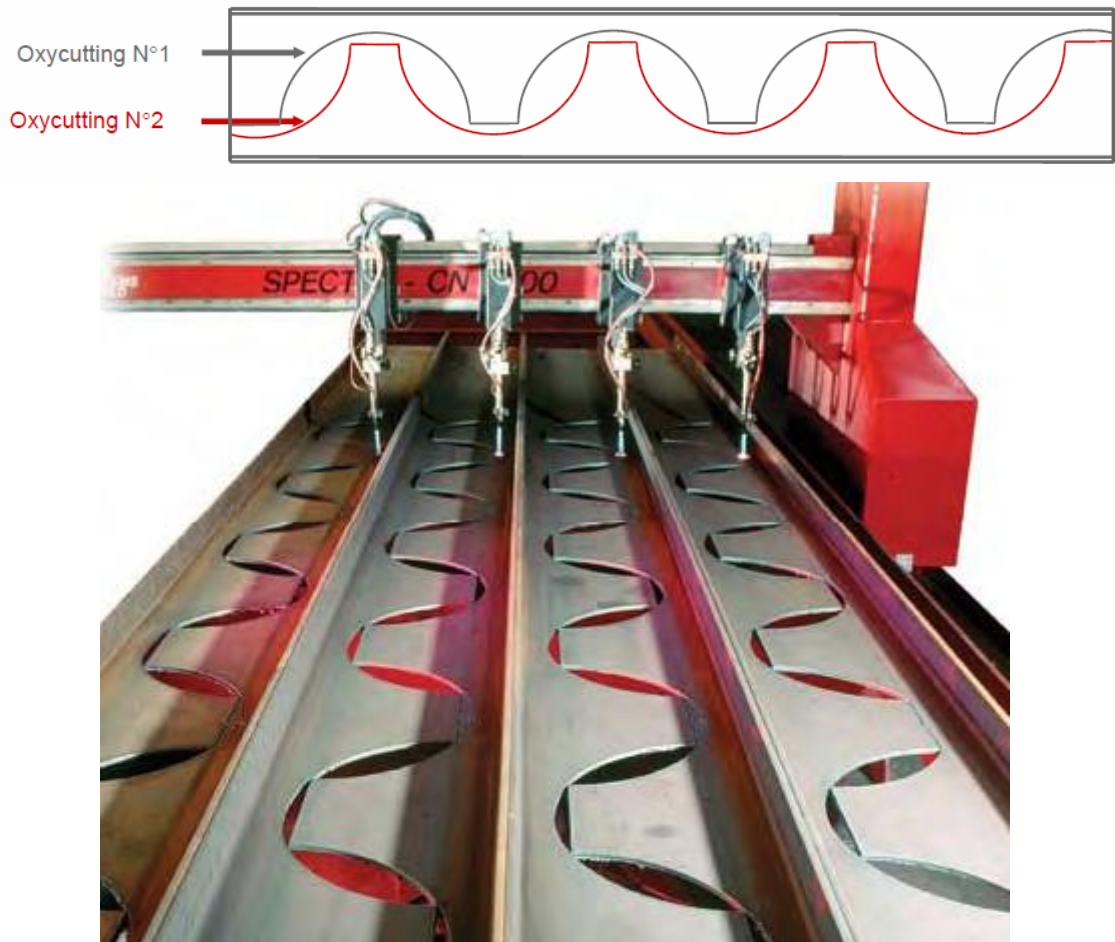
Figure 1.3 Oxycutting technology used for fabrication of the cellular tee sections
(courtesy of Westok Limited)
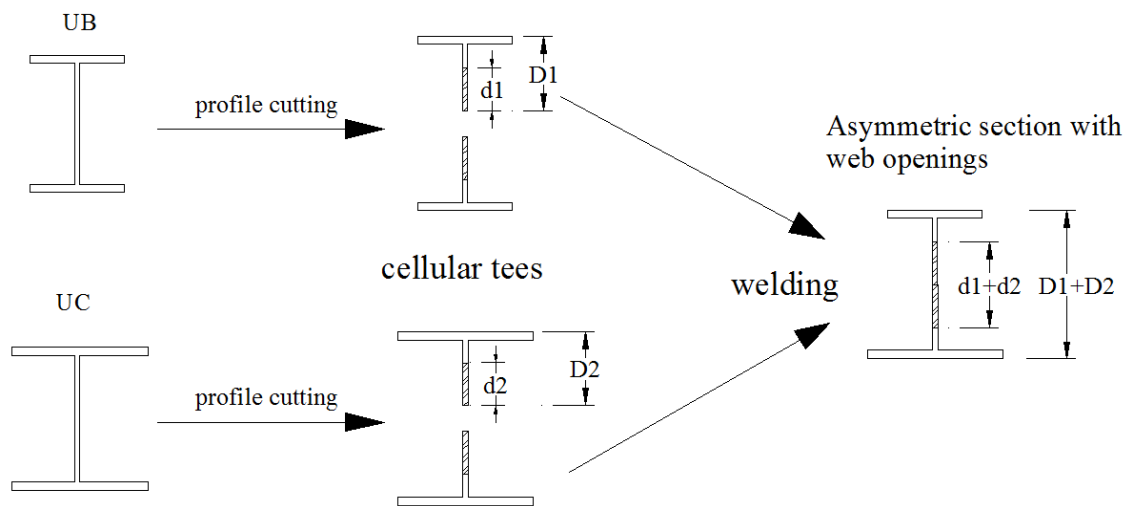
Figure 1.4 Schematic for the manufacturing process of cutting and re-welding

1.2 Shear transferring mechanism

A shear connection is an interconnecting element between the concrete and steel of a composite structure that has sufficient strength and stiffness to enable the two elements to be designed as a single structure (EC4, EN1994-1-1: 2004). The most common type of shear connection is the headed shear studs, which are normally welded on the top flange of the downstand composite beams. The shear transferring mechanism of the composite shallow cellular floor beams is formed uniquely by incorporating with the web openings. Four types of the shear transferring mechanism are investigated in this thesis, as listed below. The concrete-infill-only and tie-bar shear connection are the most commonly used shear transferring mechanism in this type of composite beam.

- Concrete-infill-only shear connection
- Tie-bar shear connection
- Ducting shear connection
- Web-welded stud shear connection

1.2.1 Concrete-infill-only shear connection

The web openings of the composite shallow cellular floor beams provide the passage for the tie-bars and building services within the structural depth. The in-situ concrete completely fills the web openings, if there are no tie-bars or building services passing through the openings, as shown in Figure 1.5. The concrete infill elements interact with the web post transferring the longitudinal shear force. This concrete infill element is called concrete-infill-only shear connection. The shear transferring mechanism of the shear connection is illustrated in the figure below.
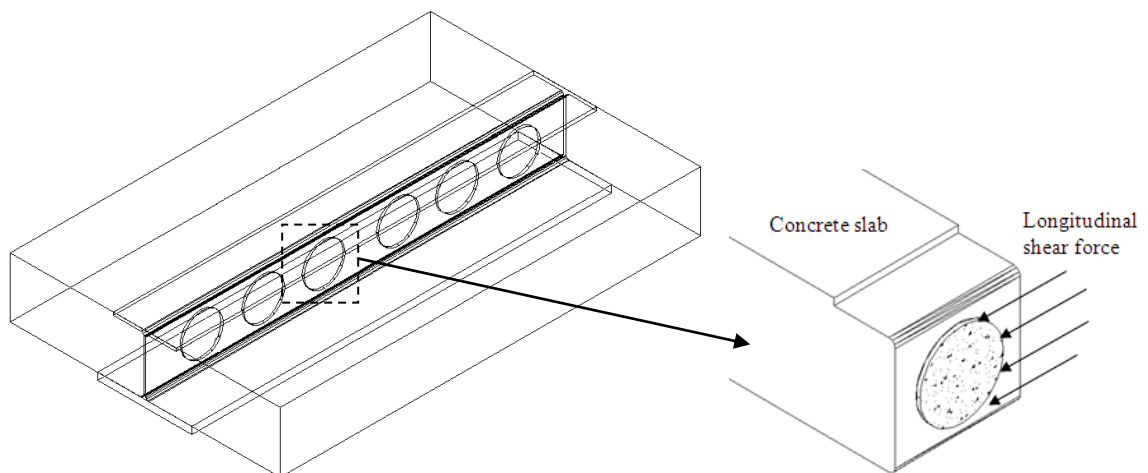
Figure 1.5 Schematic drawing of the concrete-infill-only shear connection

1.2.2 Tie-bar shear connection

One of the functions of the tie-bars used in the composite shallow cellular floor beams is to provide the tie force for the concrete slabs on both sides of the web post. Generally, high yield reinforcing bars of Ø16mm with 1m in length are used to pass through every alternative web openings. However, in the situation of the length of the tie-bars is constrained to be less than 1m; two Ø12mm tie-bars are used instead of one Ø16mm tie-bar. The in-situ concrete fills the web openings with the tie-bars. The combination of the concrete infill element and tie-bars forms tie-bar shear connection; its shear transferring mechanism is illustrated in Figure 1.6.
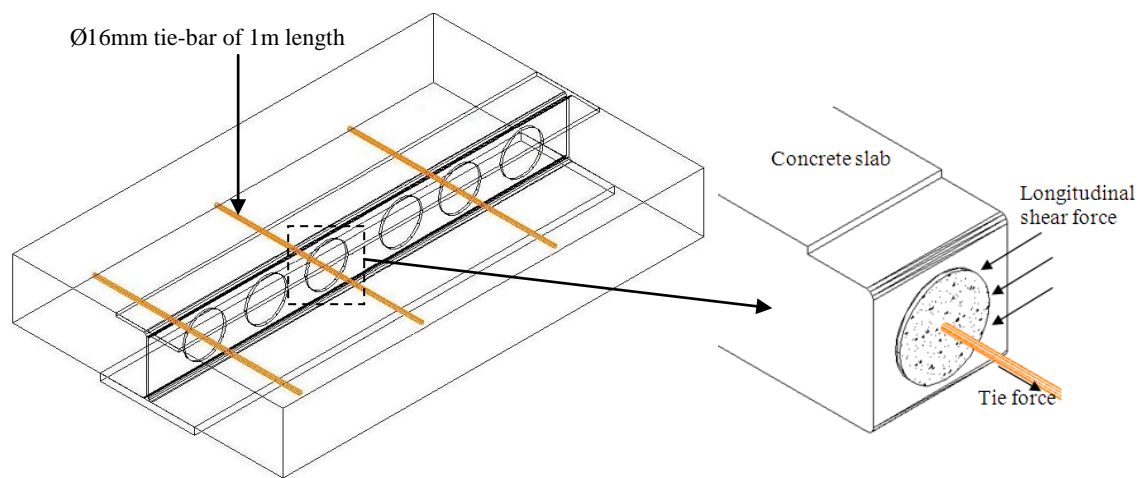
Figure 1.6 Schematic drawing of the tie-bar shear connection

1.2.3 Ducting shear connection

The ducting used for the heating, ventilation and air conditioning (HVAC) is one of the essential elements for the building services. Normally, the ducting is under-slung from the floor above; this leads to increased floor depth. The circular or elongated web openings of the composite shallow cellular floor beams provide the passage for the ducting within the structural depth, minimising the overall floor depth. Generally, the diameter of the ducting is smaller than that of the web openings; hence, there are voids between the ducting and web opening. The in-situ concrete fills the voids, creating a ring-shaped concrete element around the ducting, as illustrated in Figure 1.7. The concrete element combined with the ducting resist the longitudinal shear force; this type of shear transferring mechanism is called ducting shear connection.
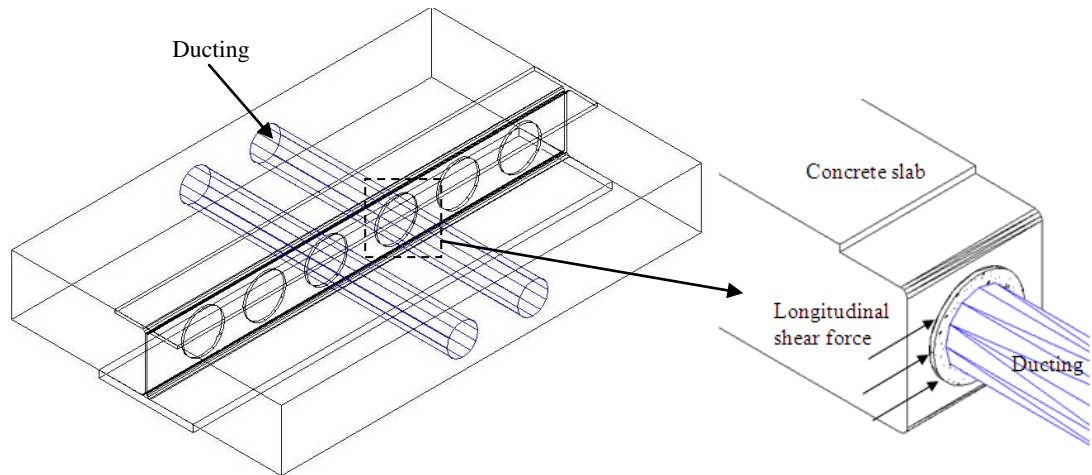
Figure 1.7 Schematic drawing of the ducting shear connection

1.2.4 Web-welded stud shear connection

The headed shear studs used for the composite shallow cellular floor beams are to provide additional shear resistance in the region where high shear occurs. The headed shear studs are welded on the web post of the top tee, as illustrated in Figure 1.8. The studs and the concrete infill element simultaneously resist the longitudinal shear force. The combination of these two elements forms the web-welded stud shear connection.
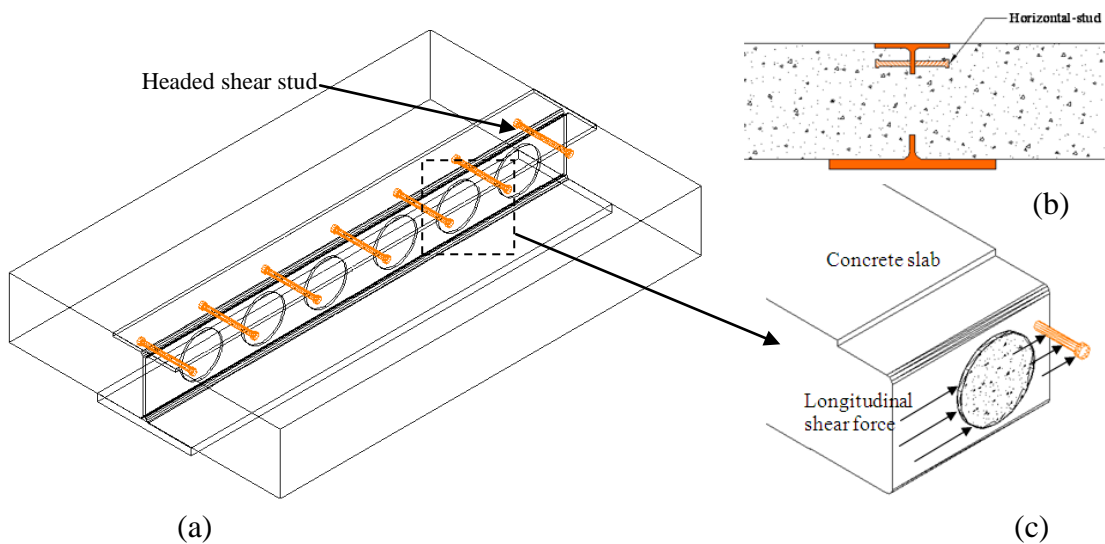
Figure 1.8 (a) Schematic drawing of the floor beam with additional headed studs;
(b) The cross sectional view; (c) Shear transferring mechanism

1.3 Composite action

The unique shear transferring mechanism used for the composite shallow cellular floor beams consist of concrete plugs with or without other elements, i.e. tie-bar, ducting and

studs. The shear transferring mechanism enables the steel beam and concrete elements to interact with each other. This interaction makes the beams behave compositely. As results of the composite action, the steel beam and concrete slab act together resisting bending. The moment resistance and stiffness of the composite beam are much increased comparing with the bare steel section. The amount of increase in strength and stiffness is also dependent on the degree of composite action. One of the experimental investigations presented in this thesis demonstrated that the typical increase of 50% in moment resistance and stiffness due to the composite action for the shallow cellular floor beams.

Because of the significant composite action achieved by the shear transferring mechanism, the shallow cellular floor beams can be designed as composite sections. Thus, the steel section sizes used for this type of composite beam are reduced comparing with the non-composite beams. The other benefits due to the composite action for the shallow cellular floor beams are:

- The depths of the composite beams are kept shallow. The unique shear transferring mechanism is formed without the increase of the structural depth, unlike the Slimflor beams which achieve the composite action with the studs welded on the top flange.
- The robustness of the composite action is enhanced by the tie-bar passing through the opening. The flexural tests presented in this thesis showed that the use of tie-bar prevented brittle failure and increased the ductility and shear performance of the shear connection. The shear transferring mechanism is different from that of the ASB which relies on shear-bond action between the concrete and steel section with embossed top flange.

1.4 Methodologies of investigation

The shear connection of the composite shallow cellular floor beams is different with the conventional headed shear studs. The behaviour and shear resisting properties of the shear connection have not been investigated previously. In order to provide information for design and further research on the shear connection, this research is carried out by using the methods of: push-out test, flexural composite beam test, analytical study and Finite Element Analysis. Details of these methodologies are summarised in the following four sections.

1.4.1 Push-out tests

Push-out test is an elemental test applies direct longitudinal shear force to the shear connection. The shear resisting capacity and load-slip behaviour of the shear connection can be obtained from the push-out test. The standard push-out test for the headed shear studs and its load-slip curve are shown in Figure 1.9. Eurocode 4 (EN1994-1-1: 2004) provides detailed specifications for the push-out test of the headed shear studs.

Push-out tests were carried out in this research to investigate the shear resisting capacity and load-slip behaviour of the shear connection used for the composite shallow cellular floor beams. Specimens of the push-out tests were designed to represent the actual configurations and shear behaviour of the shear connection. Set up and testing procedures were designed to create desired loading conditions, and to be in compliance with the specifications of Eurocode 4. The results of the push-out tests were evaluated. The behaviour and failure mechanism of the shear connection were extensively studied. The shear resisting capacities of the shear connection were analysed to establish a design method for the shear resistance of the shear connection.

(a)   (b)
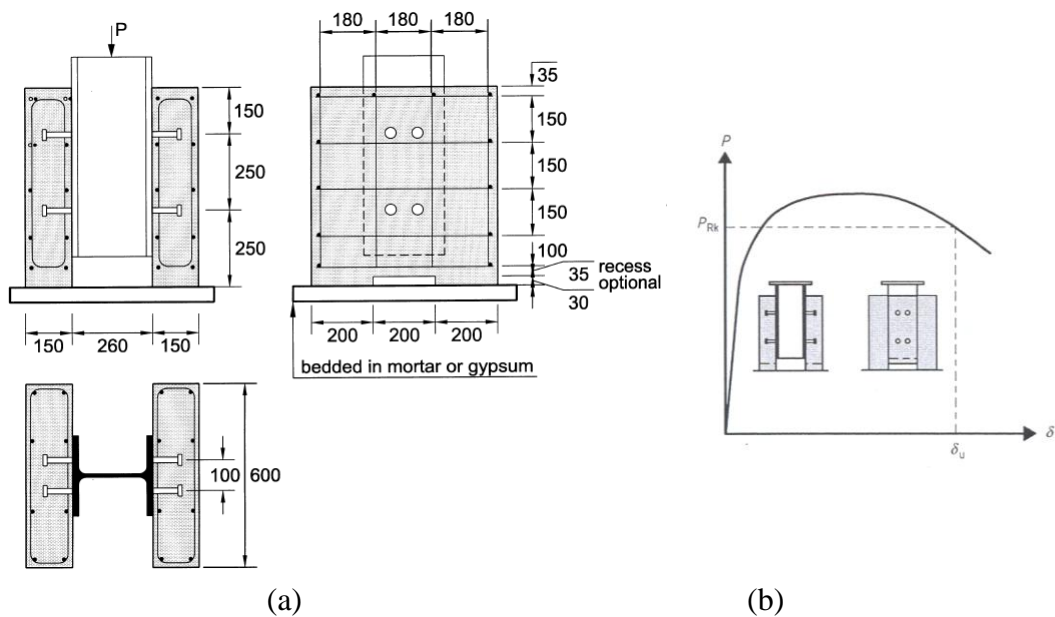
Figure 1.9 (a) Standard push-out test for the headed studs; (b) Load-slip curve of the headed studs (EC4, EN1994-1-1: 2004)

1.4.2 Flexural tests

In order to further study the shear connection, two flexural tests were carried out to investigate the shear connection when subject to bending load. A full-scale composite beam specimen was designed to represent the actual shallow cellular floor beams with a

common span range. One half span of the test beam specimen had solely the concrete-infill-only shear connection. The other half span had the combination of the concrete-infill-only and tie-bar shear connection. This layout enabled the both types of shear connection to be investigated discretely by the two flexural tests: four-point symmetric and three-point asymmetric bending tests. The results of push-out test were used in the design of the shear connection for the test beam.

The four-point symmetric bending test created a bending moment profile that was similar to that of the uniformly distributed loading (UDL). The concrete-infill-only shear connection was particularly investigated in this test phase. The four-point bending test was carried out without the plastic failure, only up to the plastification of deflection at the mid-span. This was to preserve the stiffness of the beam specimen, so that the next flexural test, three-point asymmetric bending test, could be carried out.

The three-point asymmetric bending test created a high shear within the shorter shear span, which had the combination of the concrete-infill-only and tie-bar shear connection. This flexural test was carried out to the ultimate failure. The additional tie-bar was expected to provide an enhanced composite action.

The behaviour of the shear connection in the flexural tests was compared with that in the push-out tests. The results of the flexural tests were analysed to determine the degree of shear connection and the contribution of the shear connection to the composite action.

1.4.3 Analytical study

The results of the push-out tests and flexural tests were analysed. Design methods for the shear connection and shallow cellular floor beams were developed, as listed in Table 1.1. Methodologies of the analytical studies were summarised in the following sections.

Design methods	
Push-out tests	• Design method for shear resistance of the shear connection
Flexural tests	• Design method for deflection check at the serviceability limit state (SLS) • Design method for moment resistance at the ultimate limit state (ULS)

Table 1.1 Design methods developed in the analytical studies

1.4.3.1 Analytical study of push-out test results

Base on the failure mechanism of the shear connection, a method for determining the shear resistance of the shear connection was proposed first. The test results were analysed to establish the formula for the design method. The calculated results using the established the formula was then verified with the test results, to conclude the design method for shear resistance of the shear connection.

1.4.3.2 Analysis of flexural tests

The results of the flexural tests were analysed to develop design methods at the serviceability limit state (SLS) and ultimate limit state (ULS). The flexural tests demonstrated the effect of partial shear connection on the deflections of the test beam. The calculated deflections using the method for deflection check specified in both BS5950 and EC4 were about 50% lower than the test deflections. Based on the principles of the linear partial interaction method, the method specified in BS5950 and EC4 were modified. The modified method for deflection check of the shallow cellular floor beams was then verified with the test deflections and further calculations.

The degrees of shear connection for the both flexural tests were determined in the back analysis using the plastic stress block with the measured material properties. An optimum cross section of the shallow cellular floor beams was concluded for calculating the moment resistance. By combining the findings of the push-out tests and flexural tests, a design method for moment resistance of the shallow cellular floor beams was developed which was compatible with the conventional design methods specified in both BS5950 and Eurocode 4.

1.4.4 Finite Element Analysis

Because of a complex three-dimensional stress-strain state of the concrete infill element, it is very difficult to analyse it using mathematical models. Hence, Finite Element Analysis (FEA) was carried out to perform a parametric study on the concrete-infill-only shear connection. Results of the parametric study further verify the developed design method for shear resistance of the shear connection. The variables investigated in the FEA parametric study were the diameter of the web opening and concrete strength.

1.5 Objectives

In order to investigate the shear transferring mechanism of the composite shallow cellular floor beams, with the aims of providing information on the behaviour and shear resisting properties of the shear connection, the following objectives are carried out:

1. To carry out a literature review on topics of the composite floor beams and shear connection, with emphasis on experimental studies, i.e. push-out tests and flexural tests;

2. To design and carry out two series of push-out tests. The first series of the tests was to investigate the four types of the shear connection: concrete-infill-only, tie-bar, ducting and web-welded stud shear connection. The recommendations of the first series of the tests were used to design the second series of the tests which was to further investigate the concrete-infill-only and tie-bar shear connection with the effects of loading cycles;

3. To carry out two flexural tests, four-point symmetric and three-point asymmetric bending tests, to investigate the flexural behaviour of the shallow cellular floor beams, and to investigate the concrete-infill-only and tie-bar shear connection when subject to bending load;

4. To perform analysis on results of the push-out tests and flexural tests, with the aims to develop design methods for the shear connection and shallow cellular floor beams;

5. To carry out a FEA parametric study on the shear connection to further verify the developed design method for shear resistance of the shear connection.

1.6 Aims

The experimental and analytical studies were carried out to investigate the unique shear transferring mechanism of the shallow cellular floor beams with the aims of:

- Providing information on behaviour and shear resisting properties of the unique shear connection;

- Achieving better understanding towards failure mechanism of the shear connection, which leads to improvements for the shear connection;

- Developing design methods for the shear connection and shallow cellular floor beams;

- Advancing the method of shear connection in shallow floor beam construction.

1.7 Structures of the thesis

Chapter 1   *Introduction*

Presented the background information of the composite shallow cellular floor beams and shear connection. The methodologies of the investigations with the objectives and aims were also emphasized.

Chapter 2   *Literature review*

Publications were reviewed mainly on the shear connection and composite floor beams. Emphasis was given to the investigations of the push-out tests and flexural tests. The reviewed composite floor beams were similar or have similarities to the shallow cellular floor beams. The review extended to the shear connection other than the headed shear studs.

Chapter 3   *Push-out test series-I*

Presented the investigations on four types of the shear connection used for the shallow cellular floor beams. The test specimens had variables in the diameter of the web opening and concrete strength. The relationship between the shear resistance of the shear connection and the diameter of web opening, also the concrete strength were studied. The behaviour and failure mechanism of the shear connection were particularly analysed.

Chapter 4   *Push-out test series-II*

The concrete-infill-only and tie-bar shear connection were further investigated in push-out test series-II, based on the recommendations of the push-out test series-I. Loading cycles were introduced into this test series. Its effects on the shear connection were examined.

Chapter 5   *Analytical study and Finite Element Analysis of the shear connection*

The results of the push-out tests were analysed. A design method for shear resistance of the shear connection was developed. Because of the complex stress state of the concrete infill element, a parametric study was

carried out using the FEA, which further verified the developed shear resistance design method.

Chapter 6   *Flexural tests of composite shallow cellular floor beam*

A full-scale specimen of the composite shallow cellular floor beam was investigated in two flexural tests: four-point symmetric and three-point asymmetric bending tests. Composite behaviour and flexural properties of the beam was studied. The concrete-infill-only and tie-bar shear connection were investigated in the flexural tests. Behaviour and shear performance of the shear connection were compared with that in the push-out tests.

Chapter 7   *Analysis of the flexural tests*

The results of the flexural tests were analysed. Two design methods were developed for the composite shallow cellular floor beams at the serviceability limit state (SLS) and ultimate limit states (ULS). The modified method for deflection check at the SLS was concluded based on the principle of the conventional deflection check method, which included the effect of partial shear connection. The design method for moment resistance at the ULS was compatible with the design methods of BS5950 and EC4 and implemented the developed shear resistance design method for the shear connection.

Chapter 8   *Conclusions and recommendations*

Findings of the push-out tests and flexural tests for the shear connection and the composite shallow cellular floor beams were summarised, together with the developed design methods. The recommendations were made in the areas of: improvement for the shear connection and future research topics.

Chapter 2 Literature review

In the context of investigating the shear connection of the shallow cellular floor beams, this chapter presents a review of publications about the slim-floor beams, shear connection and experimental investigations. Particular emphasis was given to experimental investigations, i.e. push-out tests and flexural bending tests. The current design codes of practice were also discussed.

2.1 Introduction

The shear connection is one of the fundamental components of a composite member. Its stiffness and capacity are primarily dependent on the performance of the shear connection. The shear connection of the shallow cellular floor beams are new types of shear connection formed by the web openings of the beam. The shear connection has not been investigated previously. A literature review on slim-floor beams, headed shear studs and other types of shear connection will nonetheless provide guidance for investigating the shear connection and the composite shallow cellular floor beams.

There are three main sections in this literature review: (1) slim-floor beams, (2) shear connection and push-out tests and (3) flexural composite beam tests.

2.2 Slim-floor beams

The slim-floor construction has become popular throughout Europe in recent years, as the concrete slabs are within the structural depth of the steel beam, thus reducing the depth of the floor construction. Hicks (2003) reviews the various composite floor beams developed for steel frame buildings: the composite downstand beam, the Slimflor beam and Slimdek beam. The span, structural depth and method of composite action of these composite beams are compared, and the comparison is summarised in Table 2.1. The optimum spans of the slim-floor construction are in the region of 6-8m. The principle benefits of the slim-floor construction are the elimination of downstand beams, leading to a flat or ribbed floor of minimum depth and the requirement for less fire protection.

Lawson et al (1999) briefly review other forms of the slim-floor constructions, as shown in Figure 2.1. The 'integrated beam' construction is the generic title of the slim-floor construction used in continental Europe: 'poutre à talon' in France, or 'Flachdecken mit integrierten Stahltragern' in Germany. This publication states that the design of the slim-floor (or integrated) beam complies with the principle rules of Eurocodes 3 and 4, and the design of all forms of the composite slabs is covered by the principles and application rules of Eurocode 4.
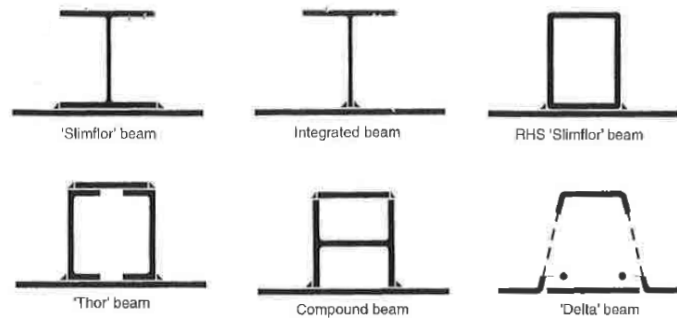
Figure 2.1 Various types of slim-floor or integrated beams (Lawson et al 1999)

	Span	Overall Depth	Method of Composite Action
Composite downstand beam	> 15m	steel beam + 120 to 160mm slab	Headed studs
Slimflor beam	5-10m	280-320mm	Headed studs
Slimdek beam (ASB)	6-7.5m*	310-340mm*	embossment on top flange

* Lawson et al (1997)

Table 2.1 General comparisons between different types of composite beam

2.2.1 The Slimflor beam

The Slimflor beam consists of a Universal Column (UC) section with a plate welded to its bottom flange, as shown in Figure 2.2; the plate supports the floor slabs directly. Mullett (1998) covers the general characteristics of Slimflor beams. The moment resistance of Slimflor beams can be determined based on two main categories: non-composite and composite sections. Design formulas of Slimflor beams are also discussed. Mullett (1992) presents design guidance for Slimflor beams using hollow core precast units. The design guidance outlined is in accordance with the BS5950: Part 1: 1990 and worked examples are also included. Mullett and Lawson (1993) present

design guidance on Slimflor beams using profiled deep decking. Design tables and worked examples are also included.

<center>(a)   (b)</center>
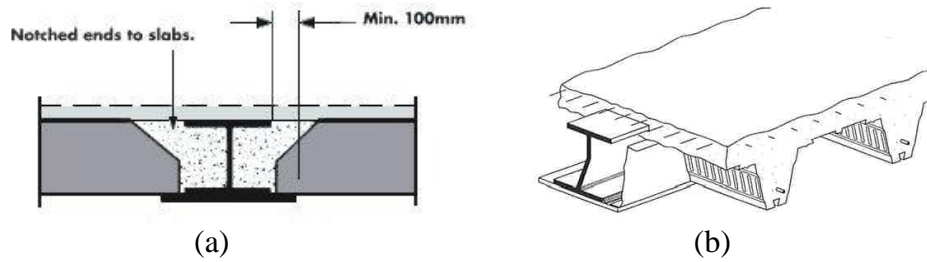
Figure 2.2 (a) Cross section of the Slimflor beam with precast units (courtesy of Precast Floor Federation); (b) The Slimflor beam with deep decking (Lawson et al 1999)

Slimflor beams using deep profile decking were experimentally investigated by Mullett and Lawson (1993), Lu and Makelainen (1995), Queiroz et al (1998), Chen et al (2002), Wang et al (2009) and Yang et al (2010). Slimflor beams using precast floor units were investigated by Bode et al (Dorka and Stengel) (1996) and Hegger et al (2009).

The results of full-scale Slimflor beam tests carried out at City University London are discussed by Mullett (1998). The test specimen had a span of 7.5m with an overall depth of 300mm, and consists of original CF210 deep decking. No shear connection were provided in the specimen. The four loading points simulated the uniformly distributed load. The test was discontinued at the total load of 1016kN with mid-span deflection of 150mm (span/50). The maximum bending moment was 925kNm, which is 1.68 of the capacity of bare steel. This increase in moment capacity due to composite action without shear connection has lead to the development of the Asymmetric Slimflor Beam (ASB).

Wang et al (2009) present experimental investigations on flexural behaviour of two Slimflor beams using deep decking with fixed end connection to a column frame. The two specimens span over 6m with an overall depth of 290mm. The width of the concrete slab is 0.75m. One of the specimens has a higher reinforcement ratio, which has no influence on the stiffness but induces a slight higher failure load, which is 476kN compared with 446kN of its counterpart. A formula for moment capacity ($M_{c,hog}$) in the hogging moment region is proposed, together with an existing formula for the sagging moment ($M_{c,sag}$). The failure load (F) of the Slimflor frame beams (span of L) is derived as Eqn. 2.1 and verified with test results.

$$F = \frac{4(M_{c,sag} + M_{c,hog})}{L} \qquad\qquad (2.1)$$

Hegger et al (2009) present four full-scale tests carried out on continuous two-span floor systems (6m x 10m) consisting of 10 slabs. In the middle of the two-span system, the slabs were supported by a Slimflor beam. The tests investigated the load bearing behaviour of Slimflor beams using prestressed hollow core slabs. The conclusions are that large deformations due to plastification of the supporting beam will cause premature failure of the slabs and that 60-70% of the shear strength of the slabs if rigid supported can be utilised.

2.2.2 The Asymmetric Slimflor Beam (ASB)

The Asymmetric Slimflor Beam (ASB) is a rolled section with a narrow top flange. The welding of an additional plate is not required. Lawson et al (1997) discuss the benefits of using ASB sections and its design procedures, which are in accordance with BS5950: Parts 1 & 3. The effective width of floor slabs is suggested as beam span/8 (or half of the value for conventional composite design in BS5950: Part 3. This is to avoid over-estimating the degree of composite action. The publication presents two full-scale tests on 280ASB and 300ASB composite beams using deep decking. Both specimens have a span of 7.5m and a width of 1m (span/8). Full shear connection is demonstrated, which is partly due to the shear-bond action, as illustrated in Figure 2.3. Design shear-bond strength of 0.6N/mm^2 is concluded. The failure moments of 280ASB and 300ASB beam specimens are 790 and 956kNm respectively.

Lawson et al (1999) review the design principles of both the Slimflor and Slimdek constructions in accordance with Eurocodes 3 and 4. Three full-scale tests on ASB composite beams are presented. Two of the tests are also presented in Lawson et al (1997) previously reviewed. The specimen of the other test has the same span of 7.5m, but with a light steel section (280ASB/100). The major differences to the other two beam specimens are the slab width of 2m and a series of elongated web openings (160mm x 240mm). However, similar conclusions are drawn from all three tests. The plastic moment resistance ($M_{pl,Rd,o}$) of a composite ASB section with web openings is concluded as Eqn. 2.2, where $M_{pl,Rd,c}$ is the plastic moment of regular composite ASB; d_o is the opening depth (d_o<160mm) and d is the depth of web post.

$$M_{pl,Rd,o} = M_{pl,Rd,c}(1 - 0.4\frac{d_o}{d}) \qquad\qquad (2.2)$$

Lawson et al (1999) also present a major load test on a two-bay (6m x 6m) Slimdek floor system, using 280ASB/100 beams and 300mm square RHS edge beams with a 300mm-deep composite slab in between. The results provide more information on the serviceability performance.
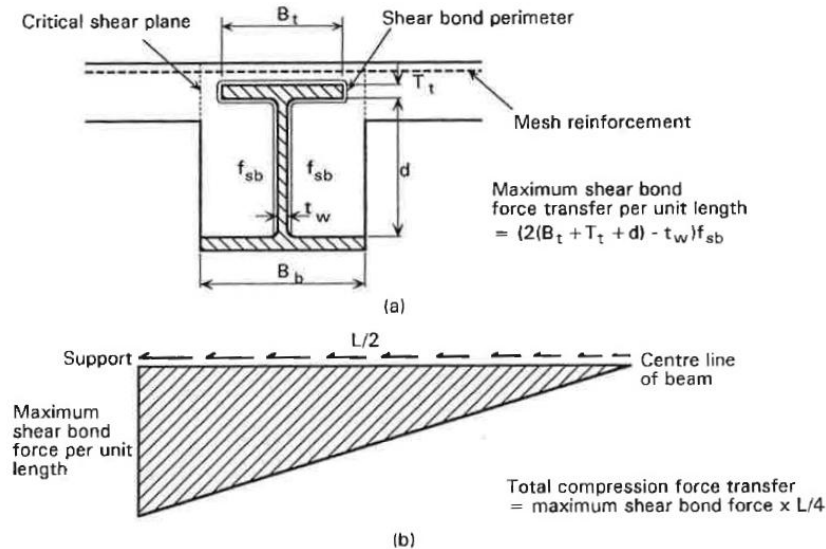
Figure 2.3 (a): Shear bond transfer around the internal surface of the ASB section; (b): Elastic shear transfer along the beam subject to UDL (Lawson et al 1997)

Rackham et al (2006) present guidance on the design of ASB using precast concrete hollow core slabs, covering two types of construction: with or without concrete structural topping. Practical guidance is given on tolerances that affect the bearing of the PC units and on the end preparation which provides clearance for the concrete encasement.

2.2.3 ITECH composite beam

The iTECH beam, shown in Figure 2.4 (a), is a new composite floor beam system developed by a Korean research group in 2002. The asymmetric steel section is fabricated by welding a top plate on to a bottom tee cut with cells of half hexagon pattern. Non-structural channels are fitted on the bottom flange supporting the decking. Both sides of the web are filled with in-situ concrete. Shear connection are not used. The composite action is provided by the bond strength at the interface between the steel beam and concrete slab, and by the bearing strength of the concrete passing through the openings. Ju et al (2003) and Ju et al (2009) investigated the flexural behaviour of the iTECH beam by carrying out full-scale composite beam tests. A slim-floor beam and a bare steel beam were also tested for comparison. The span of the specimens was 5m and

the span-to depth ratio of the composite specimens was 5.35. The ultimate strength of the iTECH beam exceeded the design value. Complete composite action and partial composite action was demonstrated before the yield and after the yield respectively. The bare steel beam failed when the top flange within the web openings buckling. Hence, the top flange is the critical member at the construction stage.

Ju et al (2005) present an experimental investigation on the shear strength of the iTECH beam. Four composite specimens with a short span of 1m were tested to determine the vertical shear contribution of the steel web, inner concrete panel and outer concrete panel. The results show that shear stirrup has a slight contribution to the vertical shear strength. However, for safety and simplicity purposes, the outer concrete panel is excluded in the proposed design method, which includes only the inner concrete panel and steel web, as illustrated in Figure 2.4 (b). Ju at al (2004) also investigated the behaviour of the moment resisting connection at the joint between an iTECH beam and a reinforced concrete column.

(a)   (b)
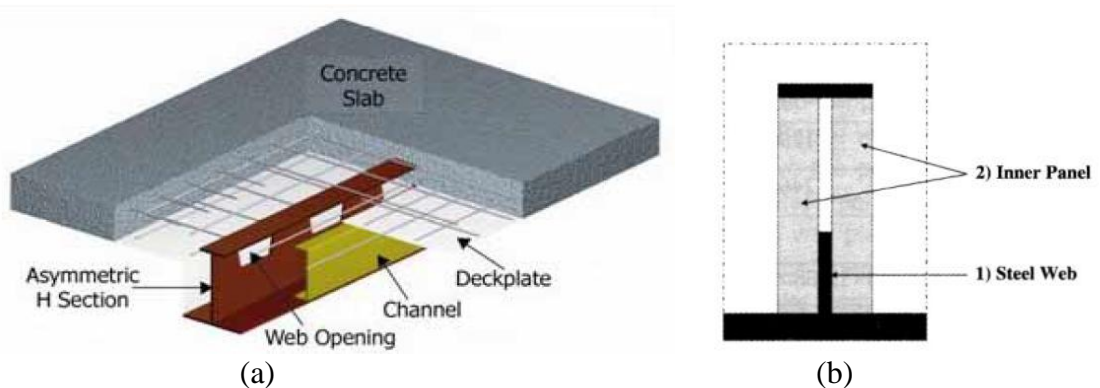
Figure 2.4 (a) Schematic of the iTECH beam (Ju et al 2004); (b) Design vertical shear force components (Ju et al 2005)

2.3 Shear connection

Headed shear studs have been extensively investigated since their initial use as shear connection in the 1950s. The current codes of practice provide detailed specifications on the use and design of headed studs. Other types of shear connection have also been developed for particular constructions. Publications for both headed shear studs and other types of shear connection will be reviewed, with emphasis on experimental investigations or push-out tests. Codes of practice will also be discussed.

2.3.1 Codes of practice

Eurocode 4 (EN1994-1-1: 2004) requires that the ultimate tensile strength of headed studs, f_u, should not be greater than 500N/mm^2 for studs used in solid slabs and concrete encasement, and 450N/mm^2 for studs used with profiled steel decking. The design shear resistance (P_{Rd}) of a headed shear stud used in a solid slab and concrete encasement can be calculated using the following formulas given in the Eurocode 4, where f_u is the specified ultimate strength of the steel, d is the diameter of the stud, γ_v is the partial factor (1.25), f_{ck} is the concrete cylinder compressive strength, E_{cm} is the elastic modulus of concrete, and h_{sc} is the height of the stud.

$$P_{Rd} = \frac{0.8 f_U \pi d^2 / 4}{\gamma_V} \tag{2.3}$$

$$P_{Rd} = \frac{0.29 \alpha d^2 \sqrt{f_{ck} E_{cm}}}{\gamma_V} \qquad \text{(whichever is smaller)}$$

British Standard BS5950-3.1: 1990 also provides detailed specifications for headed shear studs in terms of dimensions and spacing. Their design shear resistance is given as a value in BS5950, with corresponding stud dimensions and concrete strength, as illustrated in Table 2.2.

Dimensions of stud shear connectors			Characteristic strength of concrete			
Nominal shank diameter	Nominal height	As-welded height	N/mm^2	N/mm^2	N/mm^2	N/mm^2
			25	30	35	40
mm	mm	mm	kN	kN	kN	kN
25	100	95	146	154	161	168
22	100	95	119	126	132	139
19	100	95	95	100	104	109
19	75	70	82	87	91	96
16	75	70	70	74	78	82
13	65	60	44	47	49	52
NOTE 1 For concrete of characteristic strength greater than 40 N/mm^2 use the values for 40 N/mm^2.						
NOTE 2 For connectors of heights greater than tabulated use the values for the greatest height tabulated.						

Table 2.2 Characteristic shear resistance of the headed studs (BS5950-3.1: 1990)

The American Institute of Steel Construction (AISC 1994) provides a formula for calculating the ultimate strength of headed studs (Q_u), Eqn. 2.4, where A_{sc} is the stud cross-section area (mm^2), f_c' is the concrete cylinder compressive strength (MPa), E_c is the elastic modulus of concrete (MPa), and F_u is the specified tensile strength of the stud (MPa). The shear strength obtained according to AISC is about 40% higher than that of Eurocode 4 (Johnson (2008)).

$$Q_u = 0.5 A_{sc} \sqrt{f_c' E_c} \le A_{sc} F_u \tag{2.4}$$

2.3.2 Headed stud shear connection

Since the initial use of headed studs as shear connection in the 1950s (Davies (1975)), it has become the most common type of shear connection in both bridge and building construction. Many investigations of headed studs have been carried out. This review focuses on experimental studies of the studs used in both solid slabs and profiled decking.

2.3.2.1 Headed studs used in solid slabs

Chinn (1965) carried out 10 push-out tests using headed studs of $\frac{1}{2}$, $\frac{5}{8}$, $\frac{3}{4}$ and $\frac{7}{8}$ in. (13, 16, 19 and 22mm) diameter. The lengths of the stud are approximately four times its diameter. Flanges of the steel section were greased. Shear failure mode was demonstrated by studs of all diameters except the 22mm, which demonstrated slab cracking. The ultimate strength of the studs in push-out tests was found 18% to 43% higher than their direct shear strength. It was concluded that concrete strength had no effect on the ultimate strength of the studs (Q_u), as demonstrated in the concluded formula, Eqn. 2.5, where d is the stud diameter. However, this was later disapproved by conclusions of other investigations, i.e. Ollgaard et al (1971) and Hawkins (1973).

$$Q_u = 39.22d^{1.766} \tag{2.5}$$

Slutter and Driscoll (1965) present nine push-out tests using solid slabs, 12 composite beam (span of 4.5m) tests, and one two-span continuous beam test. The conclusions are that the ultimate flexural strength of the beam is related to the ultimate strength of the stud shear connection, and that the stud's diameter (d_s) and concrete cylinder compressive strength (f_c') directly govern the ultimate strength of the stud (q_u) as:

$$q_u = 930d_s^2 \sqrt{f_c'} \tag{2.6}$$

Davies (1967) studied the spacing and layout pattern of the studs by conducting 20 half-scale push-out tests using solid slabs. The studs were 10mm in diameter and 50mm in height. The results demonstrated that two studs per flange placed perpendicular to the direction of load had a 25% higher failure load than that of the studs placed parallel to the direction of load, and the ultimate strength of the studs varied linearly with the longitudinal spacing of the studs.

Goble (1968) reported an investigation into the behaviour of thin flange push-out specimens using $\frac{1}{2}$, $\frac{5}{8}$ and $\frac{3}{4}$ in. (13, 16 and 19mm) diameter studs. In total, 41

specimens were tested. It was found that the shift in failure mode from stud shearing to flange full-out occurred at a stud diameter-to-flange thickness ratio of 2.7. The studs of the thinner flange specimens were more flexible in the lower load ranges; and there was no difference in ductility between the two failure modes. The ultimate strength of studs concluded by Goble (1968) is very close to the conclusion of Slutter and Driscoll (1965) only with a different coefficient, namely 882 rather than the 930 of Eqn. 2.6.

Ollgaard et al (1971) carried out 48 push-out tests on headed studs of $^5/_8$ and $^3/_4$ in. (16 and 19mm) diameter. Normal and lightweight concrete were used. In total, seven parameters were studied: compressive and tensile strength of concrete, stud diameter, number of studs per slab, elastic modulus of concrete, type of aggregate, and density of concrete. The test results demonstrated that the strength of studs was more influenced by the concrete compressive strength and elastic modulus than by the tensile strength and density of concrete. Studs in both types of concrete showed considerable deformation after the ultimate loads were reached. The strength of studs in the lightweight concrete was 15% to 25% lower than that in the normal concrete. Three failure modes were observed: stud shearing, concrete failure and a combination of both. A formula for the ultimate strength of the stud (Q_u), Eqn. 2.7, was developed. Its simplified formula, Eqn. 2.4, achieved by rounding the exponents, was adopted by the AISC specifications. Moreover, the load-slip behaviour of the studs was mathematically expressed in Eqn. 2.8, where Q is the load (kip) and Δ is the slip (in.).

$$Q_u = 1.106 A_s f_c'^{0.3} E_c^{0.44} \tag{2.7}$$

$$Q = Q_u \left(1 - e^{-18\Delta}\right)^{2/5} \tag{2.8}$$

Hawkins (1973) conducted 47 push-out tests using solid slabs. The different parameters were: stud steel (cold formed and hot forged), stud diameter (19 and 22mm), concrete type (normal and lightweight), and concrete strength. The results show that concrete strength is the prime factor governing the capacity of studs for a given slip value, and that the properties of stud steel have a less significant effect. The important property of stud steel is its ultimate tensile strength rather than its yield strength. The other variables have considerably less influence on the capacity of studs than the strengths of concrete and steel. The author states that the behaviour of studs at low loads can be predicted by modelling studs as a flexible elastic dowel on an elastic foundation. For slips of more than 0.02 in. and for studs with a height/diameter ratio greater than 4.0, the shear stress can be predicted by empirical expression. Four distinctive failure

modes were observed: shearing of studs, punch-out of studs, pull-out of studs, and cracking of the unreinforced slab.

Johnson and Oehlers (1981) present statistical analyses of results of 125 push-out tests from 11 sources, 101 new push-out tests and 4 composite beam tests. The statistical analyses conclude that the strength of studs in push-out tests is strongly influenced by the width of the slabs, and that little of the scatter found in the results is due to experimental error. One of the parameters in the new tests is the height of the weld collar. The results show that a weld collar of $1.34d_s$ in diameter and $0.25d_s$ in height resists about 70% of the total shear, where d_s is the shank diameter. The shank failure strength of a stud increases continuously as the height of weld collar increases from 0 to $0.35d_s$. The overall conclusions are that the stiffness and strength of studs are highest when shank failure occurs and that it is possible to base the spacing of studs on shank failure loads whenever sufficient breadth of concrete slab can be provided. The minimum breadth is about twice the longitudinal spacing of the studs. Whether the maximum shear flow can be transferred to the slab without splitting the concrete depends on the layout of the studs. They should be spread as uniformly as practicable over the whole available width of the steel flange, and should never be located in a single straight line above the web.

2.3.2.2 Headed studs used with profiled decking

Grant et al (1977) present the results of 17 composite beam tests using profiled steel decking and $^3/_4$ in. (19mm) diameter studs. The variables considered were yield strength of the steel beam, geometry of steel decking and degree of partial shear connection. The specimens have spans of 24ft or 32ft (7.3m or 9.8m), with a constant thickness of 2.5 in. (64mm) for the solid part of the slabs. Four points loading was used for all beam tests. Monotonic load was applied up to the estimated working load, and then cycled 10 times. The results were analysed in conjunction with 58 additional tests conducted by other investigators, treating variables such as weight and strength of concrete, diameter and height of studs, type of reinforcement, and type of loading. It was concluded that the flexural capacity of a composite beam with profiled steel decking could be more accurately and conservatively estimated if the slab force was considered to act at the mid-depth of the solid portion above the ribs, rather than at the centroid of the concrete stress block. The capacity of a stud in ribs of composite beams with profiled steel decking (Q_{rib}) could be determined from Eqn. 2.9, where N is the number of studs in a

rib, H and h is the height of the studs and rib respectively, W is the average rib width, and Q_{sol} is the strength of the stud in a flat soffit slab (Eqn. 2.4).

$$Q_{rib} = \frac{0.85}{\sqrt{N}} \left(\frac{H-h}{h} \right) \left(\frac{W}{h} \right) Q_{sol} \leq Q_{sol} \qquad\qquad (2.9)$$

Easterling et al (1993) state that one of the important parameters identified in some of the studies to date is the position of the studs relative to the stiffener in the bottom flange of the deck. Most decks have a stiffener in the middle of the bottom flange, thus making it necessary to weld the stud off centre. This publication presents a research project conducted at Virginia Tech to evaluate the strong vs. weak stud position issue, as illustrated in Figure 2.5 (a). Four composite beam tests and eight push-out tests were carried out. All beam specimens had a span of 30ft (9.1m), a width of 81in. (2m), and a total of 12 studs of $^3/_4$ in. (19mm) diameter. The only difference in specimens was the position of the studs. The push-out test specimens were constructed using the same deck and studs used in the beam tests. Four specimens had studs in strong position and four specimens had studs in weak position. The behaviour of the studs was distinctively different between the strong and weak positions. The strong position studs failed by developing concrete shear cones or by shearing off the shank and weak position studs failed by punching through the deck rib. The response of the studs in the weak position, in terms of load vs. slip, was more ductile than that of the studs in the strong position, as shown in Figure 2.5 (b). The results of both tests, beam tests and push-out tests, were consistent with other studies to date, which showed values calculated using Eqn. 2.9 (Grant et al 1977) were higher than measured values. Modifications of Eqn. 2.9 were not proposed by the author, as further evaluation was required.

| (a) | (b) |
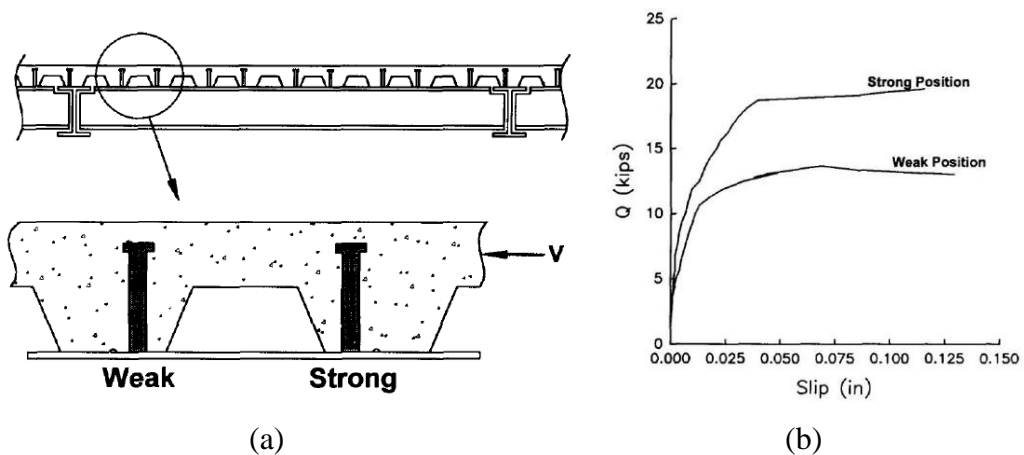
Figure 2.5 (a) Weak and strong positions of studs; (b) Load-slip curves of the studs in the strong and weak positions (Easterling et al 1993)

Johnson (2008) proposed a simple modification to the current formula in ANSI/AISC 360-05 for calculating stud strength in a trough of transverse decking. Due to the increase in yield strength of the profiled decking which was reported in Bradford et al (2006), the predication using the ANSI/AISC 360-05, Eqn. 2.10, was unconservative compared with 187 test results. The proposed modification replaces the term of $A_{sc}F_u$ with $0.5A_{sc}\sqrt{f_c'E_c}$. Lower predictions are obtained. In Eqn. 2.10, where A_{sc} and F_u is the cross-section area and tensile strength of the stud respectively, R_g is a factor which depends on the number of studs in a trough, and R_p is a factor which depends on the distance between the stud in the weak position and the deck.

$$Q_n = R_g R_p (A_{sc}F_u) \qquad\qquad (2.10)$$

2.3.3 Other types of shear connection

Apart from headed studs shear connection, there are a few other types of shear connection developed for particular constructions with specific properties. This section reviews the publications on the shear connection which are similar to those used in the shallow cellular floor beams. The reviewed shear connection consisted of: horizontal studs, concrete dowels in Deltabeam and composite bridge girders, Perfobond ribs, and Crestbond rib shear connection.

2.3.3.1 Horizontally lying shear studs

Kuhlmann and Breuninger (2000) and Kuhlmann and Kürschner (2004) present studies of horizontally lying studs shear connection, where the studs are welded on the web post of a composite girder or slim-floor tee sections, as shown in Figure 2.6. This type of shear connection eliminates the less efficient steel top flange.

Kuhlmann and Breuninger (2000) present an investigation into lying studs subject to longitudinal shear. In total, 50 push-out tests were carried out. Failure of these lying studs was mainly due to the splitting of the concrete. The splitting action of the tension force creates cracks, as illustrated in Figure 2.7 (a). Hence, vertical stirrups are used to prevent the concrete from expanding. The results show that the most important parameters for the shear strength of the lying studs are: concrete compressive strength, stud diameter, the distance from the studs to the top surface of concrete slab, and the amount and arrangement of reinforcement. The characteristic slip value of the lying studs at failure is 17.4mm, which is much higher than the specified value of 6mm in

Eurocode 4 (EN1994-1-1: 2004) which is the classification for a ductile shear connection.

In continuation of the previous paper, Kuhlmann and Kürschner (2004) further studied lying studs subjected to vertical shear, a combination of vertical and longitudinal shear, and cyclic longitudinal shear. A total of 19 cyclic push-out tests showed that a higher peak load close to static resistance causes a decrease of fatigue life, and that a rise of concrete strength leads to a slight increase of fatigue life. However, the significant influence of the stirrup diameter could not be demonstrated.

(a)   (b)
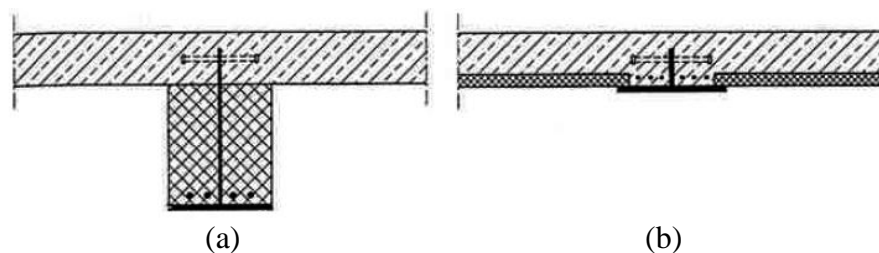
Figure 2.6 (a) Horizontal lying studs in a composite girder without top flange;
(b) Slim-floor tee section with lying studs (Kuhlmann and Breuninger 2000)

(a)   (b)
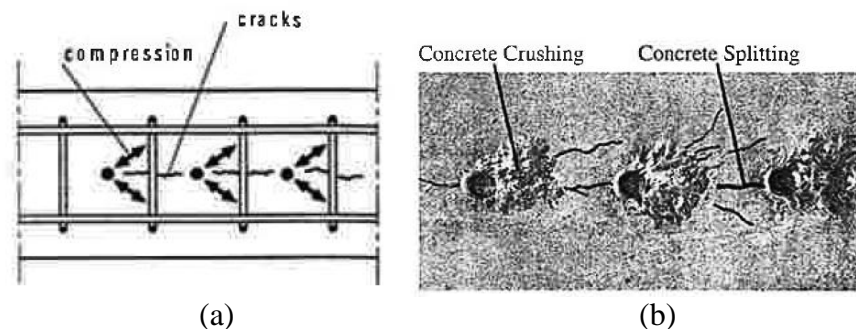
Figure 2.7 (a) Lying studs subject to longitudinal shear (Kuhlmann and Breuninger 2000); (b) Concrete failure due to cyclic loading (Kuhlmann and Kürschner 2004)

2.3.3.2 Concrete dowel in Deltabeam

The Deltabeam is a type of integrated floor beam consisting of a steel boxed section with web holes, as shown in Figure 2.8. The holes are uniformly spaced and form a shear connection with the concrete that fills the steel box section. There are two sizes of web opening in the Deltabeam: Ø75mm and Ø150mm. The openings have lipped edges that project inwards.

Peltonen and Leskelä (2004) carried out 75 push-out tests investigating the capacity of the concrete dowel using the parameters of web hole diameter, geometry of the lip (mainly the lip depth), and concrete strength. The push-out tests, as illustrated in Figure 2.9 (a), were designed based on a main assumption that only the concrete outside

of the steel box plus the concrete dowel within the lip depth are effective to the shear resistance mechanism. Hence, there was a foil parting the concrete infill to simulate the concrete dowel shear connection in the push-out test specimens. The tests demonstrated the ductile load-slip behaviour of the concrete dowel, with average maximum slips of 6-9mm. The disassembled specimens show that failure of all specimens was due to the shearing off of the concrete dowel, as shown in Figure 2.9 (b). The depth of the lip is the depth of the concrete dowel, and has less effect on the resistance of the 75mm diameter web holes. The authors developed the following shear resistance model for concrete dowel:

$$P_{max} = k_R(f_{ctm})f_{ctm}A_{\phi W} \quad\quad\quad (2.11)$$

Where f_{ctm} is the mean tensile strength of the concrete, $k_R(f_{ctm})$ is a resistance factor that depends on the geometry of the hole (depth and diameter), and $A_{\phi w}$ is the area of the hole. Three sets of the $k_R(f_{ctm})$ were concluded for both diameters.

(a)   (b)
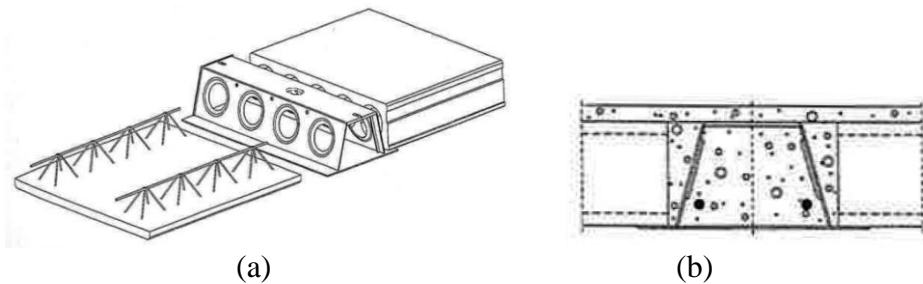
Figure 2.8 (a) Schematic of the Deltabeam; (b) Cross-section of the Deltabeam
(Peltonen and Leskelä (2004)

(a)   (b)
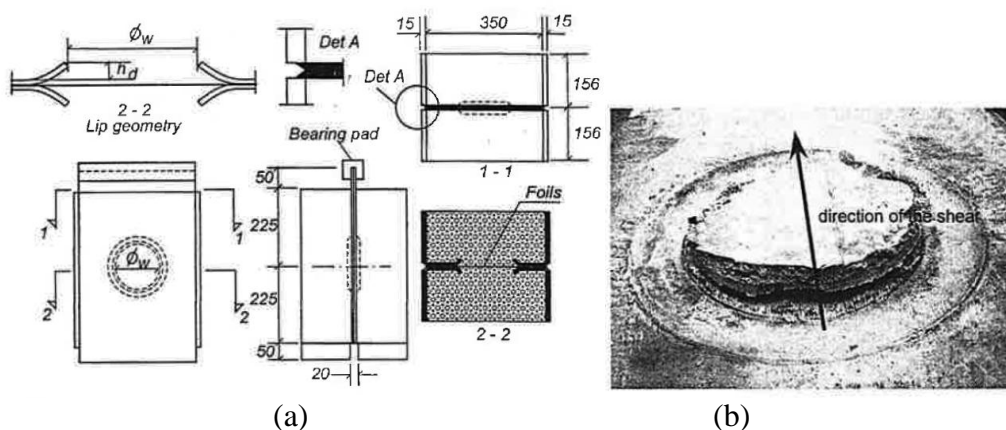
Figure 2.9 (a) Schematic of the push-out test; (b) Failure profile of the concrete dowel
(Peltonen and Leskelä 2004)

2.3.3.3 Perfobond rib shear connection

The Perfobond rib shear connection, shown in Figure 2.10, was first developed by the German firm Leonhardt, Andra and Partners as an alternative connection to eliminate progressive slips of studs in bridges that often resulted from fatigue. The perforated holes on the rectangular plate form a series of concrete dowels which provide longitudinal shear resistance.

Leonhardt et al (1987) carried out a series of push-out tests with static and fatigue loading. Perfobond ribs with two diameters of holes, 35 and 40mm, with constant spacing of 50mm and plate thickness of 12mm, were investigated. Three types of failure modes were observed: shearing of concrete dowels, bearing failure of concrete dowels within the holes, and shearing of steel strips between the holes. There was virtually no slip under static or service loading, and no fatigue problems due to dynamic loading. The load was adequately maintained after failure. Three design equations for the ultimate shear resistance of Perfobond rib, V_u, were developed representing the three potential failure modes.

$$V_u = 2\frac{\pi D^2}{4}(1.3 f_{cu}') \qquad \text{(shearing of concrete dowels)} \qquad (2.12)$$

$$V_u = Dt(8.57 f_{cu}') \qquad \text{(bearing failure of concrete dowels)} \quad (2.13)$$

$$V_u = A_s \frac{f_{sy}}{\sqrt{3}}\pi \qquad \text{(shearing of steel strips between holes)} \quad (2.14)$$

Where D is the diameter of the holes (mm), f_{cu}' is the cube compressive strength (Pa), t is the plate thickness (mm), A_s is the area of steel between adjacent holes (mm^2), and f_{sy} is the yield stress of the steel plate (Pa). However, these equations are only valid for a plate thickness of 12mm, and for 35 and 40mm diameter holes spaced at 50mm.
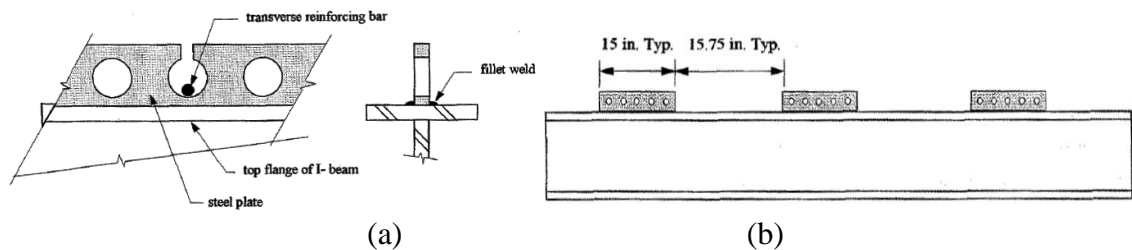
(a)   (b)
Figure 2.10 (a) Details of the Perfobond rib; (b) Positioning of the Perfobond rib
(Leonhardt et al 1987)

Veldanda and Hosain (1992) carried out 56 push-out tests as a part of an investigation to determine the feasibility of using Perfobond rib shear connection in composite floor beams. It was found the capacity of a Perfobond rib with holes of

35mm diameter was equivalent to approximately five studs of 16mm diameter. An approximately 50% increase in shear capacity of the Perfobond rib was demonstrated with the addition of a rebar passing through the hole. A shallow rib of less than 60mm in height was relatively ineffective. The stiffness of the Perfobond rib connection is greater than that of the headed shear studs under service loading. The failure was triggered by the longitudinal splitting of the floor slabs followed by the crushing of the concrete in front of the rib.

Oguejiofor and Hosain (1992) (1) tested six composite beams to verify the push-out test results of Veldanda and Hosain (1992). Three specimens had headed studs and three specimens had Perfobond rib shear connection. The same ductile behaviour was demonstrated by all specimens. The failure mode of the Perfobond rib connection in composite beam tests was the same as that in the push-out tests, namely the longitudinal splitting of concrete slabs. However, using more smaller Perfobond rib connection may result in a delay of concrete crushing and a higher ultimate load.

Oguejiofor and Hosain (1992) (2) carried out 42 further push-out tests to establish design guidelines for calculating the capacity of Perfobond rib connection. The variables investigated were: reinforcing, positioning of the holes, number of the holes, and concrete strength. An increase in shear capacity was demonstrated for an increase in the spacing of the hole up to about twice the diameter of the hole. Four holes within a 375mm length rib have less capacity than that of three holes within the length. The design formula, Eqn. 2.15, was developed, where A_c is the area of concrete in the plane of the rib (mm), f_c' is the concrete cylinder compressive strength (Pa), A_{tr} and f_y are the area and yield strength of the transverse reinforcement respectively, and A_{hs} is the total area of concrete dowels in shear.

$$V_u = 0.6348 A_c \sqrt{f_c'} + 1.1673 A_{tr} f_y + 1.6396 A_{hs} \sqrt{f_c'} \qquad (2.15)$$

The first term represents the concrete splitting, the second term represents the degree of confinement due to the transverse reinforcement, and the third term is the shear strength of the concrete dowels. This design formula was then twice modified by the same authors based on further experimental and numerical investigations. The two modified formulas, Eqn. 2.16 and 2.17 have these similar three terms; where n and d are the number and diameter of the holes respectively, and h and t are the height and thickness of the rib respectively.

$$V_u = 0.59 A_c \sqrt{f_c^{'}} + 1.233 A_{tr} f_y + 2.871 n d^2 \sqrt{f_c^{'}} \tag{2.16}$$

Oguejiofor and Hosain (1994)

$$V_u = 4.5 h t f_c^{'} + 0.91 A_{tr} f_y + 3.31 n d^2 \sqrt{f_c^{'}} \tag{2.17}$$

Oguejiofor and Hosain (1997)

Valente and Cruz (2004) investigated Perfobond rib shear connection in lightweight concrete slabs. Four push-out tests were carried out. The specimens had variables in concrete strength and position of transverse reinforcement. One specimen eliminated the bearing of the rib to the slab. The dimensions of the Perfobond ribs and concrete slabs are constant and are 375x100x13mm and 650x600x150mm respectively. The rib has three 50mm diameter holes with 112.5mm spacing. Very small slips of 1.4-2.2mm were demonstrated at the maximum load, where the failure occurred. The author concluded that Perfobond rib connection could only be used with full shear connection in lightweight concrete slabs, as the ductile of the connection was not demonstrated. The tests results were not as good as the predicted strengths obtained using the Eqn. 2.16 or 2.17 for the Perfobond rib in normal concrete. The average difference was 60-70%.

Ahn et al (2008) present a study of Perfobond rib shear connection under static and cyclic loading. A total of 18 push-out tests were carried out investigating the effects of concrete dowel, transverse rebar through rib holes, and cyclic loading. The geometry of the Perfobond rib was 500mm in length and 129mm in height with four 55mm diameter holes spaced at interval of 125mm. The same failure mechanisms were demonstrated by all specimens for both loading cases, as the initial longitudinal cracks occurred in concrete slabs on the bottom of the interface between the rib and concrete. The average slip of specimens with and without transverse rebar in static loading tests was 21mm and 3mm respectively. Similar slips were also obtained in cyclic loading tests. The effect of the concrete dowel was observed as 65% of the static shear capacity of the specimens without the transverse rebars, and the transverse rebar increased the shear capacity about twofold. In the cyclic loading tests, the residual shear capacity of the specimens without the rebar decreased to about 65% of the capacity in the static tests. However, the transverse rebar had not been shown to have had an effect on the shear capacity due to the cyclic loading.

2.3.3.4 Crestbond rib shear connection

The Crestbond rib shear connection, shown in Figure 2.11, has indented cuts which provide an easier disposition of reinforcing bars. The re-entrant angles provide resistance to longitudinal shear and transverse separation. Ver śsimo et al (2006) carried out 26 push-out tests investigating the shear capacity and ductility of the Crestbond rib shear connection. The parameters of the specimens were: diameter of the circle inscribed in the rib's dent, amount of transverse reinforcement, and concrete strength. The lengths of the ribs were 252, 315, 378, and 413mm. The heights of the ribs were 70, 81, and 93mm. The results show good load bearing capacity after the maximum load. The shear resisting capacity of a Crestbond rib is approximately equal to four 19mm headed shear studs. For an increase of 81% in concrete strength, there is a gain of 35% in the shear capacity of the Crestbond rib connection. The variation in concrete strength has a small influence on ductility when there is rebar passing through the rib.

The effect of concrete dowel is very significant, contributing to an increase of 66% in the shear capacity of the Crestbond rib. This conclusion is very similar to the 65% increase concluded by Ahn et al (2008) for the Perfobond rib connection. The presence of the rebar in the rib increases the shear capacity by 29% and 40% for concrete strength of C20/25 and C35/45 respectively. This conclusion is very different with the twofold increase of shear capacity due to rebar concluded by Ahn et al (2008) for Perfobond rib connection. The ductile behaviour of the Crestbond rib was demonstrated with an average characteristic slip of 7-8mm. The author of this thesis summarised that the slip stiffness and elastic shear resistance of both Crestbond rib and Perfobond rib connection are higher than those of headed shear studs.

(a)   (b)
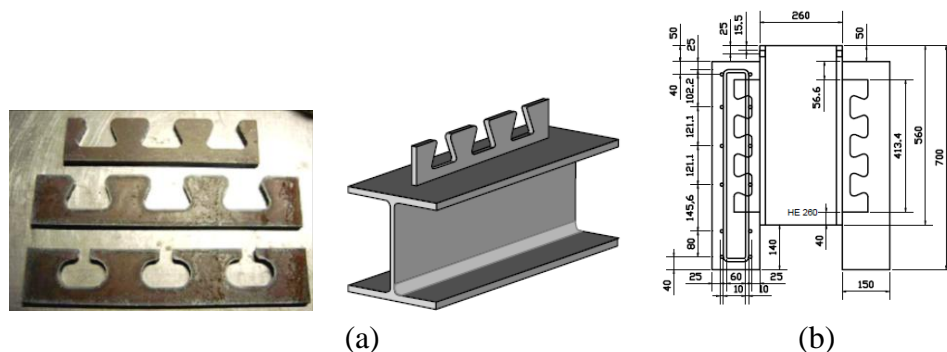
Figure 2.11 (a) Profile of the Crestbond rib shear connection; (b) Illustration of the push-out test (Ver śsimo et al 2006)

2.3.3.5 Concrete dowel in composite bridge girders

Mangerig and Zapfe (2003) investigated the effects of concrete dowels in composite bridge girders. A total of 102 push-out tests were carried out to develop a design procedure for the concrete dowels, as shown in Figure 2.12. An additional 16 push-out tests were performed with cyclic loading investigating the fatigue properties of the concrete dowels. The different variables of the specimens were: geometry of the perforation, concrete strength, and reinforcement. A further six flexural tests were carried out on composite girders without top flange, Figure 2.12 (a). The variables of the specimens were: span, dowel arrangement and utilization degree of the concrete dowel.

One of the failure modes of the concrete dowel is the punch cone, as illustrated in Figure 2.13 (a), which results from the transverse tensile stress. Its failure criterion can be defined by applying shear stress along the surface of a regular cone. The authors disagree with the general concept of the double shearing off of the concrete dowels along the planes of the web. It is suggested that the shearing surfaces are not completely parallel to the web plane, as shown in Figure 2.13 (b). The authors acknowledge that big concrete dowels require a reduction of the shear surface. A design formula of local pressure (or compressive) failure, as shown in Figure 2.12 (c), was developed:

$$P_{RD} = 72.7 h_d t_w \sqrt{f_{ck}} \, \frac{1}{\gamma_V} \tag{2.18}$$

Where h_d is the height of the concrete dowel, t_w is the thickness of the web, f_{ck} is the concrete cylinder compressive strength, and $\gamma_V = 1.25$. The ultimate load results and observed failure mechanisms in the composite girder tests demonstrated the effective shear transferring mechanism of the concrete dowel.

| (a) | (b) | (c) |
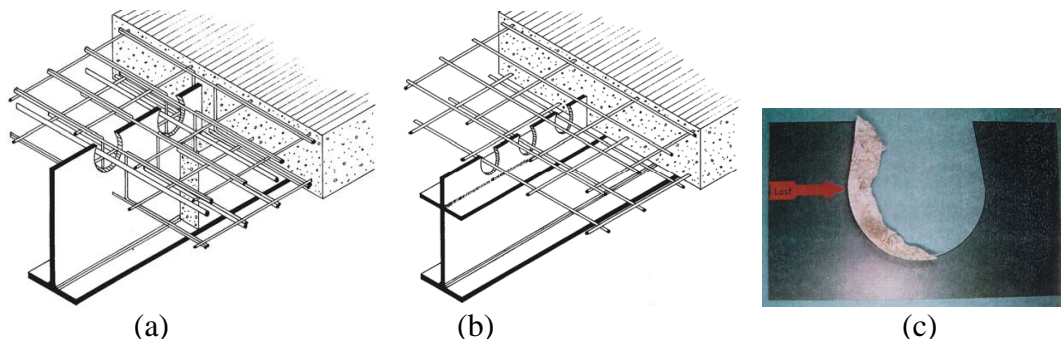
Figure 2.12 (a) Top-flangeless girder with web side filing; (b) Girder with open circular shaped plate welded on the top flange; (c) Compressed concrete in the zone of maximum local pressure (Mangerig and Zapfe 2003)

(a)   (b)
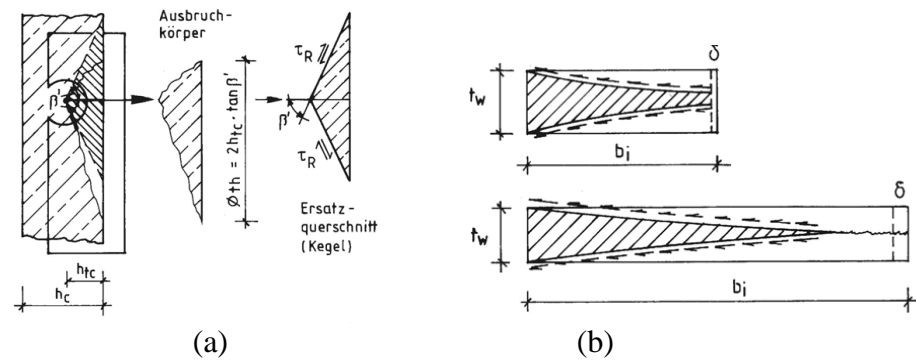
Figure 2.13 (a) Punch cone failure mode; (b) Bearing surface of the concrete dowel in plane view (t_w is the thickness of the web, b_i is the diameter of the opening) (Mangerig and Zapfe 2003)

Jurkiewiez and Hottier (2005) investigated a type of shear connection incorporating a dovetail-shaped cut on the web post with horizontal bars attached, as shown in Figure 2.14. This shear connection is similar to the Crestbond rib shear connection, but with a bigger rib formed on the web. Its original form has a very deep perforated cut, depicted in Figure 2.14 (a), providing a transverse passage for building services. However, the shallow web increases the stress concentration and reduces the vertical shear resistance. It was then modified with a shallow cut, as illustrated in Figure 2.14 (b), especially for its application in bridges. This paper presents the results of three push-out tests and a flexural composite beam test. For simplicity of fabrication in both tests, the rib was chosen as rectangular rather than curved shape. The results of the push-out tests showed that the ultimate shear capacity of one rib attached with 6 rebars of Ø16mm and 4 welded-wires of Ø10mm (depicted in Figure 2.21) was about 860kN. The failure mode was the splitting of the slabs initiated in the middle of the rib. The slip at maximum load was about 2-3mm, which was very similar to that of the Perfobond rib connection. The results of the flexural composite beam test will be reviewed in Section 2.4.3.

(a)   (b)
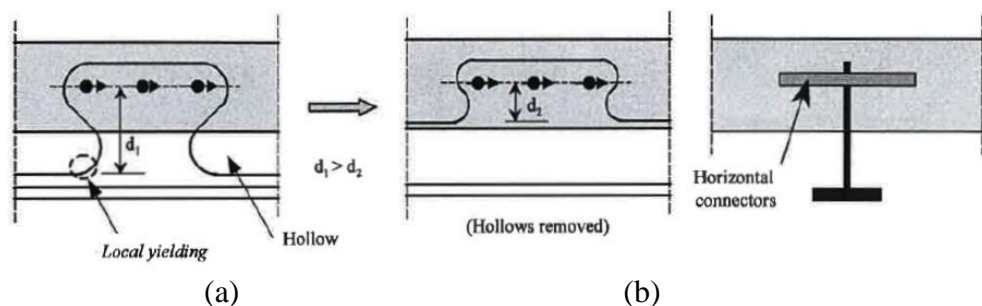
Figure 2.14 (a) Dovetail-shaped web with hollows below the slab; (b) Modified with shallow cut (Jurkiewiez and Hottier 2005)

2.4 Flexural composite beam tests

The review of flexural composite beam tests will focus on tests of: slim-floor beams, conventional downstand composite beams with web openings, and composite beams with encased web openings. This is because all these three types of composite beam have similarities with the shallow cellular floor beams, which consists of concrete slabs within the structural depth of the steel section, and encased web openings.

2.4.1 Slimflor and ASB composite beam tests

Mullett (1998) presents a flexural test of a full-scale Slimflor beam. The test was briefly reviewed in Section 2.2.1. The specimen represents a typical Slimflor beam with a deep decking composite slab. There are holes constructed on the web post providing a passage for short lengths of cylinder, as shown in Figure 2.15. However, the interaction between the cylinders and the web post was not investigated in the test. Four loading jacks were used to simulate a uniformly distributed load over the 7.5m span. Composite action was clearly demonstrated with a 68% increase of moment resistance over the steel section, although the specimen has no shear connection. The maximum bending moment including self-weight was 925kNm, which was then converted into a load intensity of 21.9kN/m^2 for a typical 6m x 7.5m bay. The composite Slimflor beam specimen could have supported an imposed load of 10.9kN/m^2 compared with the design value of 5.0kN/m^2.
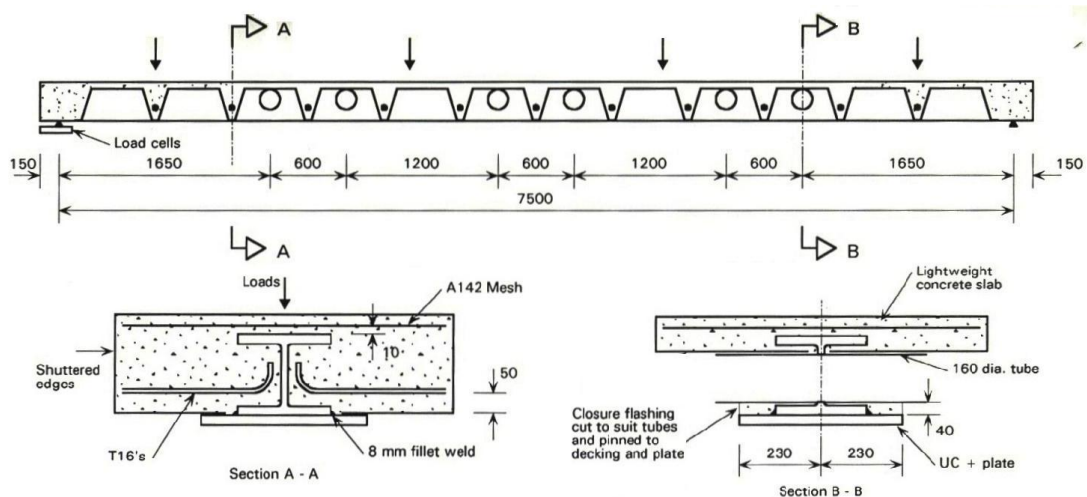
Figure 2.15 Illustration of the Slimflor beam test (Mullett 1998)

Lawson et al (1997) and Lawson et al (1999) present the flexural tests of the Asymmetric Slimflor Beam (ASB). In total, three full-scale ASB beams were tested, which were briefly reviewed in Section 2.2.2. The span of all the specimens was 7.5m.

The first two specimens had a slab width of 1m (or $^1/_8$ of the span). The third specimen had the slab width increased to 2m (or ¼ of the span). There was a series of elongated web openings (160mm deep x 240 wide) in the third specimen, as shown in Figure 2.16. All beam specimens were effectively subjected to a uniform distributed load applied by four jacks. All tests were first carried out with 1000 cycles of dynamic loading between 0 and 1.2 times the calculated working load, and then tested with monotonic loading up to the failure.

The results of the tests showed that the bending resistance of the ASB was increased by 30-50% due to the composite action, which did not deteriorate under the repeated loading. The actual degree of shear connection was high at 75-100%. The back-calculation using the measured material properties showed the longitudinal shear bond was in the range of 1.1-1.5N/mm^2. Design shear bond strength of 0.6N/mm^2 was concluded. The initial stiffness of the composite section was maintained up to 70% of the failure load. The measured stiffness was very close to the design stiffness based on the uncracked section. The effect of the elongated openings on the performance of the beam was relatively small. The shear and Vierendeel bending resistance of the reduced section were enhanced by local composite action.
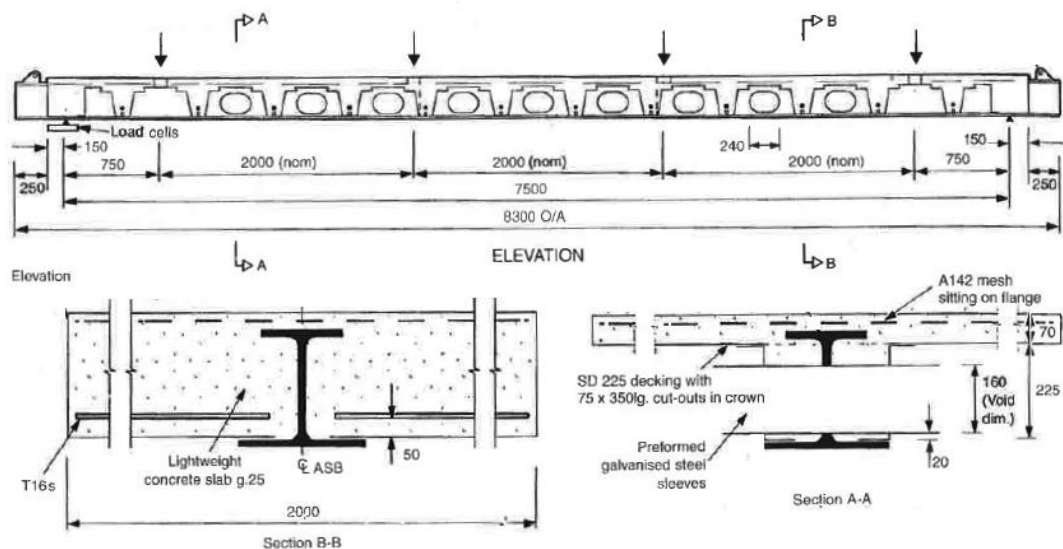
Figure 2.16 Illustration of the third ASB test (Lawson et al 1999)

2.4.2 Tests of downstand composite beams with web openings

Clawson and Darwin (1982) present an experimental investigation of downstand composite beams with rectangular web openings. Six composite beams and one steel beam were tested. Sections of W14x34 (UB356x171x51), W18x45 (UB457x191x67) and W18x46 (UB457x152x67) were used. The rectangular web openings were

concentric to the centroid of all steel sections, as shown in Figure 2.17. Opening sizes were fixed; their depths were equal to 60% of the depth of the steel beam, and their lengths were equal to twice the depth of the opening (the opening lengths were between 406mm and 550mm). The concrete slab dimensions are identical for all composite beams, namely 102mm thickness x 1220mm width. Full shear connection was provided by 19mm diameter and 76mm height headed studs placed in pairs at pitches between 203mm and 380mm. Beams with high moment-shear ratios (M/V) showed little Vierendeel effect. Beams with lower M/V ratios showed Vierendeel effect, as more shear was transferred through the opening at failure. In all cases, the compressive strains in the concrete remained low until well after the steel had begun to yield. The failure of all beams was due to the failure of the concrete. Strain hardening of steel in bottom and top tees occurred prior to the failure.

The results of the tests indicate that concrete slab significantly contributes to the flexural and shear strength of composite beams at web openings. The nature of the failure of composite beams with web openings is ductile. The concrete and steel exhibit large slips prior to the failure at the web openings. It is not clear whether this has an important effect on the strength. The M/V ratio at an opening has a pronounced effect on the mode of failure. Beams with high M/V ratios fail by the general yielding in the steel below the neutral axis and by the crushing in the concrete above the neutral axis. Beams with medium to low M/V ratios fail by the formation of plastic hinges in the bottom tee, accompanied by the diagonal tensile failure in the concrete.
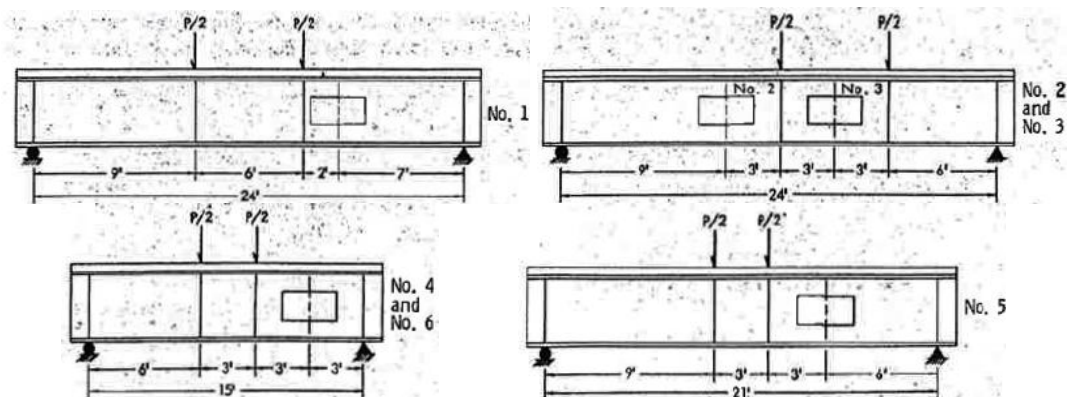
Figure 2.17 Illustration of the flexural tests of downstand composite beams with rectangular web openings (Clawson and Darwin 1982)

Redwood and Wong (1982) present an experimental investigation of the effects of web openings on downstand composite beams with steel decking. Five composite

beams were tested, as illustrated in Figure 2.18. Sections of W250x22 (UB254x102x22) and W360x51 (UB356x171x51) were used. The slabs were identical as consisted of 76mm deep steel decking with 65mm concrete cover. Shear connection was provided by headed studs of 19mm diameter and 124mm original length. The Beam 0 was a pilot beam providing guidance for designing the remaining beams. There is an eccentric opening, Hole 5, in Beam 1, offsetting upward. The effect of partial shear connection was investigated in the test of Beam 4.

Three beams with high or moderate M/V ratios (Beams 2, 3 and 4) demonstrated flexural failure mode. Local bending of the top and bottom tees due to Vierendeel action was visible, and became increasingly evident as the M/V ratio decreased. With low M/V ratios (Beams 0 and 1), the Vierendeel action at the web opening dominated the failure mode and resulted in flexural cracking of the slab. The deflection profile of Beam 1 showed large vertical displacement within the length of the opening which dominated beam behaviour. Slips were very small in the opening region at high M/V ratios, but were significant (between 2.8 and 3.6mm) near the opening at low M/V ratios. Large slips were also present near the opening of Beam 4 which had partial shear connection. In contrast, small slips were induced near the opening of Beam 3 which had a much higher degree of shear connection.

Rib separation occurred in all cases, leading to the compressive failure of the cover slab at medium and high M/V ratios and to almost complete separation of the slab at low M/V ratios. Overall, these beams exhibited some similar behaviour similar to that of the beams with solid slabs tested by Clawson and Darwin (1982). In particular, the rib separation corresponded to the inclined cracks observed in the beams of solid slabs. An improved estimation of the ultimate strength can be obtained by including additional slab compressive stresses. More information about the effect of different degrees of shear connection over the length of the opening is desirable.
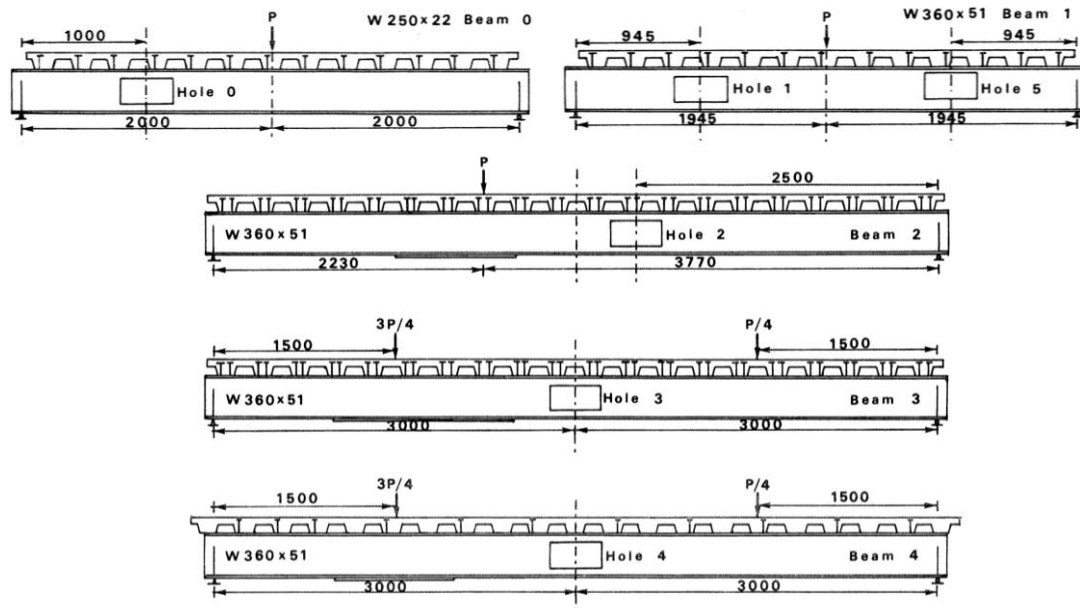
Figure 2.18 Illustration of the flexural tests presented in Redwood and Wong (1982)

Bode et al (Stengel and Zhou) (1996) present a full scale test of a downstand composite beam containing several large rectangular and circular web openings, as shown in Figure 2.19. The specimen had a total span of 12.5m. The depth and width of the composite slab was 130mm and 3m respectively. Super-Holorib decking was used with light weight concrete. Shear connection was provided by headed studs of 22mm diameter. Initial yielding of the steel beam occurred under web opening No.3, and resulted in a decrease of the stiffness of the composite beam. Due to the high M/V ratio, the behaviour of the openings was dominated by bending and a small Vierendeel effect was observed.

The mid-span deflection at the end of the test was very large at 350mm (L/35). However, no brittle or premature failure of the concrete slab was shown. The slip was very small, less than 0.9mm, at the ultimate limit state. The test results were compared with the design model which was based on the beam theory, the Vierendeel mechanism, and the inclusion of the additional contribution of the concrete slab. The calculated loading capacity using the design model with the measured material strength was 564kN. The ultimate load of the test was730kN.
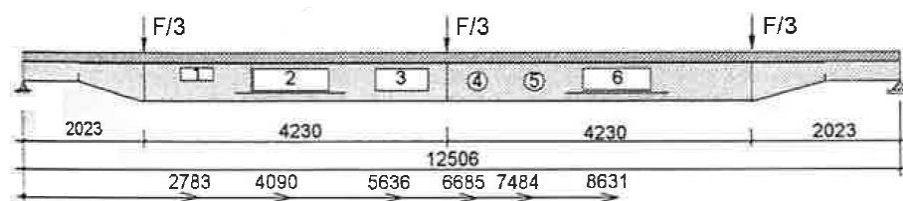
Figure 2.19 Illustration of the flexural test presented in Bode et al (1996)

2.4.3 Tests of composite beams with encased web openings

Ju et al (2009) present a flexural test of the iTECH beam, which is a new composite beam consisting of an asymmetric steel section with web openings, as illustrated in Figure 2.4 (a). A slim-floor beam and a bare steel beam were also tested for comparison, as shown in Figure 2.20. The span of all the specimens was 5m and the depth of all the steel sections was 309mm. The overall depth of the iTECH and slim-floor beam was 355mm, (span-to-depth ratio of 5.35). Four-point bending with 1.2m of pure bending region was applied to all the specimens.

The upper flange of the bare steel beam buckled without lateral torsional deformations. A buckling length of 400mm with an effective length factor of 0.75 was concluded for predicting the buckling load of the bare steel section. The iTECH beam test demonstrated full composite behaviour until yielding and sufficient longitudinal shear strength until the peak load. Buckling of its steel section was not observed before the peak load. Wide cracks were induced within the pure bending region, as there was no rebar placed within the web encasement. The end slip was 10mm at the peak load. The ultimate flexural strength exceeded the calculated value by 17%. Similar behaviour was shown by the slim-floor beam specimen, with the ultimate strength exceeding the calculated value by 8%.

The concluded design model of longitudinal shear resistance for the iTECH beam, consists of a bond strength at the interface between the concrete and steel of $0.6N/mm^2$ (concluded by Lawson et al (1997)), and a bearing strength of the concrete within the web opening of $2 \times 0.85 f_c'$ (where f_c' is the concrete compressive strength).
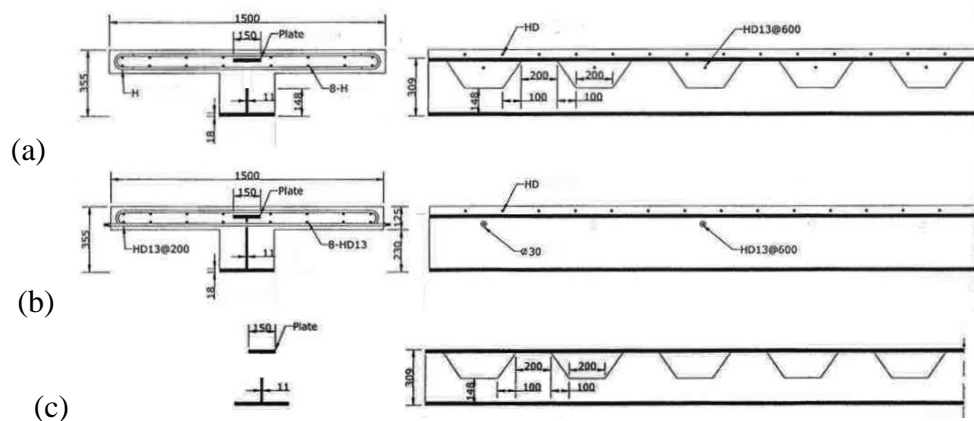
Figure 2.20 Schematic of the flexural tests of (a): iTECH beam, (b): slim-floor beam, and (c): bare steel beam (Ju et al 2009)

Jurkiewiez and Hottier (2005) present an experimental investigation of a composite beam with an encased dovetail-shaped cut on the web post, as illustrated in Figure 2.13. The longitudinal shear transferring is provided by the interaction between the dovetail-shaped rib and the concrete encasement. The push-out tests carried out by these authors were reviewed in Section 2.3.3.5. The results of the push-out tests were used in the design of the composite beam specimen. The span and width of the specimen was 8.5m and 800mm respectively. The shear connection (or the ribs) was uniformly distributed along the beam, as shown in Figure 2.21. The beam specimen was subjected to a three-point bending test. Elastic behaviour was demonstrated first and followed by significant ductile behaviour before the peak load of 532kN was reached. The non-elastic behaviour of the beam seemed to originate from the development of nonlinear behaviour of the upper fibre in the concrete at the mid-span. The failure was initiated by the crushing of the concrete. The flexural failure mode of the plastic hinge at the loading point was observed. However, failure of the shear connection was not observed. The slip at the end of the elastic deflection domain was 0.2mm, and 1.8mm at the peak load. Hence, the stiffness of the shear connection was confirmed as the same as the stiffness shown in the push-out tests.
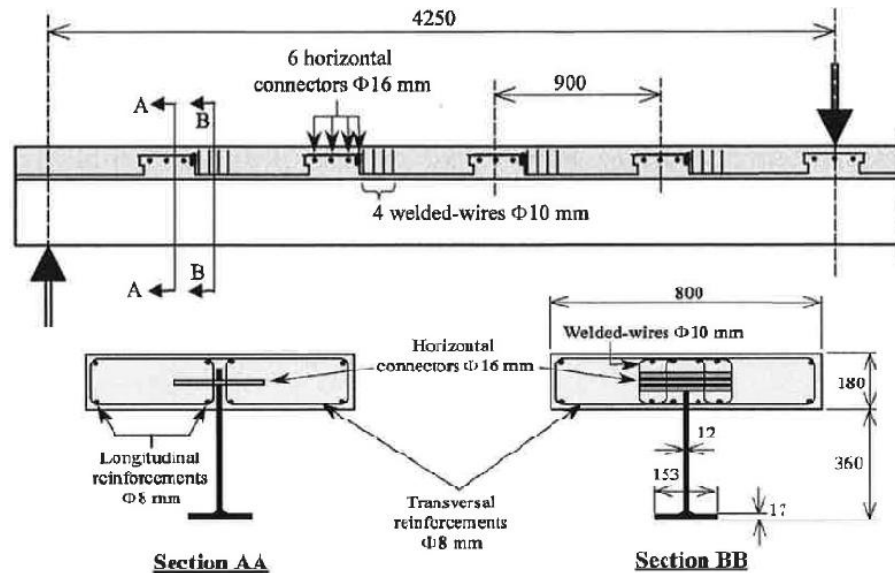
Figure 2.21 Illustration of the flexural tests presented in Jurkiewiez and Hottier (2005)

2.5 Conclusion

Although, the shear transferring mechanism of the composite shallow cellular floor beam had not been investigated previously, however the review of publications on other types of shear connection and composite floor beams had provided many useful guidelines. The collected information used in the later research was:

- methodologies of testing and analysis;

- findings of testing, i.e. characteristic behaviour, failure mechanism, shear capacities and flexural strengths;

- findings of analysis, i.e. design formulas and methods;

- benefits and disadvantages of other forms of shear connection and composite floor beams.

From the review on the shear connection, information of push-out tests was used in the current work. The shear resistance of the conventional headed studs was dependent on several parameters, i.e. stud diameter, concrete compressive strength and ultimate tensile strength of stud steel. The approach for investigating the shear connection in this thesis was first to identify the parameters that would be effective to the shear resistance of the shear connection, and then push-out tests were designed and carried out. The review on the shear connection similar to that used for the shallow cellular floor beams also provided comparable information, such as the failure modes, slip values and design formulas. For instance, the Perfobond rib shear connection had a similar configuration with concrete dowels passing through the perforated plate. The design formulas for the Perfobond rib shear connection were used in the later research to verify the developed method for shear resistance of the shear connection used for the shallow cellular floor beams.

Relevant information of flexural tests was collected in the review on the composite floor beams. The flexural tests for the composite shallow cellular floor beam were designed with the reference in the areas of: loading configurations, effective width and testing arrangement. For instance, the effective width for the concrete slab of the test specimen was designed less than the span/4 specified by both BS5950 and EC4. This was based on the approach presented in Lawson et al (1997) to avoid over-estimating the degree of composite action. And, the additional loading cycles were introduced for the flexural tests to destruct the local bond between the concrete and steel. This was similar to the testing arrangement presented in Lawson et al (1999).

Furthermore, the review of the publications on the downstand composite beams with web openings had provided information for analysing the failure modes of flexural tests, and for predicting the possible failure modes for the beam specimens when constructed with the ribbed slab.

Overall, the literature review had collected useful information for the later experimental and analytical studies. The links between the publications and information used for the later research are summarised in the table below.

Information used for later research			Publications
Code of practice for headed studs		Design formulas and design table	Eurocode 4, British Standard BS5950, American Institute of Steel Construction (AISC 1994)
Push-out tests	Headed studs	Parameters effect to the shear composite and design formulas	Chinn (1965), Slutter and Driscoll (1965), Davies (1967), Goble (1968), Ollgaard et al (1971), Hawkins (1973), Johnson and Oehlers (1981), Grant et al (1977), Easterling et al (1993), Johnson (2008)
	Horizontal lying studs	Important parameters and characteristic slips	Kuhlmann and Breuninger (2000)
	Concrete dowel in Deltabeam	Load-slip behavior, slips, failure mechanism and design formula	Peltonen and Leskelä (2004)
	Perfobond rib shear connection	Parameters, contribution of additional re-bar, failure mechanism, failure modes and design formulas	Leonhardt et al (1987), Oguejiofor and Hosain (1992), Veldanda and Hosain (1992)
Composite floor beams	Slimflor beams	Design methods	Mullett (1992)
	Asymmetric Slimflor Beam (ASB)	Advantages, benefits and design methods	Lawson et al (1997), Rackham et al (2006)
	ITECH beam	Construction system	Ju et al (2003), Ju et al (2009)
Flexural tests	Slimflor beams	Span, decking slab, test configuration, test results and flexural strength	Mullett (1992)
	Asymmetric Slimflor Beam (ASB)	Effective width, decking slab, loading procedures, composite action and failure mode	Lawson et al (1997), Lawson et al (1999)
	Downstand composite beams with rectangular web openings	Solid slab, decking slab and failure modes	Clawson and Darwin (1982), Redwood and Wong (1982)

Table 2.3 Links between the publications and information used in the later research

Chapter 3 Push-out test series-I

Push-out tests investigate the shear connection by applying direct longitudinal shear force. The shear connection of the shallow cellular floor beams is different with the conventional headed shear studs, formed uniquely by the web openings. Four types of the unique shear connection were studied in the push-out test series-I, i.e. concrete-infill-only, tie-bar, ducting and web-welded stud shear connection. The results of the push-out tests were evaluated. Particular emphasis was given to the slip behaviours and failure mechanism of the shear connection with the aim of optimizing and improving the design details. The shear resistance of the shear connection will be further analysed in Chapter 5 to develop a shear resistance design method.

3.1 Introduction

The push-out test series-I had 16 full-scale specimens investigating the concrete-infill-only, tie-bar, ducting and web-welded stud shear connection. The test specimens were designed to represent the actual configurations of the shear connection in the construction practice. The design principle was that the shear connection of the test specimens was subjected to the direct longitudinal shear force. Hence, the shear resisting capacity and load-slip behaviour of the shear connection were obtained. Set up and procedures of the push-out tests were carried out to create the desired static loading conditions and to be in compliance with the specifications of Eurocode 4.

In order to provide information on factors that influence the shear resisting capacity of the shear connection, the push-out tests specimens were designed to have two types of variables: the diameter of the web openings and concrete strength. There were two sizes of the web openings: Ø150mm and Ø200mm. This enabled the study of the relationship between the web opening diameter and shear resisting capacity of the shear connection. Two types of concrete were used to cast the slabs, i.e. the normal concrete and fibre-reinforced concrete. This enabled the study of the relationship between the concrete strengths and shear resisting capacity of the shear connection.

The push-out tests were carried out by applying monotonic loading up to the ultimate failure of the shear connection. Measurements of the longitudinal slip and transverse separation were obtained.

3.2 Test specimens

The push-out test specimens consisted of a steel section and concrete slabs flush with the steel flanges, as depicted in Figure 3.1. There were three openings fabricated on the web post of the steel section. Concrete infill passed through these web openings connecting the concrete slabs on both sides of the web post, creating the actual configuration of the shear connection. The design philosophy for the test specimens was to suitably represent the shear connection and to avoid any undesirable variables, such as the asymmetric steel section.

Shear stud

(a)   (b)
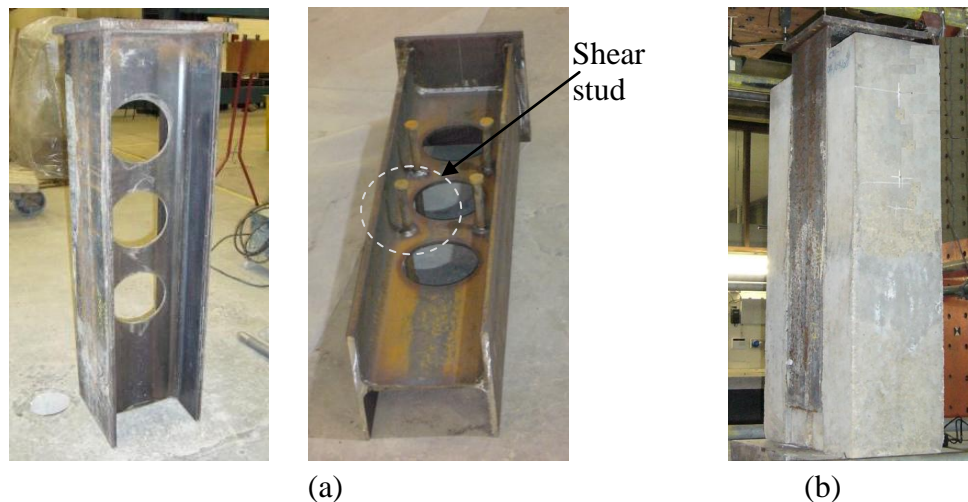
Figure 3.1 (a) Steel sections of the push-out test specimen; (b) Cast specimen for the push-out tests

3.2.1 Steel sections

The steel section of the push-out test specimen was a short universal column (UC). Three web openings were perforated on the web post. The use of the ordinary UC sections was to prevent eccentric loading, which might be created if the actual asymmetric steel section for the shallow cellular floor beams was used.

In order to study the relationship between the shear resisting capacity of the shear connection and diameter of the web opening, the steel sections were designed to have two diameters of the web openings. The web openings of Ø150mm and Ø200mm were perforated on the sections of 254x254x73UC and 305x305x97UC respectively, as

shown in Figure 3.2. A steel plate of 20mm thick was welded on the top of the steel section to evenly spread the load.

(a)   (b)
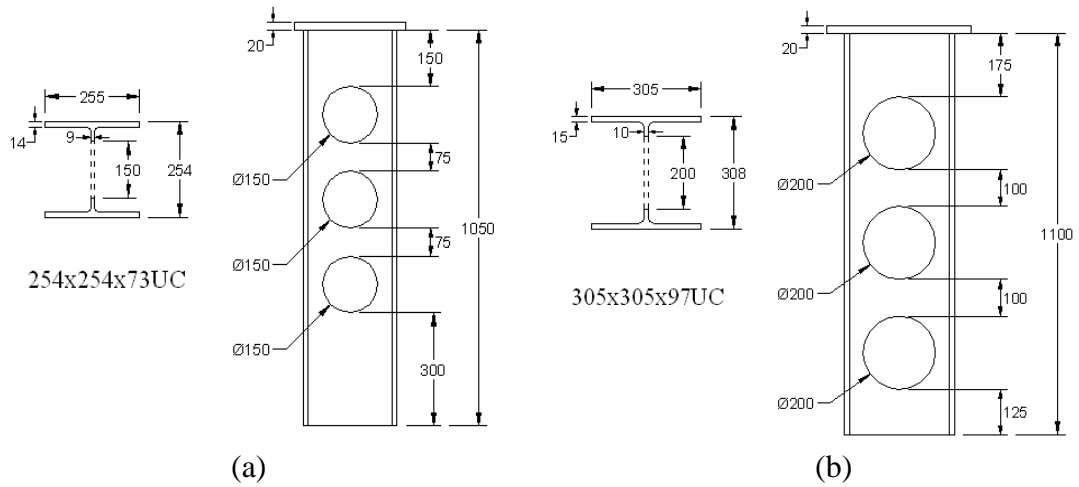
Figure 3.2 (a) the steel section of 254x254x73UC with Ø150mm openings; (b) the steel section of 305x305x97UC with Ø200mm openings

3.2.2 Concrete slabs

The total width of the concrete slabs of all specimens in the push-out test series-I was 600mm. This was to avoid undesirable variables due to the different width of the concrete slab. The depth of the slabs was the same as that of the steel section, as slabs flushed with the steel flanges.

Two types of concrete were used to cast the slabs, i.e. the normal concrete and fibre-reinforced concrete. The purpose of using the two types of concrete was to study the relationship between the shear resisting capacity of the shear connection and concrete strength. The tensile strength of the fibre-reinforced concrete was higher than that of the normal concrete with the same compressive strength. This was concluded from the concrete strength tests carried out in this research. The concrete strength comparison for the two types of concrete was shown in Appendix A. The details of synthetic fibres and superplasticizer used for the fibre-reinforced concrete were presented in Appendix A.

3.2.3 Test groups

Four types of the shear connection used for the composite shallow cellular floor beams were investigated in the push-out test series-I. There were four test groups representing each type of the shear connection, i.e. concrete-infill-only, tie-bar, ducting and web-

welded stud shear connection. Each test group had four push-out test specimens. The variable parameters of the test specimens and their labels are summarised in Table 3.1.

Test Group	Specimen No.	Web Opening	Concrete Type
T1, T2, T3, T4*	T1-A-N	Ø150mm (A)	Normal (N)
	T1-A-F		Fibre-reinforced (F)
	T1-B-N	Ø200mm (B)	Normal (N)
	T1-B-F		Fibre-reinforced (F)
*T1: concrete-infill-only	T2: tie-bar	T3: ducting	T4: web-welded stud

Table 3.1 Specimen labels and variable parameters of the test groups

3.2.3.1 Specimens of test group T1, concrete-infill-only shear connection

The specimens of the test group T1 represented the concrete-infill-only shear connection which had no other elements, i.e. tie-bar or ducting, passing through the web openings. The in-situ concrete completely filled the web opening, resisting the longitudinal shear force. The specimens were designed so that the load applied on the steel section would be directly resisted by the concrete infill elements. Hence, the shear resisting capacity and behaviour of the concrete-infill-only shear connection could be investigated. Each specimen of the test group T1 had three concrete-infill-only shear connection. Dimensions of the specimens are shown in the figure below.

(a)   (b)
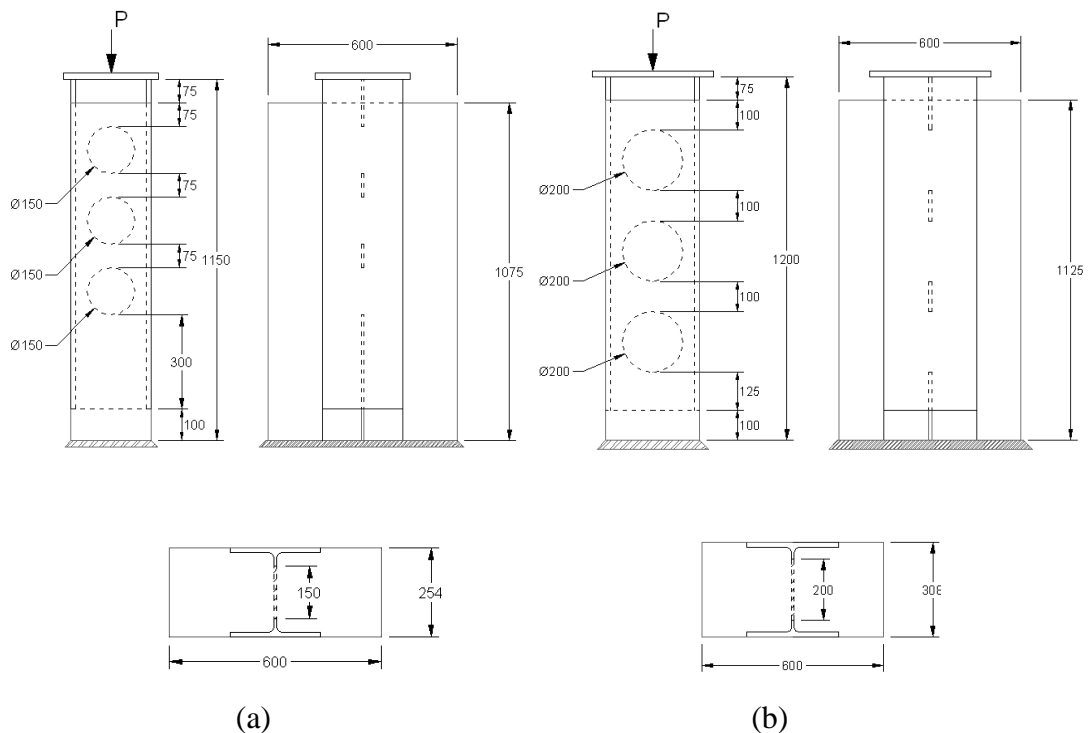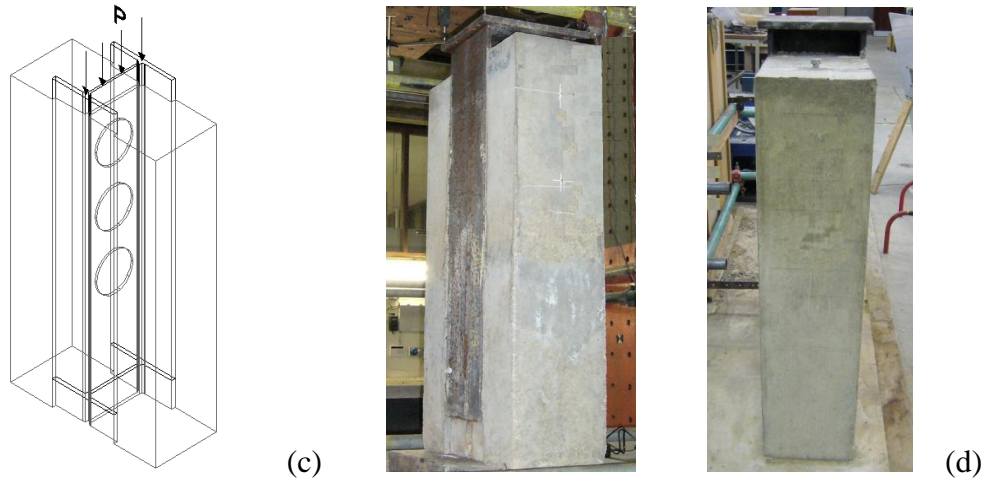
Figure 3.3 Drawings of the T1 specimens: (a) with Ø150mm web openings, (b) with Ø200mm web openings, (c) Schematic of the T1 specimens, (d) Cast test specimens

3.2.3.2 Specimens of test group T2, tie-bar shear connection

Tie-bar shear connection of the test group T2 represented the general practice of two Ø12mm tie-bars passing through each web openings when the length of the tie-bars was less than 1m (the width of the concrete slab was 600mm). The two tie-bars were positioned close to the perimeter of the web opening, as shown in Figure 3.4. The top tie-bar within each opening would be in direct contact with the movements of the steel section (or slips); hence, it would show the shear failure mode.

(a)

(b)
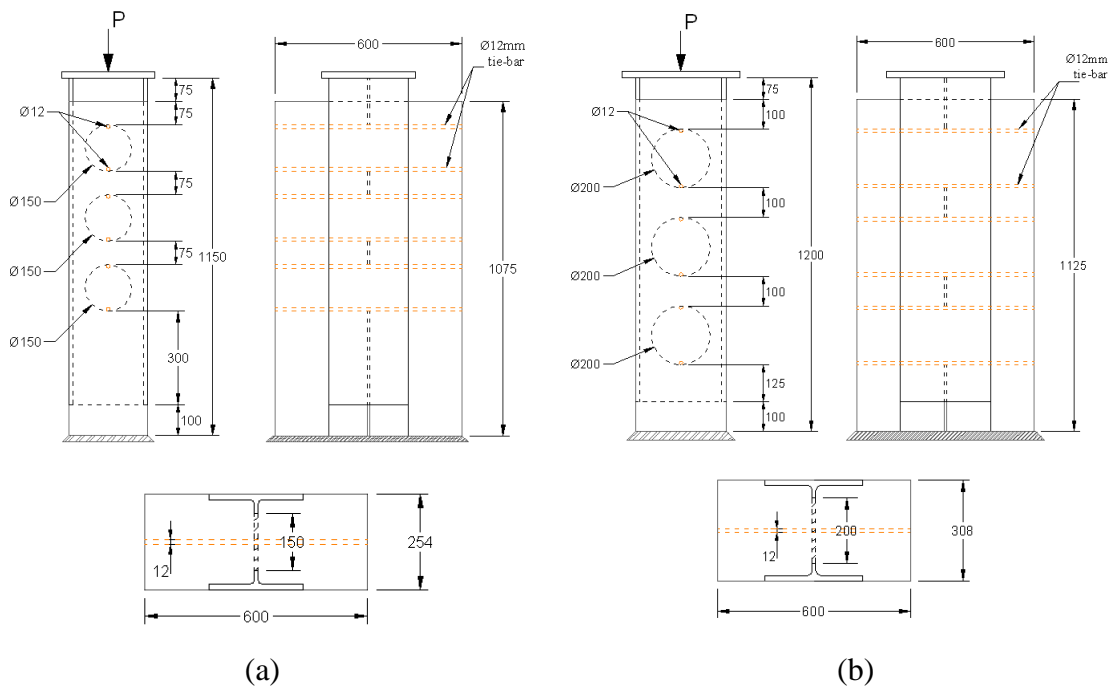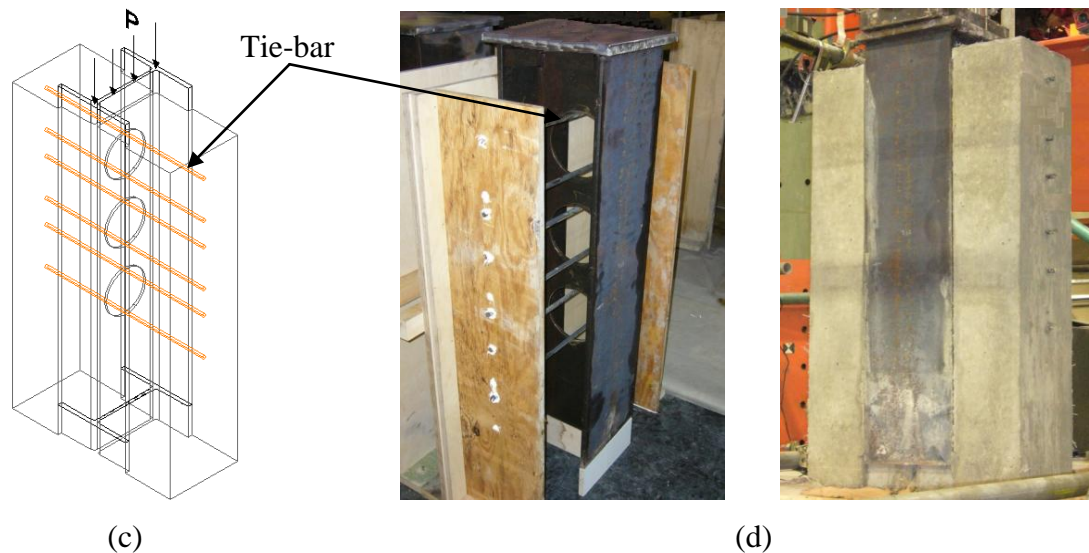
Figure 3.4 Drawings of the T2 specimens: (a) with Ø150mm web openings, (b) with Ø200mm web openings, (c) Schematic of the T2 specimens, (d) Cast test specimens

3.2.3.3 Specimens of test group T3, ducting shear connection

The ducting shear connection of the test group T3 was designed to represent the actual details of the shear connection used for the shallow cellular floor beams. In general, the diameter of the ducting would be smaller than that of the web opening. Hence, the in-situ concrete filled the voids between the ducting and web opening, creating a concrete infill element combined with the ducting resisting the longitudinal shear force.

The Ø125mm ducting was used to pass through the Ø150mm web openings; the Ø150mm ducting was used to pass through the Ø200mm web openings, as shown in Figure 3.5. The ducting was formed of 0.5mm thickness galvanised steel sheet. The ducting shear connection was expected to fail at low loads; this was due to the geometry and thickness of the ducting, which could not provide much of the shear resistance.

(a)   (b)

(c)   (d)
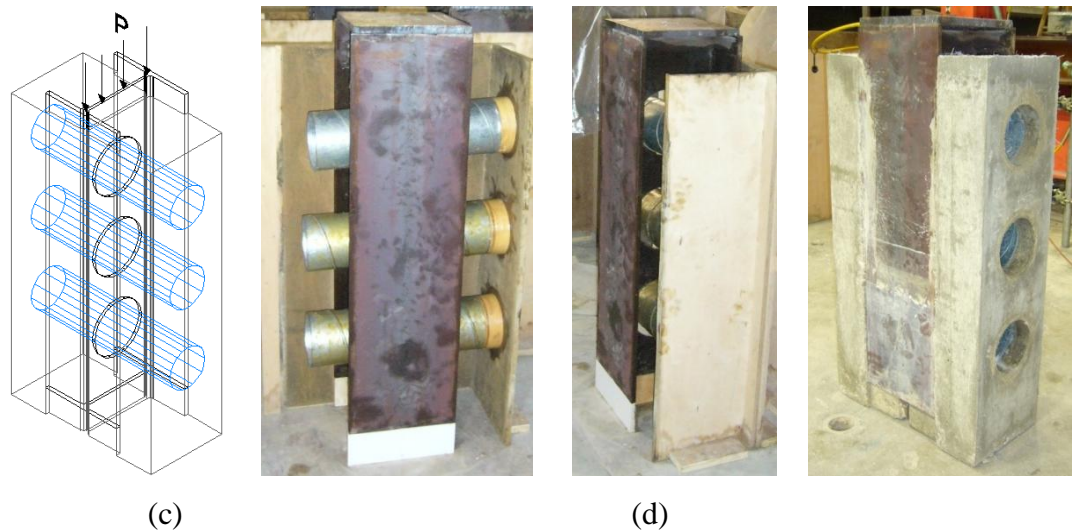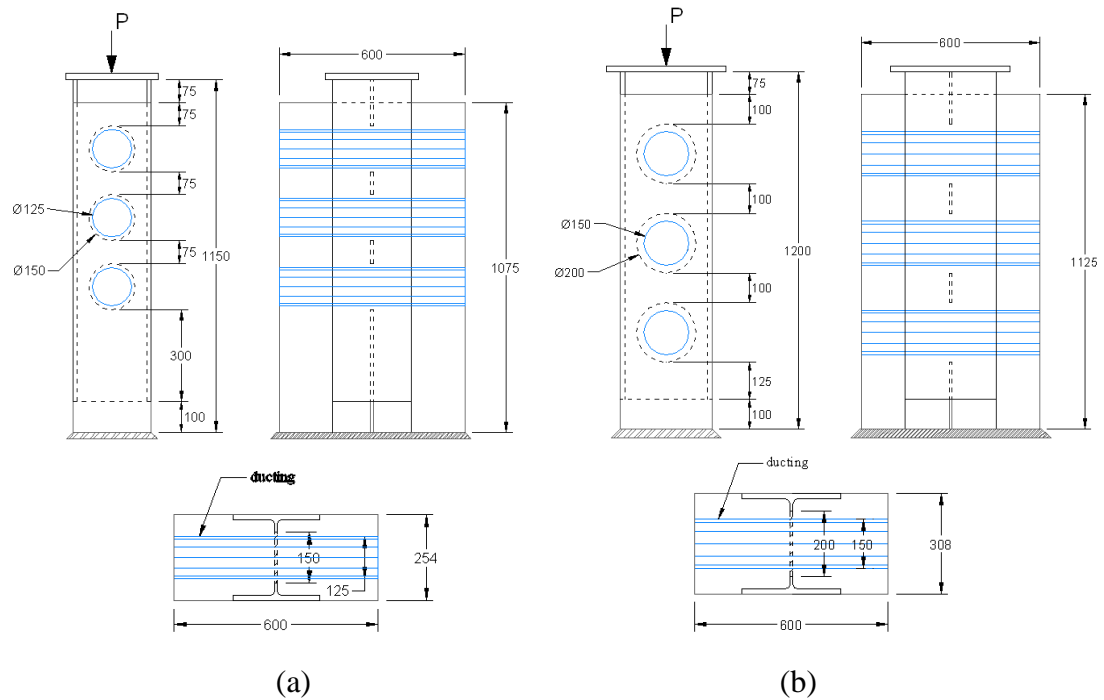
Figure 3.5 Drawings of the T3 specimens (a): with Ø150mm web openings, (b): with Ø200mm web openings; (c) Schematic of the T3 specimens; (d): Cast test specimens

3.2.3.4 Specimens of test group T4, web-welded stud shear connection

The specimens of the test group T4 comprised four headed studs welded symmetrically on each side of the web post, as shown in Figure 3.6. This layout of the studs was similar to that of the shallow cellular floor beams, which had the studs welded on the web post of the top tee, as shown in Figure 1.8. The layout design of welding studs symmetrically was to prevent the eccentric loading. The actual shear transferring mechanism of the web-welded stud shear connection was created in the push-out test specimens. The concrete infill elements and shear studs would simultaneously resist the

longitudinal shear force. The diameter of the studs was 19mm and the after welding height was 127mm, as shown in Figure 3.6.

(a)   (b)

(c)   (d)
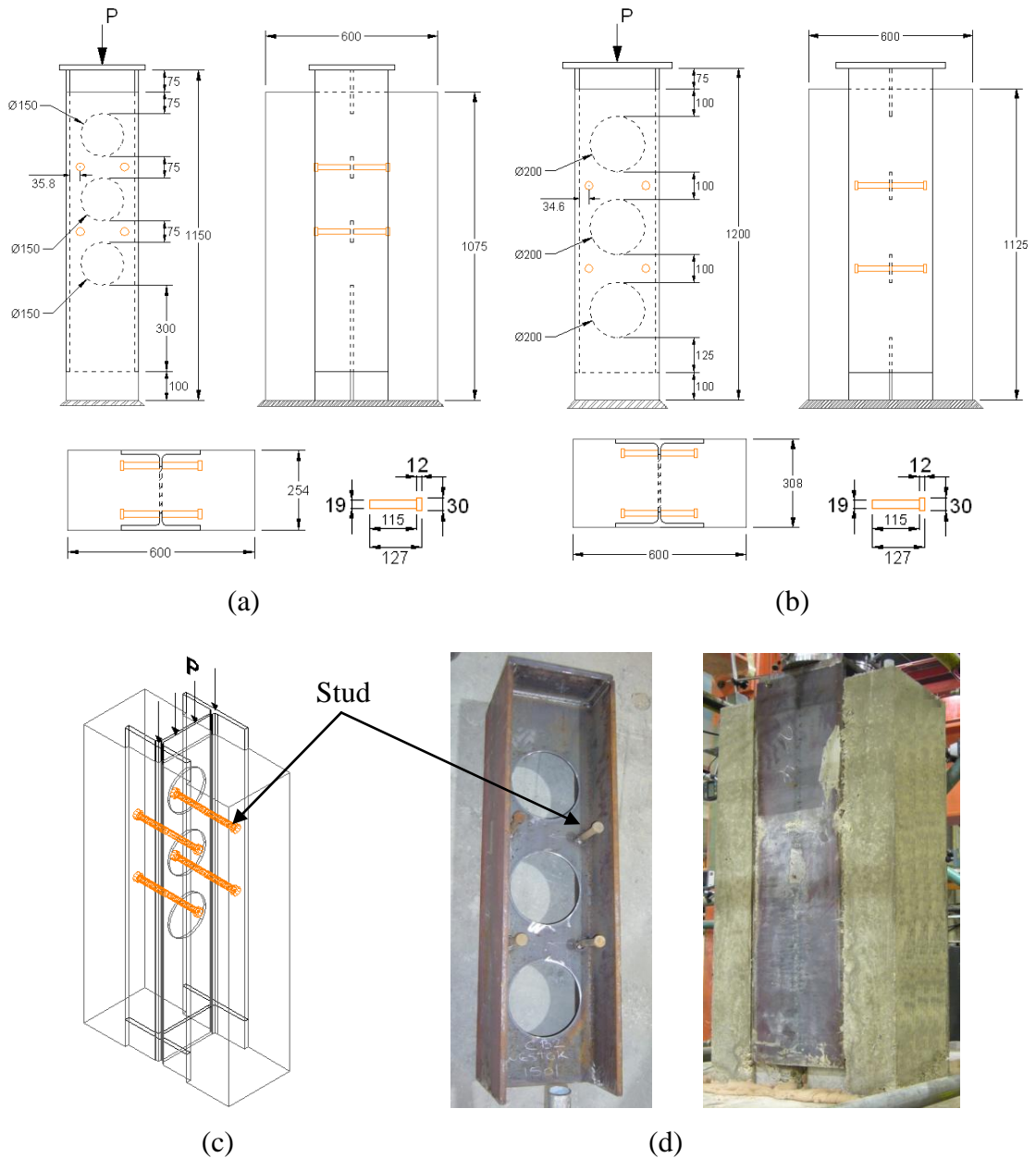
Figure 3.6 Drawings of the T4 specimens (a): with Ø150mm web openings, (b): with Ø200mm web openings; (c) Schematic of the T4 specimens; (d): Cast test specimens

3.2.4 Preparation and construction

The steel sections were applied with grease to prevent the development of the bond between the concrete and steel. But, grease was not applied on the steel sections of the T1 specimens (concrete-infill-only shear connection). This was to particularly investigate the effect of the bond on the behaviour of the shear connection.

All the push-out test specimens were cast in the Structure Laboratory of the City University London. Cubes and cylinders specimens were prepared from the same mix of the concrete used for the push-out test specimens. All the push-out test specimens, cubes and cylinders were cured under the same condition and were covered with wet sacks and plastic sheets.

3.3 Set up and testing procedures

A rig of 1900kN (200ton) capacity, depicted in Figure 3.7 (a), was used for the push-out tests. Two identical 880kN (90ton) hydraulic jacks were used to apply load. A load cell was placed under each jack, as shown in Figure 3.7 (b). Digital dial gauges were used to obtain the measurements of slips and separations. Four digital dial gauges were positioned on the top of the steel section measuring the slips in the vertical direction. Four digital dial gauges were positioned on both sides of the slabs measuring the separations in the horizontal direction. The resolution of the digital dial gauges was 0.01mm.

Reaction beam

Push-out test specimen

Reaction platform

(a)

(b)
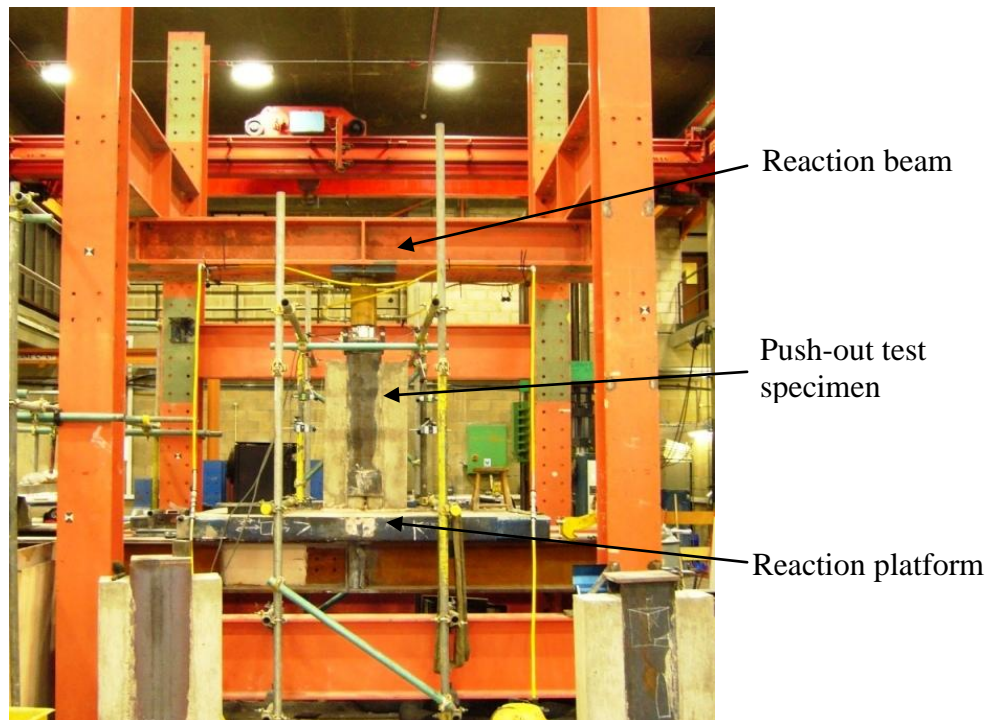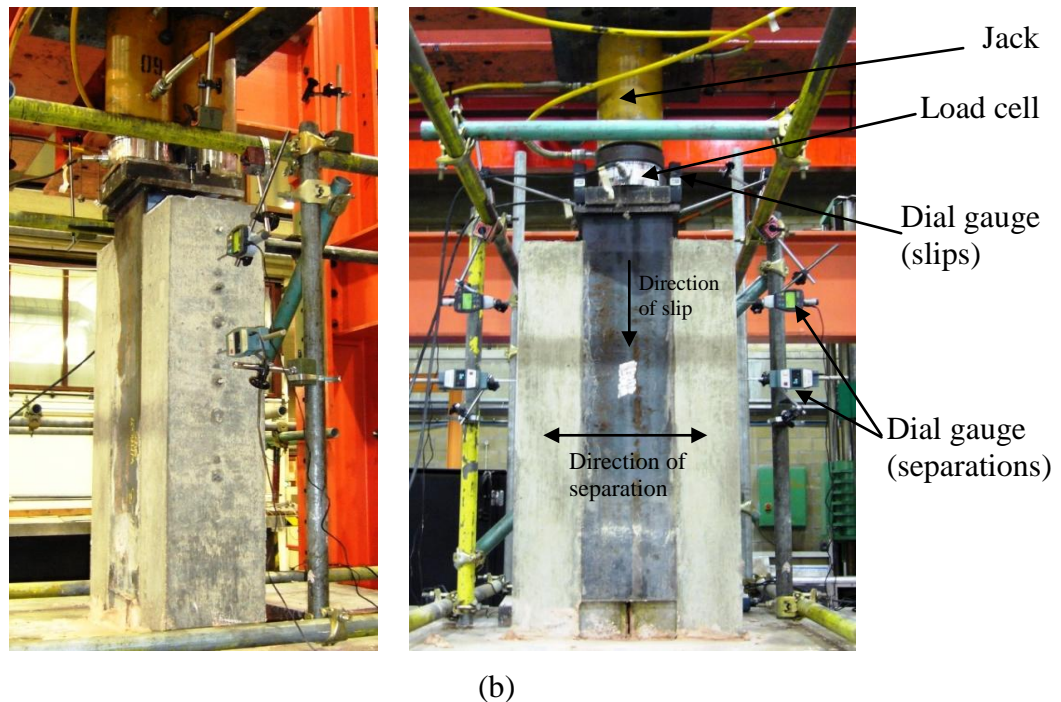
Figure 3.7 (a): The rig for the push-out tests; (b): Set up and instrumentations of the push-out tests

3.3.1 Testing procedures

The push-out tests were carried out in accordance with the specifications of Eurocode 4 (EN1994-1-1: 2004). The specimens were settled onto a layer of plaster (gypsum). This was to eliminate the uneven contact between the specimens and reaction platform. Monotonic loading was applied onto the steel sections; hence, the incremental shear force was applied to the shear connection.

The push-out tests were load-controlled. The load increments for specimens of each test groups are listed in Table 3.2. The specimens were tested until the destructive failure of the shear connection. The duration of the push-out tests was 2 hour on average, which was more than the minimum duration of 15 minutes specified in Eurocode 4. The slips were measured until the load dropped to at least 20% below the maximum load.

Test Group	Load Increment	As % of the Expected Failure Load
T1 (concrete-infill-only)	19.6kN (2ton)	2%
T2 (tie-bar)	19.6kN (2ton)	2%
T3 (ducting)	9.8kN (1ton)	3%
T4 (web-welded stud)	19.6kN (2ton)	2%

Table 3.2 Load increments of the test groups

3.4 Test results

Load-slip and load-separation curves were obtained from the push-out tests. The load-slip curves represented the characteristic behaviour of the shear connection in response to the direct longitudinal shear force. The load-separation curves represented the tie-resisting behaviour of the shear connection. The concrete strengths of all specimens are presented in Appendix B. The test results were evaluated with the aims of providing information on the specific properties of the shear connection. The criteria of the evaluation were base on Eurocode 4. The behaviour and failure mechanism of the shear connection are particularly studied with the aims of optimizing and improving the design details. The shear resisting capacities of the shear connection were further analysed in Chapter 5 to establish a shear resistance design model.

3.4.1 Load-slip curves

The load-slip curves of all test groups are shown in Figures 3.8-3.11. The load shown in these load-slip curves was the load per shear connection. Each specimen had three shear connection, as there were three web openings fabricated on the steel section. However, in the specimens of test group T4, each concrete infill element combined with 2.67 headed studs to form a web-welded stud shear connection, since there were eight studs and three concrete infill elements in each specimen, as shown in Figure 3.6.

3.4.2 Load-separation curves

The load-separation curves of all test groups are shown in Figures 3.12-3.15. The load shown in the load-separation curves was the load per shear connection. The scales of the load-separation curves were the same as those of the load-slip curves; hence, the comparison between the slips and separations could be shown. The separations of the ducting shear connection (test group T3) are very small; the enlarged load-separation curves are shown in Section 3.4.6.
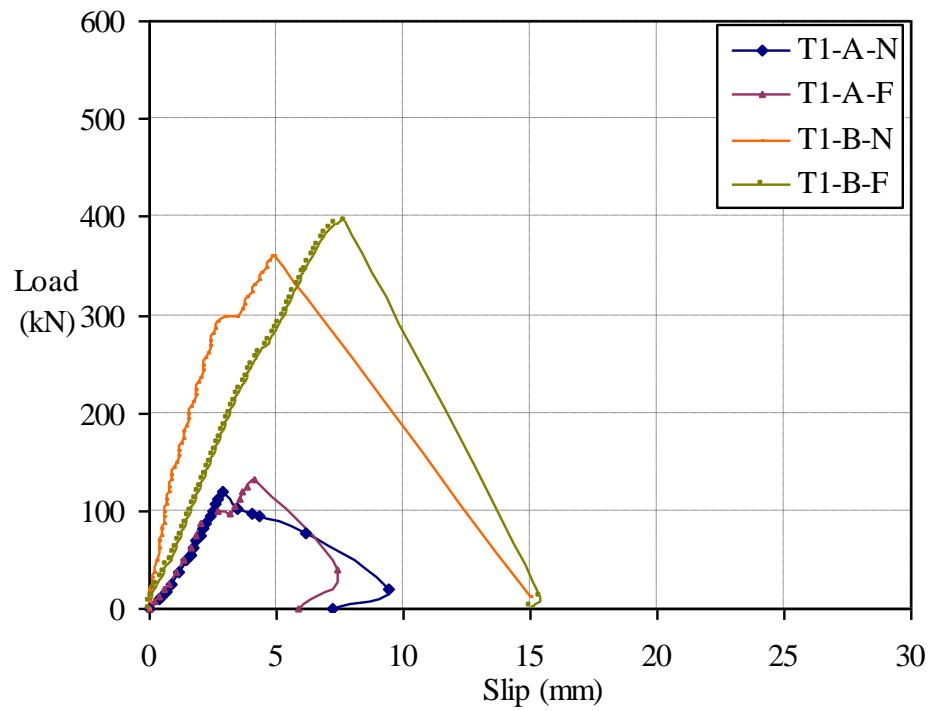
Figure 3.8 Load-slip curves of the concrete-infill-only shear connection (test group T1)
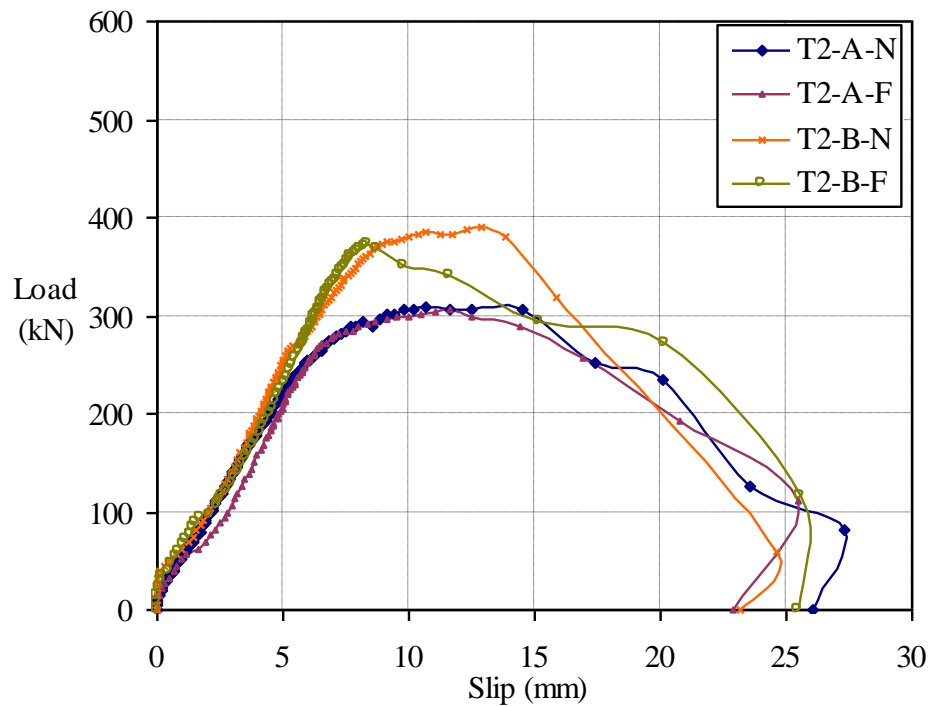
Figure 3.9 Load-slip curves of the tie-bar shear connection (test group T2)
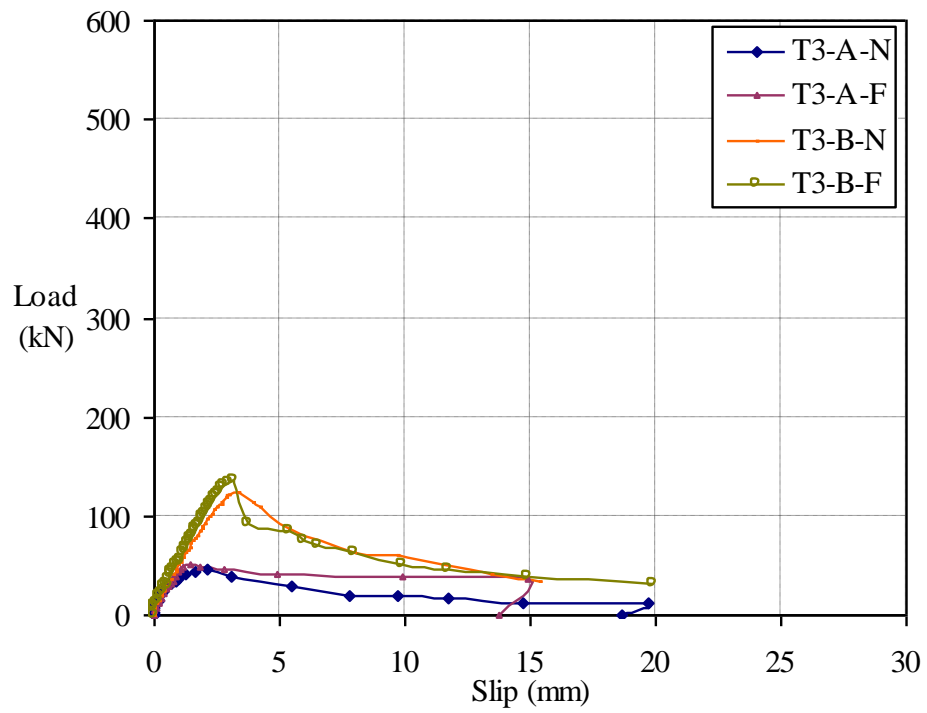
Figure 3.10 Load-slip curves of the ducting shear connection (test group T3)
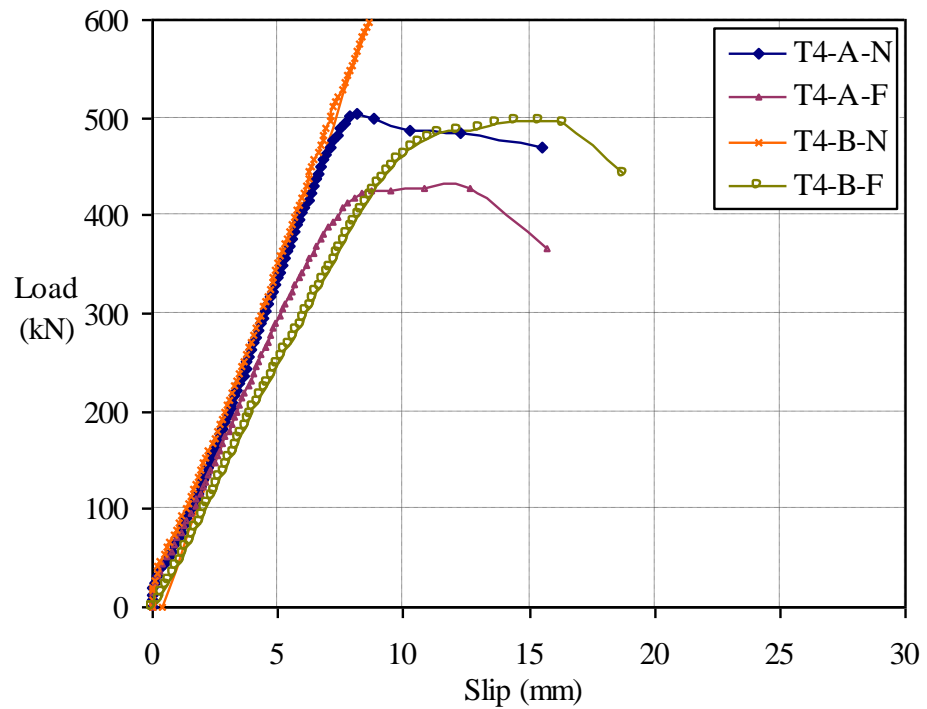
Figure 3.11 Load-slip curves of the web-welded stud shear connection (test group T4)
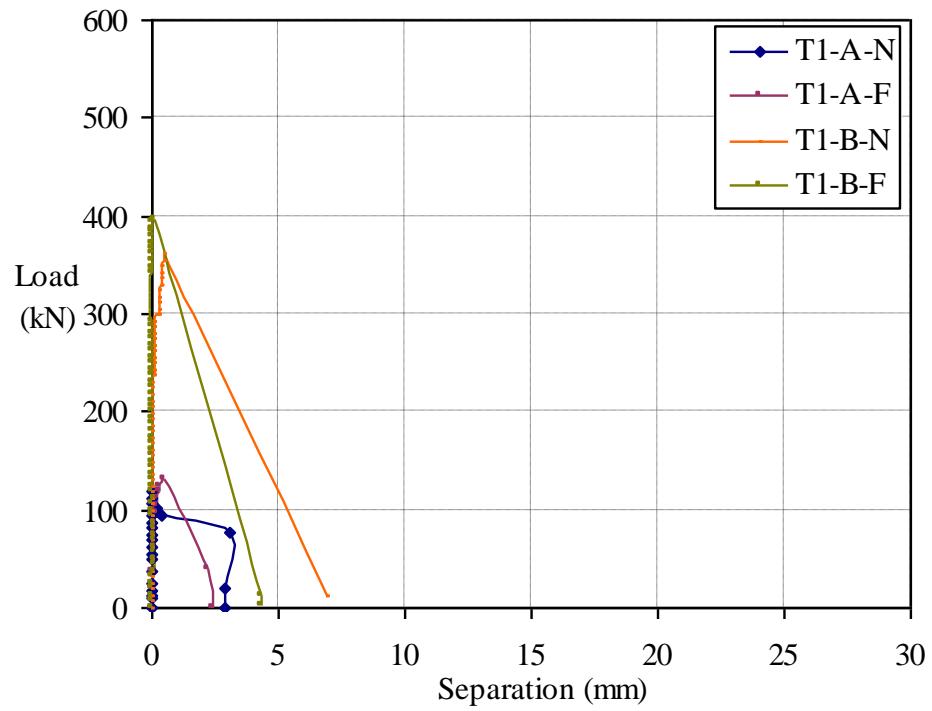
Figure 3.12 Load-separation curves of the concrete-infill-only shear connection (T1)
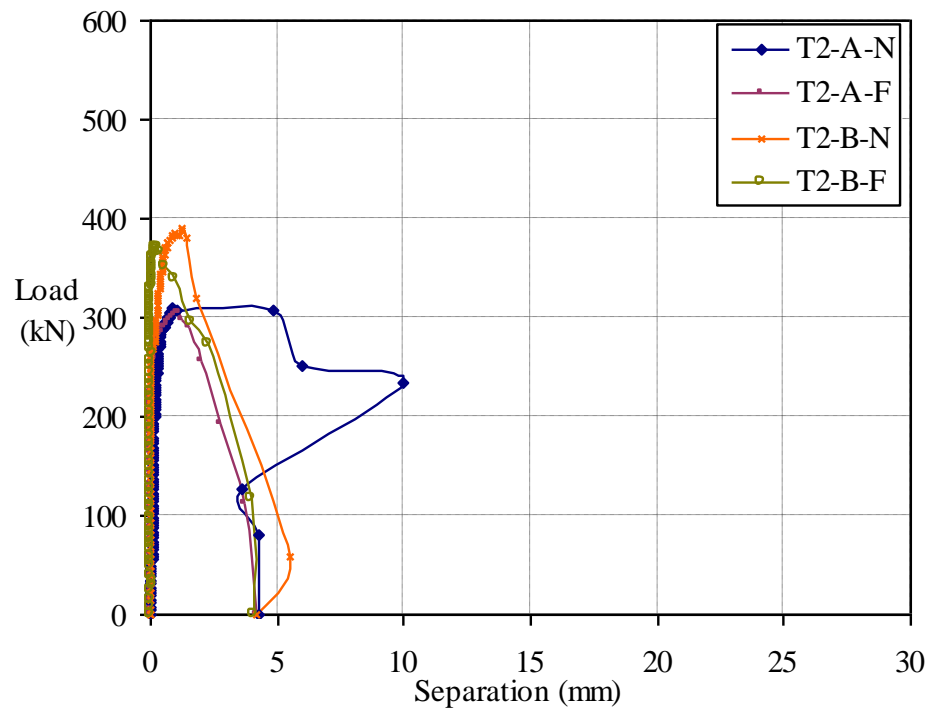
Figure 3.13 Load-separation curves of the tie-bar shear connection (T2)
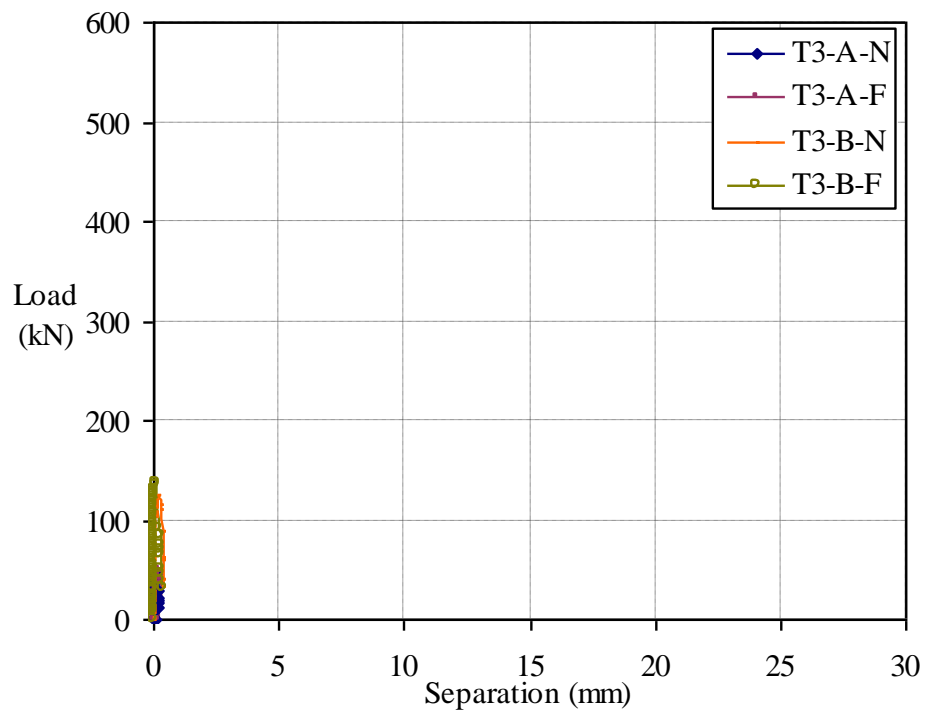
Figure 3.14 Load-separation curves of the ducting shear connection (T3)
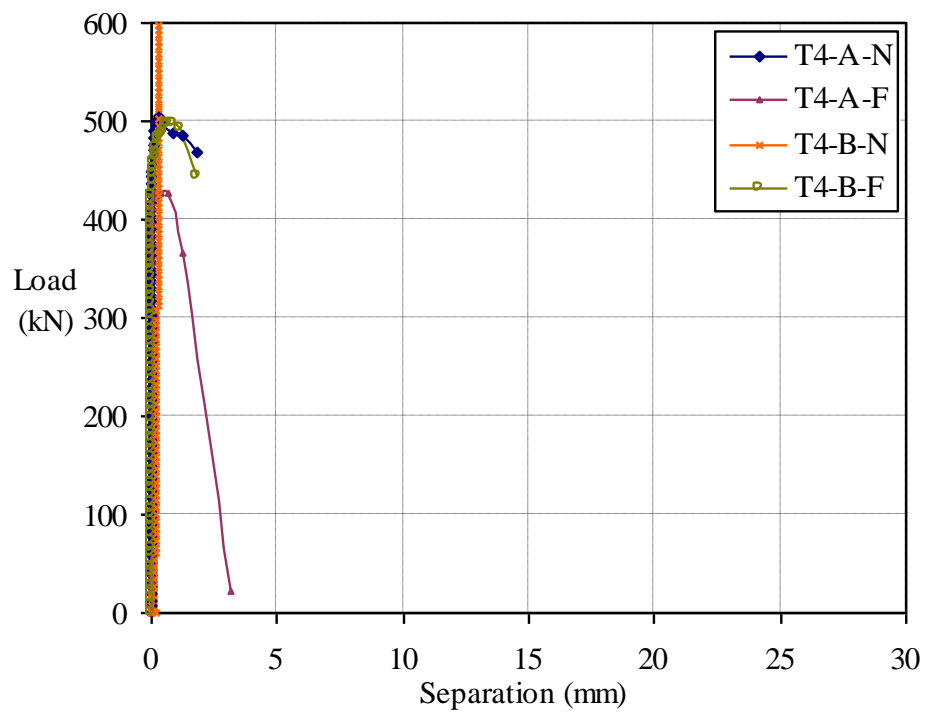
Figure 3.15 Load-separation curves of the web-welded stud shear connection (T4)

3.4.3 Result evaluation

The results of the push-out tests series-I were evaluated in accordance with the specifications of Eurocode 4. The methods and criteria used in the evaluation are outlined below.

- The ultimate shear capacity of the shear connection, P_u, was obtained by dividing the ultimate load of the specimens by the number of the shear connection;

- The slip capacity of the shear connection, δ_u, was the slip value at the load level dropped 10% below the ultimate load (EC4, EN1994-1-1: 2004). The concrete-infill-only and ducting shear connection, which showed no plastic deformations after the ultimate load was reached, as shown in Figure 3.8 and 3.10 respectively. Hence, their slip capacities, δ_u, were taken as the slip values at the ultimate load levels;

- The stiffness of the shear connection, K, was the linear stiffness of the load-slip curves;

- The criterion of tie resistance check is that the transverse separations at 80% of the ultimate load should be less than half of the slip at that load level (EC4, EN1994-1-1: 2004).

Shear connection	Specimen No.	Ultimate shear capacity P_u (kN)	Slip capacity δ_u (mm)	Stiffness K (kN/mm)	Tie resistance check (pass/fail)
Concrete-infill-only	T1-A-N	118	2.85	41	Pass
	T1-A-F	131	4.09	40	Pass
	T1-B-N	362	4.92	74	Pass
	T1-B-F	397	7.70	62	Pass
Tie-bar	T2-A-N	309	16.00	45	Pass
	T2-A-F	305	15.50	49	Pass
	T2-B-N	390	14.70	50	Pass
	T2-B-F	372	12.20	47	Pass
Ducting	T3-A-N	47	2.07	31	Pass
	T3-A-F	50	1.45	35	Pass
	T3-B-N	125	3.37	37	Pass
	T3-B-F	137	3.21	43	Pass
Web-welded stud	T4-A-N	504	8.11	66	Pass
	T4-A-F	427	14.80	58	Pass
	T4-B-N*	--	--	70	--
	T4-B-F	497	14.40	49	Pass

* The specimen, T4-B-N was not failed, as the capacity of the jacks was reached.

Table 3.3 Result evaluation of the push-out test series-I

3.4.4 Results of test group T1, concrete-infill-only shear connection

The concrete-infill-only shear connection was investigated in the test group T1. The de-bonding grease was not applied onto the steel sections. This was to investigate the effects of the bond on the behaviour of the shear connection. The results of the ultimate load and slip of the specimens are summarised in Table 3.4. The load-slip and load-separation curves of each specimen are shown in Figures 3.16-3.19. The load value of these curves was the load per shear connection.

The results of the test group T1 showed that the shear resisting capacity of the shear connection increased with the increase of web opening diameter. The failure loads of the specimens with Ø200mm web openings, T1-B-N & T1-B-F, were higher than

that of the specimens with Ø150mm web openings, T1-A-N & T1-A-F, respectively. The comparison was base on the same concrete strengths. Furthermore, the test results demonstrated that the shear resisting capacity of the shear connection increased with the increase of concrete strength. The failure loads of the specimens with higher strength of concrete, T1-A-F & T1-B-F, were higher than that of the specimens with lower strength of concrete, T1-A-N & T1-B-N, respectively. This comparison was based on the same diameter of web openings.

Slips of the concrete-infill-only shear connection were moderate, between 3-8mm. But separations were very small, close to zero. This indicated the strong tie resistance of the concrete-infill-only shear connection. The specimens, T1-A-F & T1-B-N demonstrated that the separation started at load level of the sudden slip increase. The other two specimens, T1-A-N & T1-B-F, demonstrated no separation response until the ultimate loads were reached.

Specimen No.	Web Opening	Concrete Type	f_{cu}* (MPa)	f_{ct}˜ (MPa)	Ultimate Load (kN)	Slip (mm) at Ultimate Load
T1-A-N	Ø150mm	Normal	56.5	4.53	354	2.85
T1-A-F		Fibre-reinforced	58.1	4.85	393	4.09
T1-B-N	Ø200mm	Normal	56.5	4.53	1086	4.92
T1-B-F		Fibre-reinforced	58.1	4.85	1191	7.70
* cube compressive strength of concrete			˜ tensile splitting strength of concrete			

Table 3.4 Result summary of the test group T1

Figure 3.16 Load-slip and load-separation curves of specimen T1-A-N
(Ø150mm web opening, normal concrete)

Figure 3.17 Load-slip and load-separation curves of specimen T1-A-F
(Ø150mm web opening, fibre-reinforced concrete)

Figure 3.18 Load-slip and load-separation curves of specimen T1-B-N
(Ø200mm web opening, normal concrete)

Figure 3.19 Load-slip and load-separation curves of specimen T1-B-F
(Ø200mm web opening, fibre-reinforced concrete)

3.4.4.1 Behaviour analysis

A uniform behaviour of the concrete-infill-only shear connection was shown by the four specimens. The shear connection deformed elastically until the rupture failure at the maximum load without any plastic deformations. The specimens, T1-A-F & T1-B-N, clearly demonstrated the effects of the bond (between the concrete and steel) to the slip behaviour of the shear connection, as local bond failure occurred with sudden slip increase. However, the effects of the bond did not initiate the entire failure of the specimens, as the elastic deformations resumed after the sudden slip increase.

The concrete-infill-only shear connection ultimately failed at the maximum load levels without any plastic deformations. This brittle failure mode was due to the inherent brittle material properties of concrete, as the concrete-infill-only shear connection consisted of solely the concrete infill element.

3.4.4.2 Failure mechanism study

The failed specimens were examined to study the failure profiles of the concrete-infill-only shear connection, as shown in Figure 3.20. These failure profiles showed that the top part of the concrete infill element was crushed by the web opening in the direction of the longitudinal shear force, and that the rest of the concrete infill element was ruptured due to the tensile splitting force in the transverse direction. The fibre reinforcements were pulled in the transverse direction, as depicted in Figure 3.20 (b), further illustrated the tensile failure mechanism. Hence, the failure mechanism of the concrete-infill-only shear connection was the combination of crushing and tensile rupture.

(a)

(b)
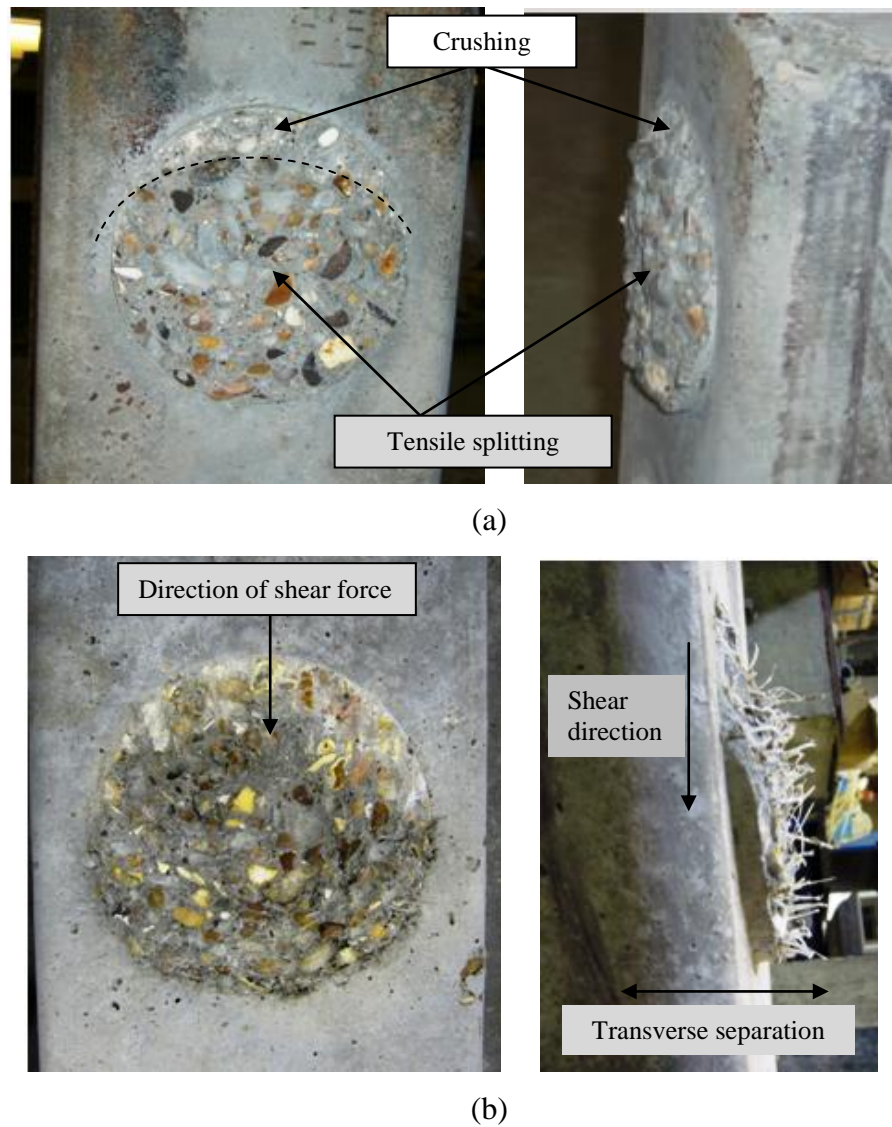
Figure 3.20 Failure profiles of the concrete-infill-only shear connection with (a) normal concrete, (b) fibre reinforcement

3.4.5 Results of test group T2, tie-bar shear connection

The tie-bar shear connection of the test group T2 consisted of two Ø12mm tie-bars passing through each web openings. The top tie-bar within each opening would be in directly contact with the longitudinal shear force, as the tie-bars were positioned close to the perimeter of the web opening. Hence, the failure profile of the top tie-bar was expected to be shear failure. The results of the ultimate loads and slips are listed in Table 3.5. The load-slip and load-separation curves of the each specimen are shown in Figures 3.21-3.24. The load values of these curves were load per shear connection.

Specimen No.	Web Opening	Concrete type	f_{cu}* (MPa)	f_{ct}˜ (MPa)	Ultimate Load (kN)	Slip (mm) at Ultimate Load
T2-A-N	Ø150mm	Normal	54.5	4.54	927	10.68
T2-A-F		Fibre-reinforced	51.9	4.07	915	11.62
T2-B-N	Ø200mm	Normal	54.5	4.54	1170	12.85
T2-B-F		Fibre-reinforced	51.9	4.07	1116	8.41

* cube compressive strength of concrete   ˜ tensile splitting strength of concrete

Table 3.5 Result summary of the test group T2

The slips of the tie-bar shear connection at the ultimate load were significant, between 8-13mm. This demonstrated the desired ductility for the shear connection. The slip stiffness of the tie-bar shear connection among the four specimens was constant. It was shown that the slip stiffness was not influenced by the diameter of web opening or the strengths of concrete. The separations at the ultimate loads were small, less than 2mm. This indicated the strong tie resistance of the tie-bar shear connection.

The relationship between the shear resisting capacity of the shear connection and web opening diameter was shown from the results. The failure loads of the specimens with Ø200mm web openings, T2-B-N & T2-B-F, were higher than that of the specimens with Ø150mm web openings, T2-A-N & T2-A-F, respectively. This comparison was base on the same concrete strengths. The test results also showed the effect of concrete strength on the shear resisting capacity of the shear connection. The failure loads of the specimens with higher concrete strength, T2-A-N & T2-B-N, was higher than that of the specimens with lower concrete strength, T2-A-F & T2-B-F, respectively. This comparison was made between the specimens with the same diameters of web opening.
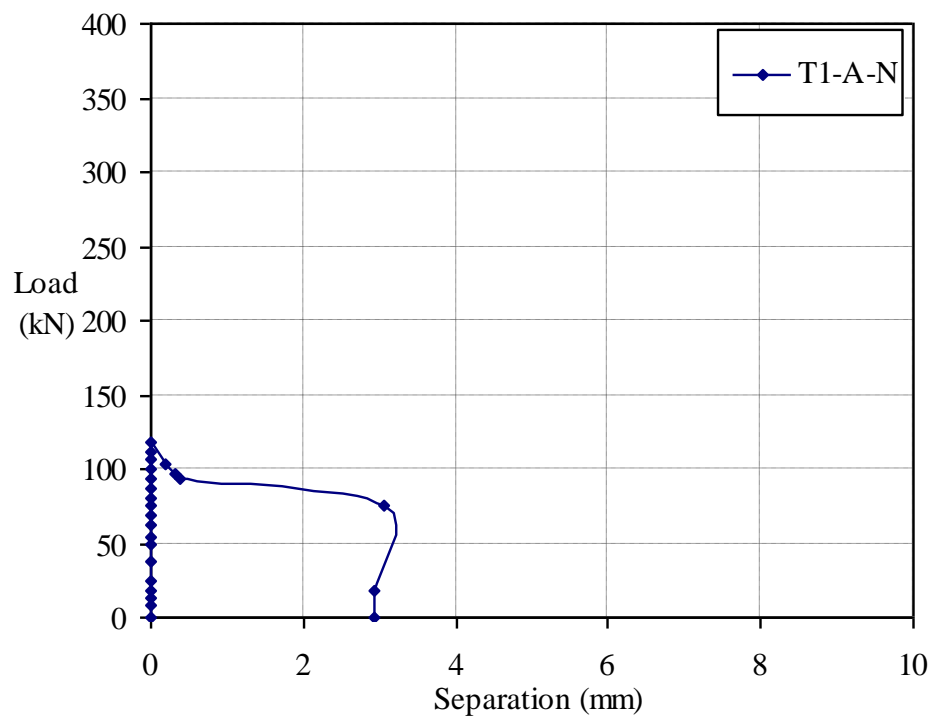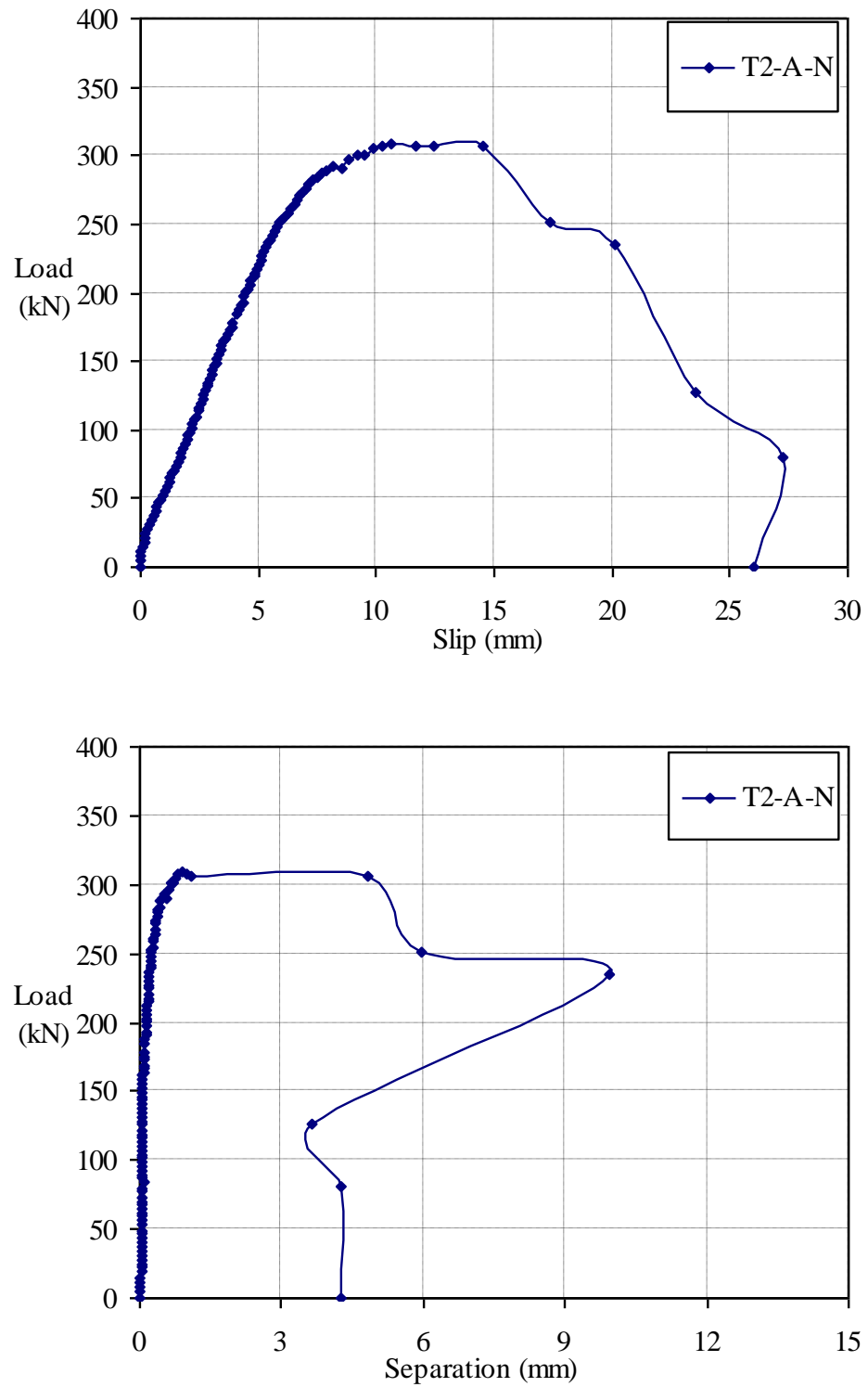
Figure 3.21 Load-slip and load-separation curves of specimen T2-A-N
(Ø150mm web opening, normal concrete)
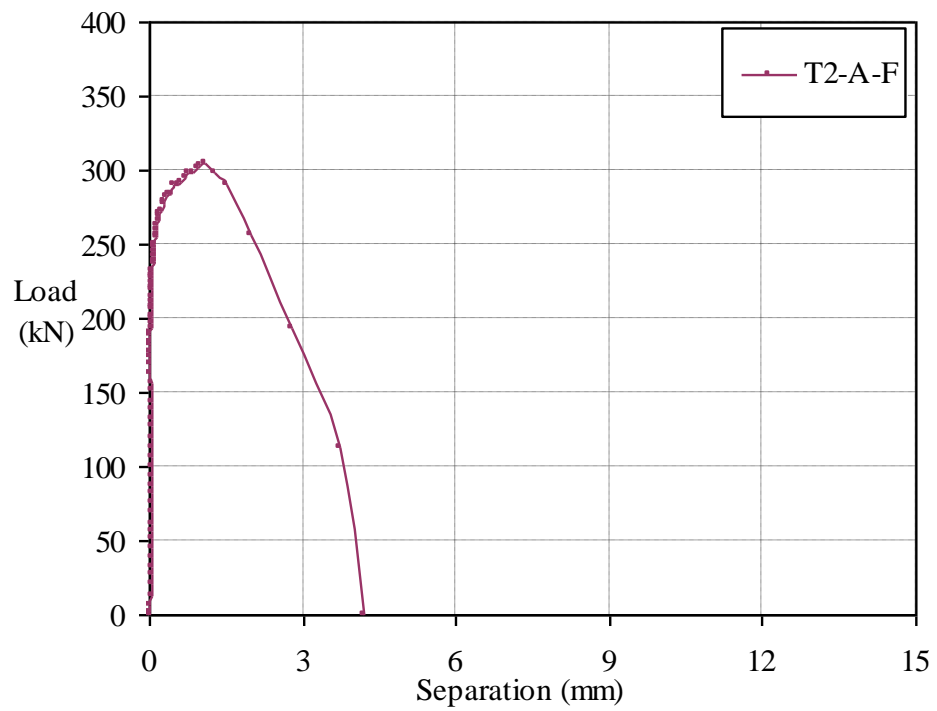
Figure 3.22 Load-slip and load-separation curves of specimen T2-A-F
(Ø150mm web opening, fibre-reinforced concrete)
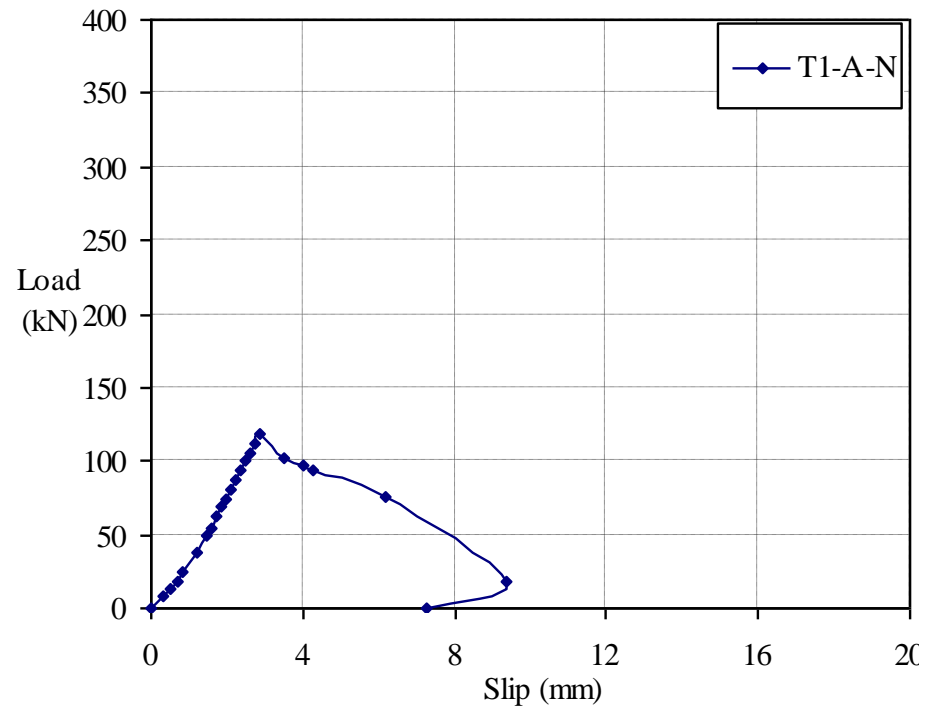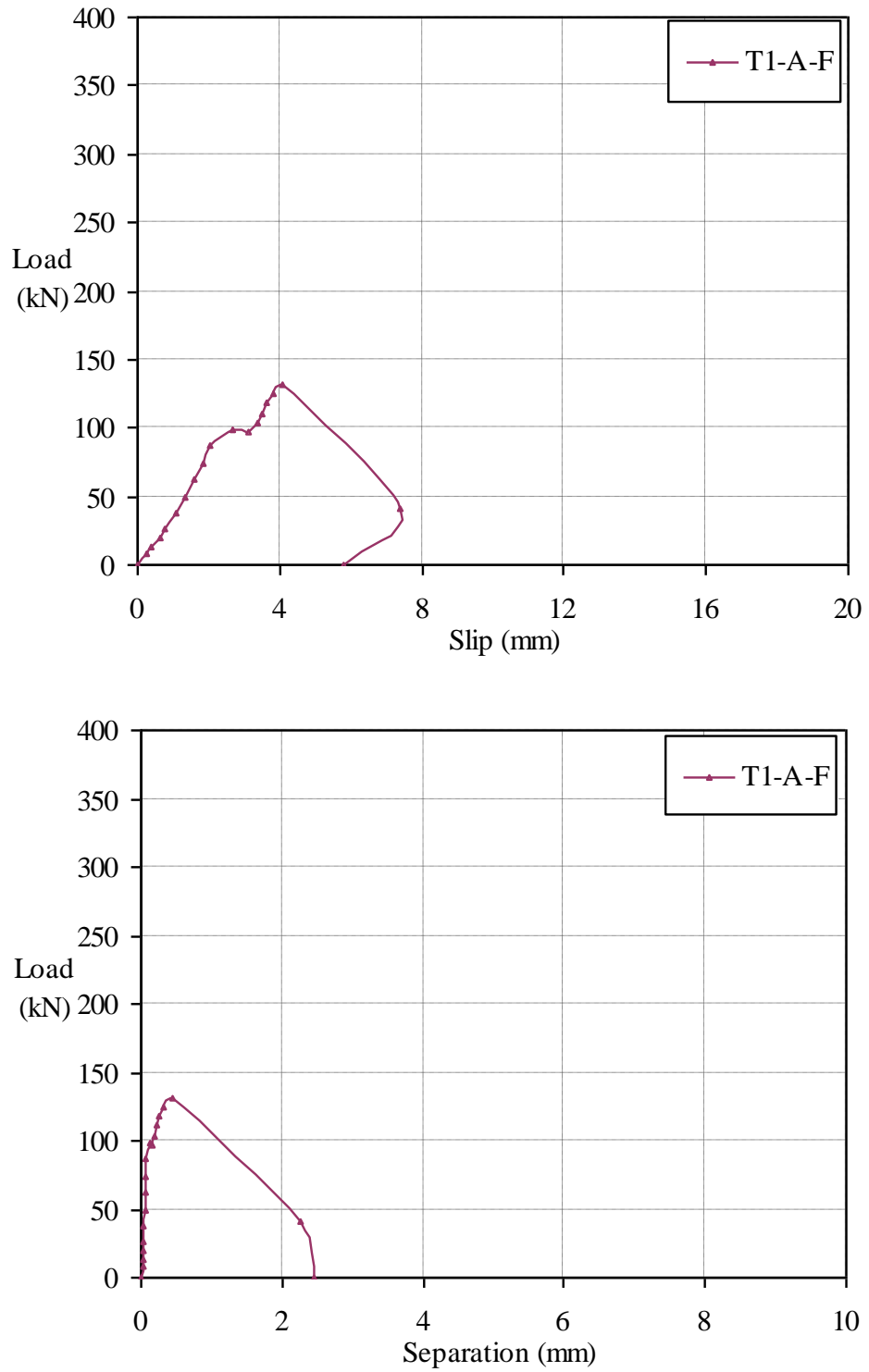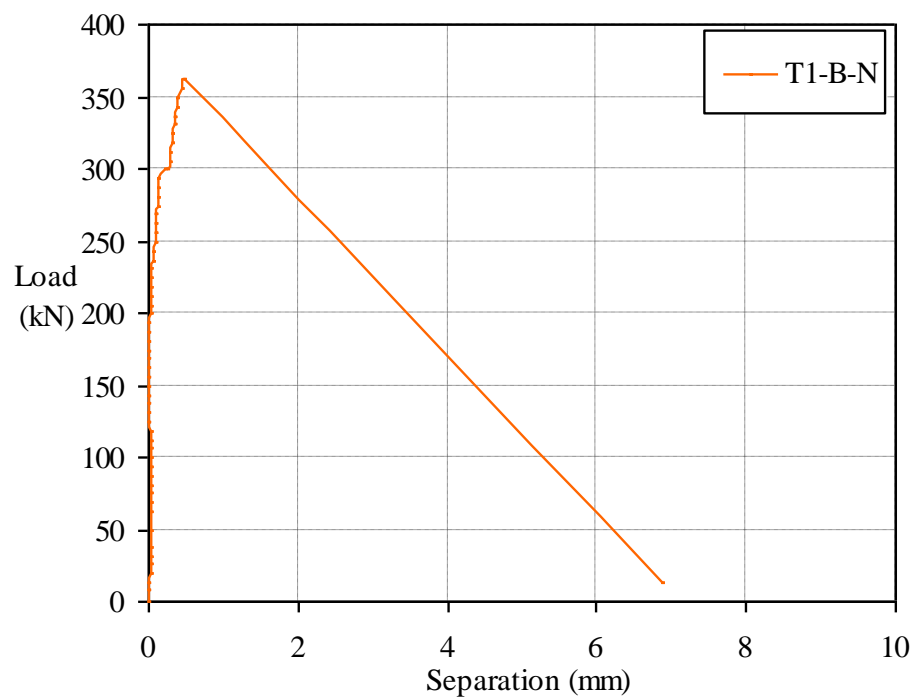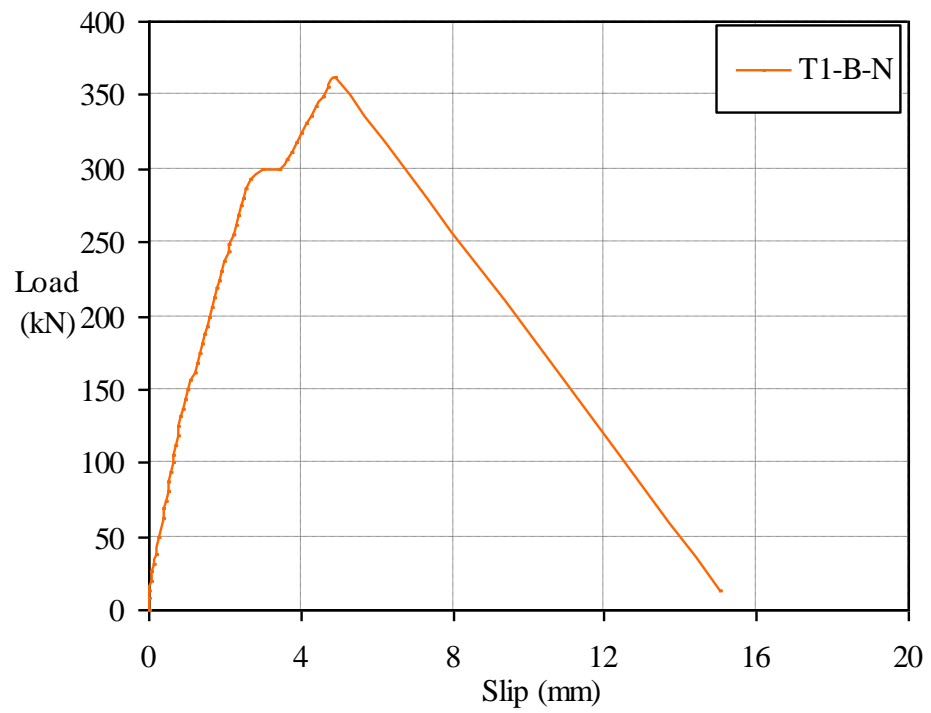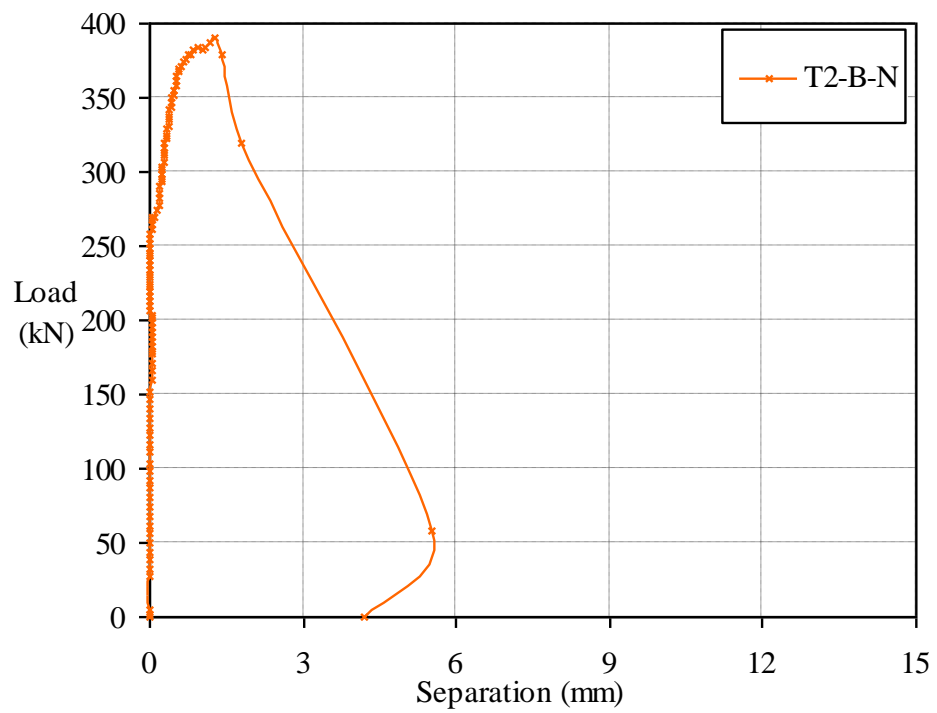
Figure 3.23 Load-slip and load-separation curves of specimen T2-B-N
(Ø200mm web opening, normal concrete)
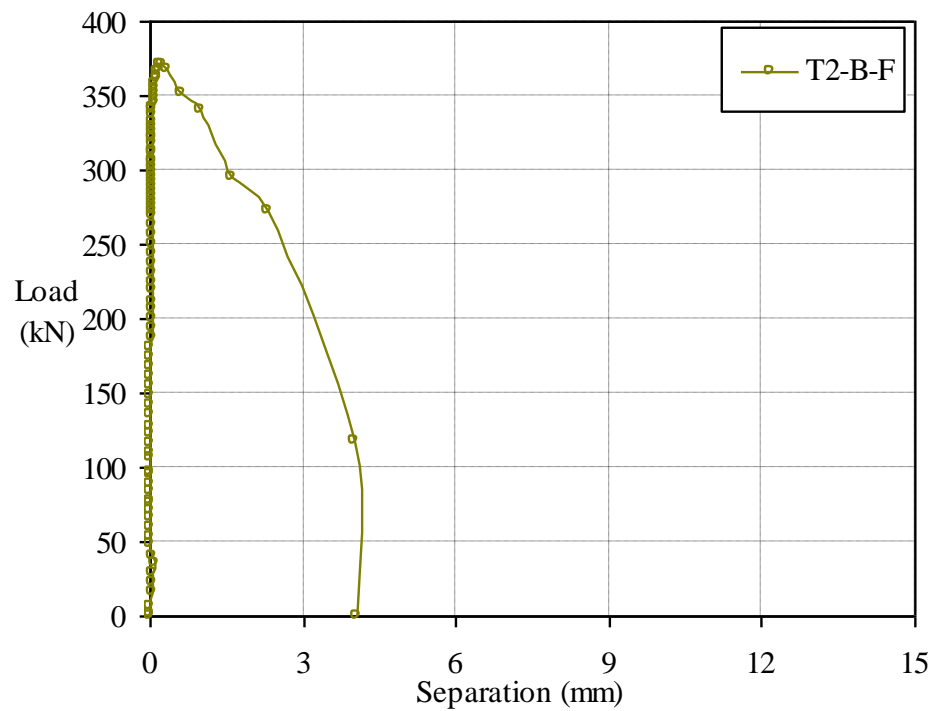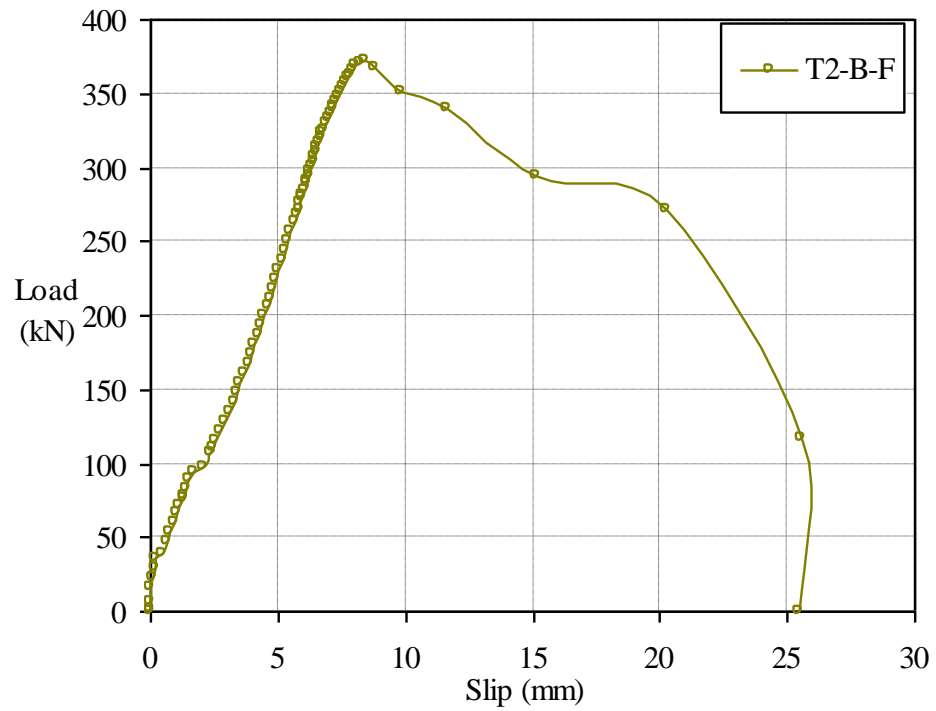
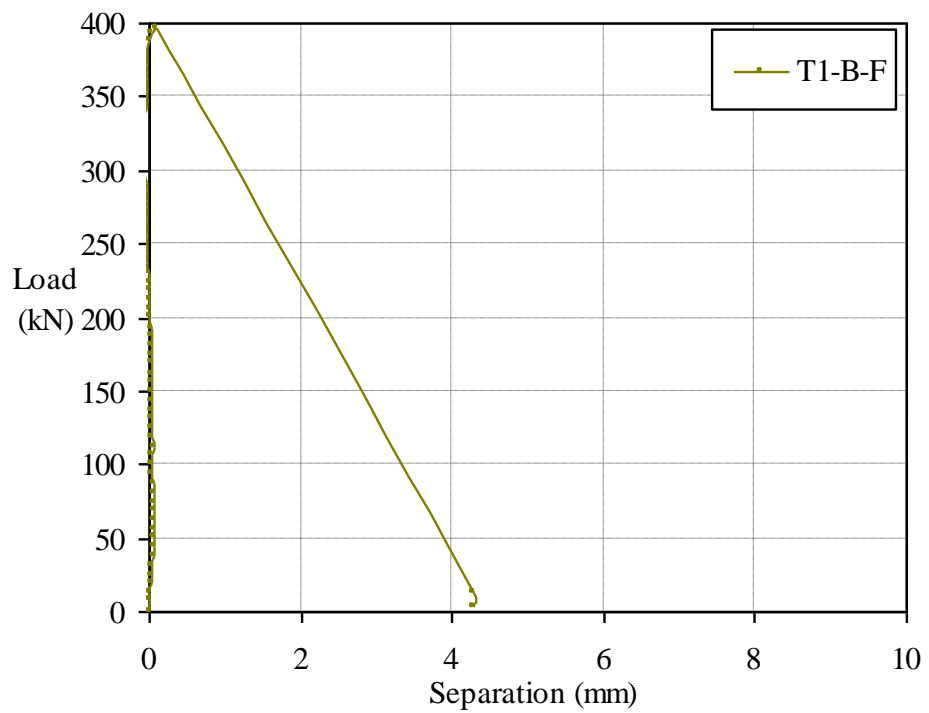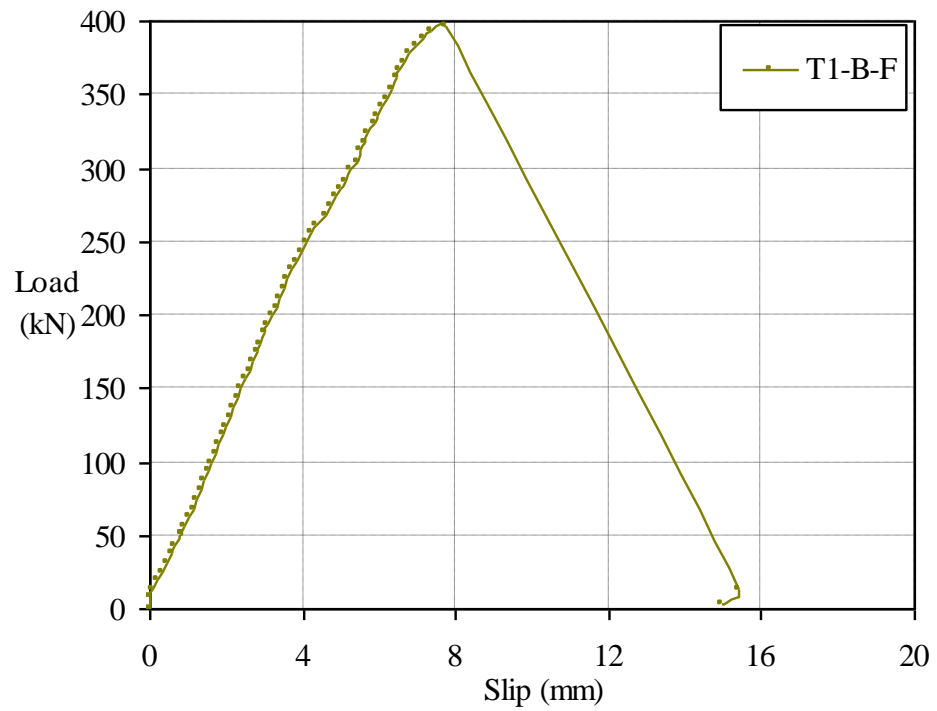Figure 3.24 Load-slip and load-separation curves of specimen T2-B-F
(Ø200mm web opening, fibre-reinforced concrete)

3.4.5.1 Behaviour analysis

The ductile behaviour was shown by the tie-bar shear connection, which initially deformed elastically before underwent plastic deformations with significant slips. Load dropped gradually and extensive slips were also occurred after the ultimate load was reached. There were minor sudden slip increases in the region of elastic deformations. This was due to the local failure of the tie-bars, as the top tie-bar within each opening was in direct contact with the slip of the steel section. However, the local failure of the tie-bars did not cause the entire failure of the specimen, as the elastic deformation resumed thereafter.

It was clearly demonstrated by all specimens of the test group that the separations (or splitting) occurred at the load levels when the slip behaviour became nonlinear. This mechanism indicated that the failure resistance (or shear strength) of the shear connection were contributed by both compressive (bearing) and tensile splitting resistances.

The cracking noise was initially heard at the end of elastic deformations. And then it was intensified during the plastic deformations. A bang went off at the end of the test, as the top of the tie-bars was sheared off.

(a)

(b)
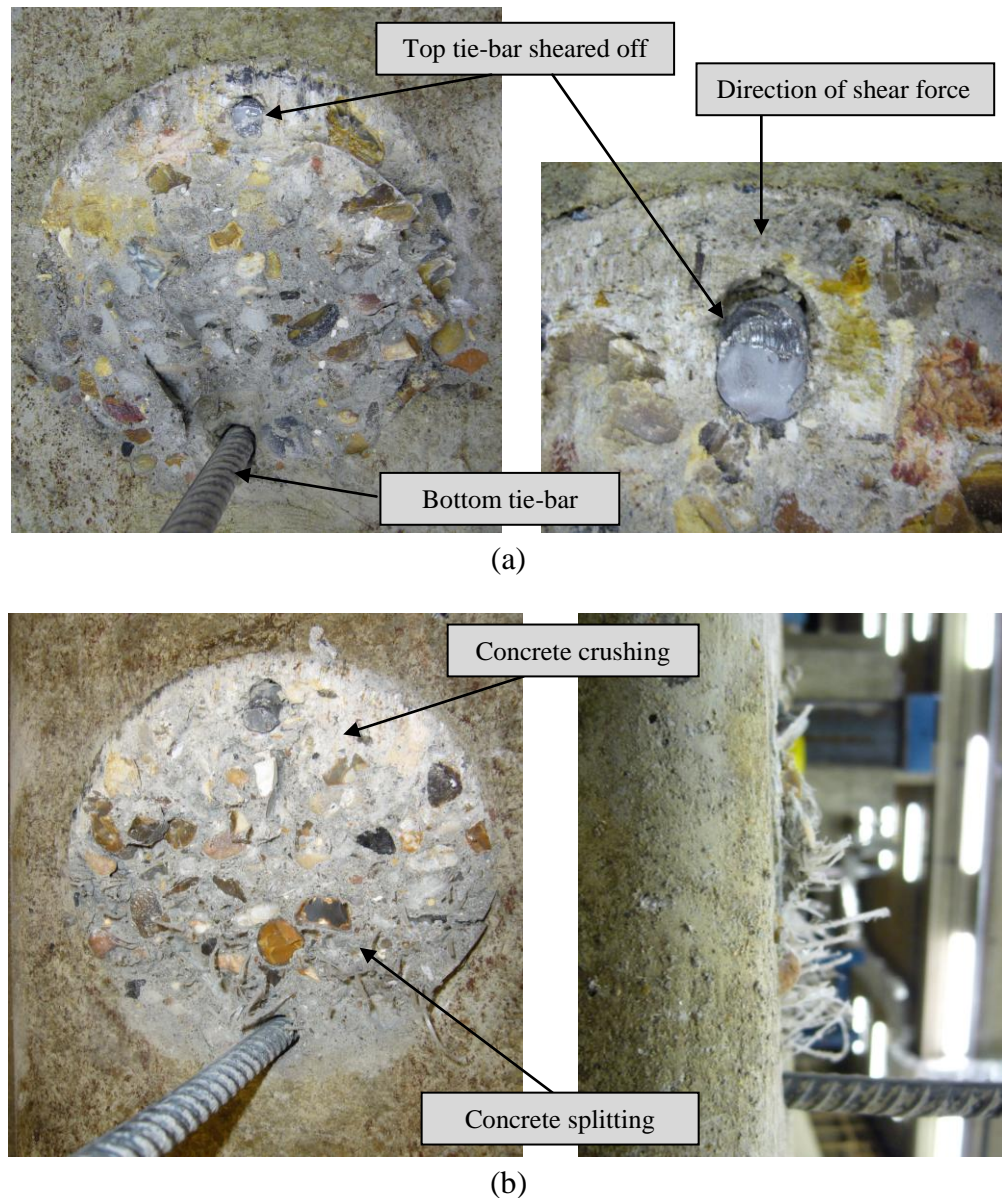
Figure 3.25 Failure profiles of the tie-bar shear connection with
(a) normal concrete, (b) fibre reinforcement

3.4.5.2 Failure mechanism study

The top tie-bar within each web opening sheared off, as shown in Figure 3.25, because the tie-bars were positioned close to the perimeter of the web openings. The top tie-bars were in direct contact with the slip of the steel section. The bottom tie-bar within the each opening remained intact from the shear failure. The bottom tie-bar was in the mechanism of providing the tensile force (or tie force) to the concrete slabs.

The failure profiles of the concrete infill element of the tie-bar shear connection were the same as that of the concrete-infill-only shear connection. The top part of the concrete infill element was crushed by the web opening in the direction of the

longitudinal shear force. The rest of the concrete infill element was ruptured by the tensile splitting force in the transverse direction.

3.4.6 Results of test group T3, ducting shear connection

The ducting shear connection of the test group T3 were formed as the concrete infill element combined with the ducting resisting the longitudinal shear force. The Ø125mm ducting was used to pass through the Ø150mm web openings of the test specimens. Similarly, the Ø150mm ducting was used to pass through the Ø200mm web openings. The results of the ultimate loads and slips are listed in Table 3.6. The load-slip and load-separation curves of each specimen are shown in Figures 3.26-3.30.

Specimen No.	Web Opening	Concrete Type	f_{cu}* (MPa)	f_{ct}~ (MPa)	Ultimate Load (kN)	Slip (mm) at Ultimate Load
T3-A-N	Ø150mm	Normal	55.2	3.91	141	2.07
T3-A-F		Fibre-reinforced	51.5	3.89	150	1.45
T3-B-N	Ø200mm	Normal	55.2	3.91	375	3.37
T3-B-F		Fibre-reinforced	51.5	3.89	411	3.21
* cube compressive strength of concrete			~ tensile splitting strength of concrete			

Table 3.6 Result summary of the test group T3

The specimens with the Ø150mm web openings and Ø125mm ducting, T3-A-N & T3-A-F, had less amount of concrete infill (between the ducting and web opening) than the other two specimens, T3-B-N & T3-B-F. The test results demonstrated the relationship between the shear resisting capacity of the shear connection and the amount of concrete infill. The failure loads of the specimens with the bigger concrete infill, T3-B-N & T3-B-F, were higher than that of the specimens with the smaller concrete infill, T3-A-N & T3-A-F. The slips at the ultimate loads were very small, less than 3.5mm. The separations were less than 0.5mm. The uniform slip stiffness of the ducting shear connectors was shown among the four specimens, as illustrated in Figure 3.26.

However, it was shown that the shear resisting capacities of the ducting shear connectors did not increase with the increase of concrete strengths. This might be due to the difference in concrete strengths was small between the specimens, and also the amount of the concrete infill was much less than other types of shear connection. Hence the effect of concrete strength was not clear.
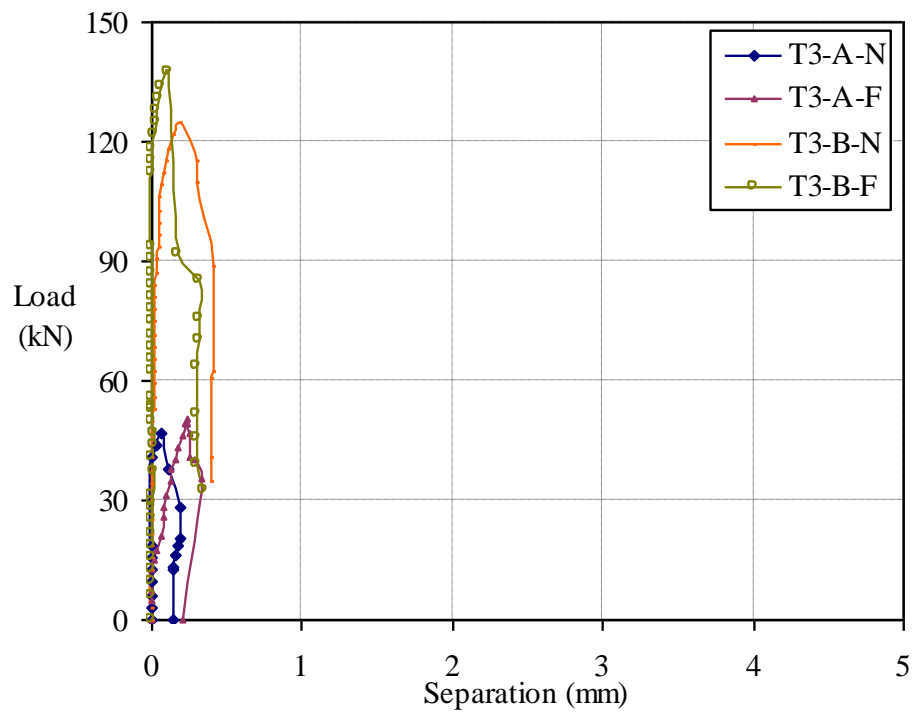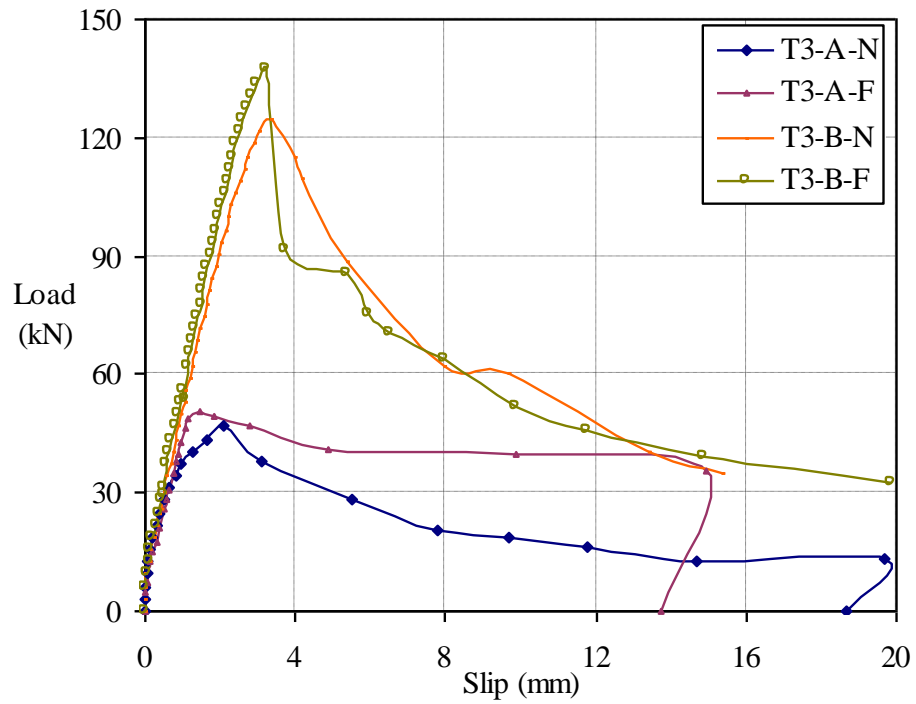
Figure 3.26 Load-slip and load-separation curves of the ducting shear connection
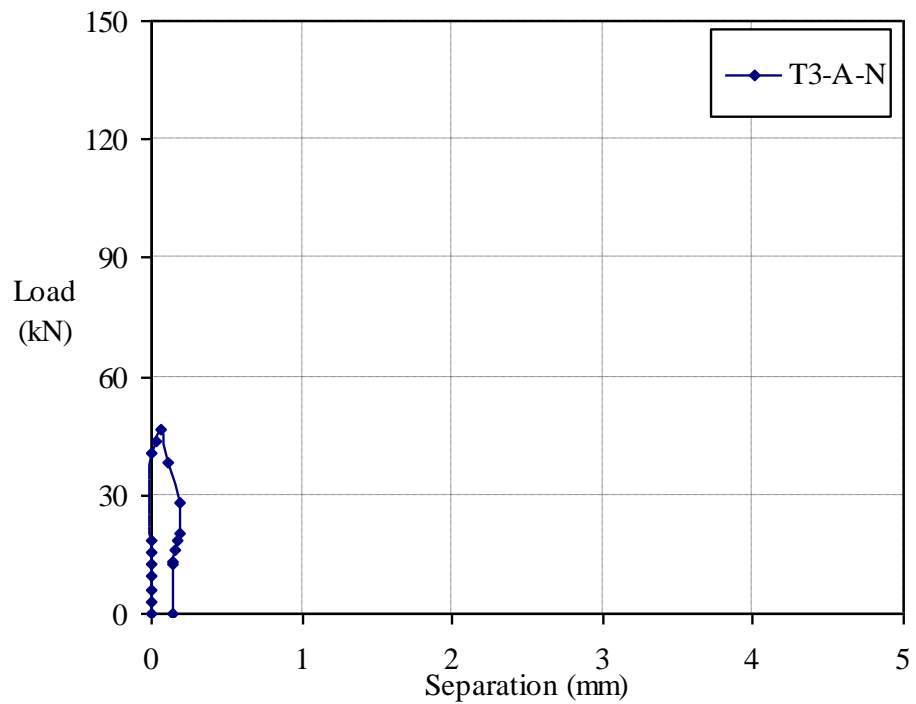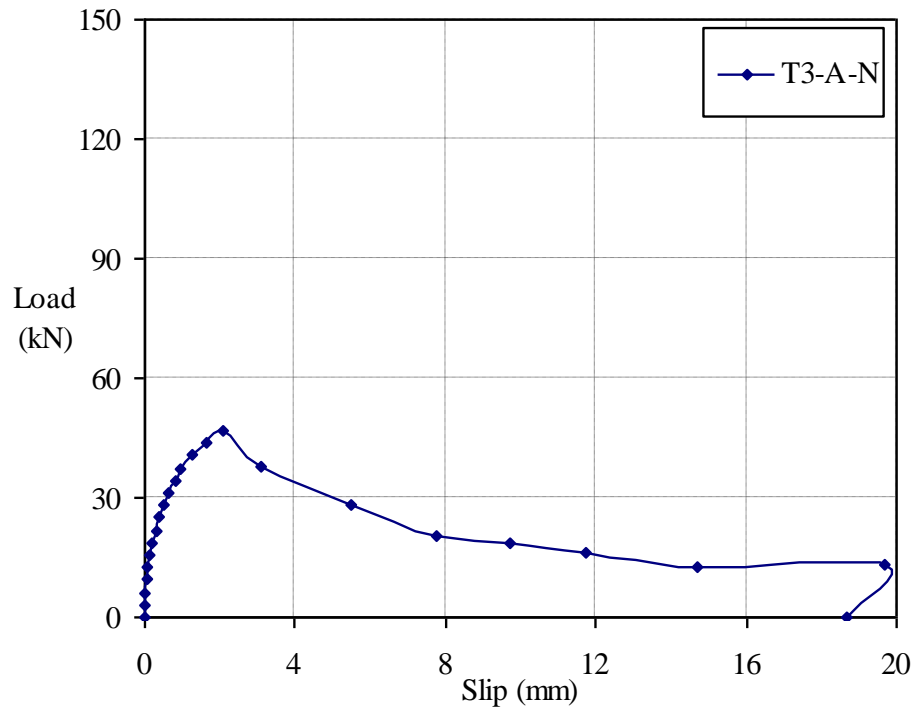
Figure 3.27 Load-slip and load-separation curves of specimen T3-A-N
(Ø150mm web opening, Ø125mm ducting, normal concrete)
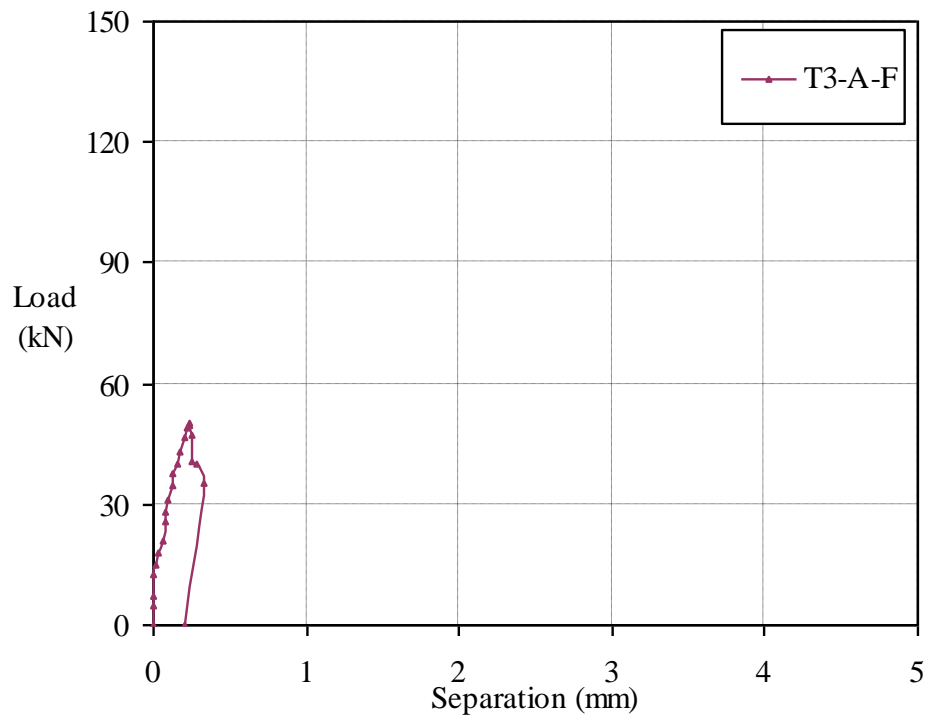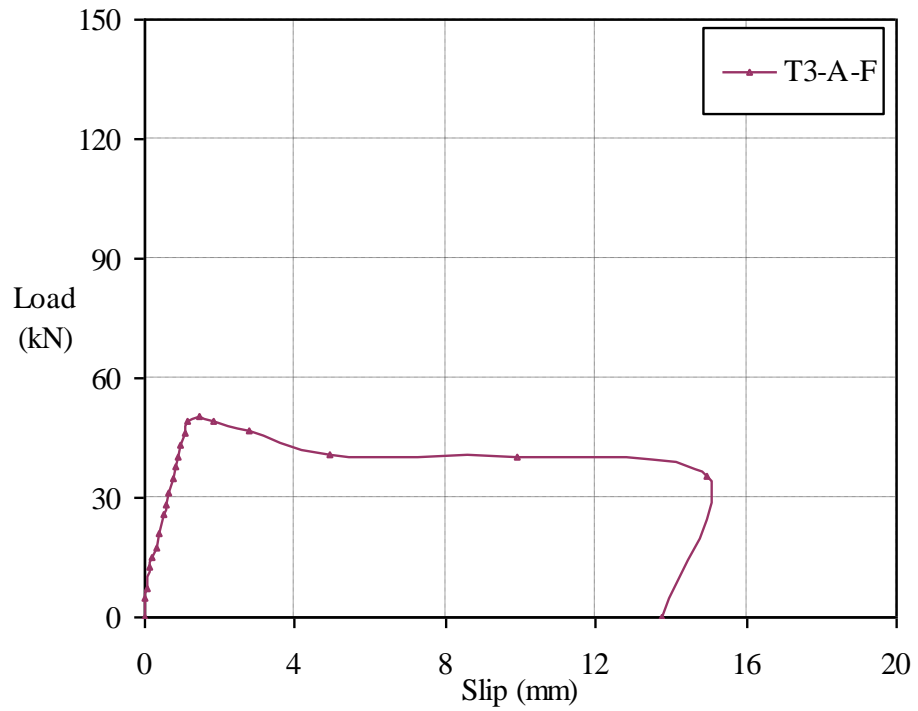
Figure 3.28 Load-slip and load-separation curves of specimen T3-A-F
(Ø150mm web opening, Ø125mm ducting, fibre-reinforced concrete)
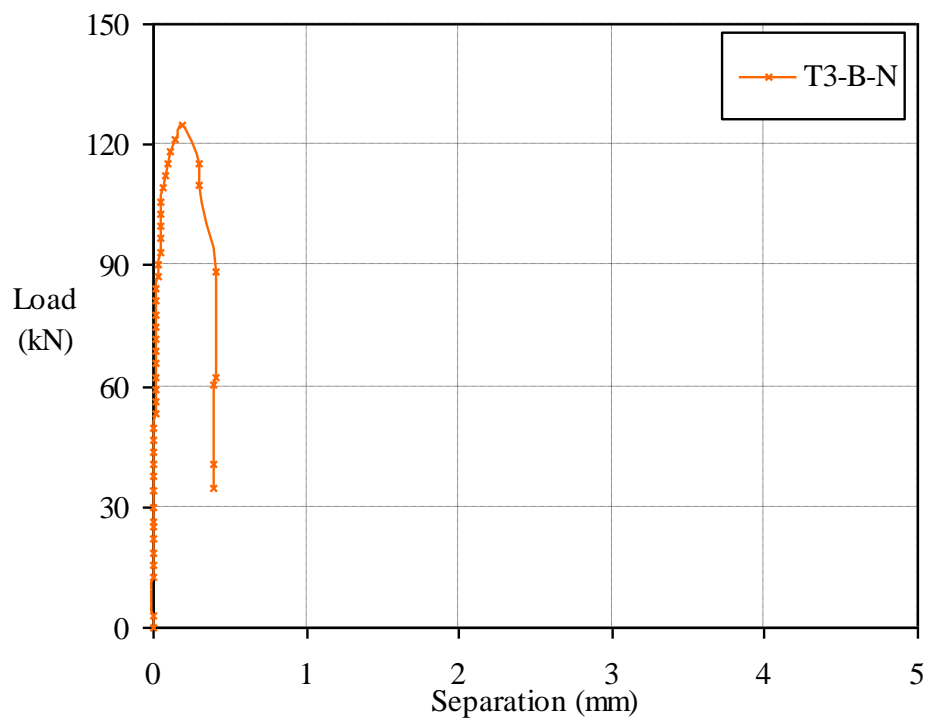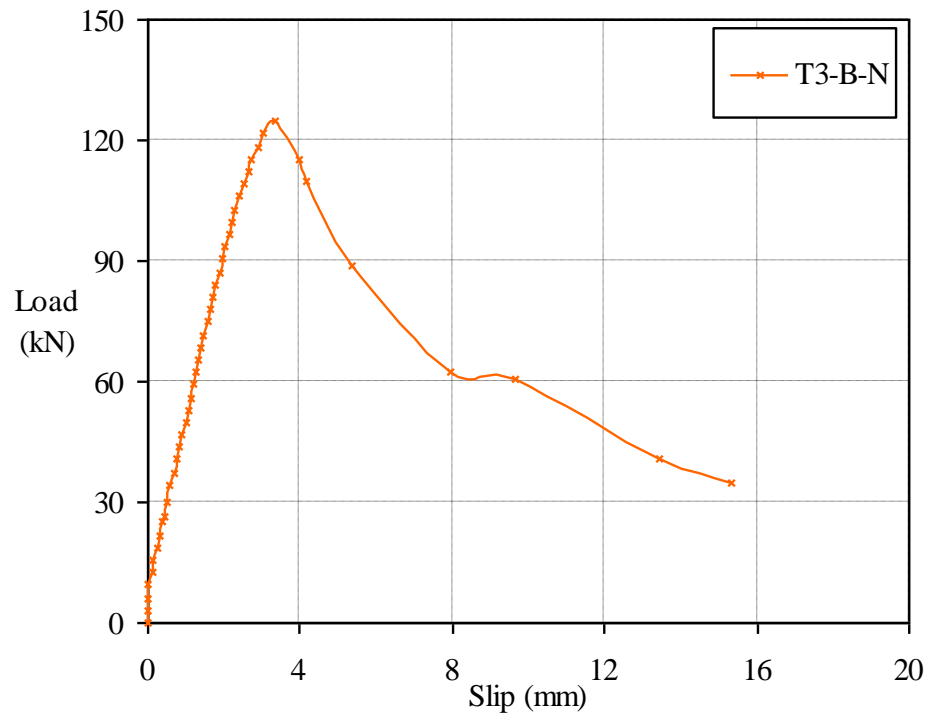
Figure 3.29 Load-slip and load-separation curves of specimen T3-B-N
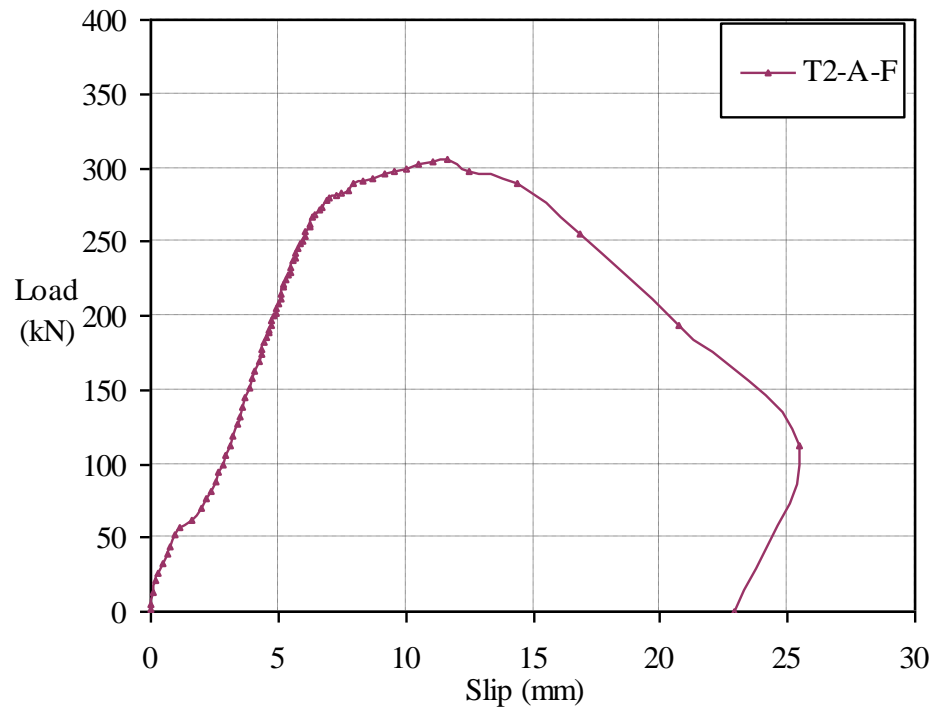(Ø200mm web opening, Ø150mm ducting, normal concrete)
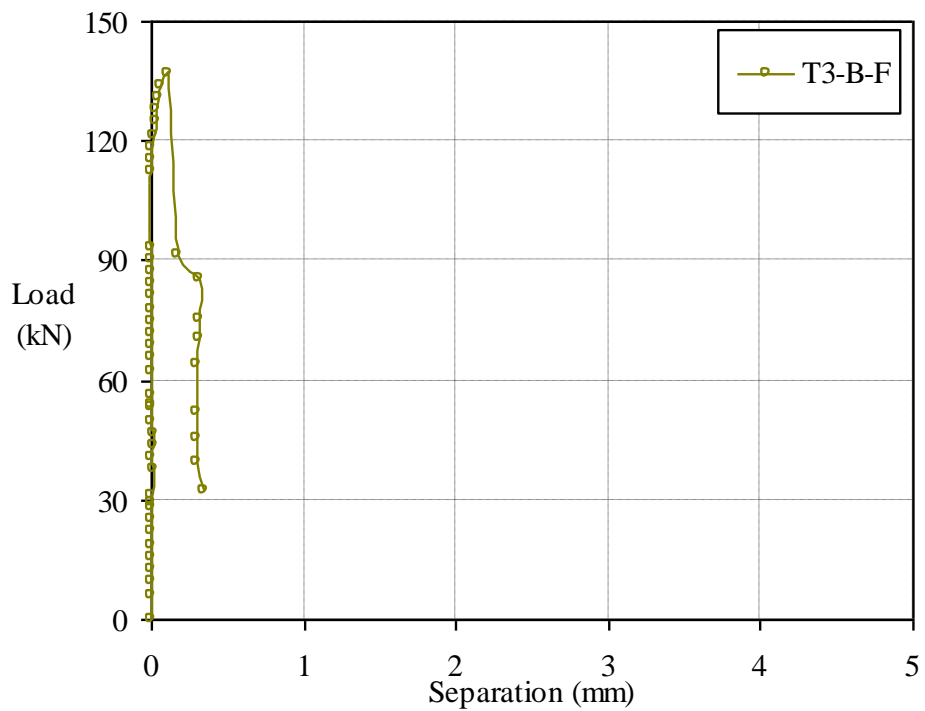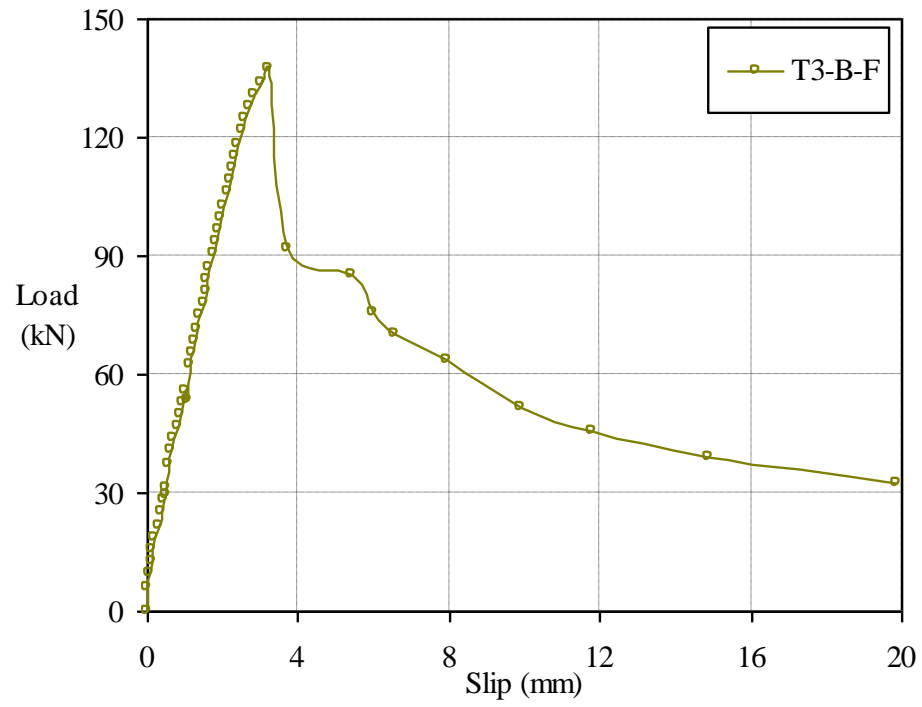
Figure 3.30 Load-slip and load-separation curves of specimen T3-B-F
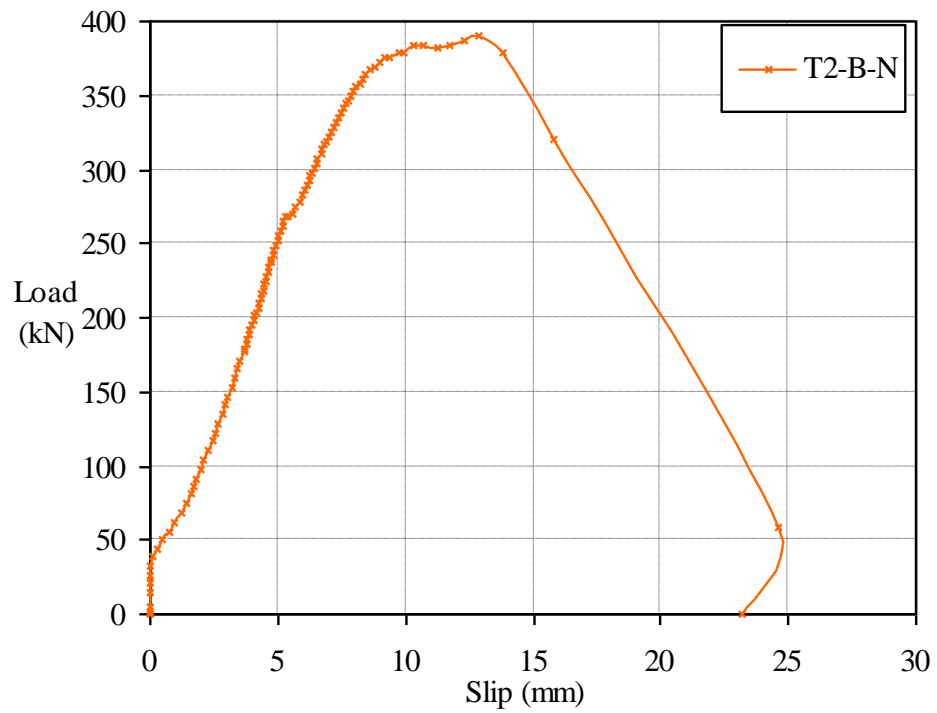(Ø200mm web opening, Ø150mm ducting, fibre-reinforced concrete)

3.4.6.1 Behaviour analysis

A uniform behaviour of the ducting shear connection was shown by the specimens. The ducting shear connection deformed elastically up to the ultimate loads. But the complete rupture failure mode was not shown by the ducting shear connection. Extensive slips were induced after the ultimate loads were reached. The presence of the ducting reduced attendance of brittle rupture failure mode, although the duct would not provide much of the shear resistance.

3.4.6.2 Failure mechanism study

The concrete infill element within the voids was initially crushed by the web opening. This led to the deformation of ducting in the direction of the longitudinal shear force, as shown in Figure 3.31 (b). Because of the thickness and geometry of the ducting, the spiral locking was eventually ruptured when the steel section further advanced in the longitudinal direction, as shown in Figure 3.31 (c).

Although, the separation values were very small, less than 0.5mm, but it indicated the tensile failure of the concrete infill element. Thus, the failure mechanism of the ducting shear connection was due to the crushing failure of the concrete infill element in the direction of the longitudinal shear force and tensile failure of the concrete infill element in the transverse direction.
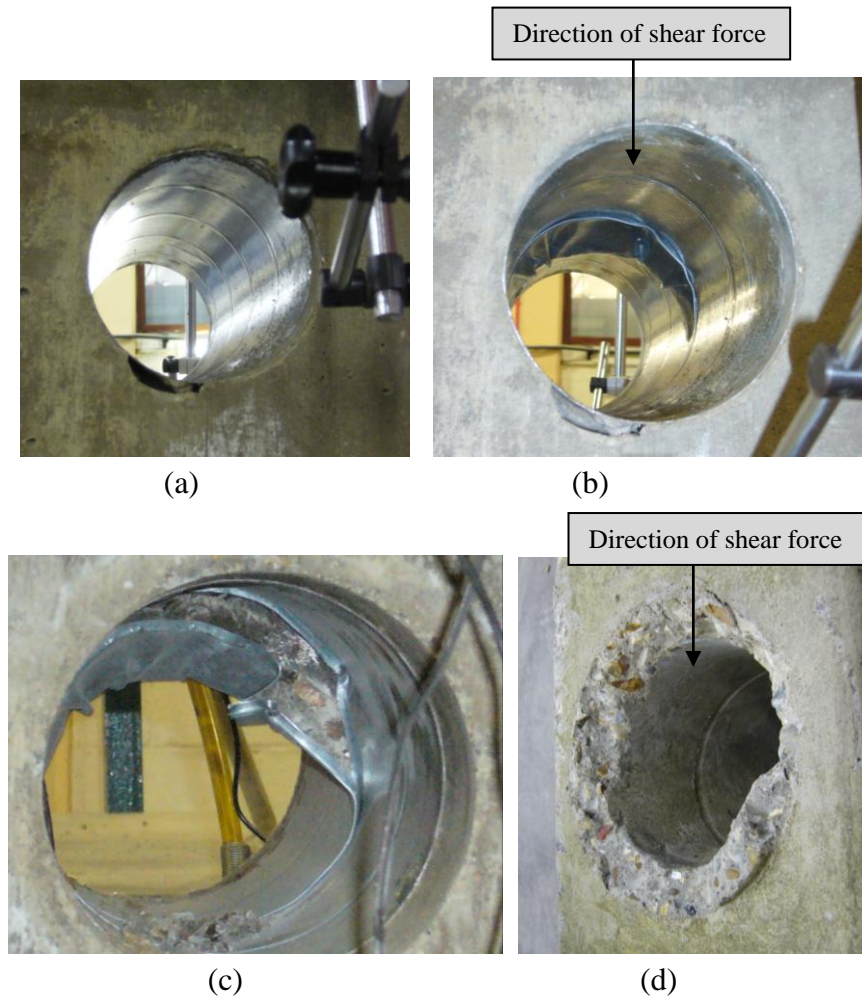
Figure 3.31 Failure profiles of the ducting shear connection (a) prior to testing, (b) deformation profile, (c) rupture profile, (d) failure profile of concrete infill element

3.4.7 Results of test group T4, web-welded stud shear connection

There were eight headed studs welded on both sides of the web post, as shown in Figure 3.6. Hence, each concrete infill element combined with 2.67 studs to form a web-welded stud shear connection. The results of the ultimate load and slip are summarised in Table 3.7. The load-slip and load-separation curves of each specimen are shown in Figures 3.32-3.35. The load of these curves was the load per shear connection.

The specimen, T4-B-N, was not failed in the push-out test, as the capacity of the hydraulic jacks was reached. Its results in Table 3.7 are the maximum value reached, but not the ultimate values. Large slips were demonstrated by all specimens. The separations were very small, which indicated the strong tie resistance of the web-welded stud shear connection.

Specimen No.	Web Opening	Concrete Type	f_{cu}* (MPa)	f_{ct}~ (MPa)	Ultimate Load (kN)	Slip (mm) at Ultimate Load
T4-A-N	Ø150mm	Normal	67.0	4.66	1521	8.11
T4-A-F		Fibre-reinforced	50.2	4.08	1281	10.79
T4-B-N$^\Delta$	Ø200mm	Normal	67.0	4.66	(1791)	(8.63)
T4-B-F		Fibre-reinforced	50.2	4.08	1491	14.43

* cube compressive strength of concrete　　　~ tensile splitting strength of concrete
$^\Delta$ specimen, T4-B-N, was not failed, as the capacity of the jacks was reached

Table 3.7 Result summary of the test group T4

The test results showed the influence of the diameter of web opening and concrete strength on the shear resisting capacity of the shear connection. The failure loads of the specimens with bigger web openings (Ø200mm), T4-B-N & T4-B-F, were higher than that of the specimens with the smaller web openings (Ø150mm), T4-A-N & T4-A-F, respectively. This comparison was based on the same concrete strengths. The failure loads of the specimens with higher concrete strengths, T4-A-N & T4-B-N, were higher than that of the specimens with lower concrete strengths, T4-A-F & T4-B-F respectively. This comparison was based on the same diameter of web openings.

3.4.7.1 Behaviour analysis

Ductile behaviour of the web-welded stud shear connection was shown by the specimens. The shear connection deformed elastically then followed by plastic deformations. Large slips were induced during the plastic deformations before and after the ultimate loads were reached. The ultimate failure of the shear connection, as the studs sheared off, occurred after the load dropped to 85-93% of the maximum loads. The slip behaviour of the web-welded stud shear connection was very similar to that of the headed studs in the standard push-out tests, as illustrated in Figure 1.9. This similar behaviour indicated that the behaviour of the web-welded stud shear connection was much influenced by the headed studs. The specimens with fibre reinforcement, T4-A-F & T4-B-F, demonstrated additional ductility comparing with the specimen, T4-A-N.

Loud cracking noises were heard as the ultimate loads were reached. The cracking noise then became intensified. A large bang went off at the destructive failure, as the shear-studs were sheared off.
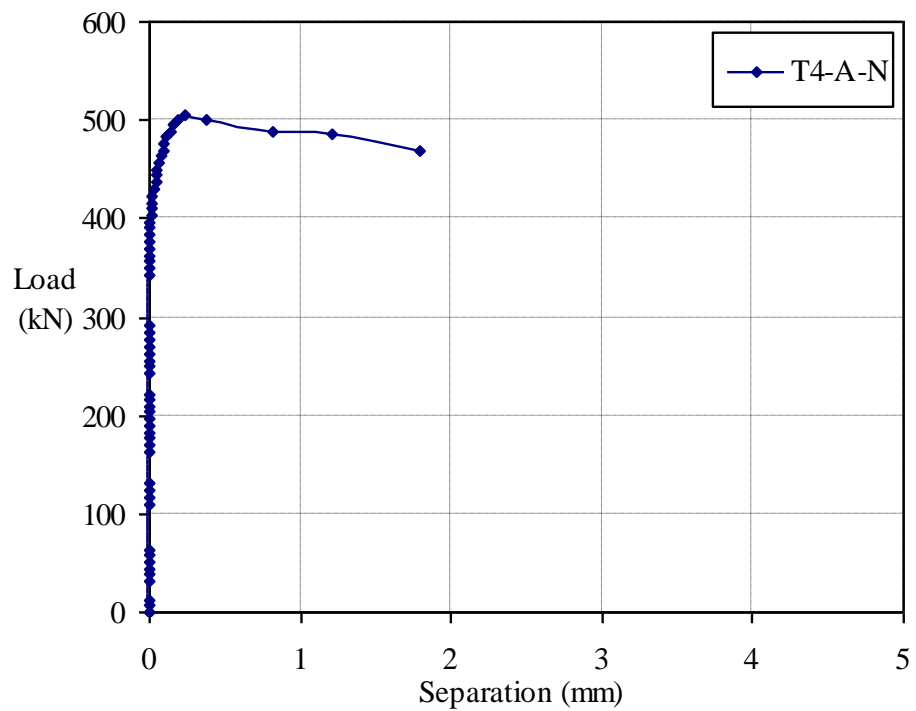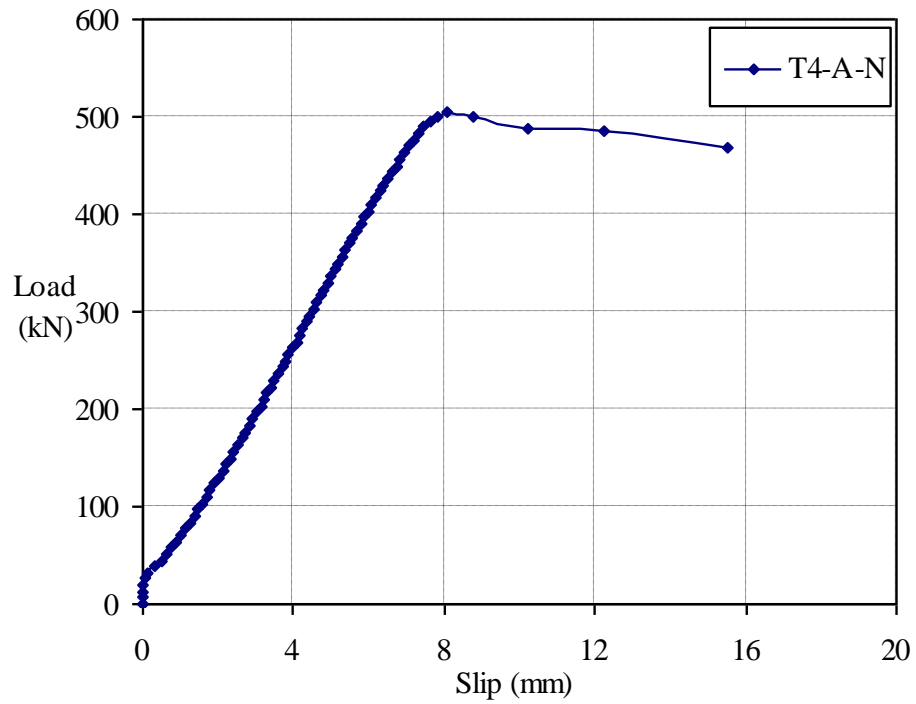
Figure 3.32 Load-slip and load-separation curves of specimen T4-A-N
(Ø150mm web opening, normal concrete)
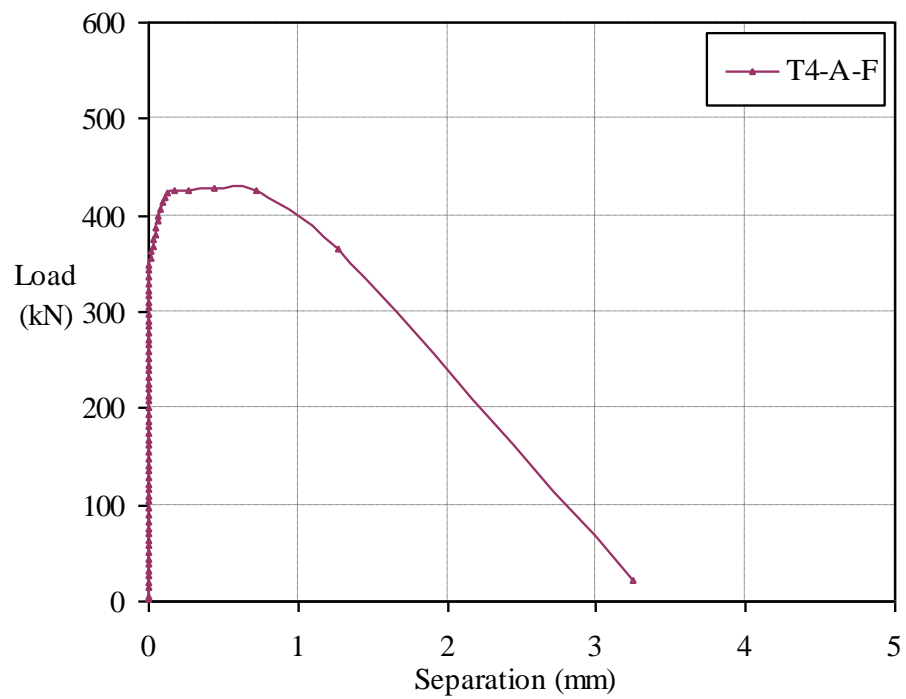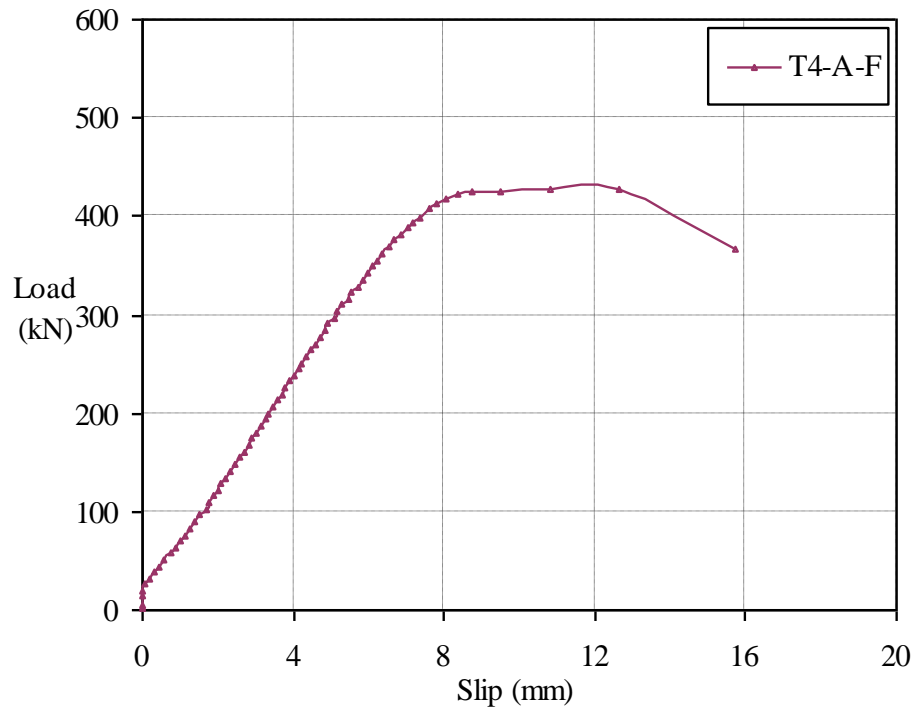
Figure 3.33 Load-slip and load-separation curves of specimen T4-A-F
(Ø150mm web opening, fibre-reinforced concrete)
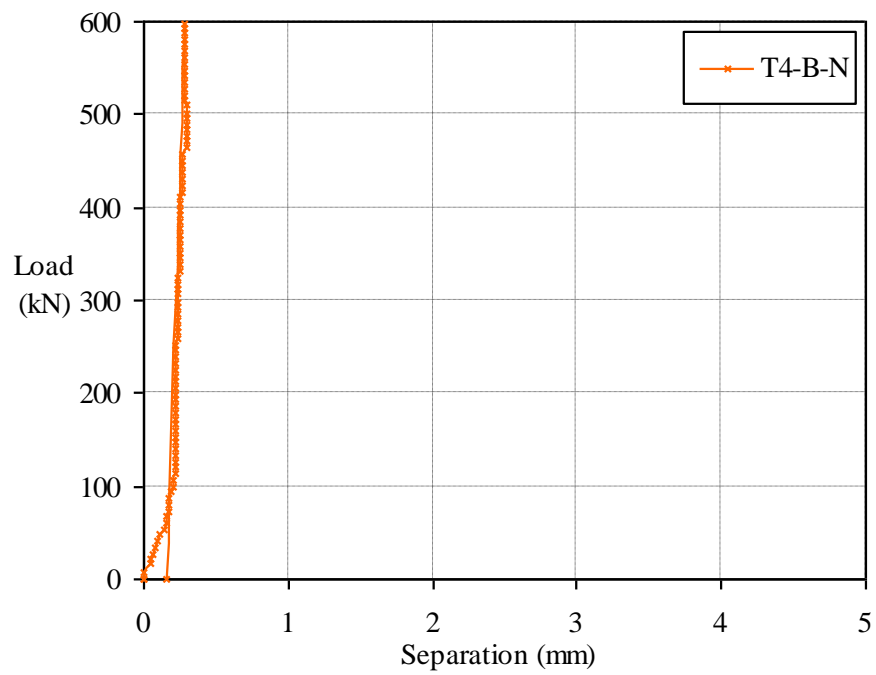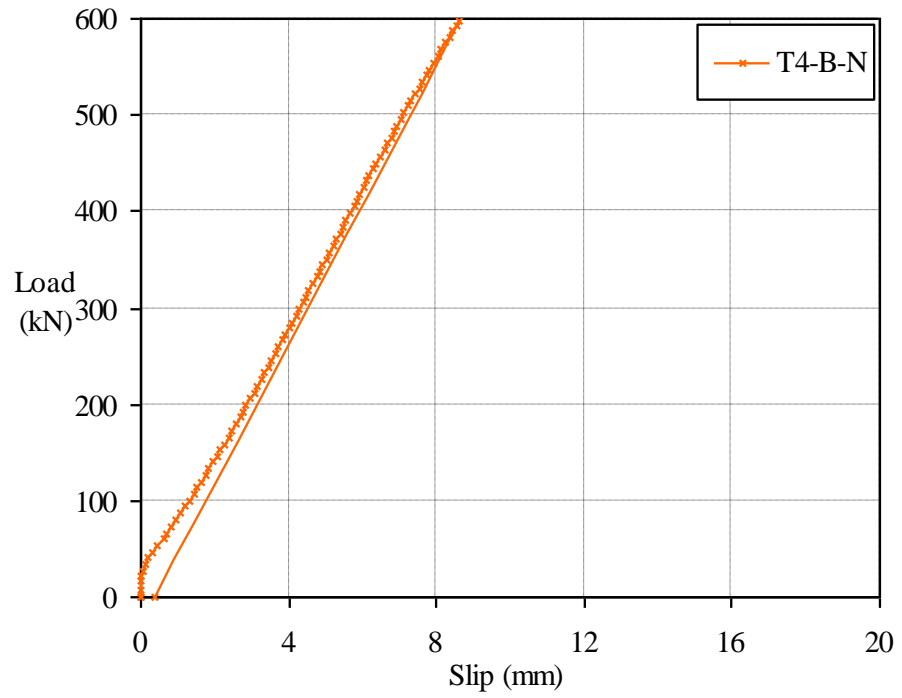
Figure 3.34 Load-slip and load-separation curves of specimen T4-B-N
(Ø200mm web opening, normal concrete)
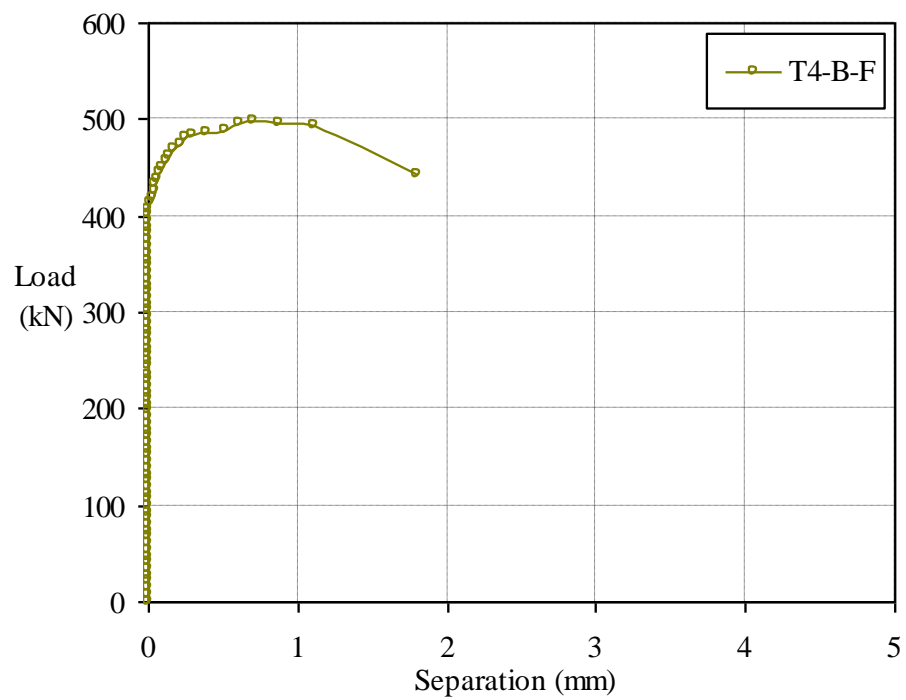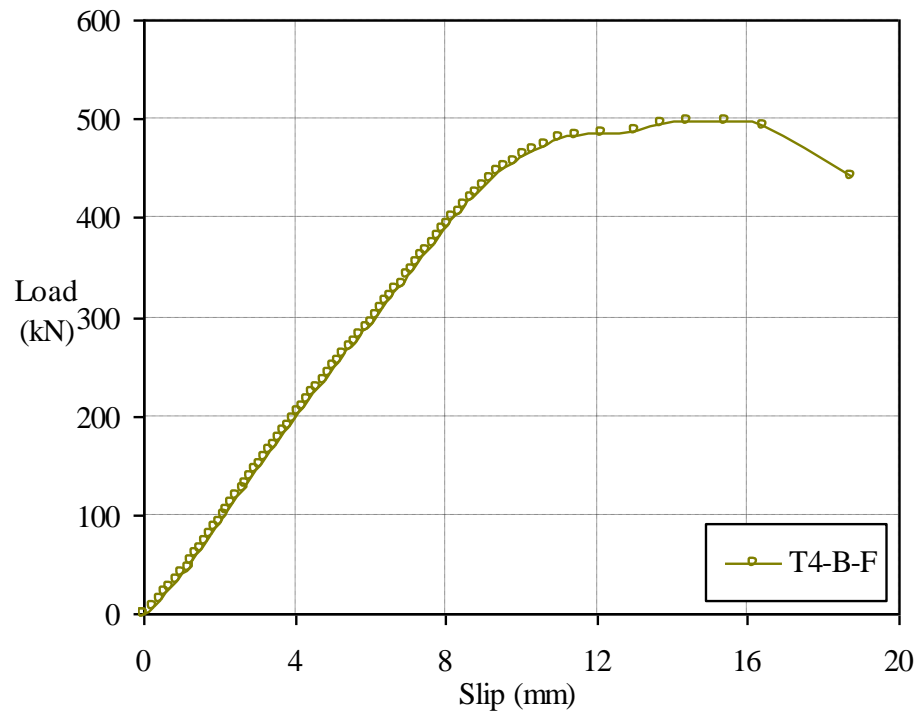
Figure 3.35 Load-slip and load-separation curves of specimen T4-B-F
(Ø200mm web opening, fibre-reinforced concrete)

3.4.7.2 Failure mechanism study

The headed studs were sheared off with bending near its root, as depicted in Figure 3.36. This failure profile was one of the main failure profile shown in the standard push-out tests, as reviewed in the Chapter 2. The concrete around the studs was crushed in the shear direction, as shown in Figure 3.36. The failure mechanism of the concrete infill element was crushing of the top part of the infill element and tensile rupture of the rest part of the infill element.
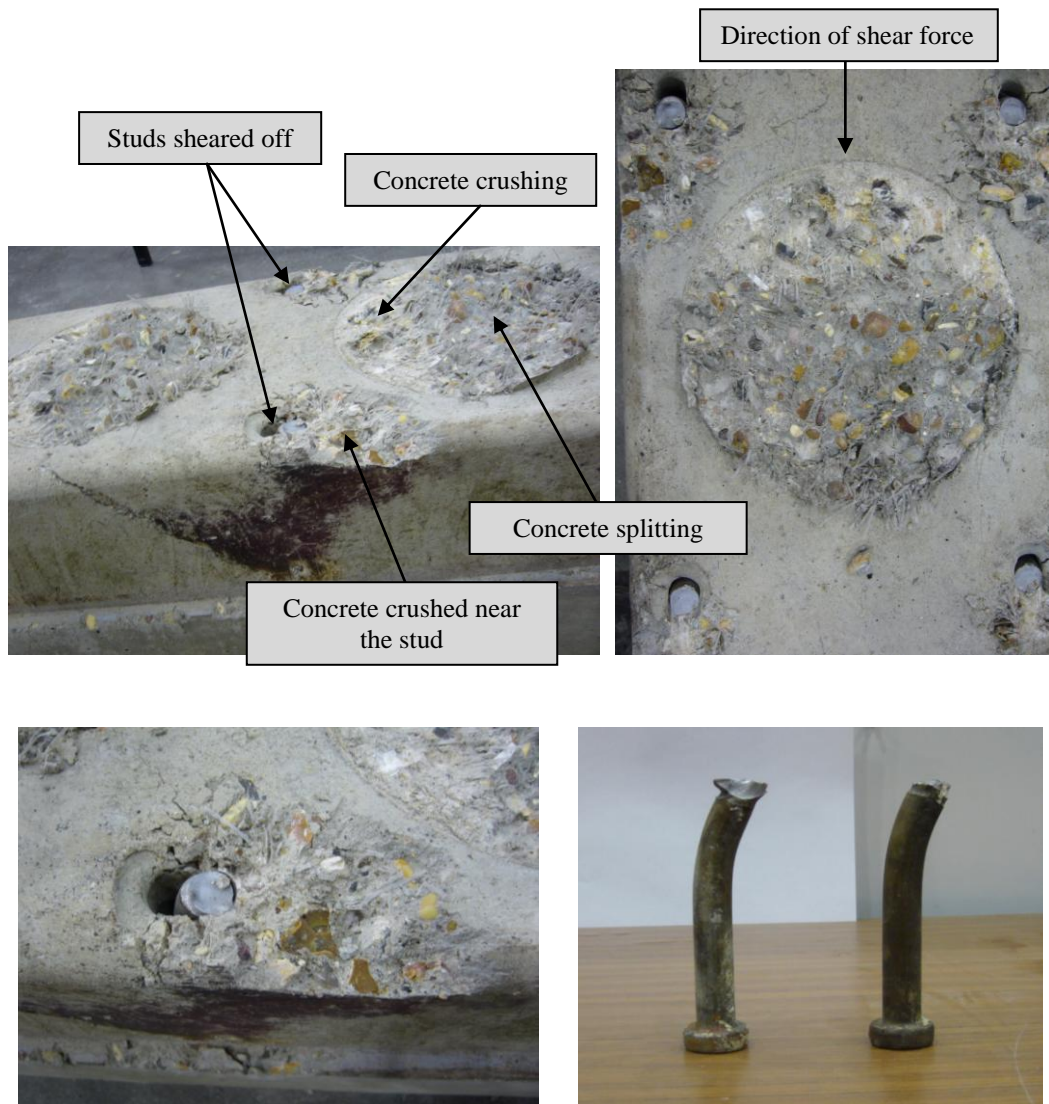
Figure 3.36 Failure profiles of the web-welded stud shear connection

3.5 Conclusions

The four types of the shear connection used for the shallow cellular floor beams were investigated in the push-out test series-I. The test results were studied and the following conclusions were made.

(1)   The concrete-infill-only shear connection showed a distinctive brittle failure mode, as the rupture failure occurred without any plastic deformations. This brittle failure mode was due to the shear connection consisted of only the concrete infill element, and that concrete was a brittle material.

(2)   The ducting shear connection showed the similar brittle behaviour mode. The ducting deformed extensively in the direction of the slips by the crushing of the concrete infill element. Large slips occurred after the ultimate loads were reached. The ducting itself had little shear resistance due to its geometry and thickness. However, the presence of the ducting reduced the attendance of the brittle failure mode.

(3)   Both tie-bar and web-welded stud shear connection demonstrated the ductile behaviour and failure mode. Plastic deformations with large slips occurred before and after the ultimate loads were reached.

(4)   Shear failure of the tie-bar was shown in the tie-bar shear connection. This were due to the tie-bars were positioned close to the perimeter of the web opening, and the tie-bars were in direct contact with the steel section in the direction of the longitudinal shear force.

(5)   The headed studs showed major influence on the behaviour of the web-welded stud shear connection, as its behaviour was the same as that of the headed studs in the standard push-out tests.

(6)   The same failure profiles of the concrete infill element were shown in four types of the shear connection. The concrete infill element was crushed in the shear direction, and was ruptured in the transverse direction. The crushing represented the compressive failure mechanism; and the rupture represented the tensile failure mechanism.

(7)   The additional elements of the tie-bars and studs used in combination with the concrete infill element had significantly increased the ductility, slip capacity and shear strength of the shear connection.

(8)   Strong tie resistance were shown by all four types of the shear connection, as very little separations were shown in the push-out tests.

(9) The effect of the bond between the steel section and concrete slabs to the behaviour of the shear connection was shown, as sudden slip increase occurred. But this local bond failure had no effect on the overall shear strengths of the shear connection, as the local bond failure did not cause the failure of the shear connection.

(10) The results of the push-out tests showed that the shear resisting capacity of the shear connection was dependent on the diameter of the web opening and concrete strength.

(11) The shear resisting capacity of the shear connection increased with increase of the web opening diameter and concrete strength.

3.6 Recommendations

The results of the push-out test series-I provided comprehensive information on the behaviour and shear resisting properties of the shear connection used for the shallow cellular floor beams. But the design details for some of the shear connection could be improved, and also that some design details for the push-out tests needed adjustment. The following recommendations were made.

(1) In order to provide information towards the design calculation for the shear connection, it was recommended that a minimum of three identical specimens should be tested for a particular shear connection.

(2) Due to the demonstrated effects of the bond on the behaviour of the shear connection, it was recommended that the steel section should be greased for future similar push-out tests.

(3) Due to the brittle failure mode of the concrete-infill-only shear connection, it was recommended that the concrete-infill-only shear connection should not be used as a sole mean to provide shear connection. It should be used in combination with other additional elements, i.e. tie-bars or studs, to provide the necessary ductility.

(4) The shear failure of the tie-bar was shown in the push-out tests because the tie-bars were positioned close to the perimeter of the web openings. It was recommended that the tie-bars should be positioned away from the perimeter of the web openings with a minimum distance of 20mm. This recommended minimum distance was based on the maximum slip capacity of the tie-bar shear connection, 16mm, shown in the push-out tests. Furthermore, if an

Ø16mm tie-bar was used passing through the web opening, it should be positioned at the centre of the web opening.

(5) The low shear resistance of the ducting shear connection was shown in the push-out tests. It was recommended that the ducting shear connection should be used only in the region of low shear. The extensive deformations of the ducting were shown at the slips of 1.5-3.5mm. It was recommended that the ducting shear connection should not be used in the region where large slips were expected.

Chapter 4 Push-out test series-II

Four types of the shear connection used for the shallow cellular floor beams were investigated in the push-out test series-I. The test results provided comprehensive information on behaviour and shear resisting properties of the shear connection. Based on the recommendations of push-out test series-I, push-out test series-II was carried out to further investigate the concrete-infill-only and tie-bar shear connection. Loading cycles were introduced to investigate its effects on the behaviour and shear resisting capacity of the shear connection. The test results were evaluated to provide specific information for the design calculation. The behaviour and failure mechanism of the shear connection were studied. The shear resisting capacity of the shear connection were analysed together with the results of the push-out test series-I to develop a design method for the shear resistance of the shear connection.

4.1 Introduction

The push-out test series-I recommended that:

- A minimum three identical specimens should be tested for a particular shear connection.
- If Ø16mm tie-bar is used, it should pass through the centre of the web opening.

Base on these two recommendations, push-out test series-II were designed to further investigate the concrete-infill-only and tie-bar shear connection. These two types of shear connection were also the most commonly used shear connection for the shallow cellular floor beams. There were two test groups in the push-out test series-II. Each test group had four identical specimens. The tie-bar shear connection had an Ø16mm tie-bar passing through the centre of the web opening.

The specimens of the push-out test series-II were modified based on the specimens of the push-out test series-I. The push-out test series-II were carried out in the same manner of the push-out test series-I. The additional loading cycles of 25 times were applied to one specimen of each test group. Load-slip behaviour of these two types

of shear connection was analysed. The failure mechanism of the tie-bar (Ø16mm) shear connection were studied, and compared with that of the tie-bar (Ø12mm) shear connection in the previous test series. The results of the tests were studied to establish the increased shear resistance due to the additional Ø16mm tie-bars.

4.2 Test specimens

The configuration of the specimens was the same as that of the push-out test series-I. The concrete slabs on both sides of the web post were connected by the concrete infill elements with or without the tie-bars. The width of the concrete slabs was increased to 1m from the previous 600mm for the push-out test series-I. This was to accommodate the increased length of the Ø16mm tie-bars. All other dimensions of the specimens were same as that of the push-out test series-I. The dimensions of specimens of both test groups were the same. This was to avoid any undesirable variables between the two test groups. The concrete strengths of the both test groups were designed at about 30N/mm^2.

4.2.1 Steel section

There was only one size of the steel section used for the specimens of the push-out test series-II. This steel section was the same steel section of 254x254x73UC used for the previous test series. There were three Ø150mm opening perforated on the web post, as shown in Figure 4.1.
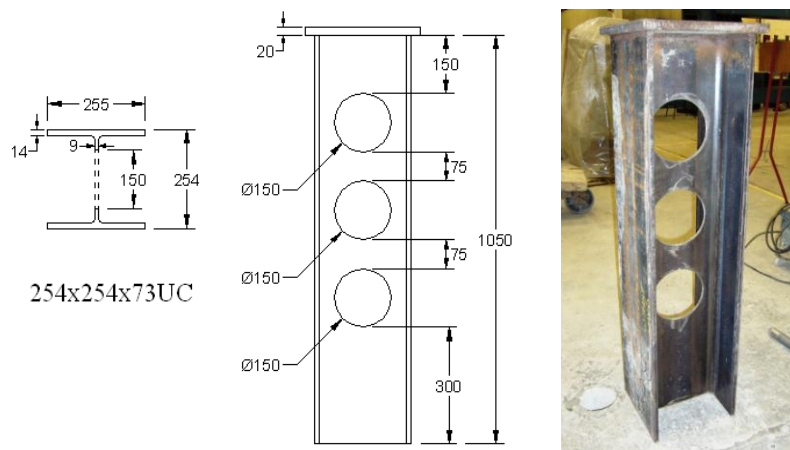
Figure 4.1 Steel section used for the push-out test series-II

4.2.2 Concrete slabs

Normal concrete was used to cast the concrete slabs for the push-out test series-II. The width of the concrete slabs was 1m, which was increased from the previous 600mm, to

accommodate the 1m length of the Ø16mm tie-bars. The 1m length was primarily to provide adequate anchorage for the Ø16mm tie-bars. The concrete slab width was the same for both test groups. The depth of the concrete slabs was 254mm. The concrete slabs flushed with the steel flanges.

4.2.3 Test groups

The two test groups of the push-out test series-II were: T5 and T6, investigating the concrete-infill-only and tie-bar (Ø16mm) shear connection respectively. Each test group had four identical specimens. This conformed to one of the recommendations of the push-test series-I.

(a)

(b)   (c)
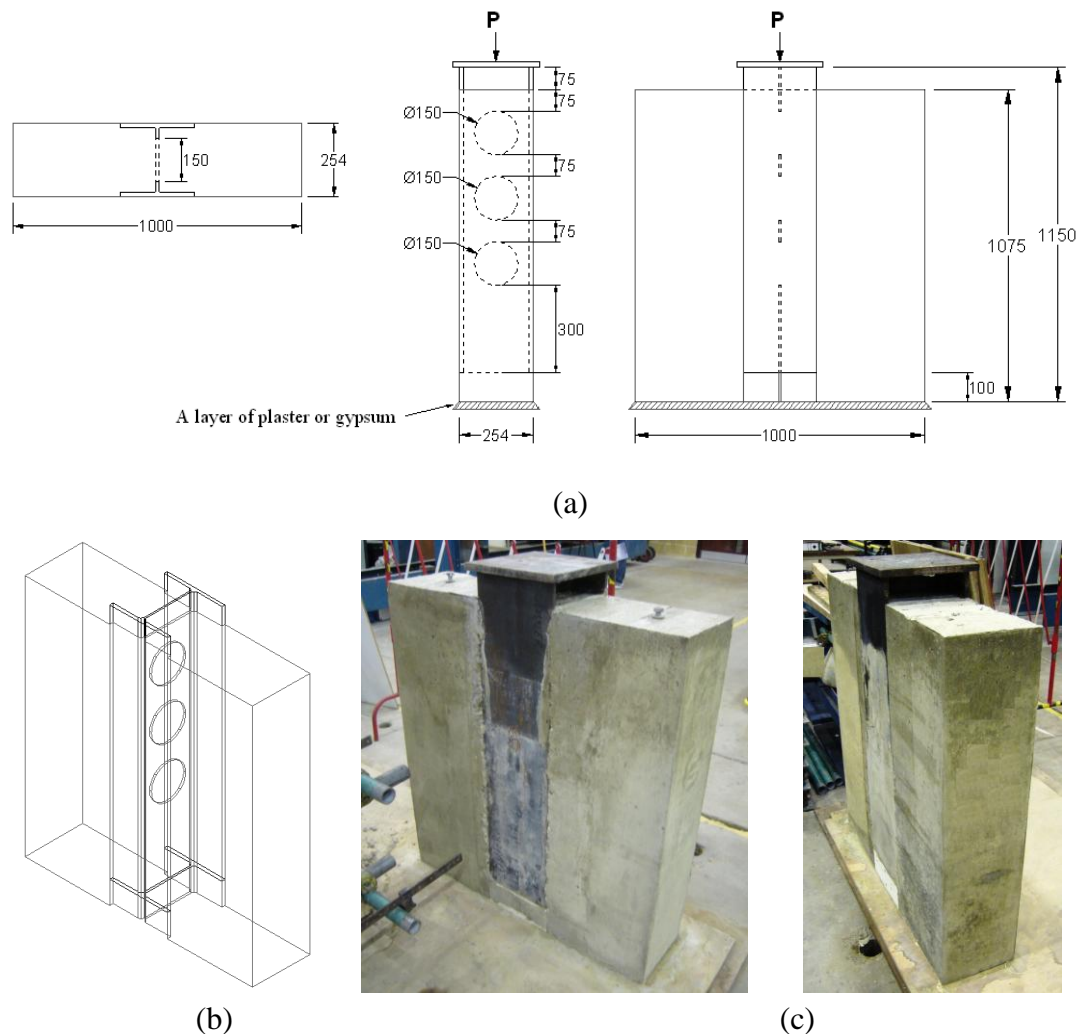
Figure 4.2 (a) Drawing of the T5 specimen; (b) 3-D illustration; (c) Cast specimens

4.2.3.1 Specimens of test group T5, concrete-infill-only shear connection

The steel sections of the test group T5 specimens were applied with de-bonding grease to prevent the load bond failure shown in the push-out test series-I. This was based on

one of the recommendations of the push-out test series-I. The dimensions of the specimen are shown in Figure 4.2. The in-situ concrete completely filled the web opening, so that applied longitudinal shear force would be directly resisted by the concrete-infill-only shear connection. The load-slip behaviour and the shear resisting capacity of the shear connection were obtained in the push-out tests.

4.2.3.2 Specimens of test group T6, tie-bar (Ø16mm) shear connection

The tie-bar shear connection of the test group T6 consisted of the concrete infill element combined with one Ø16mm tie-bar passing through the centre of each web opening, as shown in Figure 4.3. The length of the Ø16mm tie-bars was 1m, which was the same as that of the Ø16mm tie-bar used for the shallow cellular floor beams. The purpose of having the 1m length was to provide adequate anchorage resistance to the Ø16mm tie-bars, so that the tensile strength of the tie-bar would become effective.
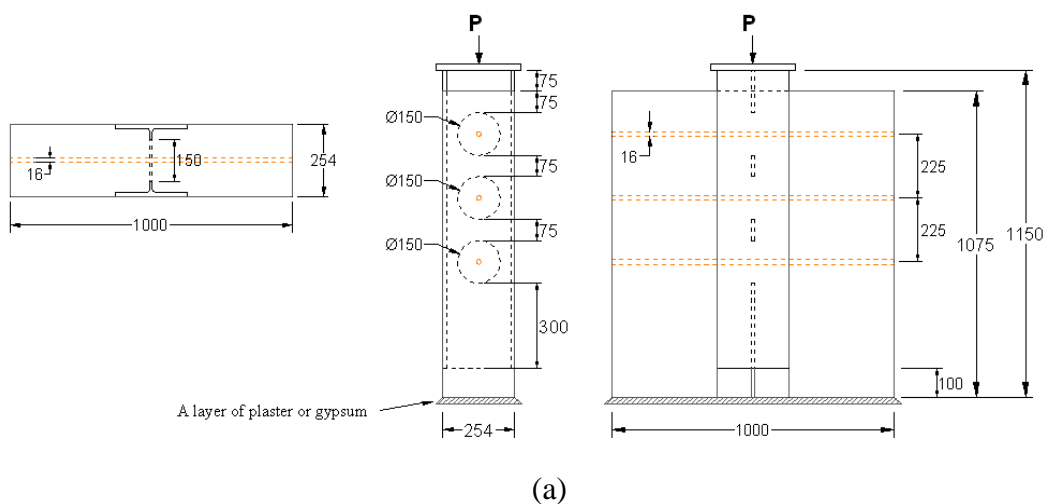
(a)
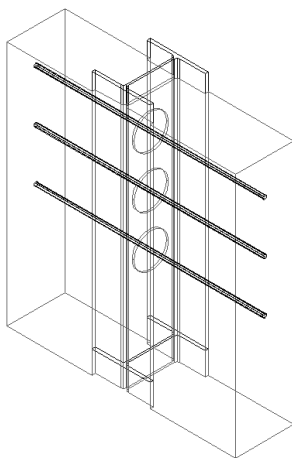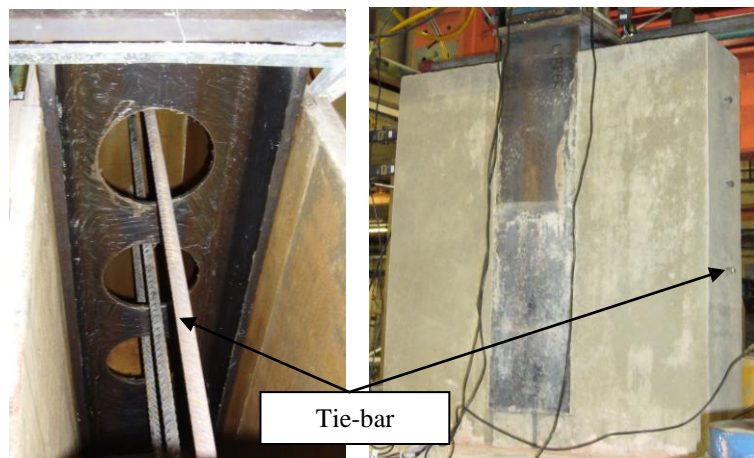
(b)   (c)

Figure 4.3 (a) Drawing of the T6 specimen; (b) 3-D illustration; (c) Cast specimen

4.2.4 Preparation and construction

The de-bonding grease was applied to the steel sections of both test groups. Hence, the development of the bond between the concrete and steel was prevented. All specimens of the push-out test series-II were cast in the Structure Laboratory of City University London. Specimens of the cubes and cylinders were prepared by using the same batch of concrete used for the push-out test specimens. The cubes, cylinders and push-out test specimens were cured under the same conditions and covered with wet sacks and plastic sheets.

(a)
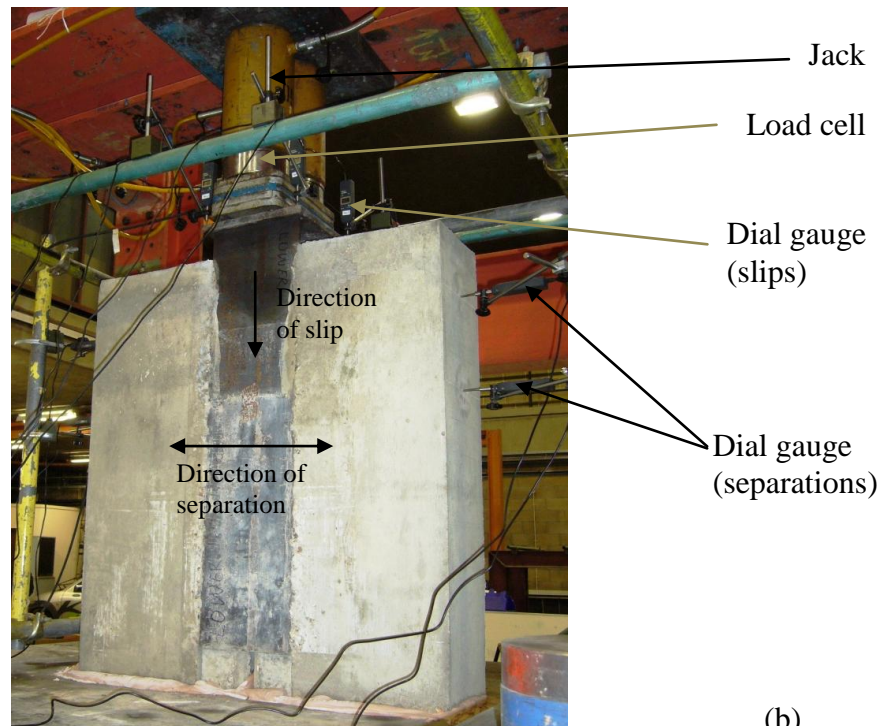
(b)

Figure 4.4 (a) Set up of the push-out test series-II; (b) Instrumentations of the test

4.3 Set up and testing procedures

The same testing rig, hydraulic jacks and load cells used in the previous test series were used for the push-out test series-II. The load cells were re-calibrated before use in the push-out test series-II. The measurements of slip and separation were obtained by using digital dial gauges. Four digital dial gauges were positioned on the top of the steel section to measure slips in the vertical direction. Four digital dial gauges were positioned on the either side of the concrete slabs, as shown in Figure 4.4 (b), to measure the separations in the transverse direction. The resolution of the digital dial gauges was 0.01mm.

4.3.1 Testing procedures

Push-out test series-II was carried out in the same manner of the previous test series. The monotonic loads were applied onto the steel section; thus, the direct shear force was applied onto the shear connection. The specimens were settled onto a layer of plaster (gypsum) creating an even contact surface between the specimens and reaction platform.

The first three specimens of each test group were tested with monotonic loads up to the destructive failure of the shear connection. The fourth specimen of each test group was tested with additional loading cycles, 25 times between 5-40% of the expected failure loads. The load increments for all specimens are shown in Table 4.1.

Test group	Specimens No.	Load increment	As % of the expected failure loads
T5 Concrete-infill-only shear connection	T5-1		
	T5-2	19.6kN (2ton)	4%
	T5-3		
	T5-4*		
	* loading cycles were applied between 29.4-205.8kN (3-21ton) with the same load increment of 19.6kN (2ton)		
T6 Tie-bar (Ø16mm) shear connection	T6-1		
	T6-2	39.2kN (4ton)	4%
	T6-3		
	T6-4 ˜		
	˜ loading cycles are applied between 49-392kN (5-40ton) with the same load increment of 39.2kN (4ton)		

Table 4.1 Load increments of the push-out test series-II

4.4 Test results

The results obtained in the push-out test series-II were presented in the load-slip and load-separation curves, as shown in Figures 4.5-4.8. The load-slip and load-separation curves were in the same scales, to enable the comparison between the slips and separations. The load-slips curves represented the behaviour of the shear connection in resisting the direct longitudinal shear force. The load-separation curves represented the tie resisting behaviour of the shear connection in the transverse direction. The load value of these curves was the load per shear connection. The concrete strengths of the specimens are presented in Appendix B.

The load-slip behaviour of the concrete-infill-only and tie-bar (Ø16mm) shear connection were analysed with the aim of optimizing the design details. The increased shear resistance due to the additional Ø16mm tie-bars were determined. The results of the tests were evaluated to provide specific information for design calculation. The shear resisting capacity of the shear connection together with the results of the previous test series were further analysed in Chapter 5 to establish a design method for the shear resistance of the shear connection.

The distinctive brittle failure mode of the concrete-infill-only shear connection was shown by specimens of the test group T5. In contrast, the ductile failure mode of the tie-bar (Ø16mm) shear connection was shown by specimens of the test group T6. The increased shear resistance and slip capacity due to the tie-bars were clearly illustrated in Figure 4.9. It was shown that the additional Ø16mm tie-bars increased the shear resistance of the shear connection by 100%. The slip stiffness of the two types of shear connection was the same.
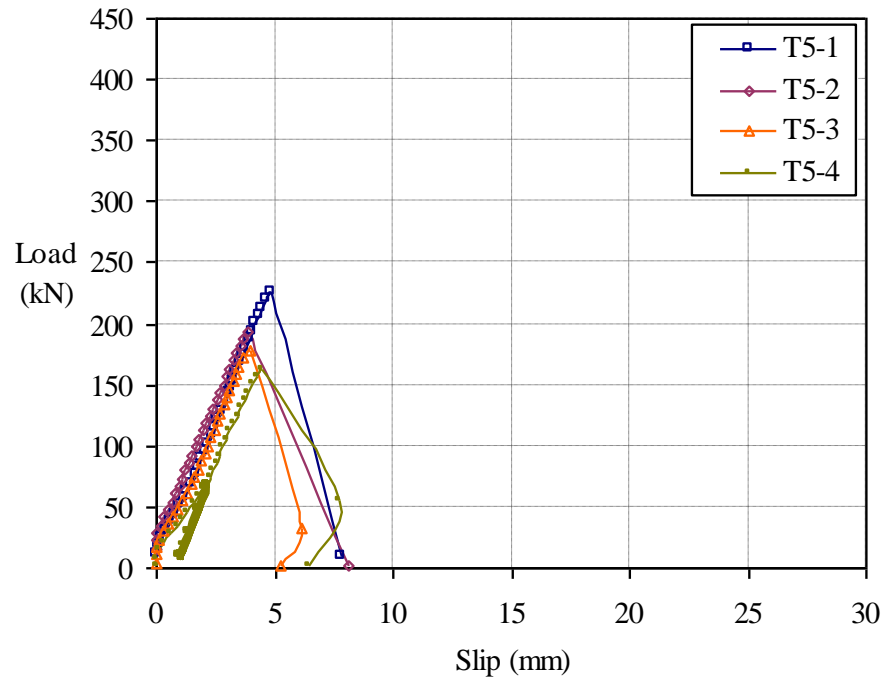
Figure 4.5 Load-slip curves of the concrete-infill-only shear connection (test group T5)
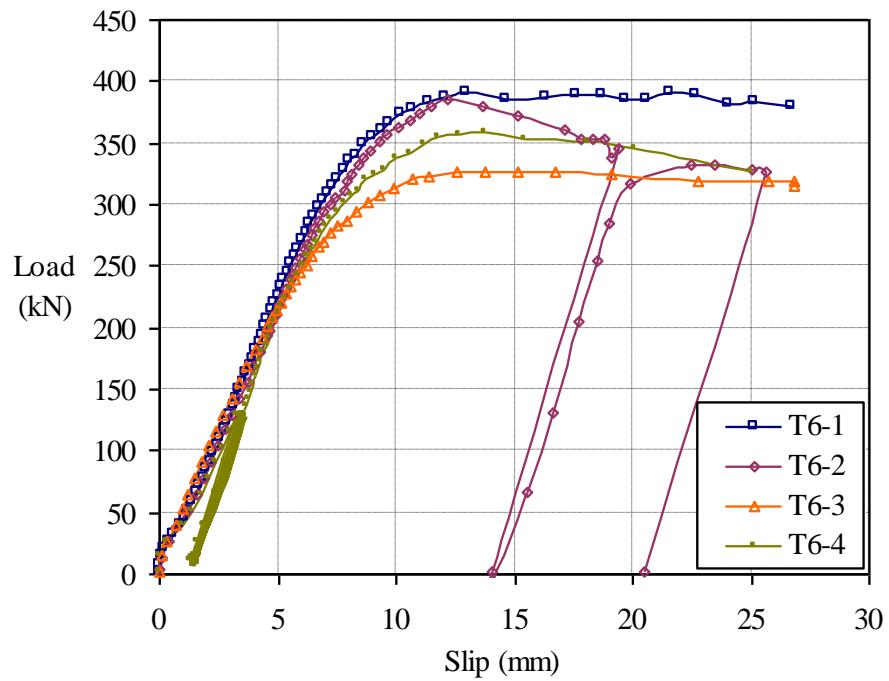
Figure 4.6 Load-slip curves of the tie-bar (Ø16mm) shear connection (test group T6)
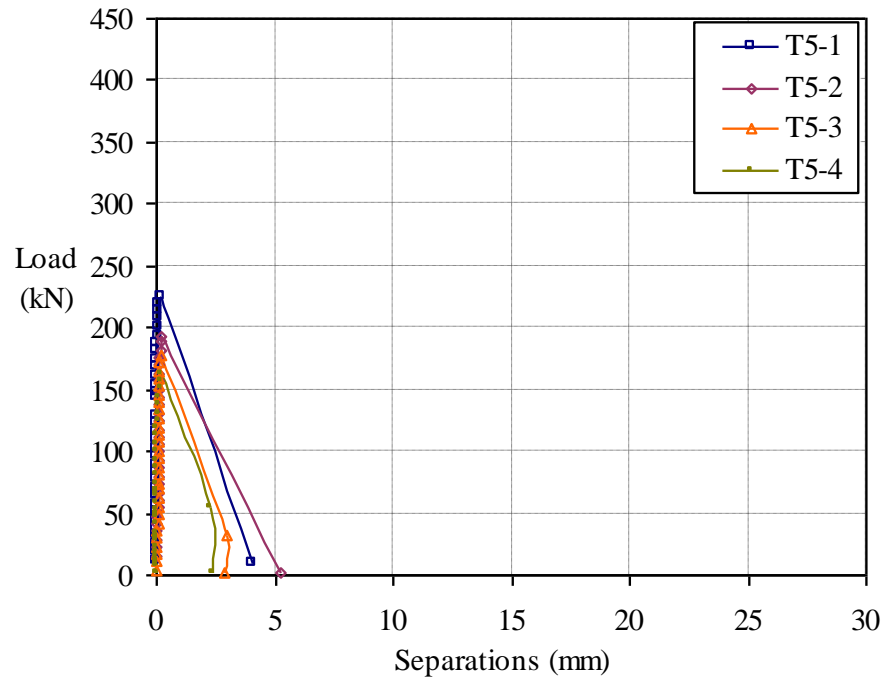
Figure 4.7 Load-separation curves of the concrete-infill-only shear connection (T5)
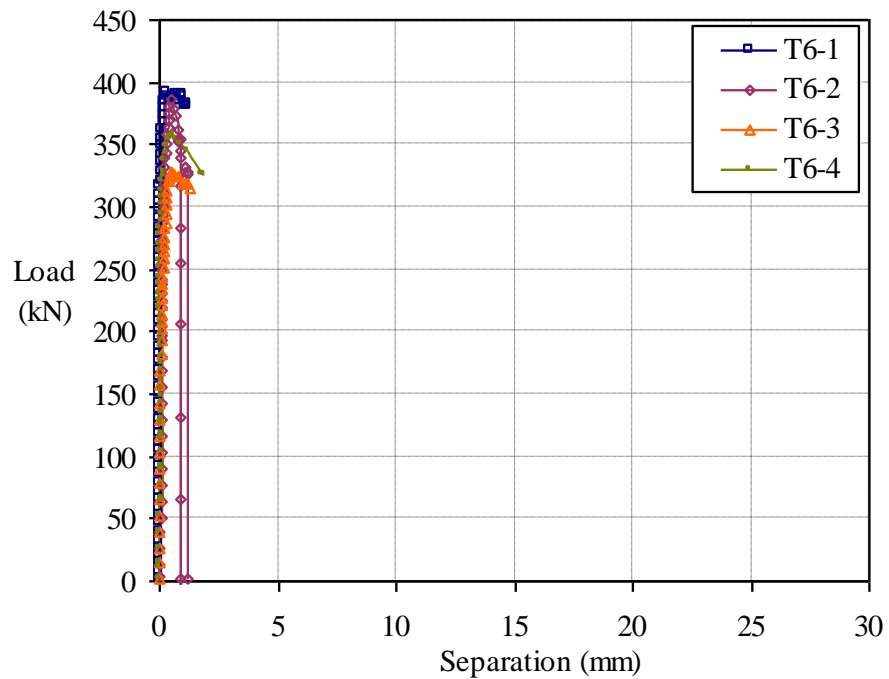
Figure 4.8 Load-separation curves of the tie-bar (Ø16mm) shear connection (T6)
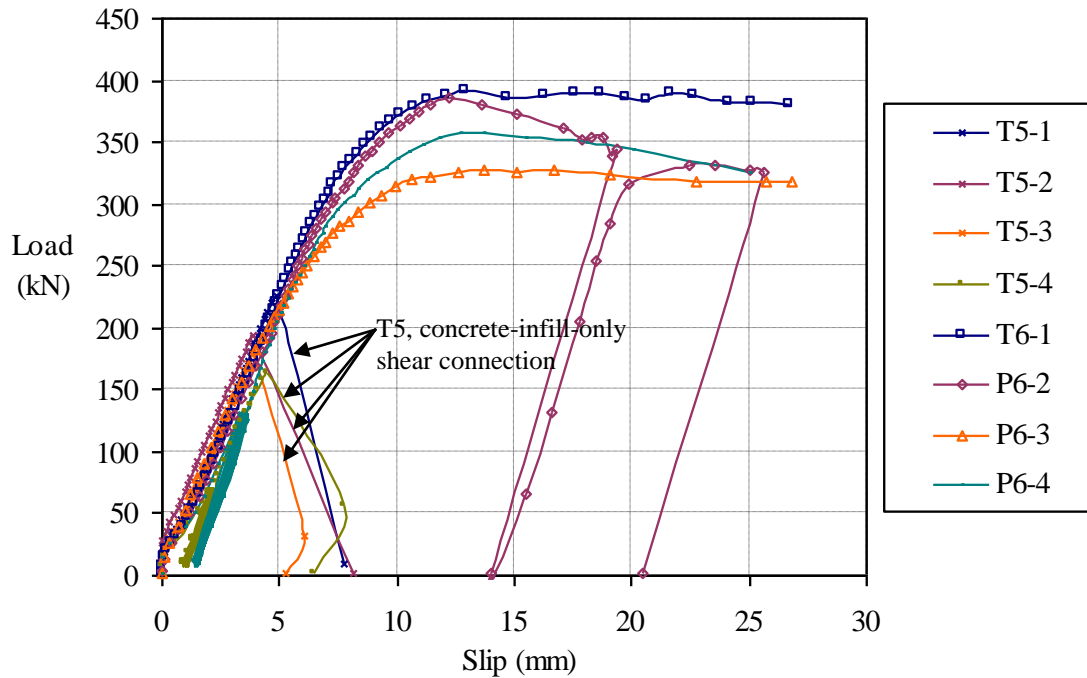
Figure 4.9 Comparison of load-slip curves between the two types of shear connection

4.4.1 Result evaluation

The results of the push-out tests series-II were evaluated with the same method and criterions that were used for the previous test series. Eurocode 4 (EN1994-1-1: 2004) specified that the slip capacity, δ_u, was the slip at the load level dropped 10% below the maximum load. The slip capacity of the concrete-infill-only shear connection was taken as the slip at the maximum load, as the rupture failure occurred at the maximum load without plastic deformations and load dropped to zero instantaneously. The slip capacity of the tie-bar shear connection was also taken as the slip at the maximum load. This was because the shear connection showed no loading dropping after the maximum loads were reached. The ultimate load levels were sustained by the tie-bar (Ø16mm) shear connection with significant slips, as shown in Figure 4.6. The evaluated properties of the concrete-infill-only and tie-bar shear connection are shown in Table 4.2.

The tie-bar (Ø16mm) shear connection showed significant slip capacity, which was three times that of the concrete-infill-only shear connection. Both types of shear connection demonstrated the strong tie resistance, as the separations were very small. Consistent results of shear resisting capacity, slip capacity and slip stiffness were shown by the shear connection of both test groups.

Shear connection	Specimen No.	Ultimate shear capacity P_u (kN)	Slip capacity, δ_u (mm)	Stiffness K (kN/mm)	Tie resistance check (pass/fail)
Concrete-infill-only	T5-1	226	4.9	47	Pass
	T5-2	194	3.9	54	Pass
	T5-3	182	3.9	47	Pass
	T5-4	175	4.4	36	Pass
Tie-bar (Ø16mm)	T6-1	391	13.0	44	Pass
	T6-2	386	12.2	42	Pass
	T6-3	327	13.7	45	Pass
	T6-4	358	13.7	40	Pass

Table 4.2 Result evaluations of the push-out test series-II

4.4.2 Results of test group T5, concrete-infill-only shear connection

The test group T5 had four identical specimens with the concrete-infill-only shear connection of Ø150mm diameter. The steel sections were applied with de-bonding grease to prevent the local bond failure, which was shown in the previous test series. The specimen, T5-4, was tested with the additional loading cycles of 25 times. The concrete strengths, ultimate loads and slips of the specimens are shown in Table 4.3. The load-slip and load-separation curves of each specimen are shown in Figures 4.10-4.13. The load value of these curves was the load per shear connection.

Specimen No.	f_{cu}* (MPa)	f_{ct}˜ (MPa)	Ultimate Load (kN)	Slip (mm) at Ultimate Load
T5-1	35	3.21	677	4.9
T5-2	35	3.21	581	3.9
T5-3	32	2.9	546	3.9
T5-4	30	3.02	525	4.4

* cube compressive strength of concrete   ˜ tensile splitting strength of concrete

Table 4.3 Result summary of the test group T5

The slips at the ultimate loads were 4.0-5.0mm, which were very similar to the 3.0-4.0mm slips shown in the previous push-out test series. It was shown that the shear

resistance of a concrete-infill-only shear connection of Ø150mm was 1.75 times the shear resistance of a headed stud with Ø19mm and 100mm height. This comparison was based on the concrete strength of 30N/mm^2. The shear resistance of the headed studs was taken as the value given in British Standard 5950 (BS5950-3.1: 1990), as shown in Table 2.2.
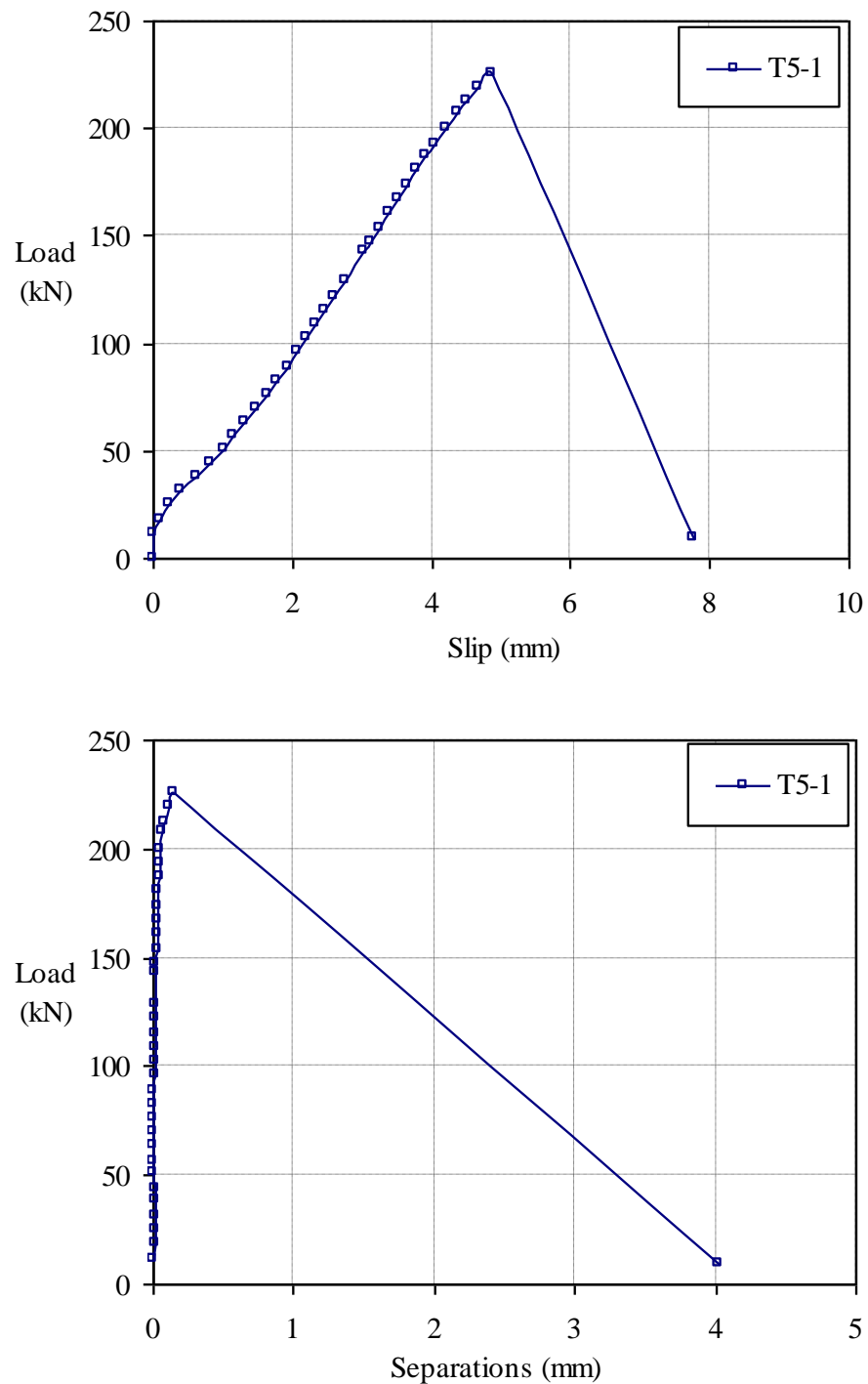
Figure 4.10 Load-slip and load-separation curves of specimen T5-1
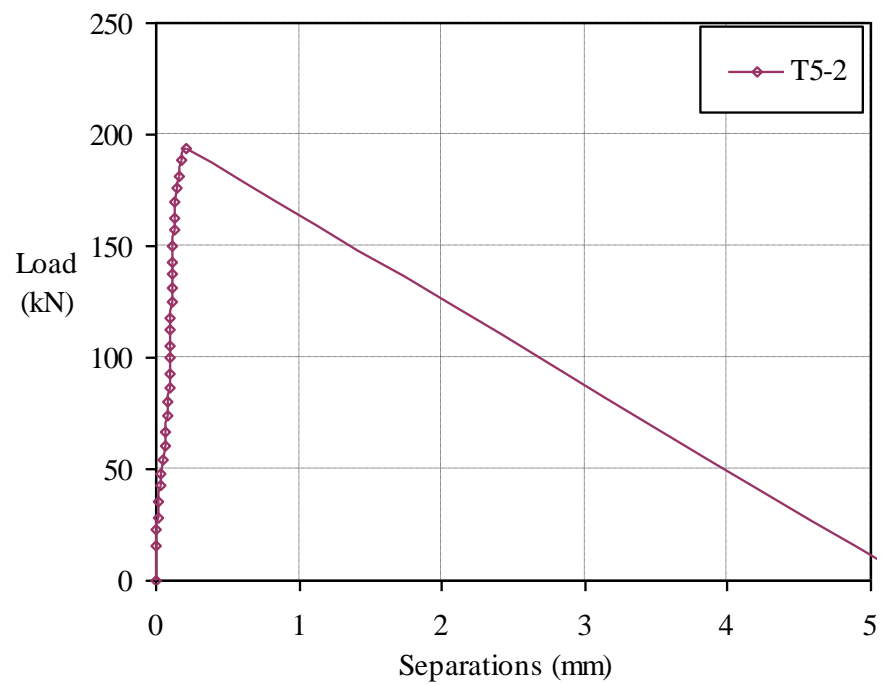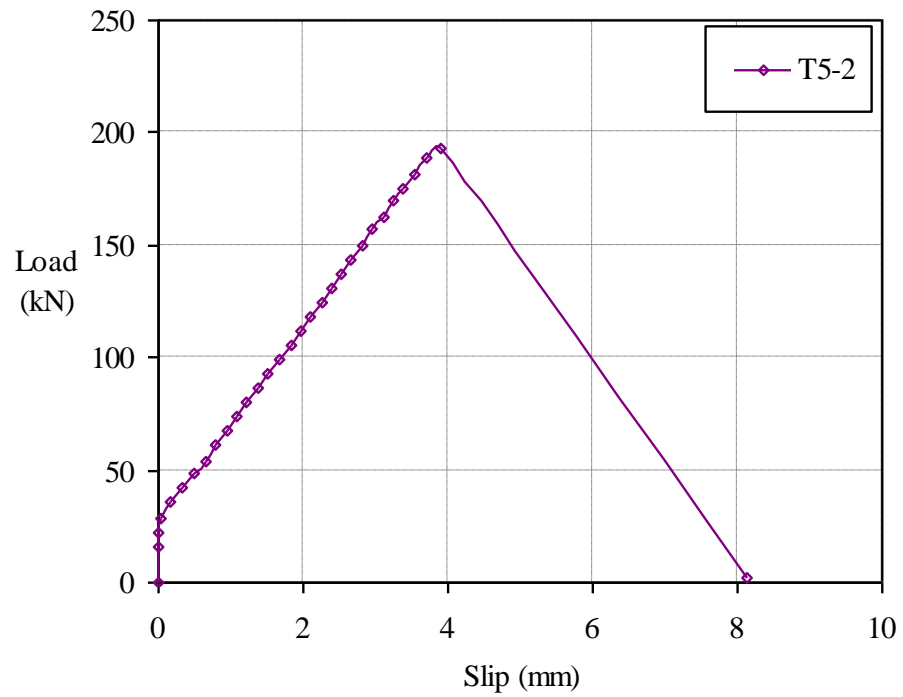
Figure 4.11 Load-slip and load-separation curves of specimen T5-2
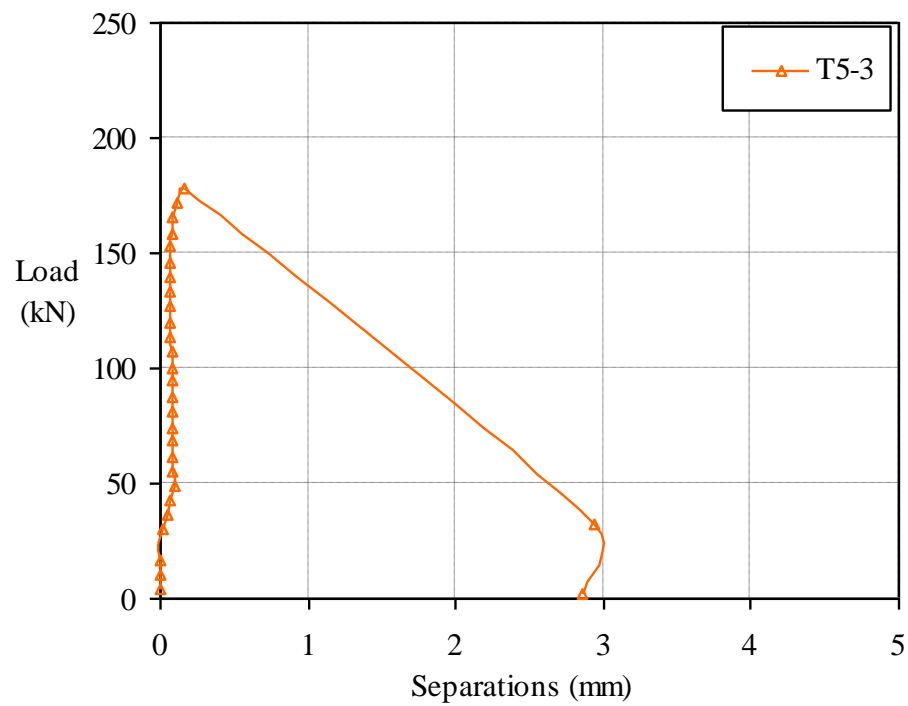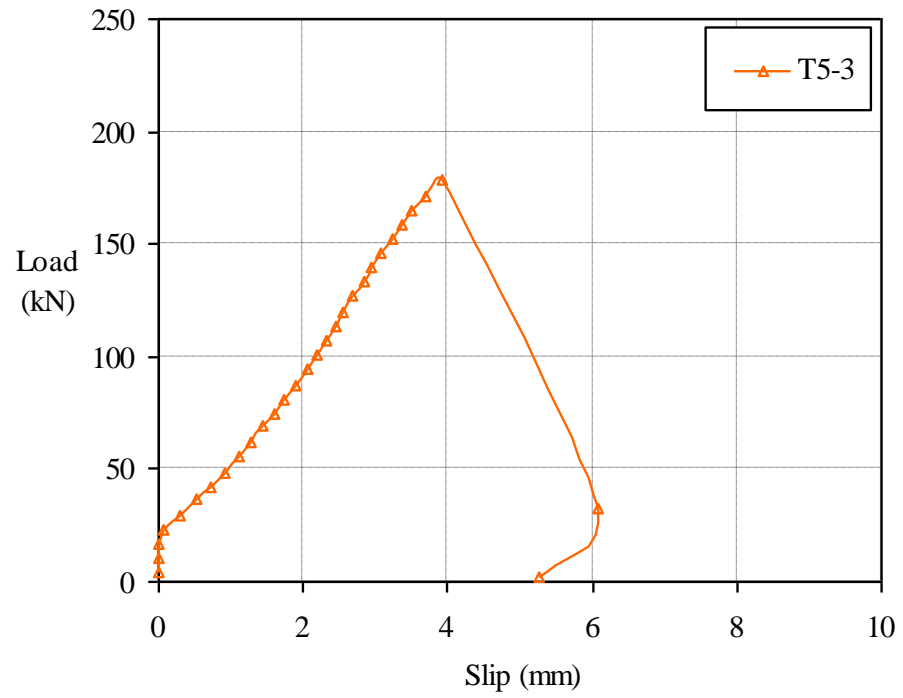
Figure 4.12 Load-slip and load-separation curves of specimen T5-3
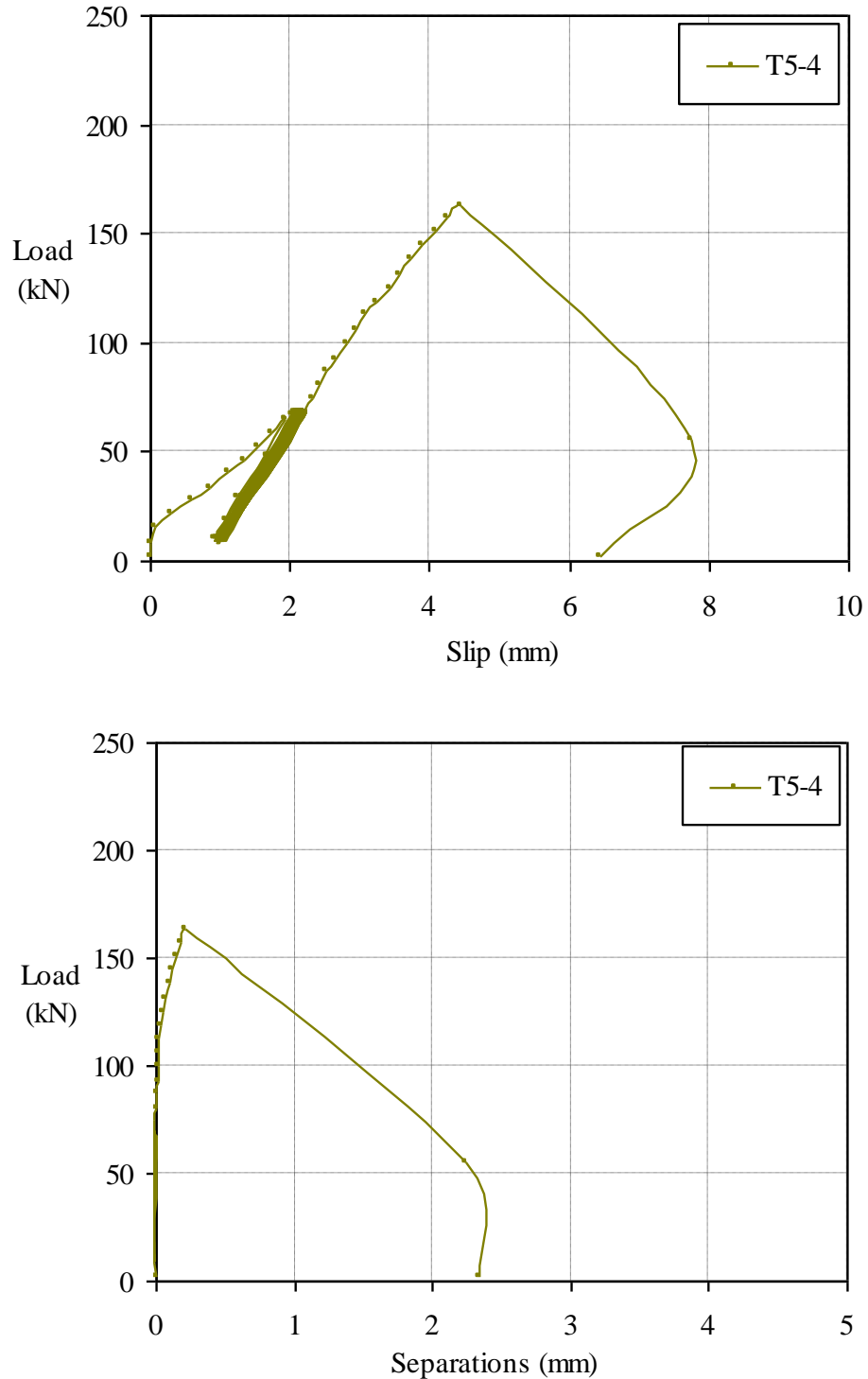
Figure 4.13 Load-slip and load-separation curves of specimen T5-4 with loading cycles

4.4.2.1 Behaviour analysis

A uniform behaviour was shown by all specimens including the specimen, T5-4, which was applied with the additional loading cycles of 25 times. The shear connection deformed elastically up to the ultimate load without any plastic deformations. The load drops instantaneously when the ultimate load was reached, as shown in the load-slip

curves. This brittle failure mode of the concrete-infill-only shear connection was mainly due to the brittle material properties of the concrete, as the shear connection consisted of solely the concrete infill element. The local bond failure or sudden slip increase shown in the push-out test series-I did not occur, because the bond was eliminated by de-bonding grease applied onto the steel sections.

4.4.2.2 Response to loading cycles

The concrete-infill-only shear connection showed the elastic behaviour during the loading cycles of 25 times, as demonstrated in Figure 4.14. The total slip increase of 0.18mm was created by these loading cycles. The slip increases were due to the crushing of the concrete as a response of the shear connection to the loading cycles. The loading cycles had no effect on the overall behaviour of the shear connection, as the elastic deformations were continued after the loading cycles.

The slip increase due to the loading cycles would be greater if the number of the cycles was higher. By analysing the increased slips over the 25 times of cycles, it was shown that the amount of slip increase during the first three cycles was almost 10 times that of the last three cycles. In other words, the rate of slip increase was reduced with the higher number of loading cycles. It was predicted that slip increase due to the loading cycles would reach a certain level if the number of the loading cycles was exceeded by a certain limit.

4.4.2.3 Failure mechanism study

The failure profiles of the concrete-infill-only shear connection, shown in Figure 4.15, demonstrated that the top part of the concrete infill element was crushed by the web post in the direction of the longitudinal shear force, and that the rest of the infill element was ruptured by the tensile splitting in the transverse direction. The failure profiles of the concrete infill element were the same as those shown in the push-out test series-I.
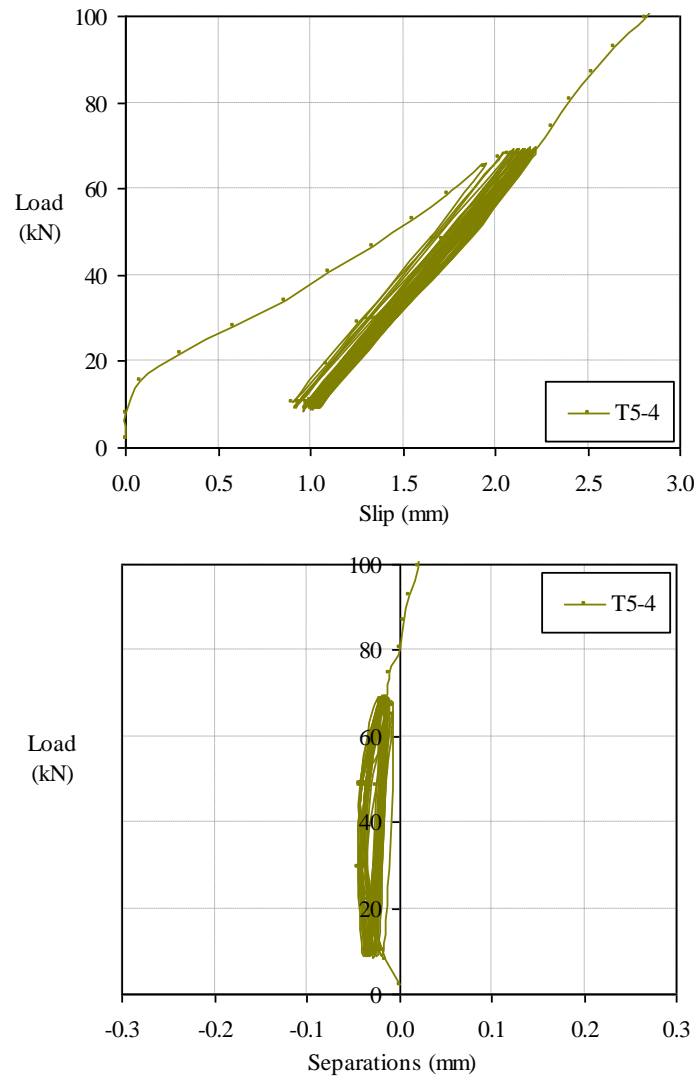
Figure 4.14 Load-slip and load-separation response of the concrete-infill-only shear connection during the loading cycles
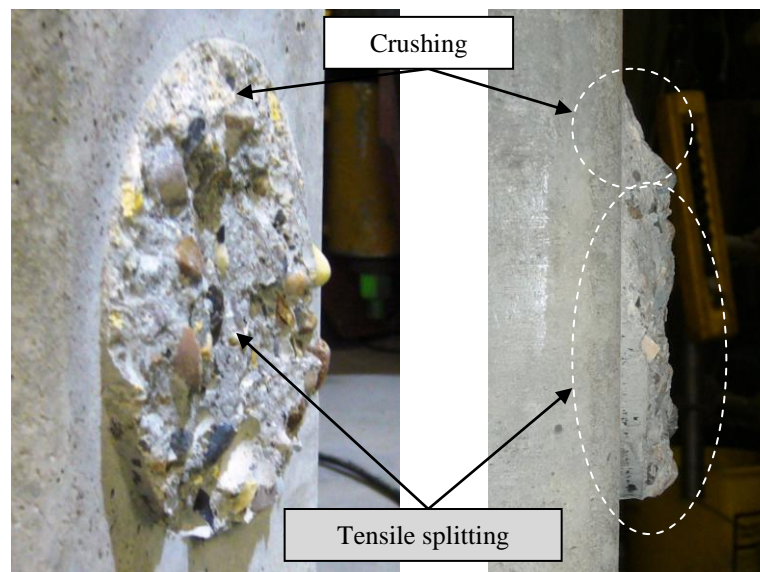
Figure 4.15 Failure profiles of the concrete-infill-only shear connection

4.4.3 Results of test group T6, tie-bar (Ø16mm) shear connection

The test group T6 investigated the tie-bar (Ø16mm) shear connection, which consisted of the concrete infill element combined with an Ø16mm tie-bar passing through the centre of each web opening. The specimen, T6-4, was tested with the additional loading cycles of 25times. The results of concrete strength, ultimate load and slip of the specimens are shown in Table 4.4. The load-slip and load-separation curves of the individual shear connection of each specimen are shown in Figures 4.16-4.19.

Specimen No.	f_{cu}* (MPa)	f_{ct} ˜ (MPa)	Ultimate load (kN)	Slip (mm) at ultimate load
T6-1	29	2.85	1173	13.0
T6-2	32	2.92	1159	12.2
T6-3	28	2.49	982	13.7
T6-4	27	2.57	1075	13.7

* cube compressive strength of concrete   ˜ tensile splitting strength of concrete

Table 4.4 Result summary of the test group T6

Slips at the ultimate loads were 12-14mm. The consistent shear resisting capacity of the shear connection was shown by the specimens. It was shown that the shear resistance of a tie-bar (Ø16mm) shear connection of Ø150mm opening was 3.7 times the shear resistance of the headed studs with Ø19mm and 100mm height. This comparison was based on the concrete strength of 30N/mm^2. The shear resistance of the headed studs was taken as the values given in British Standard BS5950 ((BS5950-3.1: 1990), as shown in Table 2.2. It was shown that the shear resistance of the tie-bar (Ø16mm) shear connection was two times that of the concrete-infill-only shear connection.

4.4.3.1 Behaviour analysis

A uniform behaviour of the tie-bar (Ø16mm) shear connection was demonstrated by all specimens, including the specimen, T6-4, which was applied with the additional loading cycles of 25 times. The shear connection deformed elastically then followed by the plastic deformations with large slips before and after the ultimate loads. The shear connection sustained the ultimate load levels while significant slips were induced, as shown in the load-slip curves. This mechanism of maintaining the shear strength during

the plastic deformations was further demonstrated during the unloading and re-loading of the specimen, T6-2, as shown in Figure 4.17. The ductile behaviour and failure mode of the shear connection indicated the tensile strength of the tie-bar had become effective. The adequate anchorage resistance of the Ø16mm tie-bar was provided by the 1m length, as no anchorage failure occurred in the push-out test.
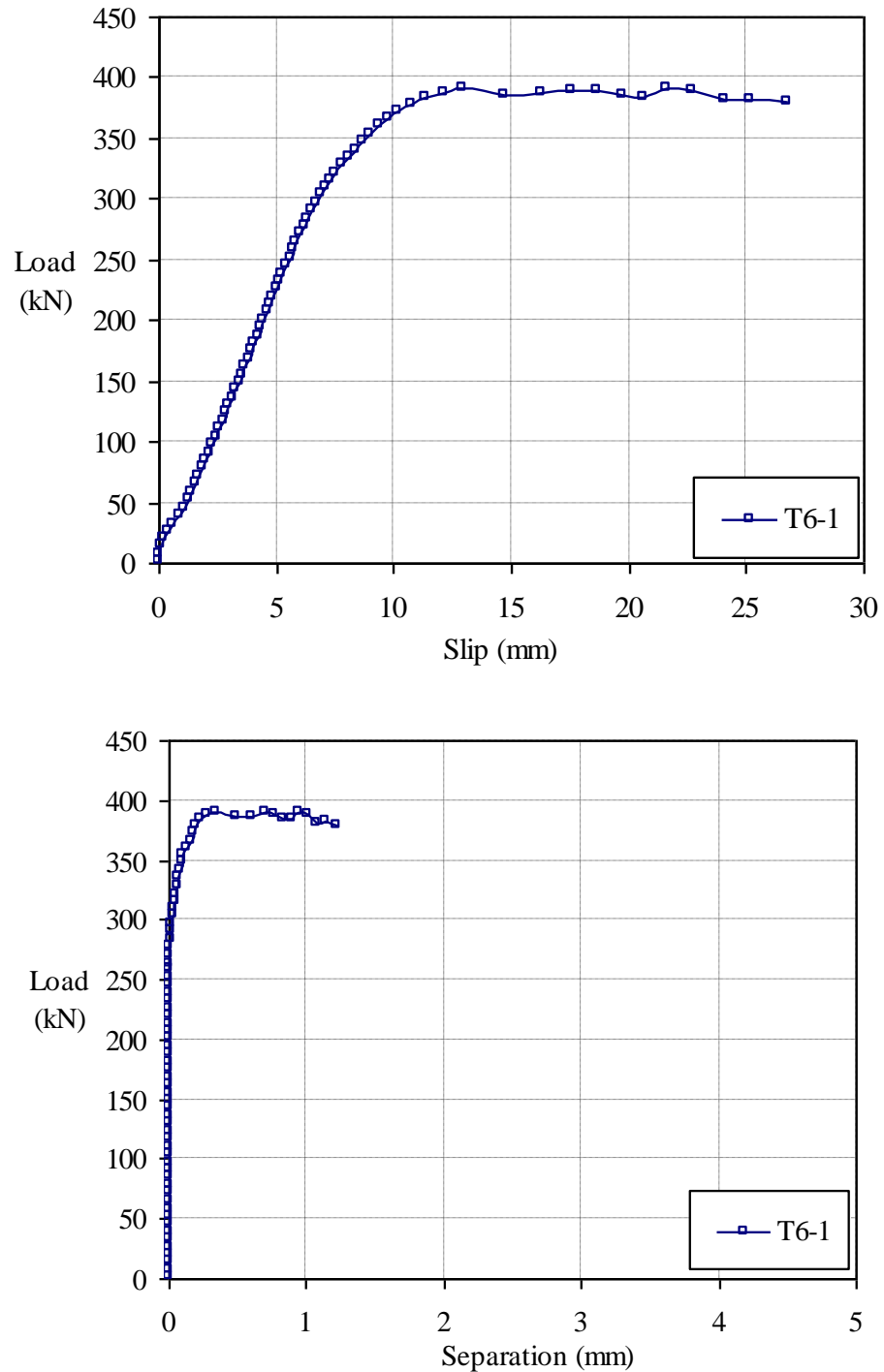
Figure 4.16 Load-slip and load-separation curves of specimen T6-1
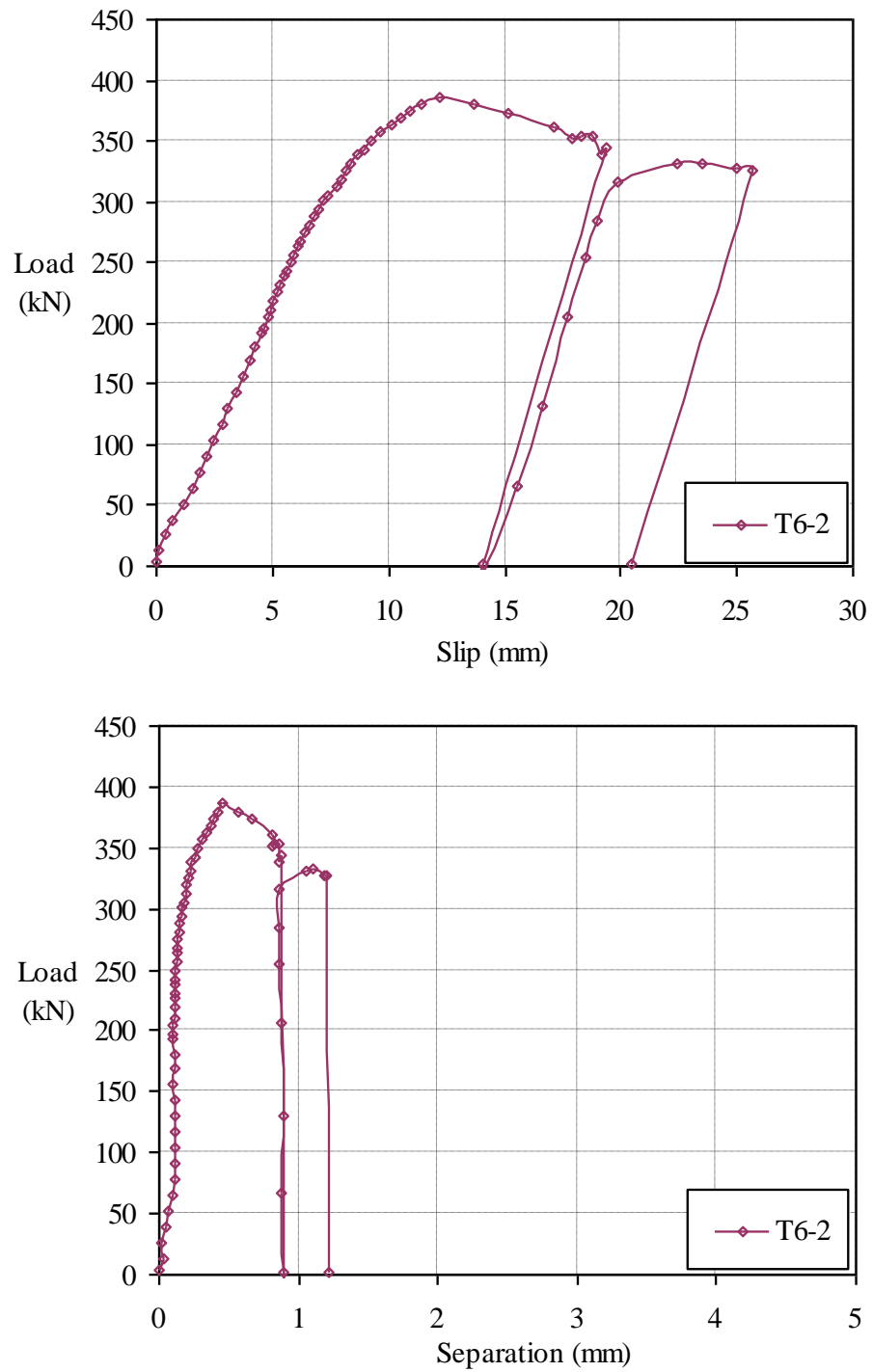
Figure 4.17 Load-slip and load-separation curves of specimen T6-2
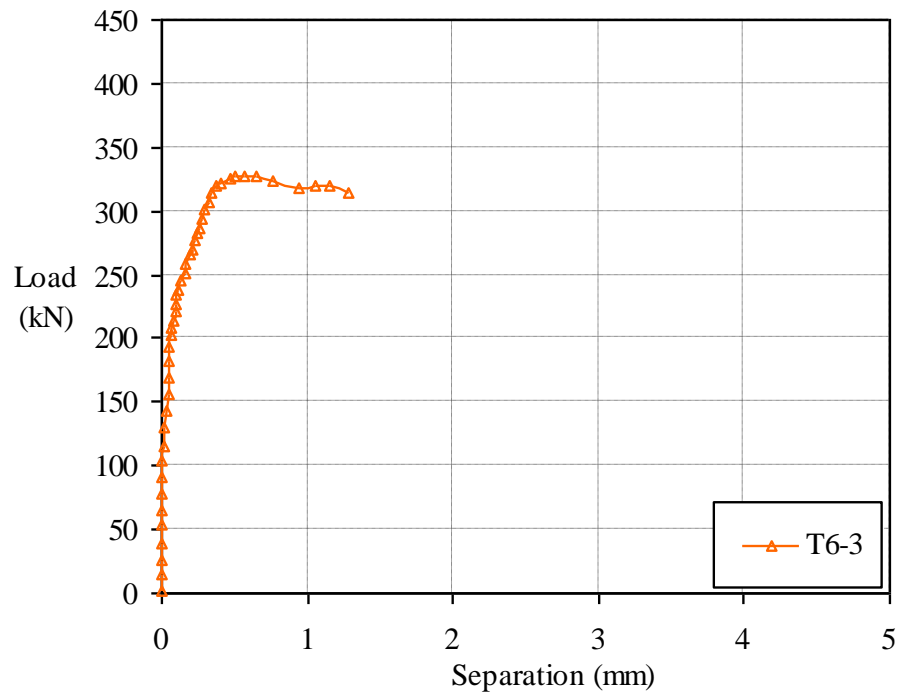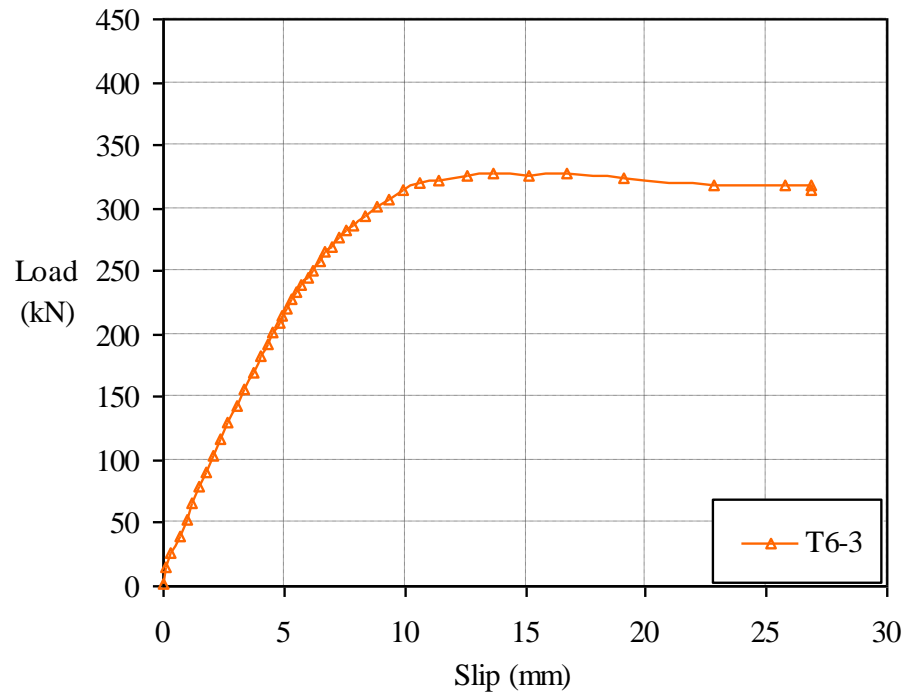
Figure 4.18 Load-slip and load-separation curves of specimen T6-3
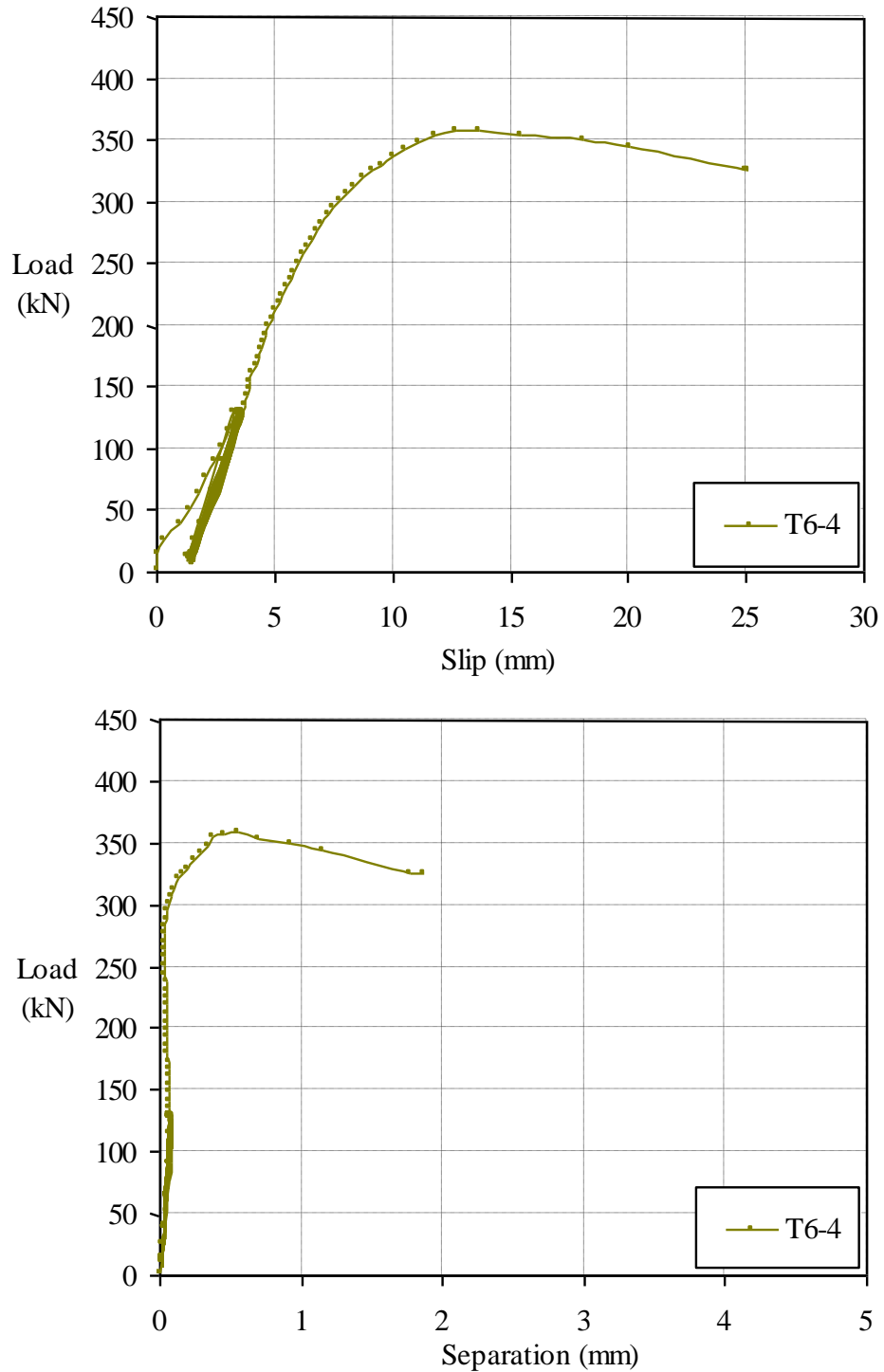
Figure 4.19 Load-slip and load-separation curves of specimen T6-4

4.4.3.2 Response to loading cycles

The loading cycles of 25 times between 5-40% of the expected failure load were applied to the specimen, T6-4. This was to investigate the effects of the loading cycles on the anchorage of the tie-bars and overall behaviour of the shear connection.

The response of the tie-bar (Ø16mm) shear connection to the loading cycles was elastic deformations, as shown in Figure 4.20. It was shown that the anchorage of the tie-bars was not affected by the loading cycles, as no load drop or sudden slip increase occurred. The overall behaviour and failure mode of the shear connection were also not affected by the loading cycles, as the elastic deformation was continued and the ductile failure mode was illustrated thereafter.

Tie-bar (Ø16mm) shear connection had slip increase of 0.19mm during the loading cycles. This was due to the crushing of the concrete infill element in the response to the loading cycles. The analysis showed that the slip increase during the first three cycles was about 8 times the slip increase during the last three cycles. The rate of slip increase became smaller with the higher number of loading cycles. Again, it was predicted that slip increase due to the loading cycles would reach a certain level if the number of the loading cycles exceeded by a certain limit.

4.4.3.3 Failure mechanism study

The tested specimens of the test group T6 could not be dissembled, as the tie-bars did not failed and concrete slabs were tied firmly together. The load-slip curves had provided comprehensive information to predict the failure profile of the shear connection.

The load-slip curves demonstrated the ductile failure mode of the shear connection with significant slips. The characteristic behaviour of maintaining the ultimate loads during the plastic deformations and no anchorage failure of the tie-bars indicated that the tensile strength of the tie-bars had became effective. The possible failure mechanism of the tie-bars would be tensile failure rather than the anchorage failure.

The large slips indicated that the significant crushing was induced by the longitudinal shear force. The separations of the specimen were shown at the ultimate load levels. The failure mechanism of the concrete infill element of the tie-bar (Ø16mm) shear connection was the crushing in the longitudinal direction force and tensile splitting in the transverse direction.
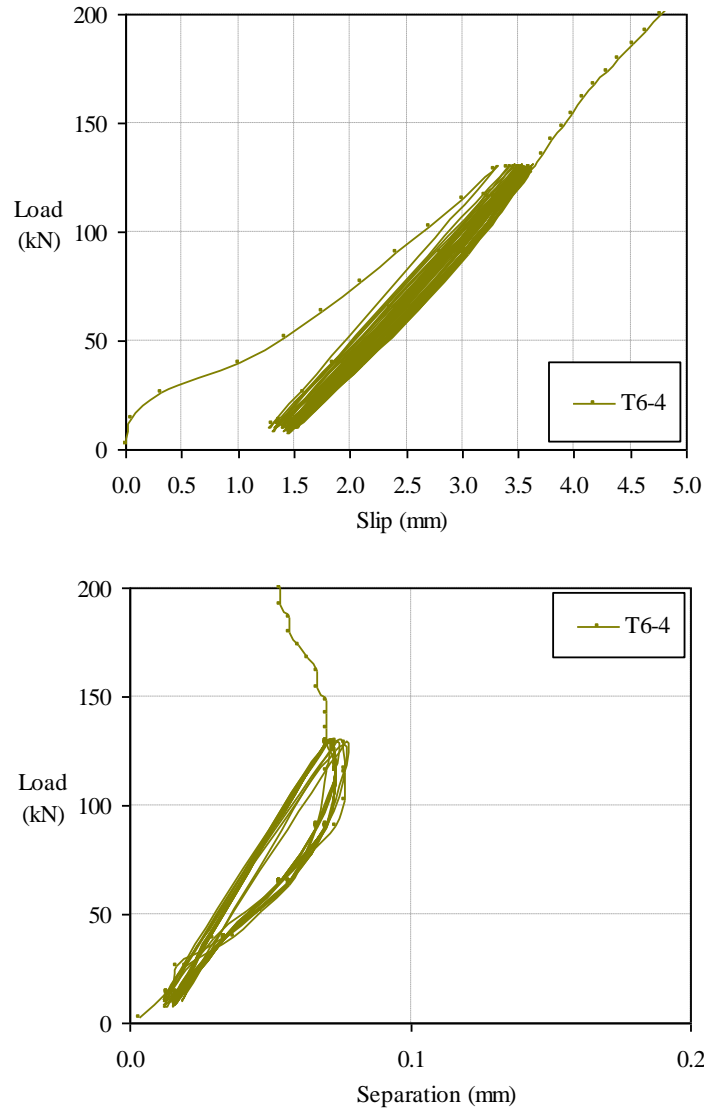
Figure 4.20 Load-slip and load-separation response of the tie-bar (Ø16mm) shear connection during the loading cycles

4.5 Conclusions

The push-out test series-II further investigated the concrete-infill-only and tie-bar (Ø16mm) shear connection. The push-out tests were designed and carried out based on the recommendations of the push-out test series-I. The tie-bar (Ø16mm) shear connection had an additional Ø16mm tie-bar passing through the centre of each web opening. There were four identical specimens in each test group. One specimen of both test groups was tested with the additional loading cycles of 25 times. The geometry of the specimens was the same between the two test groups. The results of the push-out tests were studied. The following conclusions were made:

(12)   The concrete-infill-only shear connection showed the distinctive brittle failure mode with the slip capacity of 4-5mm. The brittle failure mode was due to that the shear connection consisted of solely the concrete infill element, and that concrete was a brittle material.

(13)   In contrast, the tie-bar (Ø16mm) shear connection showed the ductile failure mode with the slip capacity of 12-14mm. It was shown that the tensile strength of the tie-bar became effective combining with the concrete infill element in the tie-bar shear connection, and that the 1m length provided the adequate anchorage resistance to the Ø16mm tie-bar.

(14)   Both types of the shear connection showed a very small amount of slip increase during the loading cycles of 25 times, 0.18 or 0.19mm. The slip increases were due to the crushing of the concrete infill element in the longitudinal shear direction. It showed that the loading cycles had no effects on the overall behaviour of the shear connection and anchorage of the tie-bars.

(15)   By comparing the two types of the shear connection, the additional tie-bars significantly increased the shear resisting capacity and ductility of the shear connection. But the tie-bars had no influence on the slip stiffness of the shear connection.

(16)   The additional Ø16mm tie-bars increased the shear resisting capacity of the shear connection by twofold. It was base on the shear connection of Ø150mm web opening with 30N/mm^2 concrete strength.

(17)   The shear resistance of a concrete-infill-only shear connection of Ø150mm web opening was 1.75 times the shear strength of a headed stud of Ø19mm and 100mm height. This comparison was base on the concrete strength of 30N/mm^2.

(18)   Similarly, the shear resistance of a tie-bar (Ø16mm) shear connection of Ø150mm web opening was 3.7 times the shear strength of a headed stud of Ø19mm and 100mm height. This comparison was base on the concrete strength of 30N/mm^2.

(19)   This tie-bar (Ø16mm) shear connection showed both desired shear resistance and ductility. This type of shear connection required no additional welding which was required for the web-welded stud shear connection. Hence, the tie-bar (Ø16mm) shear connection was an optimum shear connection for the composite shallow cellular floor beams.

4.6 Recommendation

The brittle failure mode of concrete-infill-only shear connection was again shown in the push-out test series-II.

- It was recommended that the concrete-infill-only shear connection should not be used alone to provide shear connection. It should be used in combination with other elements, i.e. tie-bars or studs, to provide the necessary ductility.

The optimum shear resistance and ductility of tie-bar (Ø16mm) shear connection was shown in the push-out test series-II.

- It was recommended the tie-bar (Ø16mm) shear connection should be further investigated in the flexural test.

The push-out tests applied the direct longitudinal shear force to the shear connection. This loading configuration might not fully represent the actual loading of the shear connection in a composite beam.

- It was recommended that flexural tests for the composite shallow cellular floor beams should be carried out to investigate the behaviour and performance of the shear connection in the composite beams.
- It was recommended that the flexural test beam specimen should be designed to represent the actual composite shallow cellular floor beams with a common span range.
- It was recommended that the web opening sizes of the flexural test beam specimen should be the same as that of the push-out test specimens, so that the results of the push-out test could be used in the design for the beam specimen. And the behaviour and performance of shear connection shown in the flexural tests could be compared with that in the push-out tests.

Chapter 5   Analytical study and Finite Element Analysis of the shear connection

The push-out tests, series-I and series-II, provided comprehensive information on the behaviour and shear resisting capacity of the shear connection used for the composite shallow cellular floor beams. The results of the push-out tests were analysed to conclude a calculation method for shear resistance of the shear connection. A parametric study was then carried out using Finite Element Analysis (FEA), to further verify the calculation method in order to establish a design method for shear resistance of the shear connection.

5.1 Introduction

The mathematical analysis on the results of the push-out tests was carried out in order to conclude a calculation method for shear resistance of the shear connection. Base on the failure mechanism shown in the push-out tests, the shear resistance of the shear connection were calculated and compared with the test results. The calculation method is then verified with results of the FEA to establish a design method for shear resistance of the shear connection.

Because of the complex three-dimensional stress-strain state of the concrete infill element, it was difficult to analyse it by using the mathematical model rather than the empirical formula. The FEA of the concrete-infill-only shear connection was carried out to further verify the calculation method concluded in the mathematical analysis. Firstly, a calibrated FEA model of the concrete-infill-only shear connection was developed. Then a parametric study was performed by using the calibrated FEA model to investigate the variables of concrete strength and diameter of web opening. Finally, the results of the FEA parametric study were compared with the calculated shear resistance using the concluded calculation method.

5.2 Mathematical analysis

The push-out test series-I investigated four types of the shear connection used for the shallow cellular floor beams, i.e. concrete-infill-only, tie-bar (Ø12mm), ducting and web-welded stud shear connection. The push-out test series-II further investigated the concrete-infill-only and tie-bar (Ø16mm) shear connection based on the recommendations of the push-out test series-I. The shear connection of both test series were formed by the concrete infills with or without other additional elements, i.e. tie-bar or shear studs, resisting the longitudinal shear force.

Type of Shear connection		Failure Mechanism
Push-out test series-I	Concrete-infill-only	• Top part was crushed in the longitudinal shear direction and the rest of concrete infill was ruptured by tensile splitting in the transverse direction.
	Tie-bar (Ø12mm)	• One of tie-bars was sheared off, as it was in direct contact with the web post; the other one remained intact (there were two bars passing each opening). • The failure mechanism of the concrete infill element was the same as that of the concrete-infill-only shear connection.
	Ducting	• Crushing of the concrete infill element led to the deformations of the ducting. • Concrete infill element was crushed with tensile splitting.
	Web-welded stud	• The headed studs were sheared off with bending near the root. • Concrete around the studs was crushed. • The failure mechanism of the concrete infill element was the same as that of the concrete-infill-only shear connection.
Push-out test series-II	Concrete-infill-only	• The failure mechanism were the same as that of the concrete-infill-only shear connection in the push-out test series-I.
	Tie-bar (Ø16mm)	• The tie-bar did not fail; the possible failure mechanism was tensile failure. • The failure mechanism of the concrete infill element was the same as those of the concrete-infill-only shear connection.

Table 5.1 Summary of the failure mechanism of the shear connection

The development of calculation method for the shear resistance of the shear connection was based on the failure mechanism shown in the push-out tests. The push-out tests demonstrated that the shear connection gained additional strength from the elements of tie-bar or studs, and there was no isolated failure between the concrete infills and the additional elements. Hence, the shear strength of the shear connection should be the combination of the resistance of both concrete infills and additional elements.

The failure mechanism of the shear connection shown in the push-out tests are summarised in Table 5.1. The failure mechanism of the concrete infill element of all shear connection was the same. The top part of the concrete infill element was crushed by the web opening in the longitudinal shear direction and the rest of the concrete infill element was ruptured by tensile splitting in the transverse direction. The cross sectional areas of the concrete infill element in compression (bearing) and tensile splitting are illustrated in Figure 5.1. The shear resistance of the concrete infill element could be calculated by taking account of both compressive (bearing) and tensile (splitting) resistance. This is expressed by a mathematical equation as Eqn. 5.1. For the shear connection other than the concrete-infill-only shear connection, the total shear resistance of the shear connection was the combination of the resistance of the concrete infill element with the resistance of other additional elements (i.e. tie-bar or studs). This mathematical combination is expressed in Eqn. 5.2.

There were two unknown coefficients within the Eqns. 5.1 and 5.2. The steps to obtain these two unknown coefficients are:

(1) To substitute the actual test data into Eqn. 5.2 (the test data includes the shear resisting capacity of the shear connection, concrete strengths and dimensions of the web opening);

(2) To form sets of simultaneous equations with the test data of any two specimens;

(3) Then to solve these sets of simultaneous equations to obtain the two coefficients of a and b ;

(4) To calculate the averages of a and b ;

(5) Finally, to substitute the calculated a and b back into Eqn. 5.2 to calculate the shear resistance of the shear connection, and to compare with the test results.

$$R_{ce} = a\left(f_{cu}A_c\right) + b\left(f_{ct}A_t\right) \tag{5.1}$$

Where: $A_c = tD, \ A_t = \dfrac{\pi D^2}{4}$

R_{ce} is the shear resistance of the concrete infill element;

f_{cu} is the concrete compressive cube strength in N/mm^2;

A_c is the area of concrete in the compression;

f_{ct} is the concrete tensile splitting strength in N/mm^2;

A_t is the area of concrete in the tensile splitting;

t is the thickness of the web;

D is the diameter of the web opening;

a, b are the coefficients.

$$P_c = a\left(f_{cu}A_c\right) + b\left(f_{ct}A_t\right) + R_{add} \tag{5.2}$$

Where: $A_c = tD, \ A_t = \dfrac{\pi D^2}{4}$

P_c is the shear resistance of the shear connection;

f_{cu} is the concrete cube compressive strength in N/mm^2;

f_{ct} is the concrete tensile splitting strength in N/mm^2;

A_c is the area of concrete in the compression;

A_t is the area of concrete in the tensile splitting;

t is the thickness of the web;

D is the diameter of the web opening;

R_{add} is the shear resistance of the additional elements i.e. tie-bar or shear studs;

a, b are the coefficients.

(a)   (b)
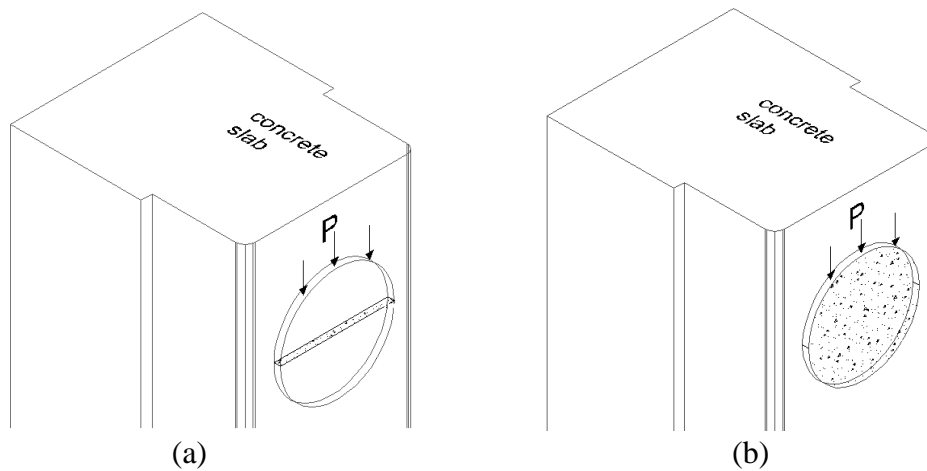
Figure 5.1 Cross sectional areas of the concrete infill element in: (a) compression (bearing), (b) tension (splitting)

The ductile behaviour and failure mode of the tie-bar shear connection clearly showed that the tensile strength of the tie-bars became effective and contributed to the overall shear strength of the shear connection. The tensile resistance of the tie-bar, as expressed in Eqn.5.3, was used in the above calculations for the coefficients of a and b. The material strength of the tie-bars used in the calculation was the results of the coupon tests. The yield strength obtained from the coupon tests for the Ø12mm and Ø16mm tie-bars was 440N/mm^2 and 442N/mm^2 respectively. Details of the coupon tests are presented in Appendix C.

$$R_{tb} = f_y \left(\frac{\pi D_{tb}^2}{4} \right) \tag{5.3}$$

Where: R_{tb} is the tensile resistance of the tie-bar;

f_y is the yield strength of the tie-bar;

D_{tb} is the diameter of the tie-bar.

The failure mechanism of the studs in the web-welded stud shear connection was shear failure, which was one of the dominant failure mechanism in the standard push-out tests for the shear studs. The resistance of studs as the additional resistance, R_{add}, in the above calculations for the coefficients of a and b was determined by using Eqn. 5.4 without the partial safety factor, γ_v. The Eqn. 5.4 was the formula given in Eurocode4 (EN1994-1-1:2004) for the design shear resistance of the headed studs. The stud's material strength used in the calculations was the results of the coupon tests. The yield strength of the studs was 452N/mm^2. There were eight studs combined with three concrete infill elements to form the shear connection for each specimen of the test group T4. Thus, the shear resistance of each shear connection was the combination of the resistance of one concrete infill element with 2.67 studs.

$$P_{Rd} = \frac{0.8 f_U \pi d^2 / 4}{\gamma_V} \tag{5.4}$$

Where P_{Rd} is the design shear resistance of the stud;

f_u is the strength of material of the stud;

d is the diameter of the shank of the stud;

γ_v is the partial factor.

By substituting the test data into Eqn. 5.2, a total of 204 sets of simultaneous equations were formed between any two push-out test specimens. There were in total of 24 test specimens in the two test series, but test results of 21 test specimens were used in

the analysis. The results of specimens, T1-A-N and T1-A-F (test group T1), were omitted from the analysis, as the set up of the push-out tests for these two specimens was different from all other specimens. No plaster (gypsum) was applied on the rig platform for these two specimens; hence, eccentric loading might have caused the specimens to fail at lower load levels. Also, specimen of T4-B-A was omitted from the analysis, as the specimen was not failed due to the capacity of the hydraulic jack was reached.

The coefficients a and b were obtained by solving the simultaneous equations of Eqn.5.2. Then the empirical values of a and b were calculated by taking averages; $a = 1.6758$ and $b = 1.4355$. Hence, Eqns. 5.1 and 5.2 became Eqns. 5.5 and 5.6, respectively as:

$$R_{ce} = 1.6758 \left(f_{cu} A_c \right) + 1.4355 \left(f_{ct} A_t \right) \tag{5.5}$$

$$P_c = 1.6758 \left(f_{cu} A_c \right) + 1.4355 \left(f_{ct} A_t \right) + R_{add} \tag{5.6}$$

Where: $A_c = tD$

$$A_t = \frac{\pi D^2}{4}$$

R_{ce} is the shear resistance of the concrete infill element;

P_c is the shear resistance of the shear connection;

f_{cu} is the concrete cube compressive strength in N/mm^2;

f_{ct} is the concrete tensile splitting strength in N/mm^2;

A_c is the area of concrete in the compression;

A_t is the area of concrete in the tensile splitting;

t is the thickness of the web;

D is the diameter of the web opening;

R_{add} is the shear resistance of the additional elements i.e. tie-bar or shear studs.

Finally, the push-out test results were compared with the calculated shear resistance of the shear connection using Eqn. 5.6. The actual concrete strengths of the specimens were used in the calculations. The comparison is shown in Table 5.2. It was shown that the results of the calculations were very close to the test results. The overall ratio of calculated shear resistance to test results was 0.935. This demonstrated that the empirical coefficients determined for Eqn. 5.6 was reliable. Also, it was further demonstrated that the method was valid for expressing shear resistance of the shear

connection using the compressive and tensile resistance of the concrete infill element combined with the resistance of other additional elements (i.e. tie-bar and studs).

The two specimens omitted from the analysis, T1-A-N and T1-A-F, also showed higher ratios of calculated shear resistance to test results, as listed in Table 5.2. It was necessary to discuss for the ducting shear connection, which showed very small shear resistance in the push-out tests. The ducting itself provided very small shear resistance due to its geometry and thickness. The other factor causing the small shear resistance for the ducting shear connection was the amount of the concrete infill element surrounding the ducting was very small. The ducting buckled when the concrete infill was crushed by the web opening in the direction of the longitudinal shear force. As the shear resistance of the ducting shear connection would barely contribute towards the overall shear transferring mechanism, hence the shear resistance of the ducting shear connection should not be included into the future design calculation.

The shear connection investigated in this research were similar to the Perfobond rib shear connection reviewed in Chapter 2, which had concrete dowels passing through the holes that perforated on the ribs. The ribs were welded onto the top flange of the steel section. The concrete dowels combined with or without rebar to transfer longitudinal shear force. But the concrete dowels of the Perfobond rib shear connection were about 35mm to 50mm in diameter which were much smaller than the concrete infills of 150 and 200mm diameter investigated in this research. The failure mechanism of the concrete dowels of the Perfobond rib was mainly due to the shear failure with crushing. Oguejiofor and Hosain (1992) (2) concluded a design formula, Eqn. 2.15, for the shear capacity of the Perfobond rib shear connection, using $\sqrt{f_c'}$ to represent the shear strength and the compressive (bearing) strength of the concrete dowels; where f_c' is the concrete compressive strength. Nevertheless, Oguejiofor and Hosain (1997) modified (or corrected) the design formula, as shown in Eqn. 2.17, using $\sqrt{f_c'}$ to represent the shear strength and f_c' to represent the compressive strength of the concrete dowels.

As the push-out tests demonstrated the compressive and tensile splitting failure of the concrete infill elements, therefore it was incorrect to calculate the resistance of the concrete infill elements based on the shear failure mechanism. Thus, the term of

$\sqrt{f_c^{'}}$ should not be used to calculate the resistance of the concrete infill elements, as $\sqrt{f_c^{'}}$ represented the shear strength, rather than the compressive or tensile strength.

The method of calculation and formula, Eqn. 5.6 concluded for the shear resistance of the shear connection in the above mathematical analysis would be further verified by using the Finite Element Analysis (FEA) presented in the next section.

Specimen No.	f_{cu} (N/mm^2)	f_{ct} (N/mm^2)	A_c (mm^2)	A_t (mm^2)	$f_{cu}A_c$ (kN)	$f_{ct}A_t$ (kN)	R_{add} (kN)	Calculation * P_c (kN)	Test results (kN)	Ratio (cal/test)
T1-A-N	56.5	4.53	1290	17671	72.89	80.05	--	237	118	~~2.009~~
T1-A-F	58.1	4.85	1290	17671	74.95	85.71	--	249	131	~~1.898~~
T1-B-N	56.5	4.53	1980	31416	111.87	142.31	--	392	362	1.082
T1-B-F	58.1	4.85	1980	31416	115.04	152.37	--	412	397	1.037
T2-A-N	54.5	4.54	1290	17671	70.31	80.23	100	333	309	1.078
T2-A-F	51.9	4.07	1290	17671	66.95	71.92	100	315	305	1.034
T2-B-N	54.5	4.54	1980	31416	107.91	142.63	100	486	390	1.245
T2-B-F	51.9	4.07	1980	31416	102.76	127.86	100	456	372	1.225
T3-A-N	55.2	3.91	215 ^	5400	11.87	21.11	--	50	47	1.068
T3-A-F	51.5	3.89	215 ^	5400	11.07	21.00	--	49	50	0.974
T3-B-N	55.2	3.91	495 ^	13744	27.32	53.74	--	123	125	0.983
T3-B-F	51.5	3.89	495 ^	13744	25.49	53.47	--	119	137	0.872
T4-A-N	67.0	4.66	1290	17671	86.43	82.35	272	535	504	1.062
T4-A-F	50.2	4.08	1290	17671	64.76	72.10	272	484	427	1.134
T4-B-N	67.0	4.66	1980	31416	132.66	146.40	272	--	--	--
T4-B-F	50.2	4.08	1980	31416	99.40	128.18	272	623	497	1.253
P5-1	35.0	3.21	1290	17671	45.15	56.73	--	157	227	0.693
P5-2	35.0	3.21	1290	17671	45.15	56.73	--	157	194	0.808
P5-3	32.0	2.9	1290	17671	41.28	51.25	--	143	179	0.798
P5-4	30.0	3.02	1290	17671	38.70	53.37	--	141	164	0.865
P6-1	29.0	2.85	1290	17671	37.41	50.36	90	225	391	0.575
P6-2	32.0	2.92	1290	17671	41.28	51.60	90	233	386	0.604
P6-3	28.0	2.49	1290	17671	36.12	44.00	90	214	327	0.654
P6-4	27.0	2.57	1290	17671	34.83	45.42	90	214	358	0.597
* Calculation uses Eqn. 5.6 with coefficients of a = 1.6758 and b = 1.4355. ^ Compressive area, A_c, calculated by using $t(D-D_d)$ where t is web thickness, D is web opening diameter, D_d is diameter of ducting.									Overall ratio	0.935

Table 5.2 Comparison of test results with calculated shear resistance using Eqn. 5.6

5.3 FEA of the concrete-infill-only shear connection

The shear connection used for the composite shallow cellular floor beams was formed by the unique feature of the web openings. The shear transferring mechanism was different from the conventional shear studs. Two series of push-out tests were carried out to investigate the behaviour and shear resisting capacity of the shear connection. In order to further verify the concluded method of calculation for shear resistance of the shear connection, the FEA was performed.

The tests results showed that the concrete infill elements were difficult to analyse using conventional mathematical models, as the concrete infill elements were in a complex stress-strain state. For this reason, the FEA was used to study the concrete-infill-only shear connection. A software package, ANSYS (11.0), was used to carry out the FEA. The results of the FEA were compared with the results of the push-out tests to establish a calibrated FEA model. A parametric study was then carried out using calibrated FEA model to investigate variables of concrete strength and diameter of the web openings. The FEA parametric study enables the verification of the shear resistance calculation method developed in the mathematical analysis.

5.3.1 Geometrical modelling

The concrete-infill-only shear connection of 150mm diameter was first geometrically modelled using the geometrical properties of the push-out test specimens. Due to the symmetric geometry of the test specimens, only a quarter of the specimen was modelled with appropriate boundary conditions. The model, as shown in Figure 5.2a, contained only one shear connection rather than three shear connection in the push-out test specimens. The purpose was to save the computing cost of the FEA.

The concrete slabs were modelled using Solid65, a three-dimensional solid element. The schematic illustration of the element is shown in Figure 5.3a. This element had plasticity, creep, swelling, stress stiffening, large deflection and large strain capabilities. Most significantly, the element was capable of modelling cracking in tension and crushing in compression. The element was defined by eight nodes with three degrees of freedom at each node: translations in the nodal x, y and z directions.

The steel section was modelled using Solid95, a solid element. The schematic illustration of this 3-D element is shown in Figure 5.3b. The element tolerated irregular shapes without losing much of its accuracy. This element was well suited to model curved boundaries. The Solid95 element was defined by 20 nodes with three degrees of

freedom per node: translations in the nodal x, y and z directions. The element had plasticity, creep, stress stiffening, large deflection and large strain capabilities.

The geometry model was then meshed using the designated mesh tool with controlled element sizes. The steel volume was meshed using a size of 12mm elements. The concrete volume was meshed using three different sizes of the element, i.e. 15, 30 and 50mm, as shown in Figure 5.2b. The region close to the steel section and containing the concrete-infill-only shear connection was meshed using the element size of 15mm. The regions away from the shear connection were meshed with 30mm elements and 50mm elements for far end section. The element size of 15mm used to mesh the shear connection was determined base on the element size analysis shown in Appendix D. The 15mm was an optimum element size for modelling concrete material, as bigger element sizes would lose accuracy and smaller element sizes would increase computational cost without the increase of accuracy.

(a)   (b)
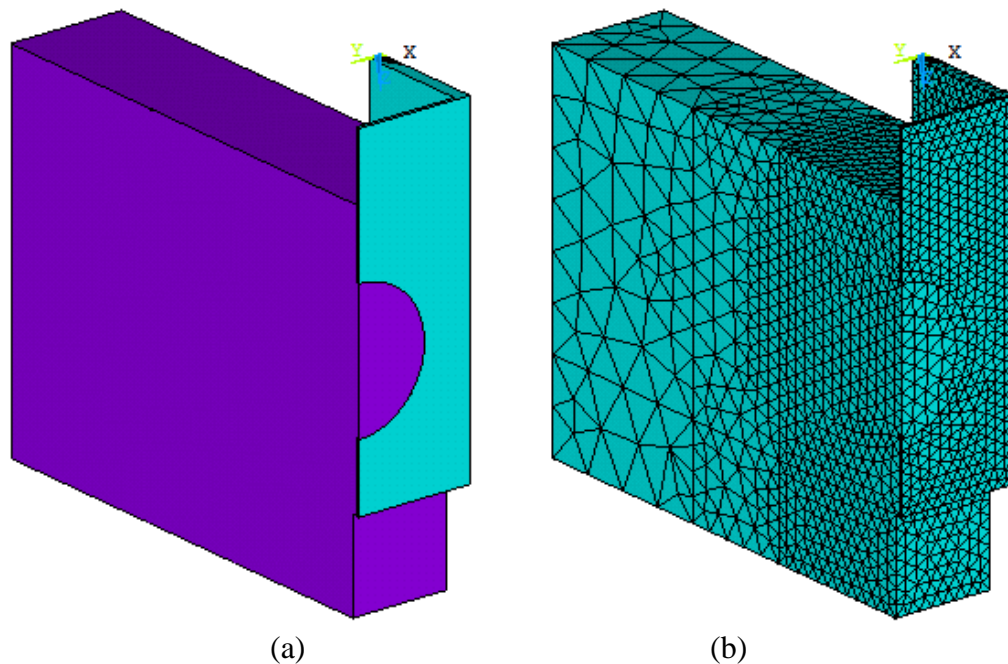
Figure 5.2 FEA model of a 1/4 of the test specimen with one concrete-infill-only shear connection of Ø150mm (a) geometry model, (b) meshed model

5.3.2 Material modelling

The measured material properties obtained in the push-out test were used as the material property inputs for the FEA calibration. The theoretical backgrounds of the concrete and steel material model are explained in the following two sections.

(a)   (b)
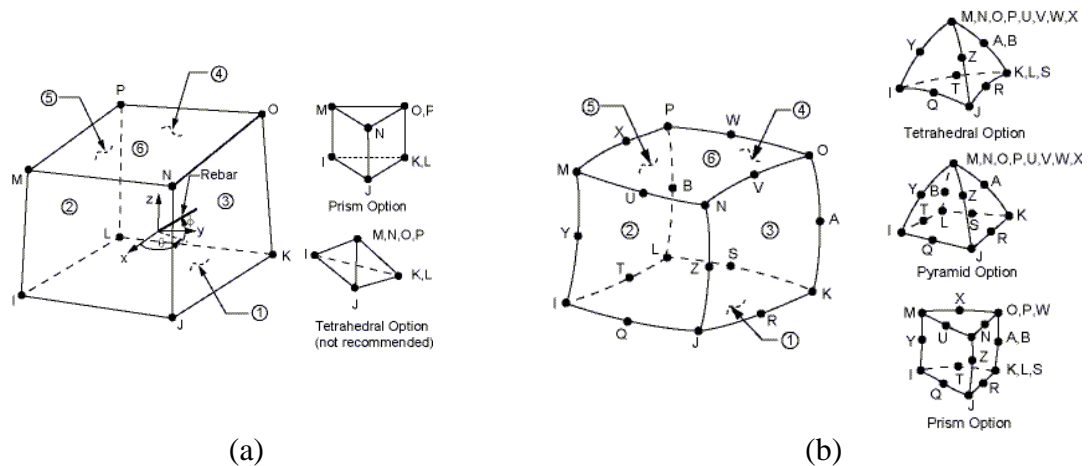
Figure 5.3 (a) Concrete element of Solid65; (b) Steel element of Solid 95

5.3.2.1 Concrete material model

The concrete element of Solid65, shown in Figure 5.3a, predicted brittle failure with cracking and crushing failure modes. The concrete material was assumed to be initially isotropic. The modulus of the elasticity of concrete, E_{cm} and the Poisson's ratio, υ, were defined for the elastic behaviour of the concrete. The input of the E_{cm} for the FEA calibration was determined based on Eurocode 2 (EN1992-1-1:2004), as shown in Eqn. 5.7. In accordance with the Eurocode 2 (EN1992-1-1:2004), the Poisson's ratio of concrete was taken as 0.2 for all strengths of concrete.

$$E_{cm} = 22[f_c /10]^{0.3} \tag{5.7}$$

Where: E_{cm} is the modulus of elasticity of concrete in 10^3N/mm^2;

f_c is the mean compressive strength in N/mm^2.

The material nonlinearity for concrete was discribed by a stress-strain curve implemented in the FEA. This stress-strain curve was considered as an isotropic material property together with the failure surface model defined by the FEA to model the concrete material. The concrete stress-strain curve for the FEA, as shown in Figure 5.4, had three sections, namely: linear elastic, parabolic nonlinearity and constant stress plateau. In accordance with Eurocode 2 (EN1992-1-1:2004), the linear elastic region was defined by the modulus of elasticity of concrete, E_{cm}, and 40% of the compressive strength as the stress limit for linear elastic. Within the parabolic region up to the peak stress, the stress and strain were determined by using Eqn. 5.8 given in Eurocode2 (EN1992-1-1:2004). Beyond the peak stress, f_c, the concrete strain would reach the maximum value of 0.0035 for all strength classes of concrete.

145

The actual declining strength of concrete after a strain of 0.0035 was not included in the material model for the FEA. It was very difficult or impossible to obtain the convergence by including the declining strength, as the numerical solution for the FEA would become highly discontinuous if the declining strength of concrete was included. These local instabilities often generated large amount of crushing which caused the model fail prematurely. The FEA used the maximum strain criteria to determine the concrete whether destruction. Crushing of the concrete started to develop in the elements located directed under the loads. Subsequently, adjacent elements crushed as load increases. Finally, the FEA model converged or the global solution finished when the convergence criteria were satisfied. These convergence criteria consisted of force and displacement tolerances. The values of these convergence criteria for the FEA were the default setting of the FEA program. The default setting was demonstrated as adequate in the later calibration study on the concrete-infill-only shear connection, as no convergence difficulties were encountered.
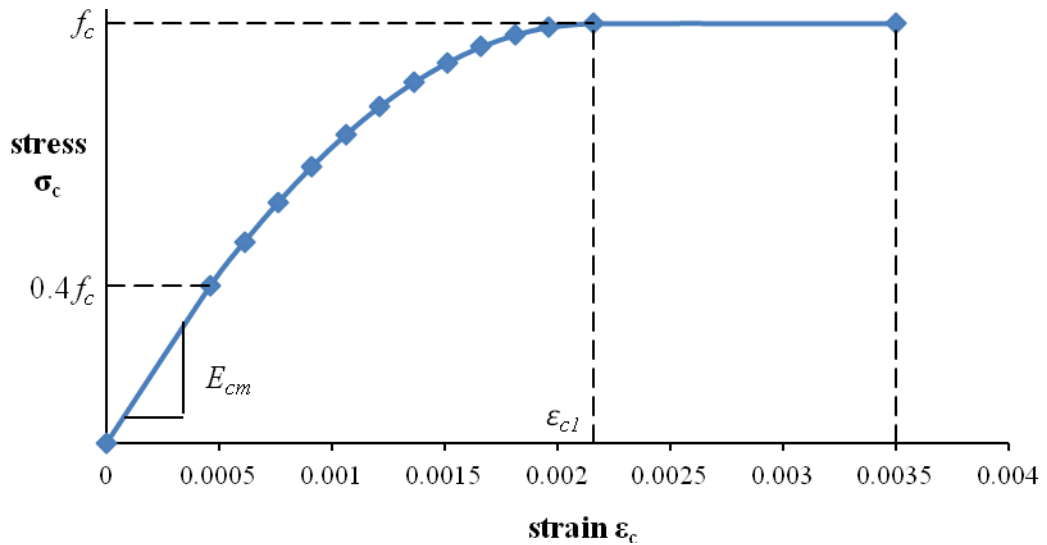
Figure 5.4, Concrete stress-strain curve for the FEA

$$\frac{\sigma_c}{f_c} = \frac{k\eta - \eta^2}{1 + (k-2)\eta} \tag{5.8}$$

Where: σ_c is the concrete compressive stress in N/mm^2;

f_c is the compressive strength in N/mm^2;

$k = 1.05 E_{cm} \times \varepsilon_{c1} / f_c$

$\eta = \varepsilon_c / \varepsilon_{c1}$

ε_c is the concrete compressive strain;

146

ε_{c1} is the concrete compressive strain at the peak stress;

$$\varepsilon_{c1} = \left(0.7 f_c^{\,0.31}\right)/10^3$$

The failure behaviour of concrete was defined as a failure surface model in the FEA. The criterion for the failure surface model due to multiaxial stress state is expressed in Eqn. 5.9 (ANSYS 11.0) as:

$$\frac{F}{f_c} - S \geq 0 \tag{5.9}$$

Where: F is a function of the principle stress state (σ_{xp}, σ_{yp}, σ_{zp},);

             S is the failure surface expressed in terms of principle stresses and five parameters (f_t, f_c, f_{cb}, f_1 and f_2) defined in Table 5.4;

             f_c is the uniaxial crushing (compressive) strength.

If Eqn. 5.9 was not satisfied, the material would not crack or crush. Otherwise, the material would crack if any principle stress was tension, while crushing would occur if all principle stresses were compression. A total of five input strength parameters were needed to define the failure surface, i.e. f_t, f_c, f_{cb}, f_1 and f_2, as listed in Table 5.3. The failure surface could be specified with a minimum of two parameters, f_t and f_c. The other three were defaults determined by Willam and Warnke (1974) as:

$$f_{cb} = 1.2 f_c \tag{5.10}$$

$$f_1 = 1.45 f_c \tag{5.11}$$

$$f_2 = 1.725 f_c \tag{5.12}$$

However, these default values were valid only for stress states where the following condition was satisfied:

$$|\sigma_h| = \sqrt{3} f_c \tag{5.13}$$

Where: σ_h = hydrostatic state $= \dfrac{1}{3}\left(\sigma_{xp} + \sigma_{yp} + \sigma_{zp}\right)$.

A shear transfer coefficient, β_t, for open cracks was defined in the concrete material model, representing a shear strength reduction factor for loads which induced sliding across the crack face. If the cracks closed, then all compressive stresses normal to the crack plane were transmitted across the crack and only a shear transfer coefficient, β_c, for close cracks was used in the model. Typical shear transfer coefficients ranged from 0 to 1.0, with 0 representing a smooth crack (complete loss of

shear transfer) and 1.0 representing a rough crack (no loss of shear transfer). This specification was made for both the closed and open cracks.

The concrete material inputs for the FEA calibration are summarised in Table 5.3. The uniaxial compressive strength, f_c, was the mean compressive strength obtained in the push-out tests. The uniaxial tensile strength, f_t, was the mean cylinder splitting strength obtained in the push-out tests. The biaxial compressive strength, f_{cb}, was determined by using Eqn. 5.10. The concrete stress-strain curves for uniaxial compressive strength of 30, 32 and 35N/mm^2 are shown in Appendix L.

The input of β_t and β_c were 0.25 and 0.75 respectively, which enabled some shear transfer for the material model. The results of the FEA calibration showed that the variation in these two parameters had almost no influence on the behaviour and results of the shear connection.

The input of the parameters of σ_h^a, f_1 and f_2 should have been omitted, as the push-out tests were not carried out in a hydrostatic stress state. However, the model was unable to run if these inputs were left blank or zero. A very small input of 10E-6 was chosen for these parameters. The input of the stiffness multiplier, μ_s, was the default value of 0.6.

Parameters	Descriptions	Input		
E_{cm}	Modulus of the elasticity of concrete (10^3N/mm^2)	32800	33300	34000
υ	Poisson's ratio	0.2	0.2	0.2
β_t	Shear transfer coefficient for an open crack	0.25	0.25	0.25
β_c	Shear transfer coefficient for a close crack	0.75	0.75	0.75
f_t	Ultimate uniaxial tensile strength (N/mm^2)	2.85	3.0	3.25
f_c	Ultimate uniaxial compressive strength (N/mm^2)	30	32	35
f_{cb}	Ultimate biaxial compressive strength (N/mm^2)	36	38.4	42
σ_h^a	Ambient hydrostatic stress state	10E-6	10E-6	10E-6
f_1	Ultimate compressive strength for a state of biaxial compression superimposed on σ_h^a	10E-6	10E-6	10E-6
f_2	Ultimate compressive strength for a state of uniaxial compression superimposed on σ_h^a	10E-6	10E-6	10E-6
μ_s	Stiffness multiplier for cracked tensile condition (default=0.6)	0.6	0.6	0.6

Table 5.3 Concrete material property inputs for the FEA calibration

5.3.2.2 Steel material model

The steel section of the push-out test specimens showed no yielding or plastic deformations in the push-out tests. In order to capture the full response of the steel section, material nonlinearity was also included in the steel material model for the FEA.

Bilinear kinematic hardening was used with von Mises yield criteria to model the elasto-plastic behaviour of steel. This bilinear kinematic hardening was described by a bilinear stress-strain curve, as shown in Figure 5.5. The initial slope of the curve was the elastic modulus of the material. At a specified yield stress, the curve continued along the second slope defined by the tangent modulus. The kinematic hardening assumed that the yield surface remained constant in size and that the surface translated in the stress space with progressive yielding, as illustrated in Figure 5.6.

The steel material property inputs are summarised in Table 5.4. The steel yield stress and tangent modulus were obtained in the coupon tests.

Young's Modulus	Poisson's Ratio	Yield Stress	Tangent Modulus
200 (10^3N/mm^2)	0.3	420 (N/mm^2)	15 (10^3N/mm^2)

Table 5.4 Material properties of the steel used for the FEA calibration
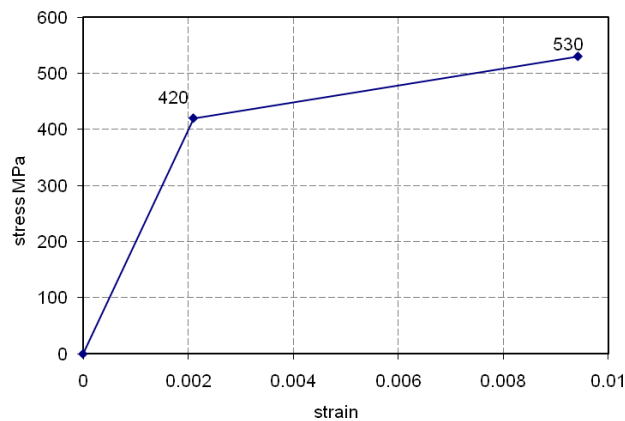
Figure 5.5 Idealised steel stress-strain curve based on the coupon test results

(a)   (b)
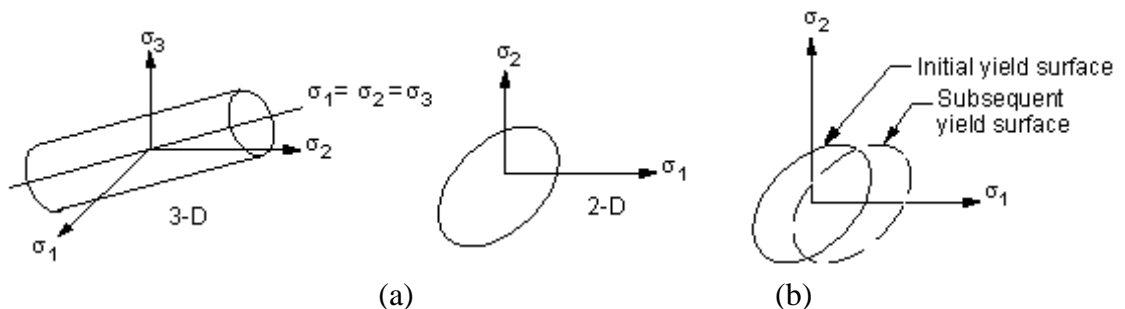
Figure 5.6 (a) Failure surface of bilinear kinematic hardening; (b) Schematic kinematic hardening (ANSYS 11.0)

5.3.3 Boundary conditions

Boundary conditions were applied on the support and planes of symmetry. All degrees of freedom were restricted for the nodes on the support. The nodes on the cutting plane of the steel web and concrete infill element were restricted in the x direction due to symmetry. Similarly, the nodes on the cutting plane of the concrete slab were restricted in the y direction due to symmetry, as shown in Figure 5.7.
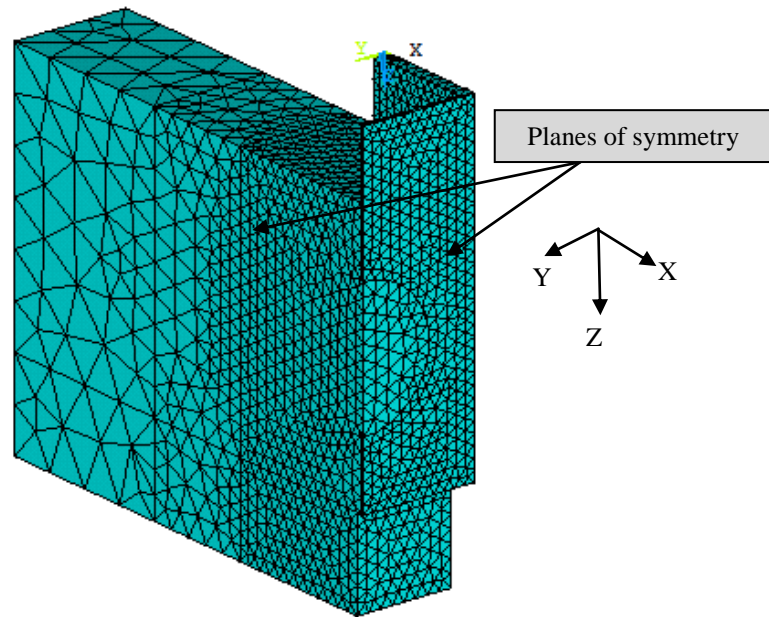
Figure 5.7 Planes of symmetry for the boundary conditions

5.3.4 Contact model

The interaction between the steel elements and concrete element was modelled using contact elements for the FEA calibration. Contact models were highly nonlinear and their response could have made solution convergence difficult. It was therefore paramount to define a correct contact model for the FEA, as the amount of penetration between the two materials should be equal to the slip results of the shear connection.

The model used for the FEA was treated as a rigid-to-flexible contact problem. The steel section was considered as a rigid volume, which had a higher stiffness relative to the deformable concrete volume. The steel elements at the interface were modelled as a target surface using the element, TARGE170. The concrete elements at the interface were modelled as a contact surface using the element, CONTA174. Both contact elements were capable of modelling 3-D curved surfaces and permitting large sliding. The behaviour of the contact model for the FEA was largely influenced by several factors, which are discussed in the following three sections.

Initial contact conditions

The rigid body motions were constrained only by the presence of the contact elements in the FEA for the shear connection. It had to be designed in such a way that the contact pairs would be in contact in the initial geometry. In the other words, the contact pairs had to be "just touching". The initial penetration was excluded in the contact model for the FEA calibration to ensure the correct initial contact. These small initial penetrations were caused by numerical round-off during the mesh generation.

Penetration tolerance

The penetration tolerance, FTOLN, was used in conjunction with the augmented Lagrangian method, the default contact algorithm for surface-to-surface contact elements. FTOLN was a factor based on the thickness of the element to specify an allowable maximum penetration for the augmented Lagrangian method. If any penetration larger than this tolerance was detected, the global solution would be unconverged, even though the residual forces and displacements were within the convergence criteria. The default FTOLN was 0.1. The FEA calibration showed that the default, 0.1, caused an excessive number of iterations and non-convergence at very small slips. By using an FTOLN of 1.0, a good comparison for the slips between the FEA and the push-out tests was achieved.

Contact stiffness

The amount of penetration between the two surfaces was dependent on contact stiffness. Higher contact stiffness could lead to a decrease in the amount of penetration and convergence difficulties. The FEA program estimated a default value for the contact stiffness based on the material properties of the underlying deformable elements. A real constant, FKN, was used to specify either a scaling factor or an absolute value for contact stiffness. If the FKN was underestimated, global convergence difficulties might be caused by too much penetration rather than by residual forces. If the FKN was overestimated, global convergence might require many equilibrium iterations for achieving convergence tolerance of forces and displacement rather than penetration. An optimum FKN of 0.08 was achieved for the FEA calibration.

5.3.5 Application of load

The pressure was applied as load to the steel section in the FEA. The total amount of load was divided into a number of substeps in the FEA to simulate the incremental loads applied in the push-out tests. The Automatic Time Stepping (ATS) was enabled in the FEA to ensure that the optimum load increment was used when the nonlinear response of the model occurred. The ATS option also permitted bisection to allow recovery if convergence failed.

By default, the FEA automatically enabled the Newton-Raphson option. The line search option in the FEA was turned on to improve a Newton-Raphson solution by scaling the solution vector by a scalar value called the line search parameter.

5.3.6 The calibration results

The FEA of the concrete-infill-only shear connection was carried out by using the material strengths obtained in the push-out tests. The results of the FEA were calibrated with the results of the push-out tests. The results of the test group T5 were used in the calibration to compare with the results of FEA, as the test group had four identical specimens and the test results were consistent.

The comparisons for the failure loads and slips between the push-out tests and the FEA are summarised in Table 5.5. The identical slip stiffness was shown between the results of the FEA and push-out tests are illustrated in Figures 5.8 and 5.9. Both failure loads and slips of the FEA were very close to those of the push-out tests. The average ratio for the failure loads between the results of the FEA and push-out tests was 0.9. The average ratio for the slips between the results of the FEA and push-out tests was 1.01.

Test Reference	Concrete strength f_c (MPa)	Failure load			Slip		
		Push-out Test (kN)	FEA (kN)	Ratio (Test/FEA)	Push-out Test (mm)	FEA (mm)	Ratio (Test/FEA)
T5-1	35	227	221	1.03	4.84	4.51	1.07
T5-2	35	194	221	0.88	3.90	4.51	0.86
T5-3	32	182	212	0.86	3.92	4.21	0.93
T5-4	30	164	196	0.84	4.44	3.83	1.16
			average	0.90		average	1.01

Table 5.5 Comparisons between the results of the push-out tests and FEA

The brittle failure mode of the concrete-infill-only shear connection was shown by the FEA, as illustrated in Figures 5.8 and 5.9. The FEA models converged at the failure point as the maximum load was reached. The slip and stress contour plots of the FEA for the model with f_c of 30N/mm^2 are shown in Figures 5.10 and 5.11, respectively. The Figure 5.11 contained stress plots of three different dimensions, namely vertical direction (compression), direction in line with the web post, and transverse direction (tensile splitting).

The stress plots clearly demonstrated the compression and tension region of the concrete infill shear connection when subjected to the direct longitudinal shear force. The compression region was at the top part of the concrete infill, as shown in Figure 5.11a. It was shown that the ultimate compressive strength of the concrete was reached, but the yield stress of the steel was not reached. The tensile splitting region of the shear connection was also clearly shown in the stress plot, Figure 5.11c, as the tensile stress reaches 2.969N/mm^2 which was slightly greater than the concrete tensile strength of 2.90N/mm^2. These stress results of the FEA confirmed the failure mechanism of the shear connection concluded from the push-out tests, which the failure of the concrete infill element was due to the combination of compression and tension. The contour plots for the FEA models with the concrete compressive strength, f_c, of 32N/mm^2 and 35N/mm^2 are shown in Appendix E.

The calibration had shown the excellent agreements between the results of the FEA and push-out tests, in the terms of the failure load, slip, stress results and failure mode. It was demonstrated that the FEA model used for the calibration was reliable and could be used to carry out a parametric study on the concrete-infill-only shear connection, in order to further verify the Eqn. 5.6 which was the formula obtained for the shear resistance of the shear connection from the mathematical analysis, as shown in Section 5.2.
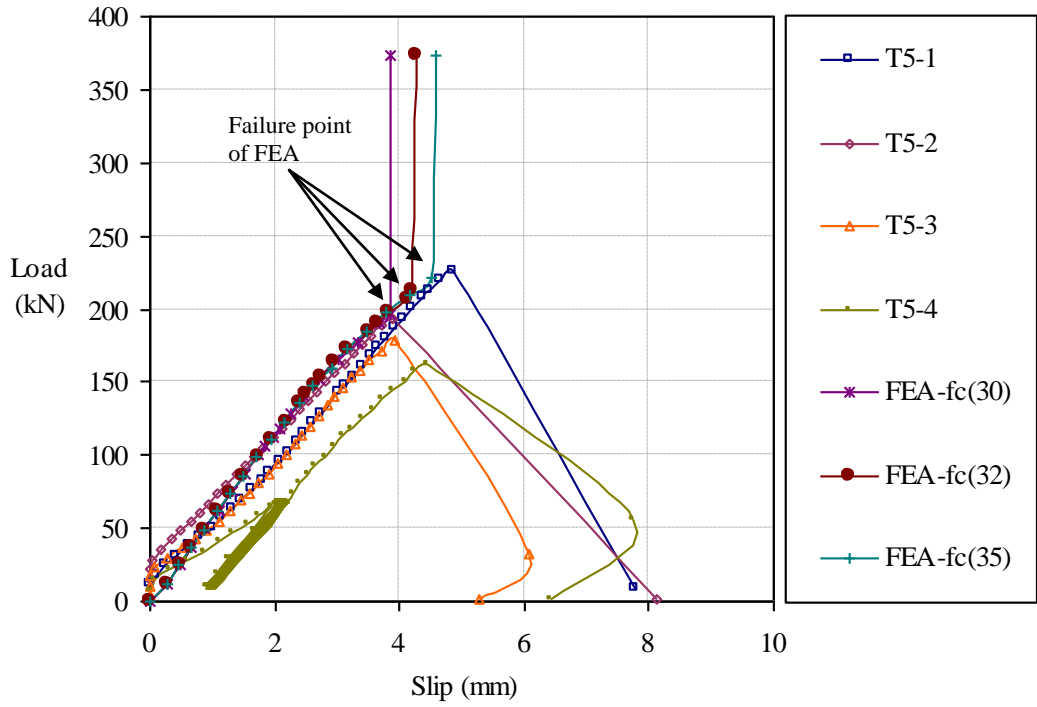
Figure 5.8 Comparison of load-slip curves between FEA models and push-out tests
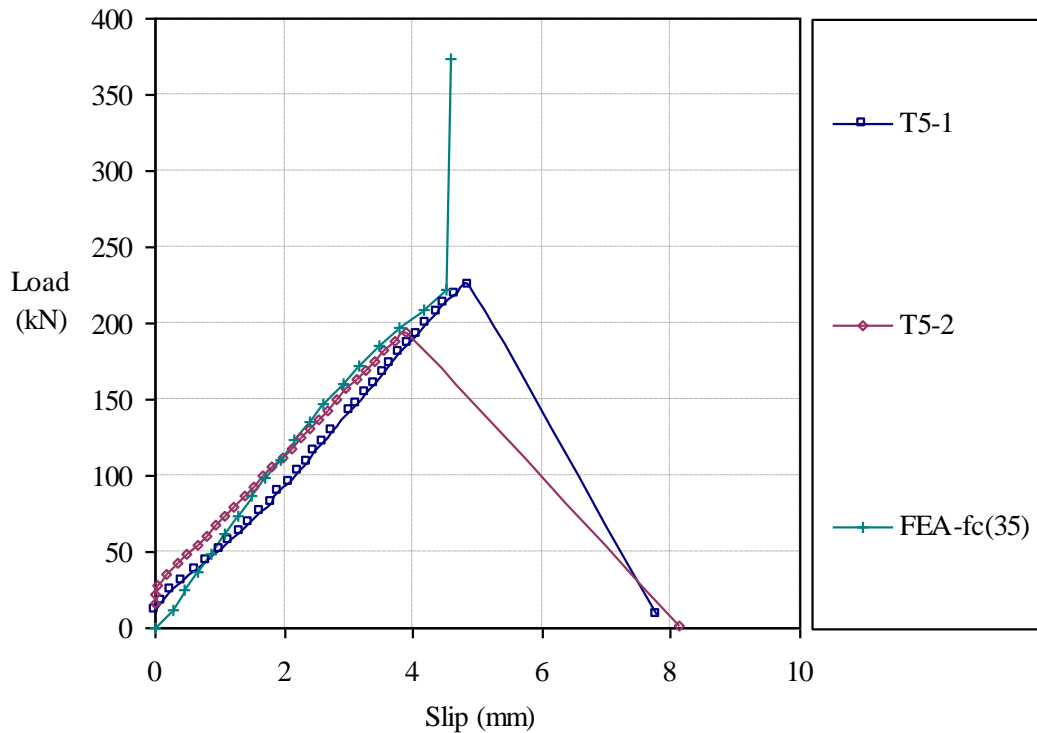
Figure 5.9 Comparisons of load-slip curves between the FEA model and push-out tests for the concrete compressive strength, f_c, of 35 N/mm^2

154

(a)   (b)
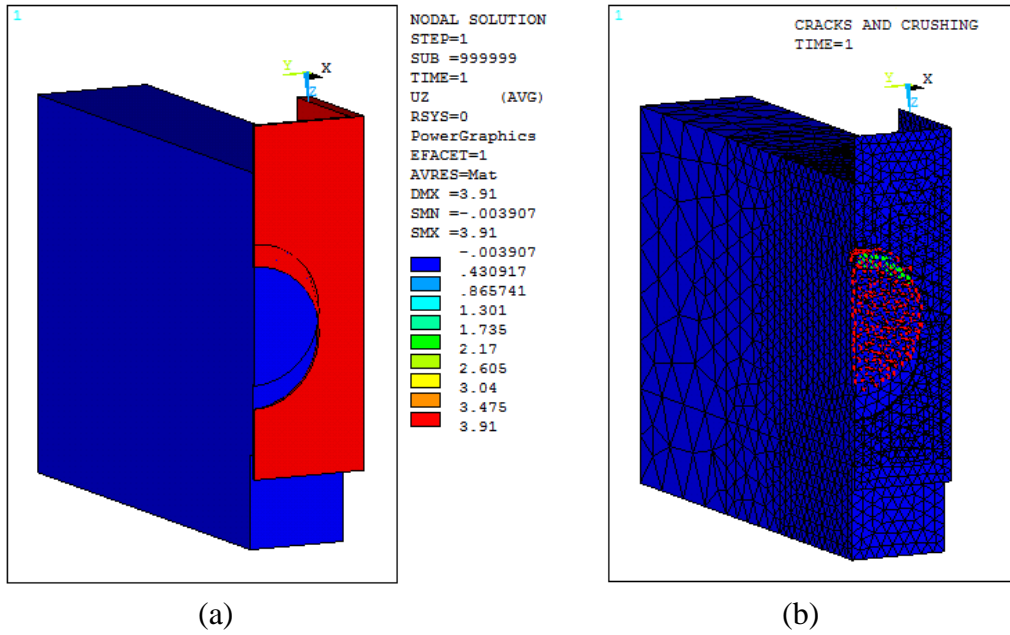
Figure 5.10 Contour plots of: (a) vertical displacement (slips); (b) cracks

(a)

(b)

(c)
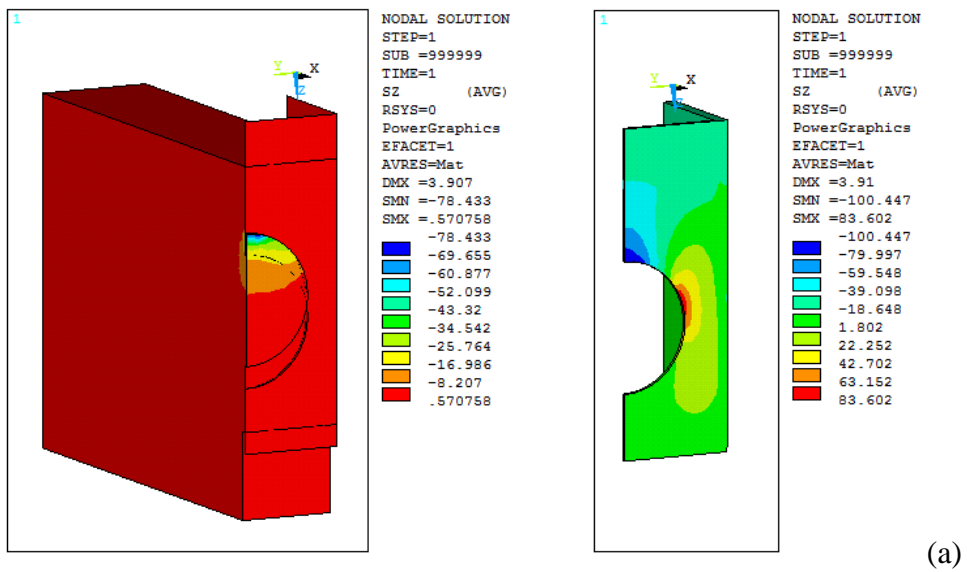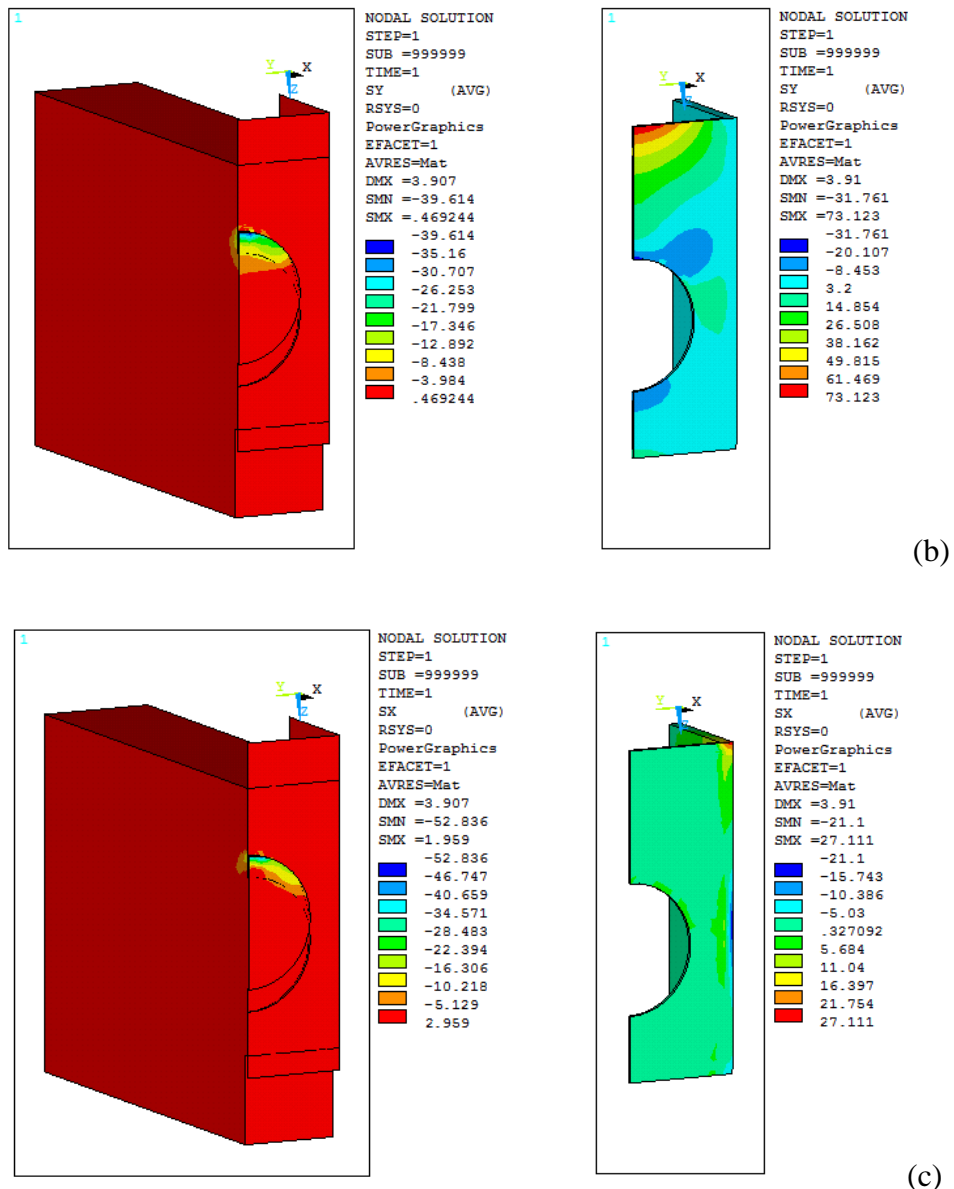
Figure 5.11 Stress contour plots of concrete and steel volumes: (a) compression (vertical direction), (b) stress in line with web post (y-directional), (c) tensile (x-direction)

5.3.7 Parametric study

The calibrated FEA model of the concrete-infill-only shear connection was used to carry out a parametric study. The variable parameters investigated in the FEA parametric study were strength of concrete and diameter of the web opening. The concrete strength was varied between 25 to 60N/mm^2, and the web opening diameter was varied between 100, 150 and 200mm.

The FEA models for the concrete-infill-only shear connection with Ø100mm and Ø200mm web openings were developed. These FEA models contained the same types of elements, boundary conditions and contact model with that calibrated FEA model

with Ø150mm web opening. The FEA model with Ø100mm web opening, as shown in Figure 5.12a, had the same geometry properties as that of the calibrated FEA model with Ø150mm web opening apart from the size of the web opening. The FEA model with Ø200mm web opening was developed by using the geometry properties of the push-out test specimens, T1-B-N or T1-B-F, which had web openings of Ø200mm. The meshed FEA model with Ø200mm web opening is shown in Figure 5.12b.

The results of the FEA parametric study are summarised in Table 5.6. The load-slip curves of the FEA models with the web opening diameter of 100, 150 and 200mm, are illustrated in Figures 5.13, 5.14 and 5.15 respectively. These load-slip curves demonstrated that the FEA models with the same web opening diameter had the same slip stiffness, but the failure loads and slips varied with the concrete strengths.

The slip results were also compared for the FEA models with different web opening diameters at the concrete strengths of 30, 45 and 60N/mm^2, as shown in Figures 5.16, 5.17 and 5.18 respectively. It was shown that slip stiffness of the concrete-infill-only shear connection was influenced by the diameters of the web openings, as the slip stiffness of the FEA models increased with the increase of web opening diameter. The FEA of the concrete-infill-only shear connection also demonstrated that the failure loads were dependent on the diameter of the web opening. For the shear connection with the same concrete strengths, the failure loads increased with the increase of web opening diameters.

(a)   (b)
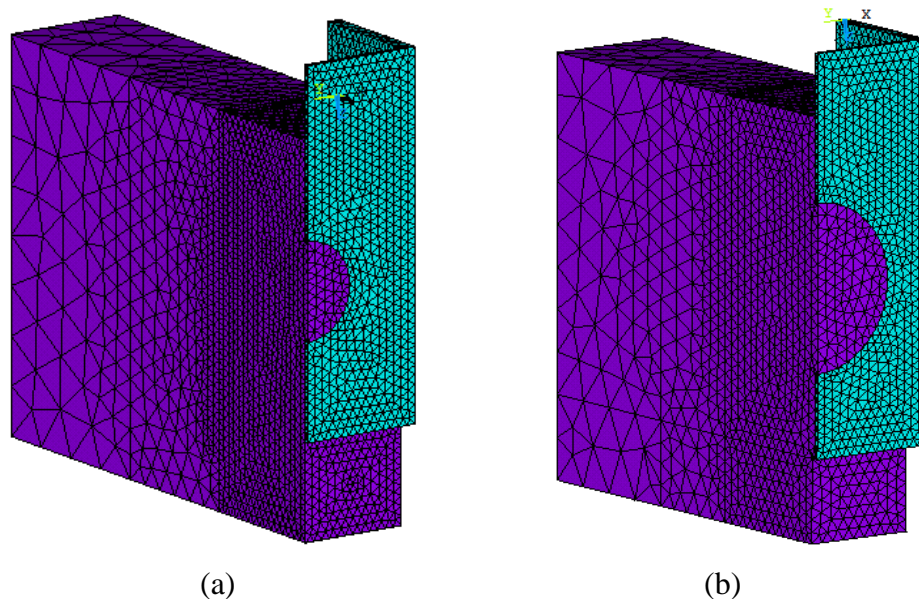
Figure 5.12 FEA models of the concrete-infill-only shear connection with web opening diameters of (a) 100mm, (b) 200mm

Concrete Strength		Failure Load (kN) of the FEA Model			Ultimate Slip (mm) of the FEA Model		
f_c (MPa)	f_t (MPa)	Ø100mm	Ø150mm	Ø200mm	Ø100mm	Ø150mm	Ø200mm
25	2.56	82	171.4	263.6	2.62	3.19	3.93
28	2.77	84.1	187.0	276.5	2.68	3.56	4.22
30	2.90	86.3	196.4	286.3	2.76	3.84	4.43
32	3.02	91.5	212.4	299.1	2.92	4.21	4.63
35	3.21	94.2	221.7	311.5	3.01	4.51	4.83
38	3.39	97.1	237.1	324.2	3.12	4.95	5.07
40	3.51	99.8	249.3	336.8	3.18	5.28	5.36
42	3.62	104.6	268.0	347.6	3.38	5.87	5.59
45	3.80	108.6	280.5	361.3	3.54	6.21	5.85
48	3.96	113.2	286.3	375.1	3.71	6.45	6.04
50	4.07	120.1	301.7	382.7	3.96	6.84	6.21
52	4.12	125.8	307.9	398.8	4.14	7.11	6.49
55	4.21	132.1	314.1	406.2	4.39	7.34	6.78
58	4.30	137.5	329.4	423.0	4.67	7.79	7.27
60	4.35	143.2	332.5	430.9	4.83	7.95	7.47

f_c is the concrete compressive strength , f_t is the concrete tensile strength

Table 5.6 Results of the failure loads and slips of the FEA parametric study
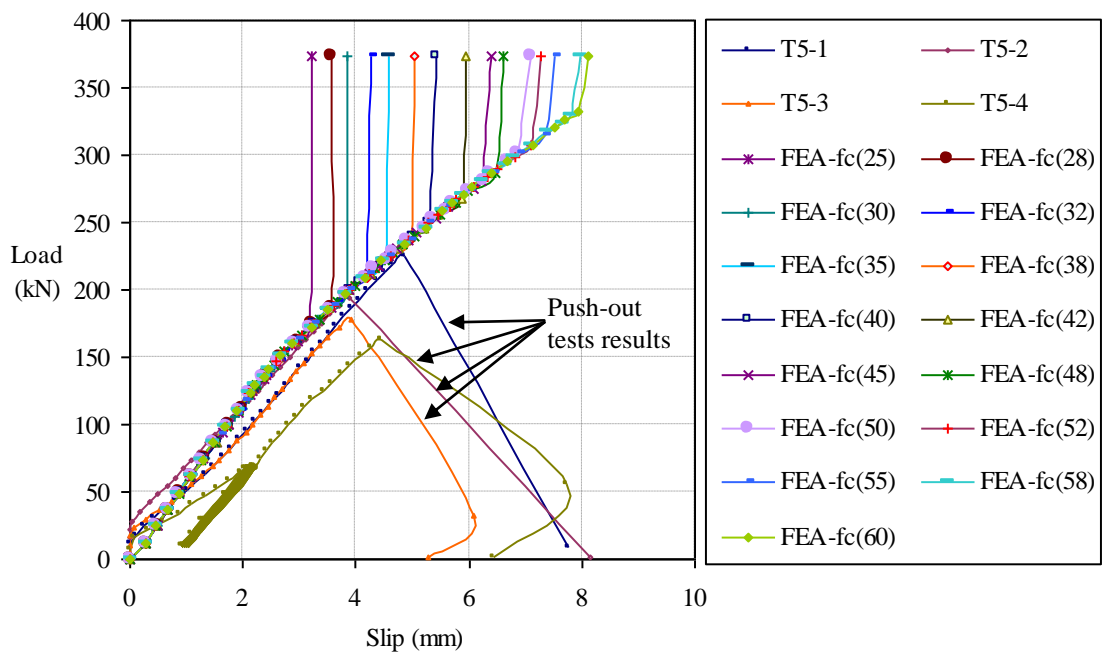
Figure 5.13 Load-slip curves of the FEA concrete-infill-only shear connection with Ø150mm web opening
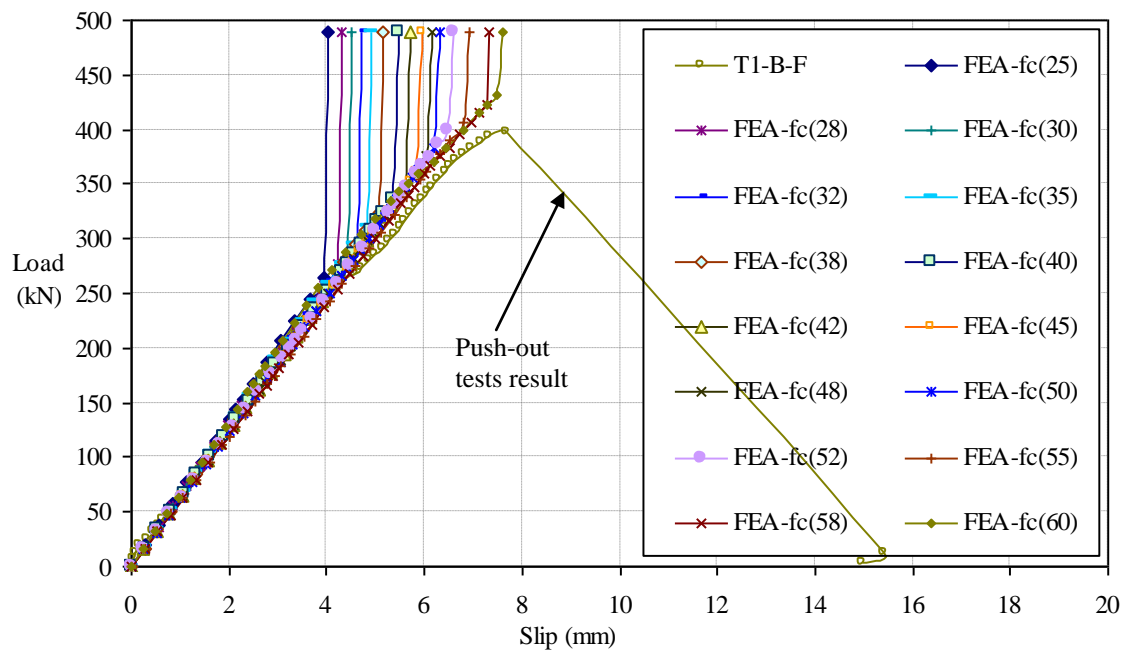
Figure 5.14 Load-slip curves of the FEA concrete-infill-only shear connection with Ø200mm web opening
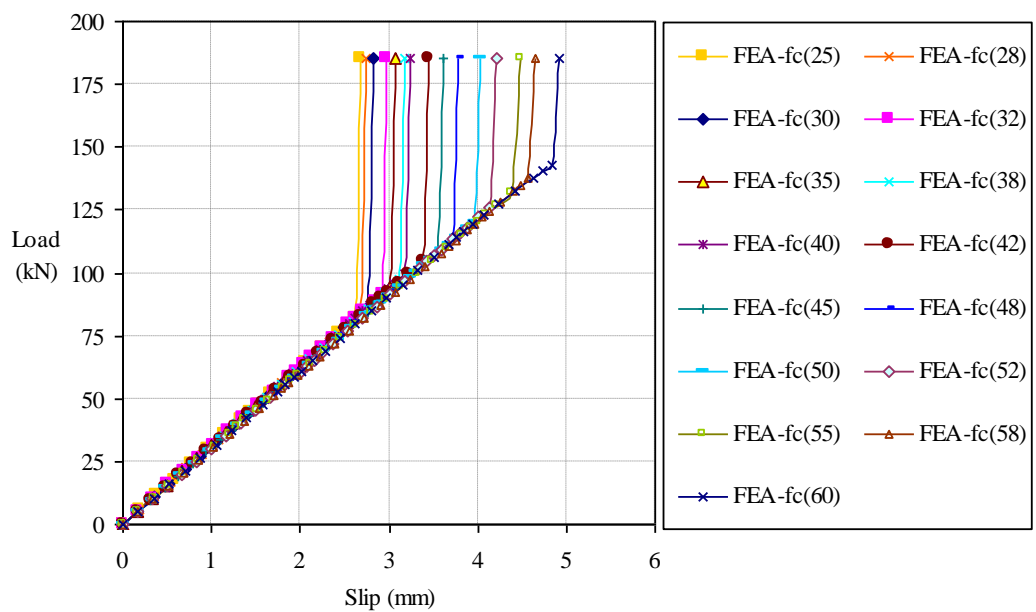
Figure 5.15 Load-slip curves of the FEA concrete-infill-only shear connection with Ø100mm web opening
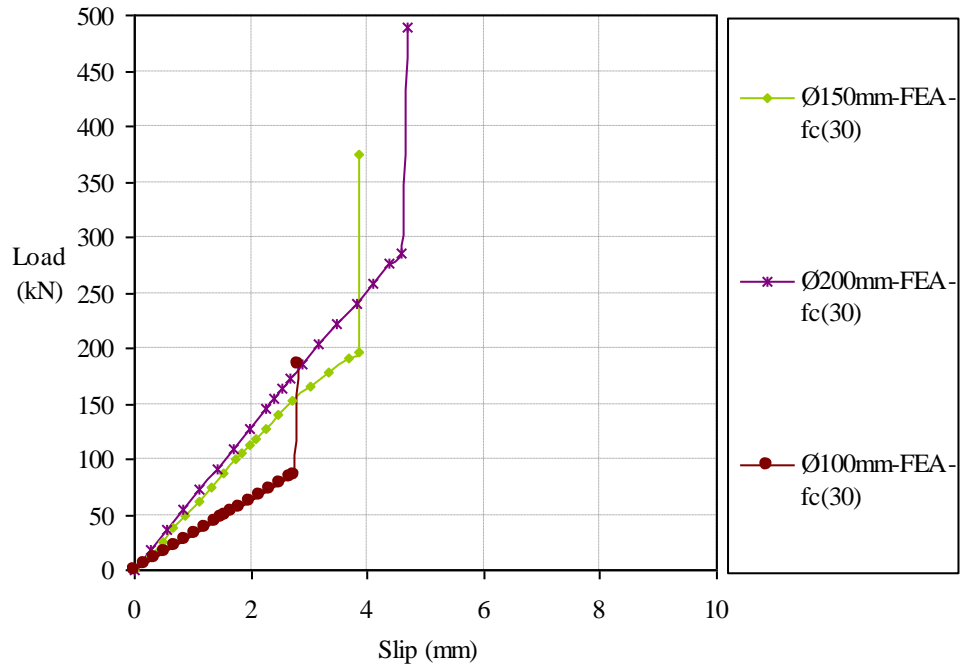
Figure 5.16 Load-slip curves of the FEA concrete-infill-only shear connection with concrete strength of 30N/mm^2 but different diameters of web opening
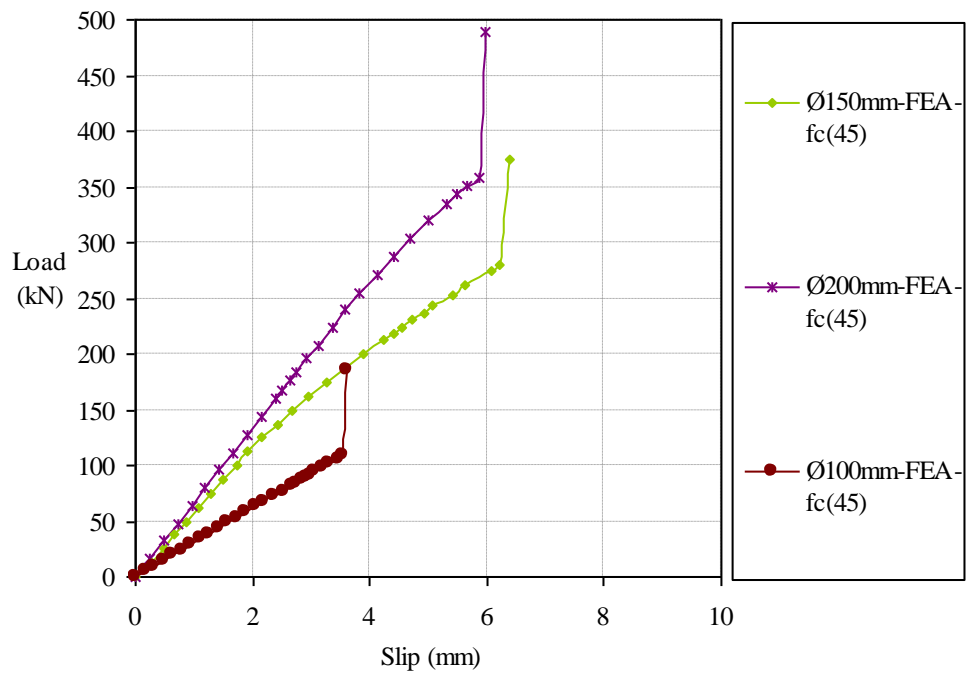
Figure 5.17 Load-slip curves of the FEA concrete-infill-only shear connection with concrete strength of 45N/mm^2 but different diameters of web opening
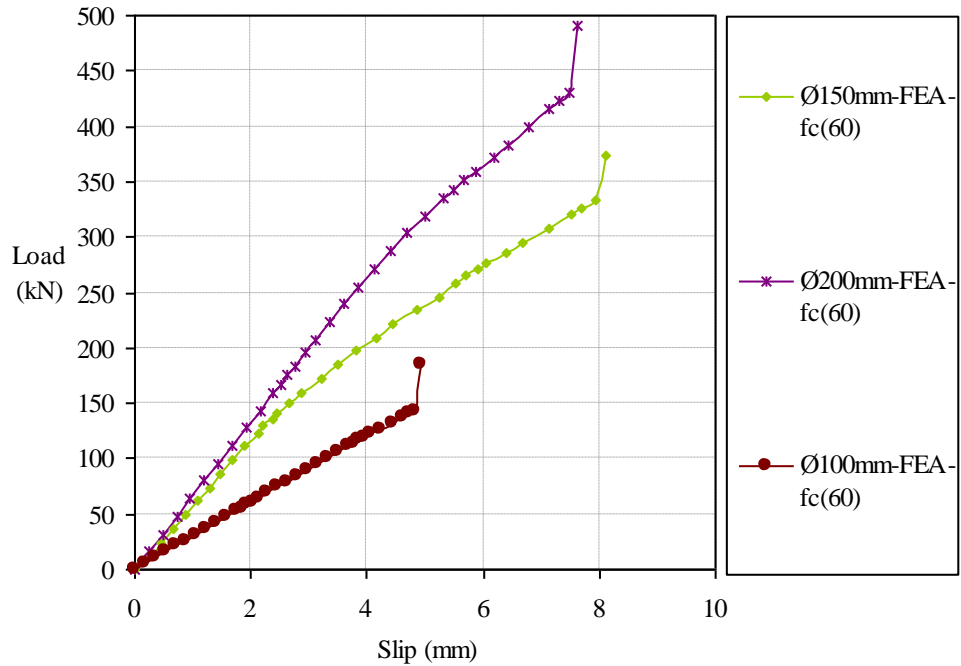
Figure 5.18 Load-slip curves of the FEA concrete-infill-only shear connection with concrete strength of 60N/mm^2 but different diameters of web opening

5.3.8 Verification of the shear resistance calculation method

The method for calculating the shear resistance of the shear connection, Eqn. 5.6, was the sum of three terms: the compressive resistance and tensile resistance of the concrete infill element, and the resistance of the additional elements, i.e. re-bar or studs. The first two terms constituted the shear resistance of the concrete infill element. The method of combining the compressive and tensile resistance to calculate the shear resistance of the concrete infill element was based on the failure mechanism shown in the push-out tests. This failure mechanism was further confirmed by the FEA, as analysed in Section 5.3.6.

The method of combining the shear resistance of the concrete infill element with the resistance of the additional elements to calculate the total shear resistance of the shear connection was based on a number of grounds.

- The push-out tests showed the significantly gained shear resistance from the additional elements, i.e. tie-bar or studs. The calculation for the additional shear resistance was based on the failure mechanism of the additional elements.

- The test group T4 and T6 for the web-welded stud and tie-bar (Ø16mm) shear connection showed there was no isolated failure between the additional elements and concrete infill elements. Hence, the shear resisting

161

mechanism of the shear connection was due to the combined effect of both the concrete infills and the additional elements; and they both contributed to the shear resistance of the shear connection.

- Although, the test group T3 for the tie-bar (Ø12mm) shear connection showed the local shear failure of the tie-bar positioned close to the edge of the web openings. But a minimum distance of 20mm between the tie-bar and web openings was recommended for the construction practice in order to prevent the shear failure for the tie-bar and to utilise its tensile resistance.

- By comparing the results of test group T5 (concrete-infill-only) and T6 (tie-bar Ø16mm), as illustrated in Figure 4.9, the combined effect of the concrete infill and the tie-bar was very apparent. The only difference between the specimens of these two test groups was the additional Ø16mm tie-bar passing through the centre of the web openings. The shear resistance of the shear connection increased by twofold with the additional Ø16mm tie-bar. Nevertheless, the slip stiffness of the two types of shear connection was the same. Thus the additional tie-bar had no contribution toward to the slip stiffness of the shear connection. If the additional tie-bar altered the shear resisting mechanism of the concrete infill element, then the slip behaviour of the shear connection would be different. Therefore, the method for calculating the shear resistance of the concrete infill (used in combination with the tie-bar) should be unchanged as expressed in Eqn.5.5.

- Comparing with the concrete-infill-only shear connection, ductile slip behaviour was shown by the shear connection with the additional tie-bar. It was indicated that the tensile resistance of the tie-bar became effective and contributed to the overall performance of the shear connection. Moreover, there was no anchorage failure of the tie-bar, nor the shear failure of the tie-bar as positioned at the centre of the web opening. Therefore, the resisting mechanism of the tie-bar combined with the concrete infill element in transferring the longitudinal shear force was the tensile resistance, as illustrated in Figure 5.19b.

- The tensile resistance of the tie-bar was in the same direction as the tensile splitting force of the concrete infills, as shown in Figure 5.19b, thus the additional tie-bar eliminated the brittle failure mode. The tie-bar acted together with the concrete infill providing much increased resistance in the transverse direction (or horizontal direction shown in Figure 5.19).

- Based on the above evidence, the tensile resistance of the tie-bar could be added to the shear resistance of the concrete infill element to calculation the shear resistance of the shear connection.

The FEA did not consider the combined effect of the tie-bar reinforcement. The main reasons were:

- The shear resisting mechanism of the reinforcing tie-bar and its contributions towards to shear resistance of the shear connection were shown in the push-out tests.

- Unlike the concrete infill element whose shear resisting mechanism need to be confirmed by the FEA, and the empirical formula concluded for the shear resistance of the concrete infill element need to be further verified by the FEA parametric study.

- As the tensile resisting mechanism and contributions of the tie-bar was clearly shown in the push-out tests, hence, it would be certain to add the tensile resistance of the tie-bar to the combined shear resistance.
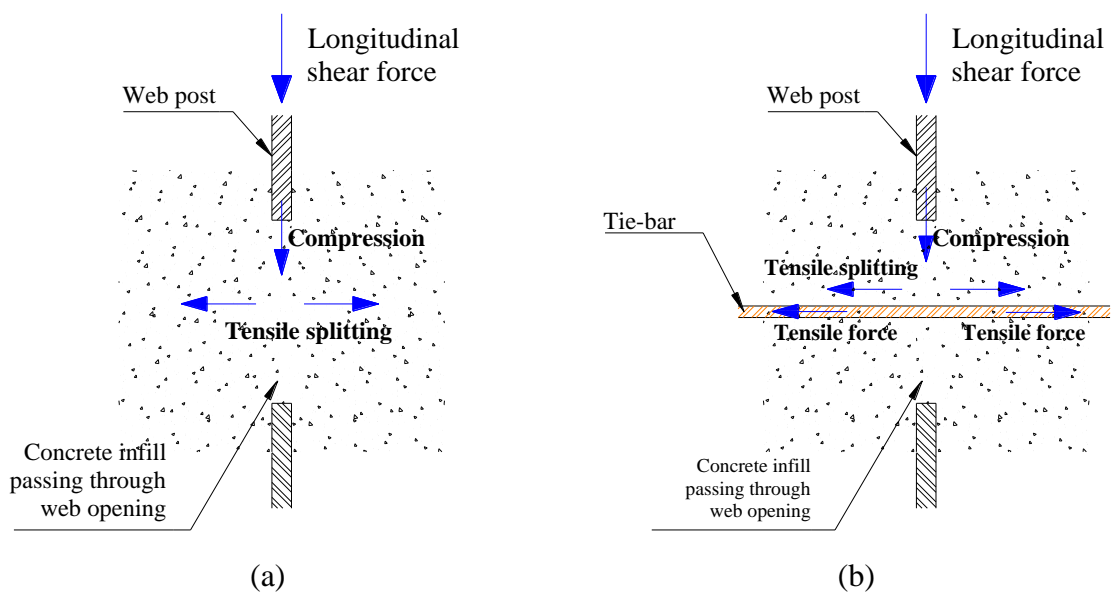
Figure 5.19 Illustration of the failure mechanism for (a) concrete infill element, (b) concrete infill element with the additional tie-bar

The results of the FEA parametric study was used to further verify the mathematical formula, Eqn. 5.5, obtained for calculating the shear resistance of the concrete infill element. The FEA parametric study investigated concrete-infill-only shear connection with the concrete strengths varied between 25 to $60N/mm^2$ and web opening diameters of 100, 150 and 200mm. The results of the FEA were compared with the calculated results using Eqn. 5.5, the method obtained from the mathematical analysis.

The comparison showed that the calculated shear resistance of the shear connection using Eqn. 5.5 were lower than that obtained in the FEA, as demonstrated in the Tables 5.7, 5.8 and 5.9. The average ratios for the shear resistance of the calculation to FEA were 0.935, 0.703 and 0.863 for the web opening diameters of 100, 150 and 200mm, respectively. The results of the FEA represented the shear resisting capacity of the shear connection in the push-out tests, as the FEA models were calibrated with the push-out tests. Based on the above verifications, the calculation method, Eqn. 5.5, could be further developed into a design method for shear resistance of the shear connection.

	f_{cu} (N/mm^2)	f_{ct} (N/mm^2)	A_c (mm^2)	A_t (mm^2)	P_c * (kN)	FEA (kN)	Ratio Cal/FEA
Web opening 100mm, and web thickness 8.6mm	25	2.56	860	7854	64.9	82.0	0.792
	28	2.77	860	7854	71.5	84.1	0.851
	30	2.90	860	7854	75.9	86.3	0.879
	32	3.02	860	7854	80.2	91.5	0.877
	35	3.21	860	7854	86.6	94.2	0.920
	38	3.39	860	7854	93.0	97.1	0.958
	40	3.51	860	7854	97.2	99.8	0.974
	42	3.62	860	7854	101.4	104.6	0.969
	45	3.80	860	7854	107.6	108.6	0.991
	48	3.96	860	7854	113.8	113.2	1.006
	50	4.07	860	7854	118.0	120.1	0.982
	52	4.12	860	7854	121.4	125.8	0.965
	55	4.21	860	7854	126.8	132.1	0.960
	58	4.30	860	7854	132.1	137.5	0.961
	60	4.35	860	7854	135.6	143.2	0.947
* calculated using Eqn. 5.6							Average 0.935

Table 5.7 Comparison between results of calculation and FEA for web opening of 100mm

	f_{cu} (N/mm^2)	f_{ct} (N/mm^2)	A_c (mm^2)	A_t (mm^2)	P_c * (kN)	FEA (kN)	Ratio Cal/FEA
Web opening 150mm, and web thickness 8.6mm	25	2.56	1290	17671	119.1	171.4	0.695
	28	2.77	1290	17671	130.7	187.0	0.699
	30	2.90	1290	17671	138.3	196.4	0.704
	32	3.02	1290	17671	145.9	212.4	0.687
	35	3.21	1290	17671	157.1	221.7	0.709
	38	3.39	1290	17671	168.2	237.1	0.709
	40	3.51	1290	17671	175.5	249.3	0.704
	42	3.62	1290	17671	182.7	268.0	0.682
	45	3.80	1290	17671	193.6	280.5	0.690
	48	3.96	1290	17671	204.3	286.3	0.714
	50	4.07	1290	17671	211.4	301.7	0.701
	52	4.12	1290	17671	217.0	307.9	0.705
	55	4.21	1290	17671	225.8	314.1	0.719
	58	4.30	1290	17671	234.5	329.4	0.712
	60	4.35	1290	17671	240.2	332.5	0.722
* calculated using Eqn. 5.6							Average 0.703

Table 5.8 Comparison between results of calculation and FEA for web opening of 150mm

	f_{cu} (N/mm^2)	f_{ct} (N/mm^2)	A_c (mm^2)	A_t (mm^2)	P_c * (kN)	FEA (kN)	Ratio Cal/FEA
Web opening 200mm, and web thickness 9.9mm	25	2.56	1980	31416	198.6	263.6	0.754
	28	2.77	1980	31416	217.7	276.5	0.787
	30	2.90	1980	31416	230.2	286.3	0.804
	32	3.02	1980	31416	242.5	299.1	0.811
	35	3.21	1980	31416	260.9	311.5	0.838
	38	3.39	1980	31416	279.0	324.2	0.861
	40	3.51	1980	31416	291.0	336.8	0.864
	42	3.62	1980	31416	302.8	347.6	0.871
	45	3.80	1980	31416	320.5	361.3	0.887
	48	3.96	1980	31416	338.0	375.1	0.901
	50	4.07	1980	31416	349.5	382.7	0.913
	52	4.12	1980	31416	358.5	398.8	0.899
	55	4.21	1980	31416	372.5	406.2	0.917
	58	4.30	1980	31416	386.5	423.0	0.914
	60	4.35	1980	31416	395.5	430.9	0.918
* calculated using Eqn. 5.6							Average 0.863

Table 5.9 Comparison between results of calculation and FEA for web opening of 200mm

5.4 Conclusion of design method

The calculation method for the shear resistance of the shear connection was obtained from the mathematical analysis; it was based on the failure mechanism of the shear connection shown in the push-out tests. The calculation method combined the shear resistance of the concrete infill element with resistance of the additional elements, i.e. tie-bar or studs, to calculate the total shear resistance of the shear connection. The mathematical formula of the method was expressed in Eqn. 5.6. The results of the calculation method compared well with the results of the push-out tests. The ratio for the shear resistance of the calculation to test results was 0.935.

The FEA further verified the empirical formula obtained for the shear resistance of the concrete infill element, as expressed in Eqn. 5.5. The calculated results were very close to the results of the FEA parametric study, as the average ratios of the calculated shear resistance to results of the FEA were 0.935, 0.703 and 0.863 for web opening diameters of 100, 150 and 200mm, respectively.

Overall the shear resistance of the shear connection obtained from the calculation method, Eqn. 5.6, were very close to the results of the push-out tests. In order to develop a design method for the shear resistance of the shear connection, a partial safety factor was added into the mathematical formula, Eqn. 5.6, as expressed in Eqn. 5.14.

$$P_{uc} = \frac{1.6758\left(f_{cu}A_c\right) + 1.4355\left(f_{ct}A_t\right) + R_{add}}{\gamma} \tag{5.14}$$

Where: $A_c = tD$

$$A_t = \frac{\pi D^2}{4}$$

P_{uc} is the design shear resistance of the shear connection;

f_{cu} is the concrete cube compressive strength in N/mm^2;

f_{ct} is the concrete tensile splitting strength in N/mm^2;

A_c is the area of concrete in the compression;

A_t is the area of concrete in the tensile splitting;

t is the thickness of the web;

D is the diameter of the web opening;

R_{add} is the shear resistance of the additional elements i.e. tie-bar or shear studs;

γ is the partial safety factor.

The shear resistance obtained from the design method, Eqn. 5.14, with the partial safety factor of 1.5 were compared with the results of the push-out tests, as shown in Table 5.10. The ratio of the design shear resistance (P_{uc}) to test results was 0.624 for the partial safety factors of 1.5.

Specimen No.	f_{cu} (N/mm^2)	f_{ct} (N/mm^2)	A_c (mm^2)	A_t (mm^2)	Test results (kN)	Partial safety factor $\gamma = 1.5$	
						Design resistance P_{uc} (kN) *	Ratio (P_{uc} /test)
T1-A-N	56.5	4.53	1290	17671	118	~~158~~	~~1.339~~
T1-A-F	58.1	4.85	1290	17671	131	~~166~~	~~1.265~~
T1-B-N	56.5	4.53	1980	31416	362	261	0.721
T1-B-F	58.1	4.85	1980	31416	397	274	0.691
T2-A-N	54.5	4.54	1290	17671	309	222	0.718
T2-A-F	51.9	4.07	1290	17671	305	210	0.689
T2-B-N	54.5	4.54	1980	31416	390	324	0.830
T2-B-F	51.9	4.07	1980	31416	372	304	0.817
T3-A-N	55.2	3.91	215	5400	47	33	0.712
T3-A-F	51.5	3.89	215	5400	50	32	0.649
T3-B-N	55.2	3.91	495	13744	125	82	0.656
T3-B-F	51.5	3.89	495	13744	137	80	0.581
T4-A-N	67.0	4.66	1290	17671	504	357	0.708
T4-A-F	50.2	4.08	1290	17671	427	323	0.756
T4-B-N	67.0	4.66	1980	31416	--	--	--
T4-B-F	50.2	4.08	1980	31416	497	415	0.835
P5-1	35.0	3.21	1290	17671	227	105	0.462
P5-2	35.0	3.21	1290	17671	194	105	0.539
P5-3	32.0	2.9	1290	17671	179	95	0.532
P5-4	30.0	3.02	1290	17671	164	94	0.576
P6-1	29.0	2.85	1290	17671	391	150	0.384
P6-2	32.0	2.92	1290	17671	386	156	0.403
P6-3	28.0	2.49	1290	17671	327	142	0.436
P6-4	27.0	2.57	1290	17671	358	142	0.398
* Design shear resistance calculated using Eqn. 5.14.						Ratio 0.624	

Table 5.10 Comparison for shear resistance between the design values and test results

Chapter 6   Flexural tests of composite shallow cellular floor beam

The behaviour and shear resisting capacity of the shear connection used for the composite shallow cellular floor beams were investigated in two push-out tests series, which applied the direct longitudinal shear force to the shear connection. In order to further investigate the characteristic of the shear connection in the actual composite beam, two flexural tests were carried out: four-point symmetric and three-point asymmetric bending tests. The concrete-infill-only and tie-bar shear connection were investigated in the flexural tests. Behaviour and shear performance of the shear connection were compared with those shown in the push-out tests. Composite behaviour and flexural strength of the shallow cellular floor beam were studied.

6.1 Introduction

A full scale test beam specimen was designed to represent the actual composite shallow cellular floor beams of a common span range with solid concrete slab. The reasons of using the solid slab are explained in Section 6.2. The two most commonly used shear connection for the composite shallow cellular floor beams were investigated in the flexural tests, namely the concrete-infill-only and tie-bar shear connection. The two flexural tests carried out in this research were: four-point symmetric and three-point asymmetric bending tests. The results of the push-out tests were used in the design for the shear connection of the beam specimen.

      The layout of the shear connection was designed to enable the discrete investigation of the both types of the shear connection in two flexural tests. In order to particularly investigate the concrete-infill-only shear connection in the four-point symmetric bending test, only one half span of the beam specimen had solely the concrete-infill-only shear connection. In order to investigate the combined effect of the concrete-infill-only and tie-bar shear connection in the three-point asymmetric bending test, the other half span of the beam had a combination of both shear connection; there was an Ø16mm tie-bar of 1m passing through every alternative web opening.

The four-point symmetric bending test created a loading profile that was similar to the uniformly distributed load (UDL), with a region of constant bending moment and regions of constant shear within the shear spans. This flexural test was to particularly investigate the concrete-infill-only shear connection. The four-point symmetric bending test was carried out only up to plastification of deflection at the mid-span without failure of the beam specimen. It was to preserve the stiffness of the beam specimen, so that the three-point asymmetric bending test could be carried out thereafter.

The three-point asymmetric bending test created a region of high shear within the shorter shear span, which had the combination of concrete-infill-only and tie-bar shear connection. This flexural test was a failure test to particularly investigate the combined effect of both shear connection.

The behaviour and shear performance of the shear connection in the flexural tests were compared with that in the push-out tests. The flexural behaviour and failure mechanism of the shallow cellular floor beam were studied. The flexural test results were back analysed by using the measured material properties to determine the degrees of shear connection. By combining with the findings of the push-out tests, the results of the flexural tests were further analysed in Chapter 7 with the aims of establishing design methods for the composite shallow cellular floor beams at the serviceability limit and ultimate limit states.

6.2 Test specimen

The full-scale composite beam specimen for the flexural tests was designed to represent the composite shallow cellular floor beams used in the construction practice. The composite action of the composite beam specimen was provided by both the concrete-infill-only and tie-bar shear connection. The composite beam specimen had an asymmetric steel section with circular web openings and cast with solid concrete slab. The overall length of the specimen was 6.2m. The span between the supports was 6m. The total width of the concrete slab is 1m. The reasons for using the solid slab rather than the ribbed slab are:

- To be consistent with the push-out tests where the solid slab were used; the shear resistance and behaviours of the shear connection obtained from the push-out tests could be used to design the shear connection of the composite beam specimen.

- The characteristics of the shear connection shown in the flexural tests could be compared with those in the push-out tests.

- To accommodate the Ø16mm tie-bar of 1m length for the tie-bar shear connection; the required anchorage length for the tie-bar was 1m.

- To simplify the tests and reduce the number of variables in the study.

If using the ribbed slab for the composite beam specimen, the following results might be different.

- The main differences would be the failure mode, stiffness and degree of composite action.

- The failure modes for the beam specimen with solid slab would be different with the ribbed slab; this was explained more in Section 6.3.3.

- The elastic stiffness of the composite beam specimen with the ribbed slab would be less than that of using the solid slab. This was demonstrated in stiffness calculations carried out in Section 7.2.2.

- The degree of shear connection would be increased for using the ribbed slab. The compressive resistance of the ribbed slab in full shear connection, R_c, was reduced comparing with that of the solid slab. For the same longitudinal shear resistance of the shear connection, R_q, the degree of shear connection, $\eta = R_q/R_c$, would be therefore increased. The increase in composite action would reduce the slips of the beam specimen.

- One of the reasons for the using the ribbed slab was to represent the construction practice for service integration, such as ducting passing through the web openings; this would lead to web openings unfilled, which would complicate the flexural tests. The unfilled web openings would make the section less resistance to Vierendeel bending effects, especially for the region of low Moment/Shear (M/V) ratio. As the steel section used for the composite beam specimen was shallow, with big web openings and its web thickness is unmodified (unlike the ASB with the modified web); hence the Vierendeel bending would very likely to occur at the unfilled web openings. Furthermore, the Vierendeel bending effect was not part of the investigations for the flexural tests, as the main purposes were to investigate performance of the shear connection and its contributions to the composite action.

- The width of the concrete slab of 1m was designed for the effective width and Ø16mm tie-bar used for the tie-bar shear connection. Thus, transverse reinforcements should be needed to control cracking for the thin concrete flanges when using the ribbed slab. This reinforcement would increase the degree of shear connection for the composite beam specimen as was demonstrated in the ASB flexural tests (Lawson et al 1999).

- For the case of topping was constructed over the top flange for the ribbed slab, the concrete cover would also increase the degree of shear connection as it was also shown in the ASB flexural tests (Lawson et al 1999).

6.2.1 Steel section

The steel section was fabricated by welding two highly asymmetric cellular tees together along the web. The top tee was cut from the 305x165x54UB and the bottom tee was cut from the 305x305x97UC. The width of the top flange was 167mm and the width of the bottom flange was 305mm. The degree of asymmetry in flange width was 55%. The net projection between the two flanges was 69mm. The dimensions of the steel section are shown in Figure 6.1 (a) & (b).

The diameter of the web openings was 150mm, which was the same as that of the push-out test series-II. There were 22 web openings spaced at 265mm. The steel section had no end plates. It was to avoid confinement of the slips. The steel grade of the steel section was S355. The actual strengths were obtained from the coupon tests, as shown in Appendix C. Coupons were cut from the leftover of the actual steel sections. The average yield and ultimate strengths were 414 and 527 N/mm^2 respectively.

(a)

(b)

(c)
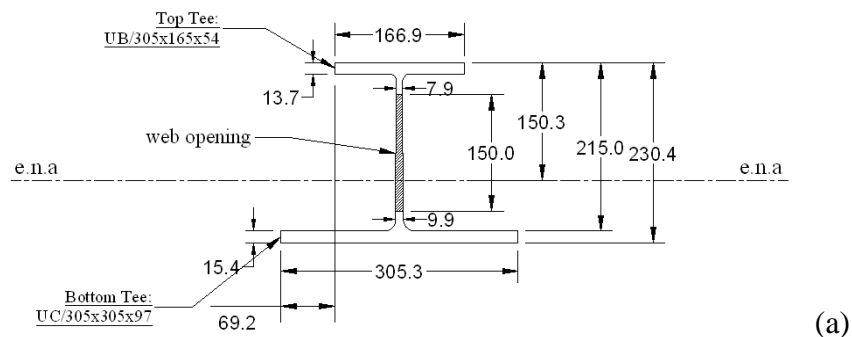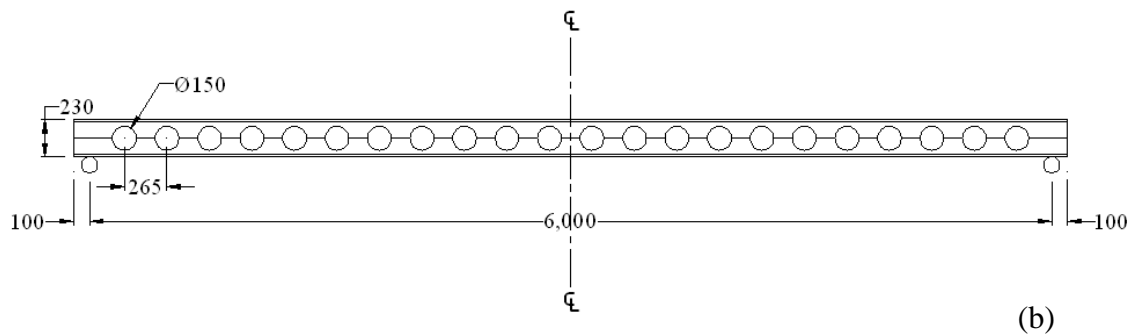
Figure 6.1 Steel section of the composite beam specimen: (a) drawing of cross section, (b) drawing of side view, (c) actual steel section

6.2.2 Concrete slab

The total width of the concrete slab was 1m, which was the same as that of the push-out test series-II. It was to accommodate the 1m length of Ø16mm tie-bar used for the tie-bar shear connection. For beam span of 6m, this concrete width was smaller than the effective width of 1.5m (1/4 span) calculated in accordance with both Eurocode 4 (EN1994-1-1:2004) and BS5950 (BS5950-3.1:1990). The smaller concrete width was also based on the approach presented in Lawson et al (1997) to avoid over-estimating the degree of composite action.

The concrete slab sit on the bottom flange of the steel section and flushed with the top flange of the steel section, as depicted in Figure 6.2 (a). The depth of the concrete slab was 215mm. The concrete slab on both sides of the web post were connected by the

concrete infill elements with or without the Ø16mm tie-bars. The 28-day concrete cube compressive strength was designed at 30N/mm^2.

6.2.3 Layout of shear connection

Both the concrete-infill-only and tie-bar (Ø16mm) shear connection were investigated in the flexural tests. The layout of the shear connection enabled discrete investigations of the two types of shear connection in two flexural tests. In order to particularly investigate the concrete-infill-only shear connection in the four-point symmetric bending test, one half of the beam span had solely the concrete-infill-only shear connection. In order to investigate the combined effect of the concrete-infill-only and tie-bar shear connection in the three-point asymmetric bending test, the other half of the beam span had the combination of both shear connection; there was an Ø16mm tie-bar of 1m passing through every alternative web opening, as illustrated in Figure 6.2b.

The longitudinal shear resistance of the shear connection were calculated based on the results of the push-out tests. The loading configurations for both flexural tests were designed to show the full composite action of the test beam.

6.2.4 Preparation and construction

The full-scale flexural test beam specimen was constructed in the Structural Laboratory of City University London. The steel section was greased to prevent the development of bond between the steel section and concrete. The elimination of the shear-bond strength would enable the flexural tests to demonstrate the shear transferring mechanism of the shear connection without the influence of other mechanism. The test beam specimen was propped during the concreting and curing. The test beam was cast using concrete of Ordinary Portland cement with 20mm maximum size of coarse aggregate. The cube and cylinder specimens were cast from the same batch of concrete used for the test beam specimen. All the specimens were cured under the same conditions and covered with plastic sheets.

(a)

(b)
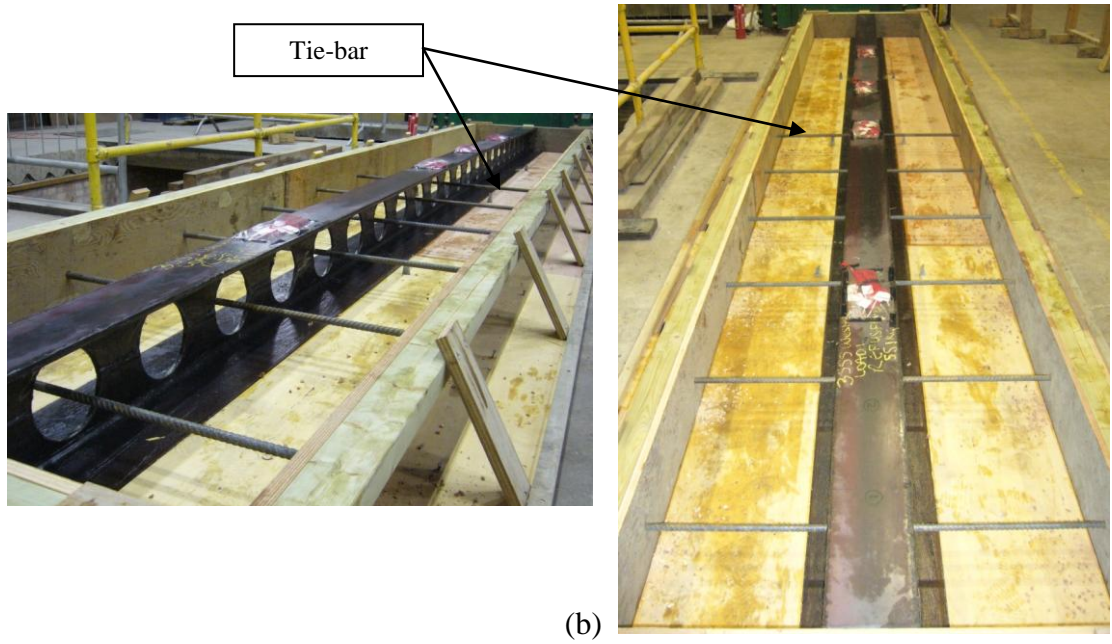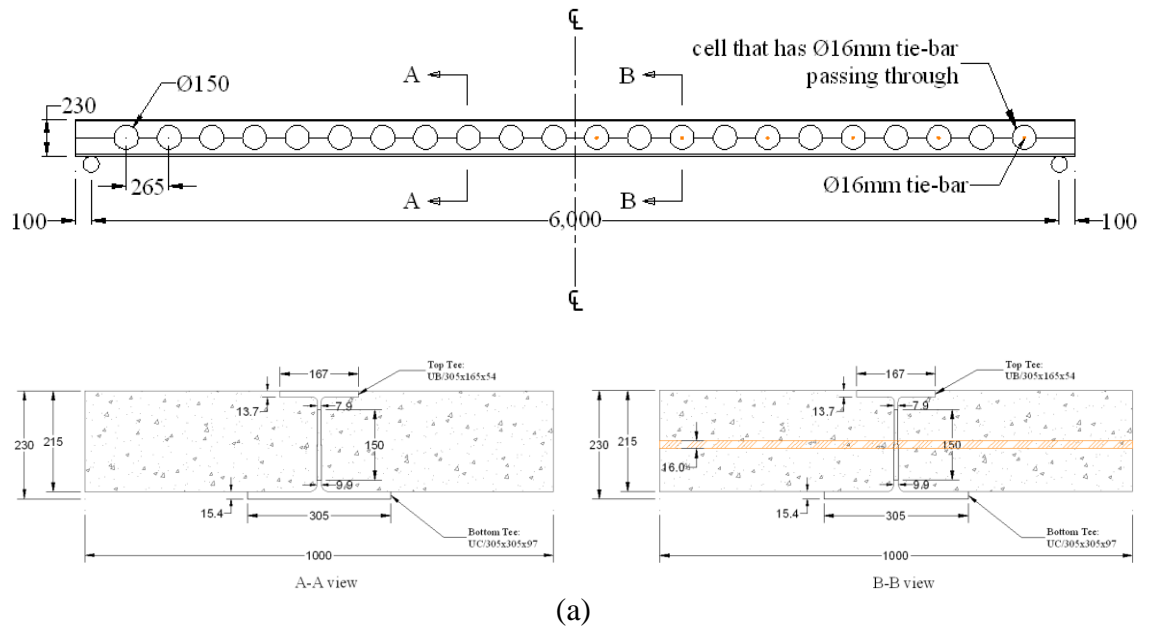
Figure 6.2 (a) Drawing of the test beam specimen, (b) Layout of the tie-bars

174

Figure 6.3 Casting and curing of the test beam specimen

6.3 Flexural tests

Two flexural tests, four-point symmetric bending and three-point asymmetric bending tests, were carried out to investigate the behaviour and performance of the composite shallow cellular floor beam and its shear connection. The loading positions were designed based on the results of the push-out test and in accordance with the design methods specified in the codes of practice, i.e. Eurocode 4 (EN1994-1-1:2004) and BS5950 (BS5950-3.1:1990).

Four-point symmetric bending test was carried out first without the failure of the beam specimen. Thereafter, three-point asymmetric bending test was carried out up to the failure of the beam specimen. Details of the two flexural tests are presented in the following two sections.

6.3.1 Four-point symmetric bending test

The four-point symmetric bending test created a bending moment profile that was similar to that of the UDL, with a region of constant moment. The four-point symmetric bending test was not a failure test. Three incremental loading cycles were applied before the test beam was loaded up to the occurrence of plastification in the mid-span deflection. It was to preserve the stiffness of the test beam for the next flexural test, three-point asymmetric bending test. The applied loading cycles were to establish the residual deflections and slips within the elastic loading range and also to break local bond, although de-bonding grease was applied onto the steel section.

    The loading position of the four-point symmetric bending test is shown in Figure 6.4. There were nine web openings within each shear span and four web openings within the region of constant moment.
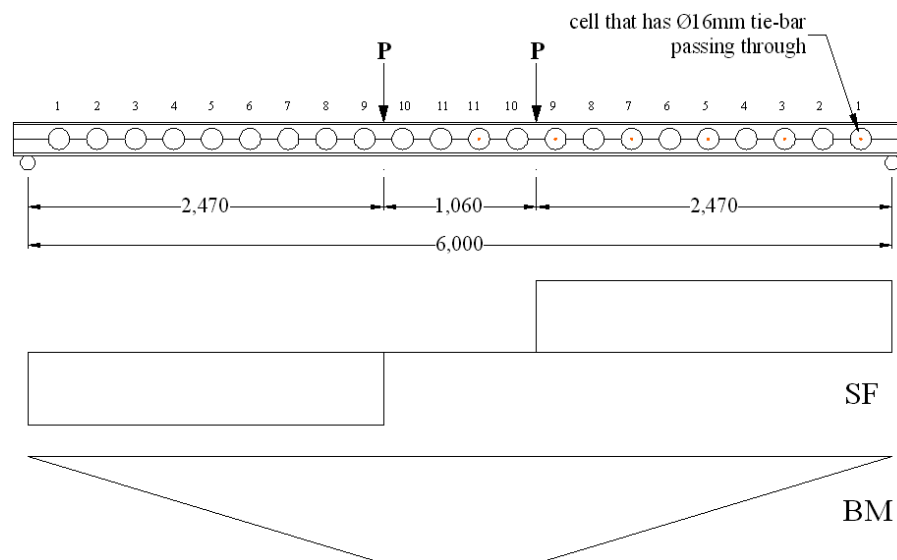
Figure 6.4 Loading position, shear force and bending moment diagrams of the four-point symmetric bending test

    The shear connection within the left and right shear spans provided 1575kN and 2545kN longitudinal shear resistance respectively, which were calculated by using the results of the push-out test series-II. The required longitudinal shear resistance for full shear connection was 898kN, calculated in according with Eurocode 4 and BS5950. The full composite action was expected for both shear spans. The shear resistance of the shear connection was assumed not affected by depth of plastic neutral axis of the beam specimen. The design full moment resistances for both shear spans were the same, which was 354kNm calculated in accordance with the methods of Eurocode 4 and

BS5950. The calculation details of the design moment resistance are shown in Appendix K.

The deflection stiffness of both shear spans under the elastic loading was expected to be the same, as the two shear spans had the same elastic (uncracked) section properties. The four-point symmetric bending test created the same magnitude of constant shear force within each shear span. Hence, the slip distribution along both shear spans was expected to be uniform. The elastic slip stiffness of the two types of shear connection shown in the push-out tests was the same. Therefore, the elastic slip values of the shear connection within both shear spans were expected to be the same.

The shear span/depth ratio of the four-point symmetric bending test was 10.7, which was much greater than the minimum limit of 2.5 (Oehlers and Bradford (1995)) for creating the flexural failure mode. Although the four-point symmetric bending was not a failure test, yielding of the bottom flange at the loading point was expected. This prediction was based on the conclusion of the publications reviewed in the literature as that the dominate failure mechanism of the composite beams was yielding of the steel beam occurred prior to the failure of the concrete slab.

6.3.1.1 Objectives and aims

The objectives and aims of the four-point symmetric bending test were:

1. To demonstrate the composite action for the test beam of the composite shallow cellular floor beam;

2. To provide results for determining the degree of shear connection and shear performance of the shear connection, with the aim of establishing design methods for the composite shallow cellular floor beams;

3. To observe the yielding in the steel bottom flange as an indication of the flexural failure mode;

4. To demonstrate the same elastic deflection stiffness of the two shear spans;

5. To demonstrate the uniform slips distribution within both shear spans;

6. To demonstrate the same elastic slip stiffness of the two shear spans as predicted based on the same slip stiffness of the two types of shear connection shown in the push-out tests.

(a)

Reaction
beam

Jacks

Load cell

(b)

Steel flange

Roller

Neoprene
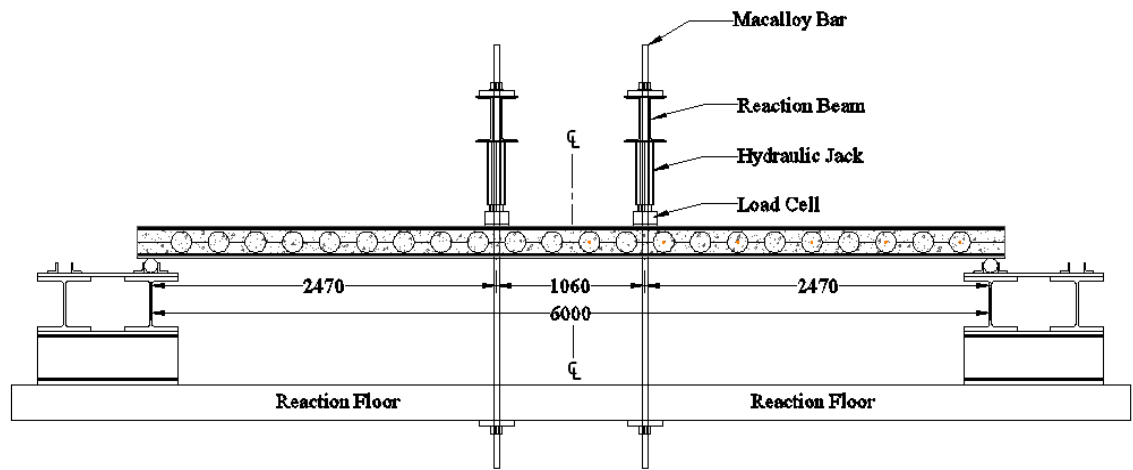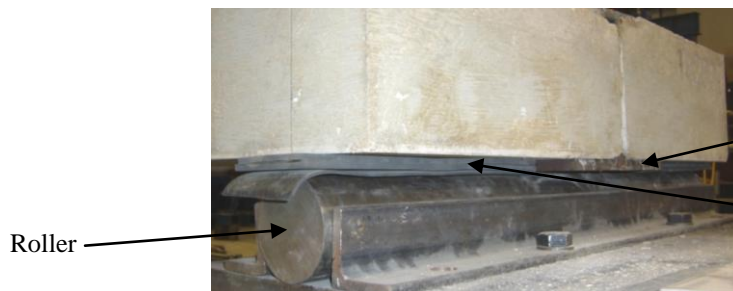
(c)

Figure 6.5 Set up of the four-point symmetric bending test: (a) illustration drawing,
(b) loading arrangement, (c) end support

178

6.3.1.2 Set up and instrumentation

The set up for the four-point symmetric bending test is illustrated in Figure 6.5a. The specimen was simply supported by the footings. The steel bottom flange was in contact with the rollers. The concrete slab was not in contact with the rollers. There was neoprene placed between the rollers and concrete slab, as depicted in Figure 6.5c. It was to create even supports for the concrete slab as the test beam might tilt during the flexural tests.

A 498kN (50ton) hydraulic jack was attached to each reaction beam which was held by high tensile Macalloy bars that were connected through the reaction floor. A load cell was placed beneath the hydraulic jack, as shown in Figure 6.5b. There was a small load spreader placed between the load cell and steel top flange.

Applied load was measured by using the load cell, which was calibrated prior to the flexural test. Deflections were measured by using digital dial gauges and linear voltage displacement transducers (LVDT) at mid-span and quarter-spans, as illustrated in Figure 6.6a. Both the digital dial gauges and LVDTs were positioned at the same locations, as shown in Figure 6.6b. The dial gauges measured the deflections at the beginning of the test with a high resolution of 0.01mm. After the range of the dial gauges was exceeded, the deflections were measured by the LVDTs with a resolution of 1mm.

The slips between the steel section and concrete slab were measured by using the digital dial gauges at mid-span, quarter-spans and end supports, as illustrated in Figure 6.6a. Tags were cast in the concrete slab. The digital dial gauges were attached to the steel section, as depicted in Figure 6.6c. Hence, the relative movements or slips were measured.

The strain of the steel section was measured by using strain gauges at various locations, as shown in Figure 6.7. The strain measurements were acquired via a data logger. At each location, there were strain gauges glued on the top flange, the web posts of the top and bottom tees, and the bottom flange.

(a)

(b)

(c)
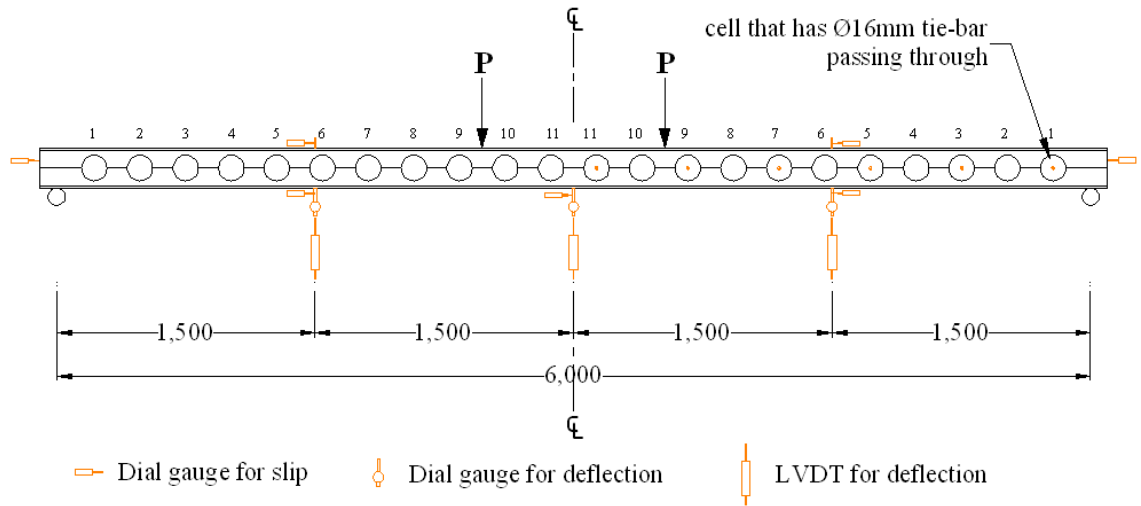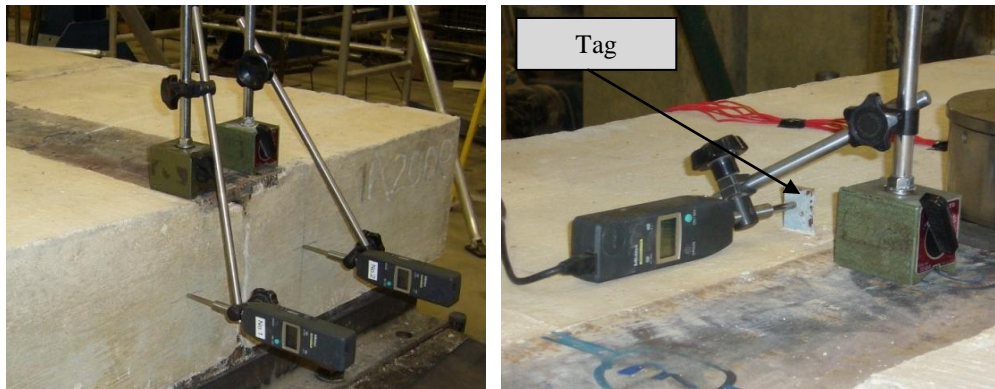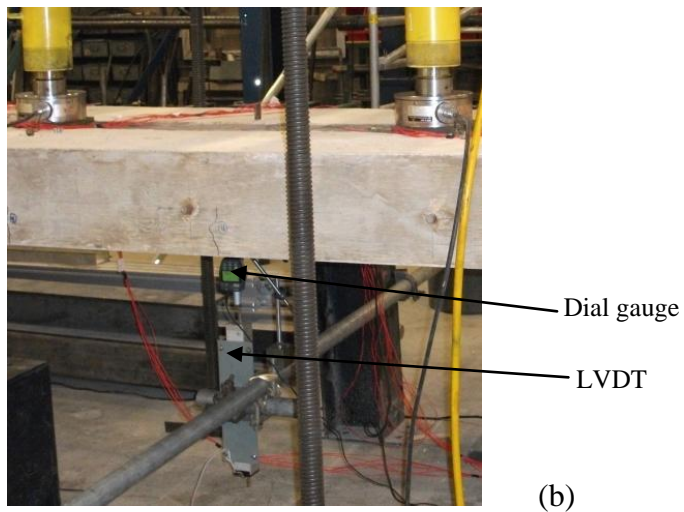
Figure 6.6 Instrumentation for deflections and slips: (a) measuring locations, (b) deflection instrumentation, (c) slip instrumentation

6.3.1.3 Testing procedure

Three incremental loading cycles were applied before the test beam was loaded up to the occurrence of plastification in the mid-span deflection. The four-point symmetric bending test was load-controlled, with load increments of 9.8kN (1ton) applied to a load level of 49kN (5ton). Smaller load increments of 4.9kN (0.5ton) were then applied up to the designated load levels. The load reached at each stage in the four-point symmetric bending test is shown below.

	Load Reached*
1st loading cycle	54kN (5.5ton)
2nd loading cycle	69kN (7ton)
3rd loading cycle	88kN (9ton)
The end of the test	106kN (10.8ton)

* load at each loading point
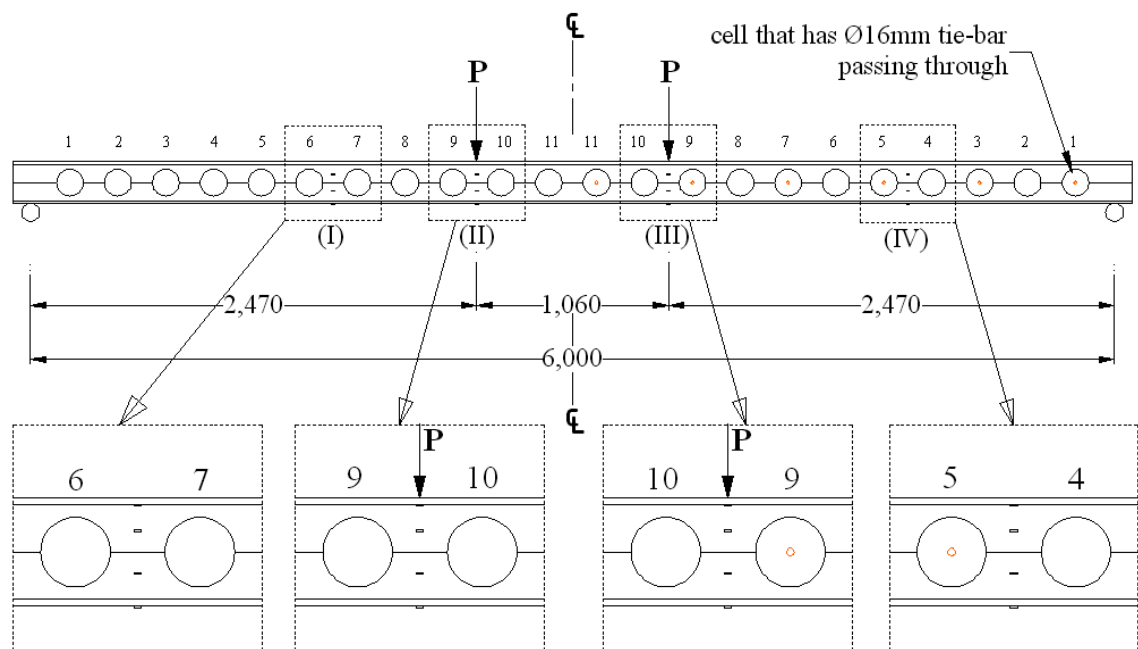
(a)
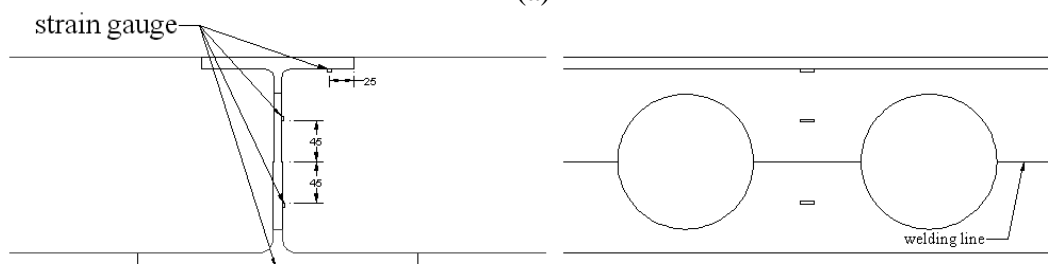
(b)

Figure 6.7 (a) Locations of the strain gauges; (b) Positions of the strain gauges

6.3.2 Three-point asymmetric bending test

The three-point asymmetric bending test was carried out after the four-point symmetric bending test. The loading point was placed between the fifth and sixth web opening, as shown in Figure 6.8. There were two concrete-infill-only shear connection and three tie-bar shear connection within the shorter shear span. The total longitudinal shear resistance of the shear connection was 1475kN, which was much greater than the required longitudinal shear resistance, 898kN, for the full composite action. Hence, full degree of shear connection was expected. This was based on the following two assumptions:

1.   The shear resistance of the shear connection was not affected by the position of the plastic neutral axis.

2.   There was a uniform behaviour and non-discrete failure between the two types of shear connection which would have a combined effect towards the composite action.
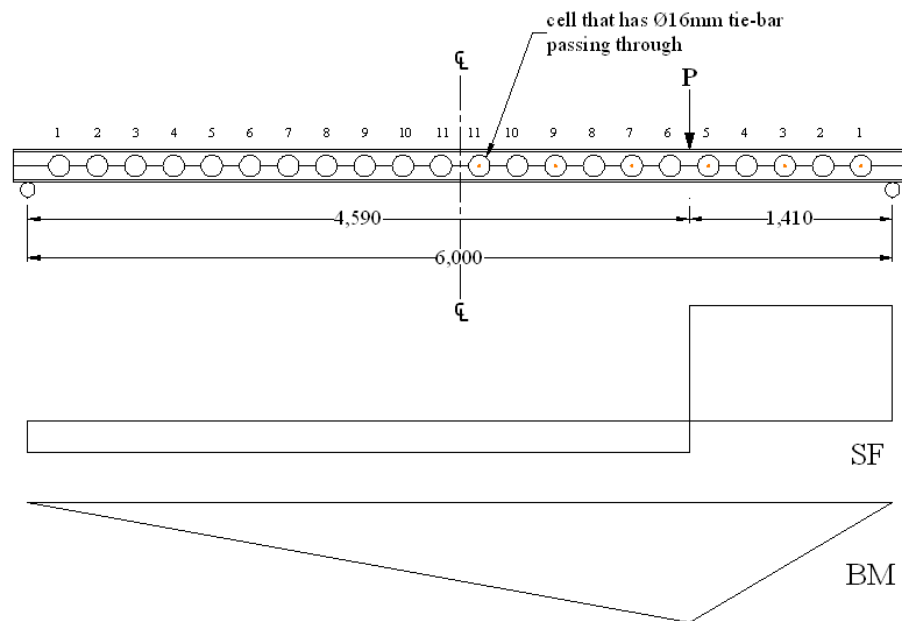
Figure 6.8 Loading position, shear force and bending moment diagrams of the three-point asymmetric bending test

At the end of the four-point symmetric bending test, the residual deflection at the mid-span was 16mm (=span/372), which was less than the deflection limit of span/360 at the serviceability limit state. The residual slip of the shear span that had both types of shear connection was 0.5mm, which was negligible. Hence, the shear connection within this shear span remained intact and could be further investigated.

The three-point asymmetric bending test created a high shear within the shorter shear span. This high shear might induce the Vierendeel bending, which generally occurred at the web opening of low moment-shear ratio. The Vierendeel bending failure mode was shown at rectangular web openings in flexural tests on the downstand composite beams carried out by Clawson and Darwin (1982) and Redwood and Wong (1982) reviewed in the literature. However, the steel section of the test specimen for the composite shallow cellular floor beams was partially encased, which increased the vertical shear capacity of the beam specimen. The web openings of the beam specimen were filled with in-situ concrete, which enhanced the shear resistance of the web opening. Furthermore, the shear span/depth ratio of the three-point bending test was 6.5, which was greater than the minimum limit of 2.5 (Oehlers and Bradford (1995)) for creating the flexural failure mode. Hence, the flexural failure mode of the beam specimen, rather than the Vierendeel bending, was expected in the three-point asymmetric bending test.

6.3.2.1 Objectives and aims

The objectives and aims of the three-point asymmetric bending test were:

1. To provide results for determining the degree of shear connection and shear performance of the shear connection;
2. To establish design methods for the composite shallow cellular floor beam by combining the results of the four-point symmetric bending test;
3. To observe the flexural behaviour and failure mode of the composite beam specimen under high shear;
4. To observe the behaviour of the combined shear connection and to demonstrate the combined effect of the two types of shear connection to the composite action.

6.3.2.2 Set up and instrumentation

The three-point asymmetric bending test was set up by moving the loading position of the previous flexural test, without changing the conditions of support. The set up is shown in Figure 6.9. The same hydraulic jack and reaction beam were used. The same load cell was re-calibrated prior to the flexural test.

The deflection measurements were taken at loading point, maximum deflection point and quarter-span, as shown in Figure 6.10a. The maximum deflection point,

367mm off the mid-span, was an approximate location determined by using the McCaulay's method with the steel section properties. The objective was to demonstrate the amount of deflections rather than the actual location.

The slips were measured by using the dial gauges at various locations, as shown in Figure 6.10a. The slip differences between the top and bottom of the slab and between slab on both sides of the web post were monitored.

The strains of the steel section were measured by using the same strain gauges used in the previous flexural test. The locations of the strain gauges are shown in Figure 6.7. The location IV, between the fourth and fifth cells, was the previously planned loading point for the three-point asymmetric bending test. The strains under the actual loading point were not obtained. Nevertheless, the strains at the location IV would show the similar strain development to that of the actual loading point.

6.3.2.3 Testing procedure

Two incremental loading cycles were applied before the beam specimen was tested up to the ultimate failure. The three-point asymmetric bending test was load-controlled. Load increments of 9.8kN (1ton) were applied to the load level of 49kN (5ton). Smaller load increments of 4.9kN (0.5ton) were then applied up to the designated load levels. The designated load level for each loading stage and the ultimate load level are listed below.

	Load Reached
1st loading cycle	144kN (15ton)
2nd loading cycle	191kN (20ton)
Maximum load	340kN (34.5ton)
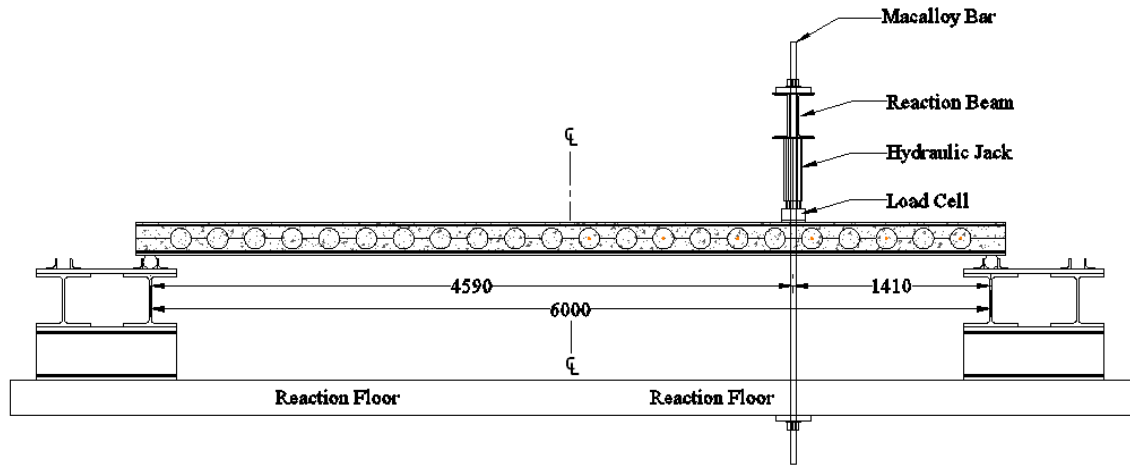
(a)
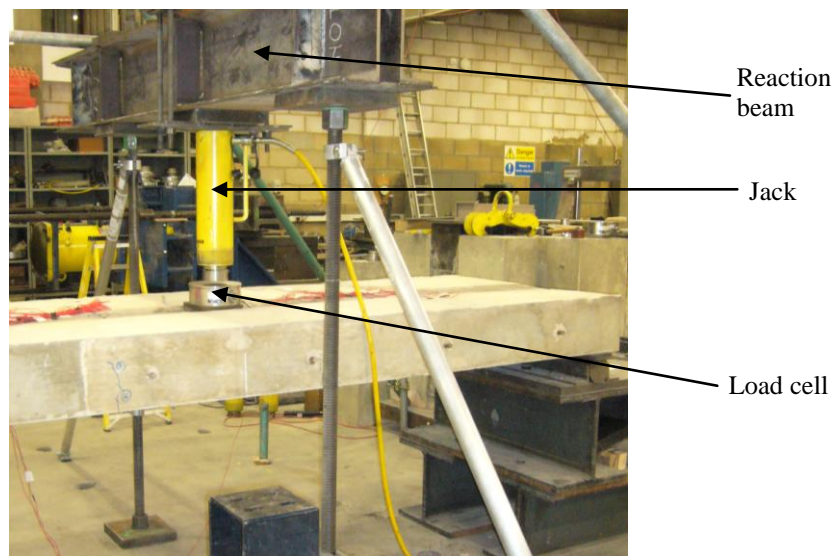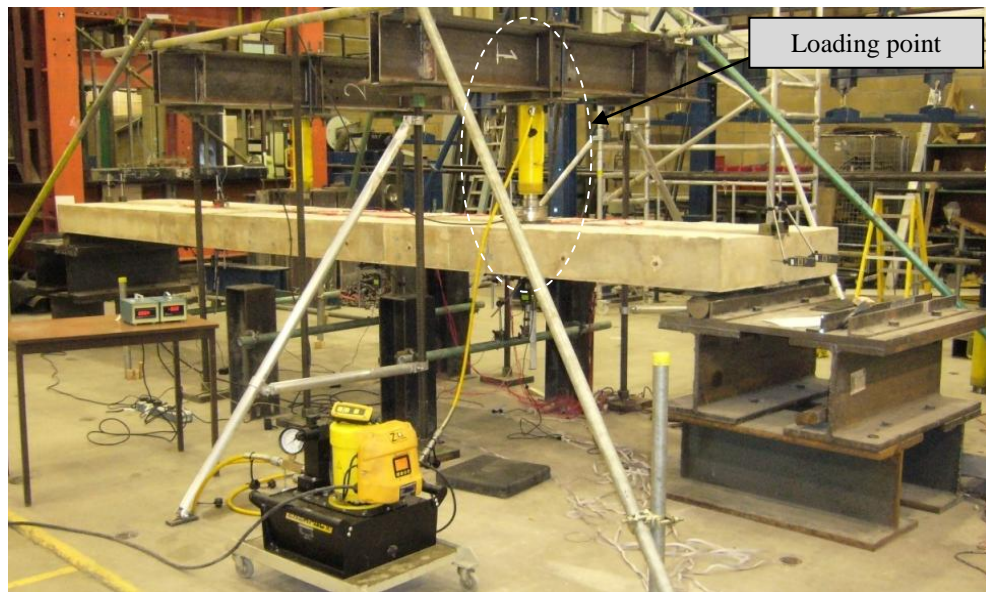
(b)

Figure 6.9 Set up for the three-point asymmetric bending test: (a) illustration drawing, (b) loading arrangement
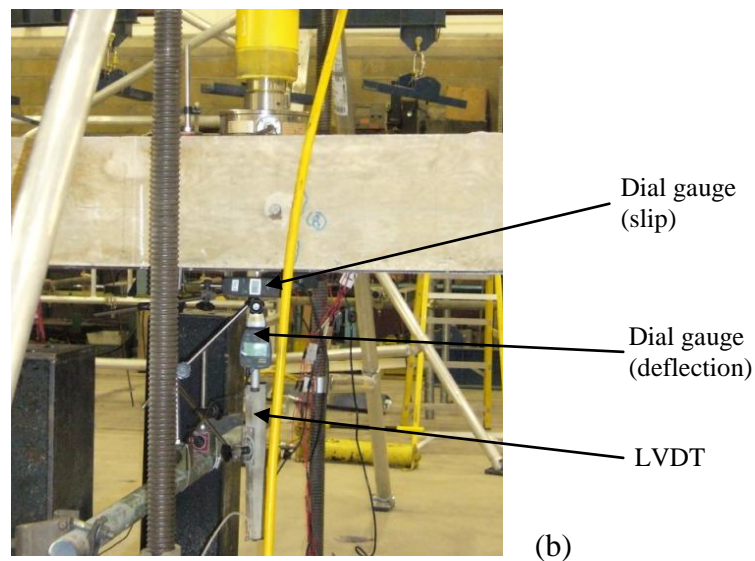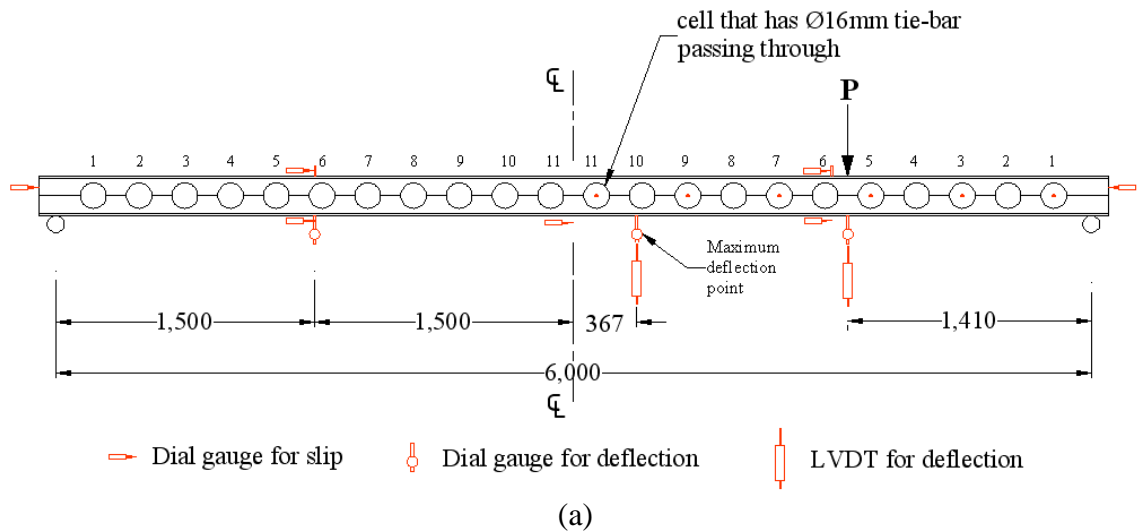
Figure 6.10 (a) Locations for slip and deflection measurement, (b) Instrumentation of slip and deflection at the loading point

6.3.3 Possible failure modes

The composite beam specimen was tested in two discrete flexural tests. The possible modes of failure for the test beam specimen are listed below. The possible failure modes for a beam specimen with ribbed slab were also discussed.

Four-point symmetric bending test

- Flexural failure mode was expected in the four-point symmetric bending test, as the shear span/depth ratio of 10.7 which was much higher than the minimum limit of 2.5 for the flexural failure mode. Yielding on the bottom flange should be the initial indication for flexural failure mode. Crushing failure of the concrete slab was not expected as the test was not an ultimate failure test.

186

- Vierendeel bending was not the possible failure mode for the beam specimen, as the flexural test created low shear with a high M/V ratio at the web openings close to the loading points. Furthermore the concrete slab increased the shear resistance of the composite section, and the concrete infills passing through the openings strengthened the shear capacity of the web opening; hence the Vierendeel bending effect should be prevented.

For test beam with the ribbed slab in four-point bending test

- A possible failure mode was the flexural failure with crushing of the concrete thin flange and yielding of the steel bottom flange at the loading points.

- If there were web opening unfilled to represent the composite beam for service integration, the Vierendeel bending effect might be noticeable at the web openings close to the loading points, as the steel section was shallow, with large web openings. This might lead to diagonal inclining cracking or diagonal tensile failure of the thin concrete flange. (The cross section for the beam specimen with the ribbed slab and web openings unfilled would be very similar to the cross sectional drawings illustrated in Figures 2.15 and 2.16.)

Three-point asymmetric bending test

- One of the possible failure modes was the flexural failure, as the shear span/depth ratio for the three-point asymmetric bending test was 6.5 which was much higher than the minimum limit of 2.5 for the flexural failure mode.

- The occurring of the Vierendeel bending was due to the transfer of shear forces across the web openings. The three-point asymmetric bending test created high shear with low M/V ratio, which was very likely to create the Vierendeel bending effect at the web openings. However, the web openings of the composite beam specimen were filled with in-situ concrete which enhanced the shear resistance of the web opening. Furthermore, the section was partially encased with solid slab, which increased the vertical shear capacity of the composite section and might prevent the Vierendeel bending. Nevertheless, Vierendeel bending was one of the possible failure modes of the beam specimen in the three-point asymmetric bending test. If the Vierendeel effect occurred, there would be diagonal cracks in the solid slab at the web opening.

For test beam with the ribbed slab in three-point bending test

- The reduced cross section for the ribbed slab increased the possibility of the Vierendeel bending effect at the web openings under the high shear created in the three-point bending test.

- Moreover, the Vierendeel bending effect would be more likely if there were web openings unfilled to represent for service integration. The Vierendeel bending moments would be resisted by local bending of the top and bottom tees, when the shear force was transferred across the openings. As the top tee had increased resistance from the composite action, a plastic hinge was likely to occur in the bottom tee. It would be followed by diagonal tensile failure of the thin concrete flange.

6.4 Test results

In this section, the results of the four-point symmetric and three-point asymmetric bending tests were presented in terms of bending moment, deflection, slip, strain, stress, cracking pattern and failure mode.

6.4.1 Results of four-point symmetric bending test

The results of the four-point symmetric bending test at the final load level are listed in Table 6.1. The final load at the two loading points was almost the same, 104kN and 108kN. The shear forces (SF) and bending moments (BM) were calculated by including the self weight of the beam specimen. The SF and BM diagrams are shown in Figure 6.12.

	Load (kN)	SF (kN)	BM (kNm)	Mid-span Deflection (mm)	Quarter-span Deflection (mm)	End Slip* (mm)
Left loading point	104	-108	-285		44.6	5.96
				64.9		
Right loading point	108	109	-287		41.4	0.41

* slip at end span

Table 6.1 Results of the four-point symmetric bending test
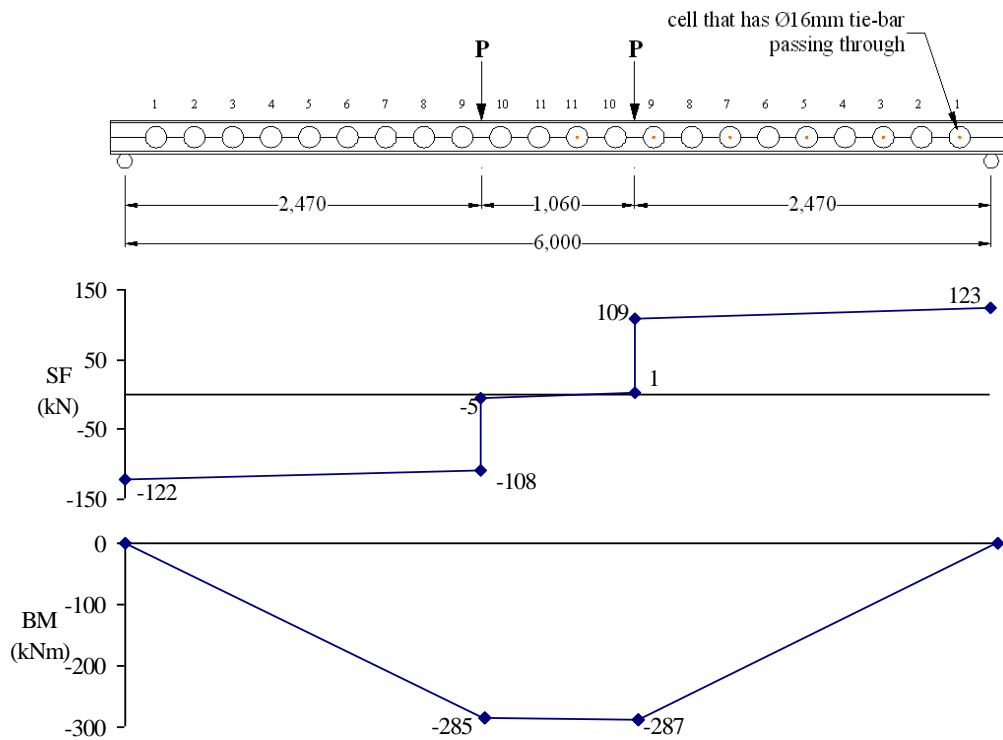
Figure 6.12 SF and BM diagrams for the four-point symmetric bending test

A uniform shear force was shown within each shear span. A small variation of the shear force along the shear span was due to the self weight of the beam specimen. The quarter-span deflections at final load level were very similar, 46.4mm and 41.4mm. This confirmed the prediction of the same deflection stiffness for the two shear spans, as their elastic (uncracked) section properties were the same. The residual deflection of the beam specimen at the mid-span was 16mm after the test. The state of the beam specimen after the four-point symmetric bending test is depicted in Figure 6.13. The two end slips at the final load were in complete contrast, 5.96mm and 0.41mm. These test results were further discussed in the following five sections.
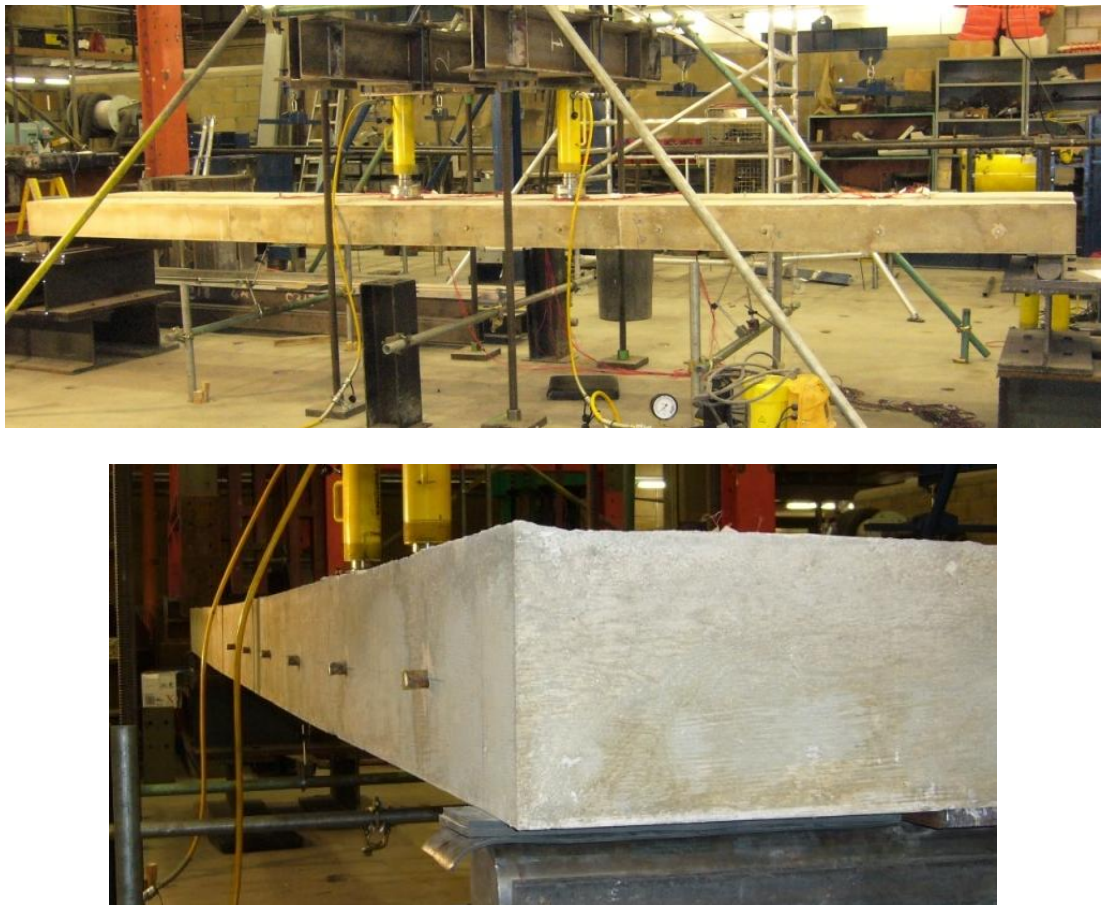
Figure 6.13 The state of the beam specimen after the four-point symmetric bending test

6.4.1.1 Bending moment

Bending moments at the loading points were 285kNm and 287kNm. The test bending moments and calculated moment resistances were compared in Table 6.2. The moment resistance of the beam specimen in full composite action and moment resistance of the steel section were calculated by using plastic stress block method with measured

material properties. The details of the calculation are shown in Appendix G. The comparisons are further shown in the deflection curve, Figure 6.14.

The significant composite action of the beam specimen was shown in the four-point symmetric bending test. The test bending moment was 1.5 times the plastic moment resistance of the steel section. The actual degree of shear connection and performance of the shear connection are further determined in Chapter 7.

Test Moment* (kNm)	Full Moment Resistance of the Test Beam (kNm)	Plastic Moment Resistance of the Steel Section (kNm)
286	348	196

* average bending moment of the two loading points

Table 6.2 Comparison for moment resistance of the four-point bending test

6.4.1.2 Deflection

The deflections were measured at mid-span and quarter-spans, as shown in Figure 6.6a. The deflections were plotted with the mid-span moments, which included the self weight of the beam specimen. The deflection curves are shown in Figures 6.14 - 6.17. The beam specimen was essentially elastic when the serviceability deflection limit of span/360 was reached. The test was stopped when the plastification of the mid-span deflection occurred. The residual mid-span deflection was 16mm (=span/372) after the test, which was less than span/360. The deflections at the different loading stages are illustrated in Figure 6.17.

The elastic behaviour of the beam specimen was clearly demonstrated well after the serviceability deflection limit of span/360 and plastic moment resistance of the steel section was exceeded, as shown in the deflection curves. After the third loading cycle, the residual deflection at mid-span was 5mm, which was negligible. This indicated there was no local failure of the beam specimen occurred within the loading cycles. The deflection behaviour of the beam specimen after the third loading cycle was slightly different, as the deflection stiffness dropped. This might be caused by local failure of the shear connection.

The deflection stiffness of both shear spans was the same. This confirmed the prediction made, in Section 6.3.1, based on the two shear spans had the same elastic (uncracked) section properties.
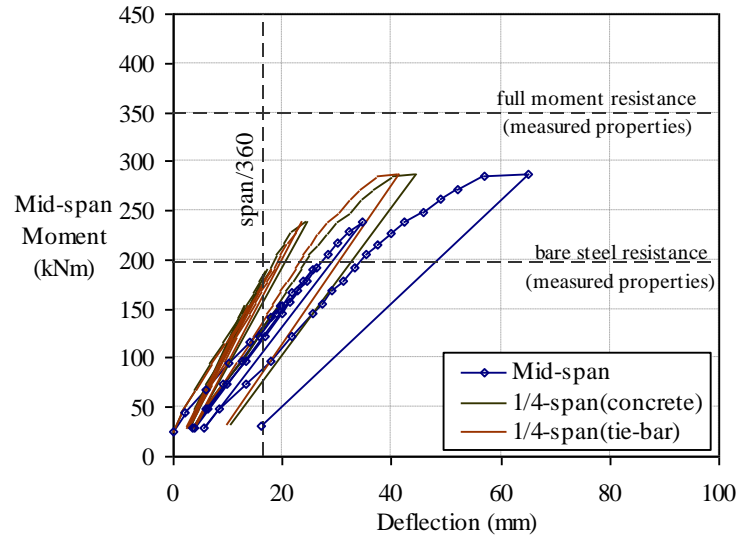
Figure 6.14 Deflections at mid-span and quarter-spans of the four-point bending test
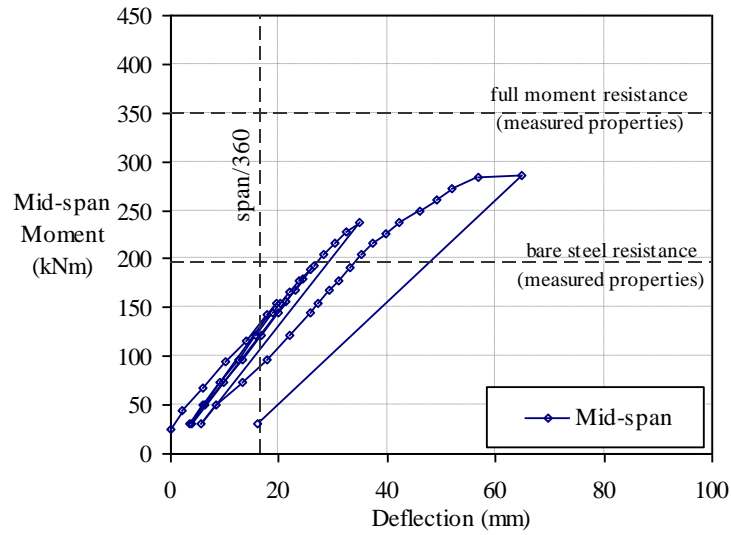
Figure 6.15 Deflections at the mid-span of the four-point bending test
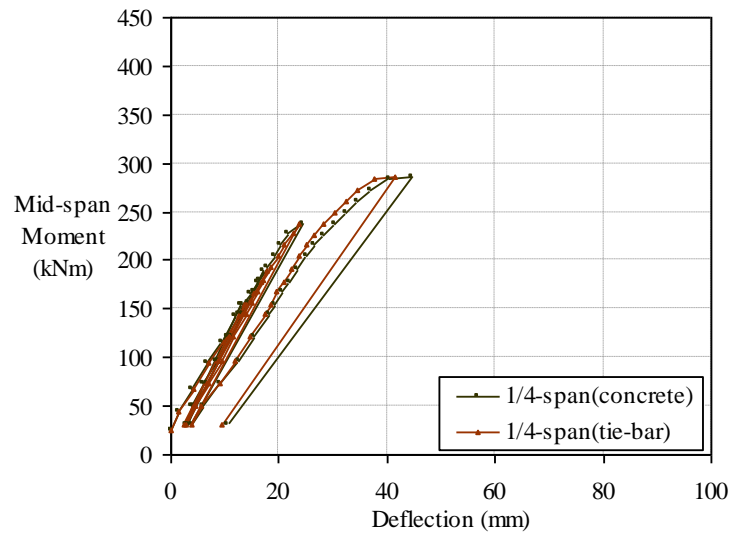
Figure 6.16 Deflections at the quarter-spans of the four-point bending test
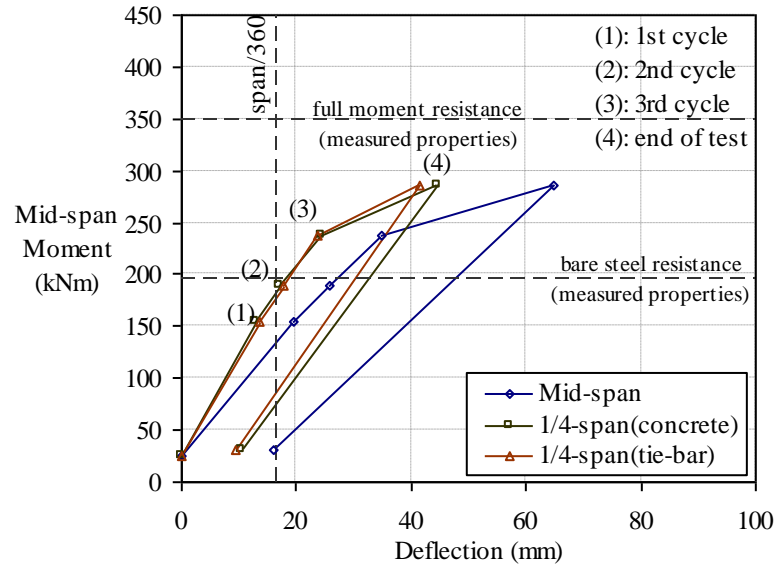
Figure 6.17 Deflections at different loading stages in the four-point bending test

6.4.1.3 Slips

The slips were measured at the end-spans, quarter-spans and mid-span, as shown in Figure 6.18. The slips over the span at the different loading stages were plotted in Figure 6.19. It was shown that both shear spans had the same uniform slip distributions during the first two loading cycles. This was due to the longitudinal shear force was uniform along the two shear spans, and the elastic slip stiffness of the two types of shear connection was the same in the push-out tests; hence the same uniform slip distributions should be shown for the two shear spans. The slip at the end of the first two loading cycles was 0.25mm, where the mid-span deflection was 26mm exceeding the serviceability deflection limit of span/360, 16.7mm. Therefore the slips of the shear connection were negligible when the serviceability limit state was reached.

The shear span had solely the concrete-infill-only shear connection showed a major slip increase at the third loading cycle, as shown in Figure 6.19. The end-span slip curves, depicted in Figure 6.20, further demonstrated the failure of the concrete-infill-only shear connection at the end of the third loading cycle. This indicated that the drop of deflection stiffness after the third loading cycle was due to the failure of the shear connection. The brittle failure mode of the concrete-infill-only shear connection was further demonstrated in the flexural test, was the same as that shown in the push-out tests.

The distinctive slip difference between the two shear spans at the end of the flexural test was illustrated in Figure 6.19. The end-span slip of the left shear span was 6mm, which was similar to the 5mm slip capacity of the concrete-infill-only shear

connection shown in the push-out tests. The slip of the right shear span at the end of the flexural test was 0.41mm, which was negligible. The combination of the concrete-infill-only and tie-bar (Ø16mm) shear connection within the right shear spans remained intact. It was demonstrated that the additional tie-bars significantly increased the longitudinal shear resistance for the composite beam specimen. The elastic slip stiffness of the two shear spans were the same, as shown in Figure 6.21b. The slip behaviour between the top and bottom of the slab, and between the slab on both sides of the web post were the same, as shown in Figure 6.22.
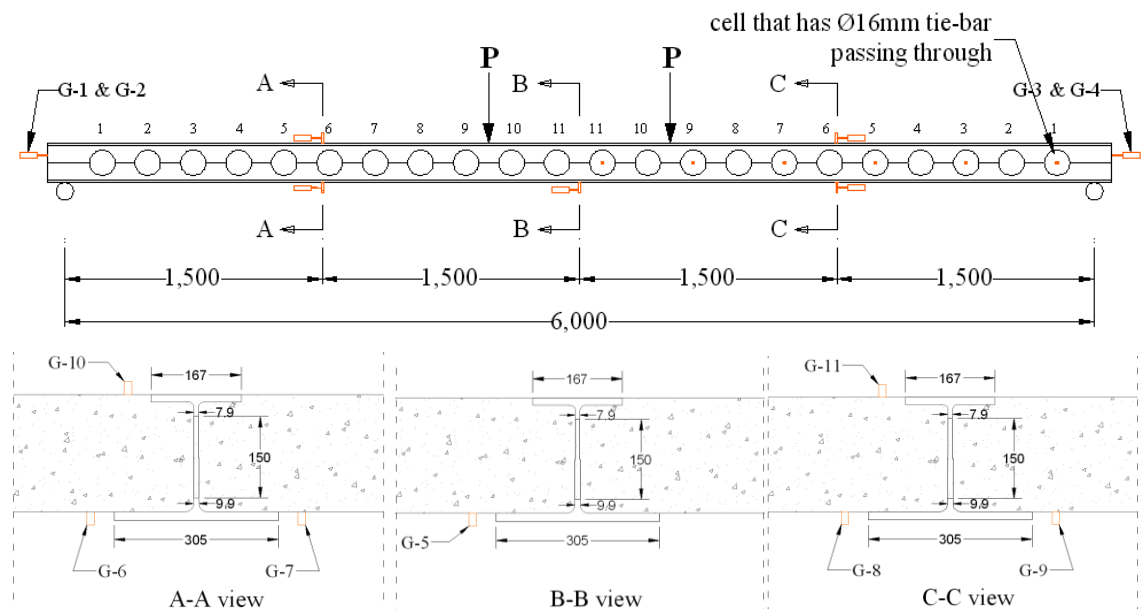
Figure 6.18 Locations of slip instrumentation and labels of the dial gauges
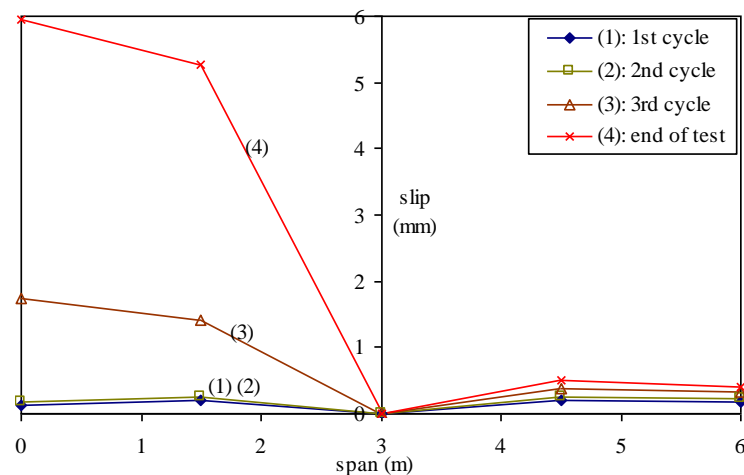
Figure 6.19 Slips over the span at the different loading stages

(a)

(b)
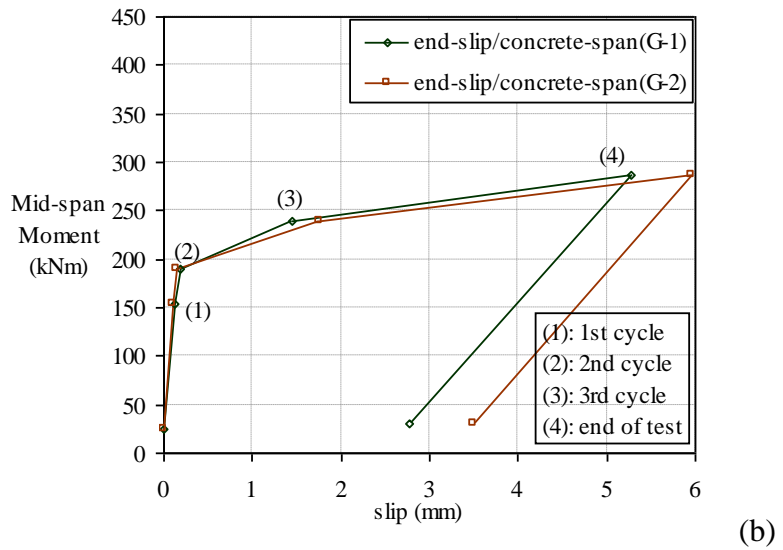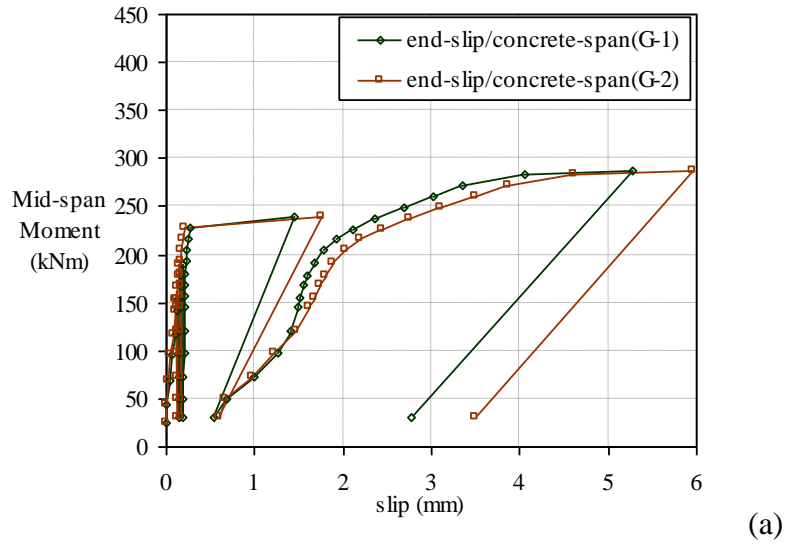
Figure 6.20 End-span slip curves of the left shear span with the concrete-infill-only shear connection: (a) slip curves, (b) slips reached at different loading stages

(a)
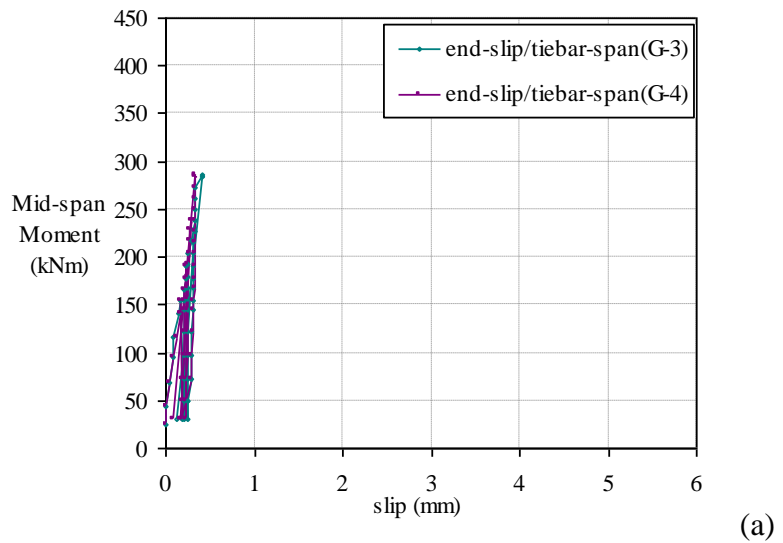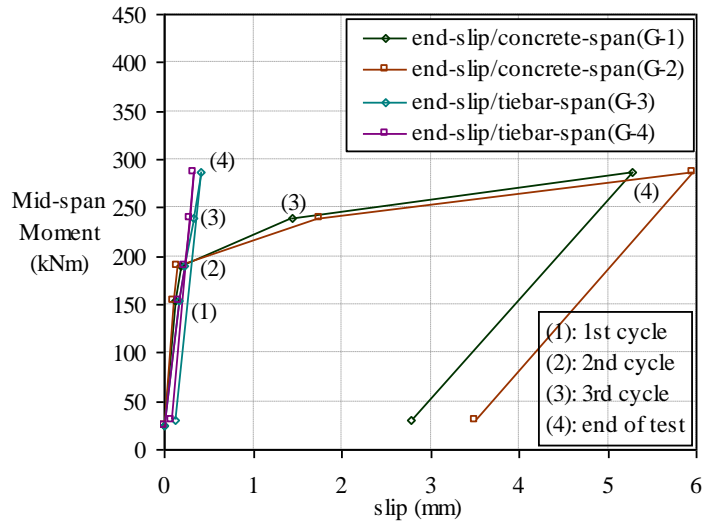
Figure 6.21 (a) End-span slip curves of the right shear span with the combination of shear connection; (b) Comparison of the slips between the two shear spans
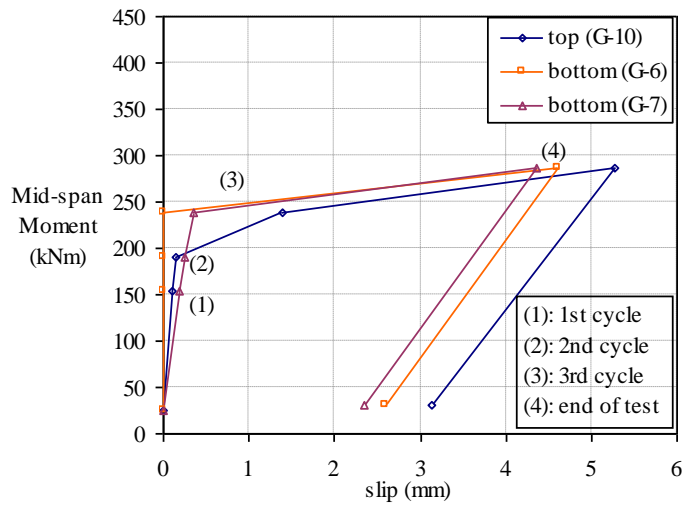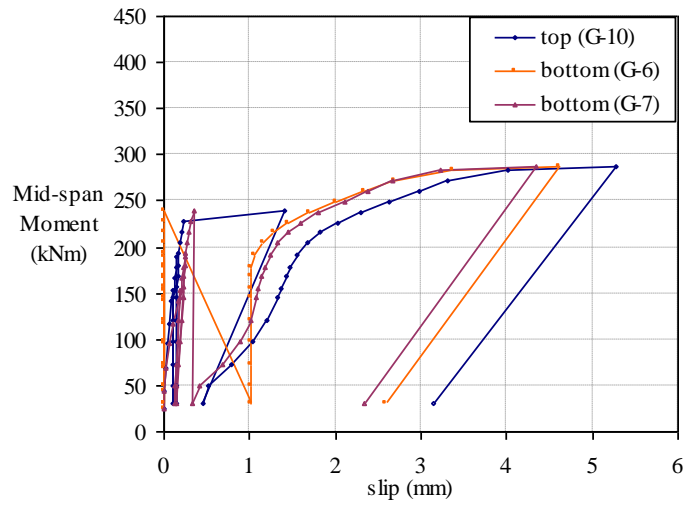
Figure 6.22 Quarter-span slips of the left shear span with the concrete-infill-only shear connection: (a) slip curves, (b) slips reached at different loading stages

6.4.1.4 Strain and stress

Strains of the steel section were measured at various locations, as shown in Figure 6.7. The strain curves at these locations are presented in Figure 6.23. It was shown there were nonlinear strains on the top flange and the web post of the top and bottom tees. Linear strains were shown on the bottom flange at all locations. Significant nonlinear compressive strains were shown on the top flange at the left loading point, location II. This indicated possible buckling of the top flange due to compression. Nonlinear strains with large residuals of 75-80% were shown on the web posts at both loading points. At the end of the test, small nonlinear tensile strain was also shown on the bottom flange at left loading point, location II. This was an initial indication of the flexural failure mode, as the bottom flange started to yield.
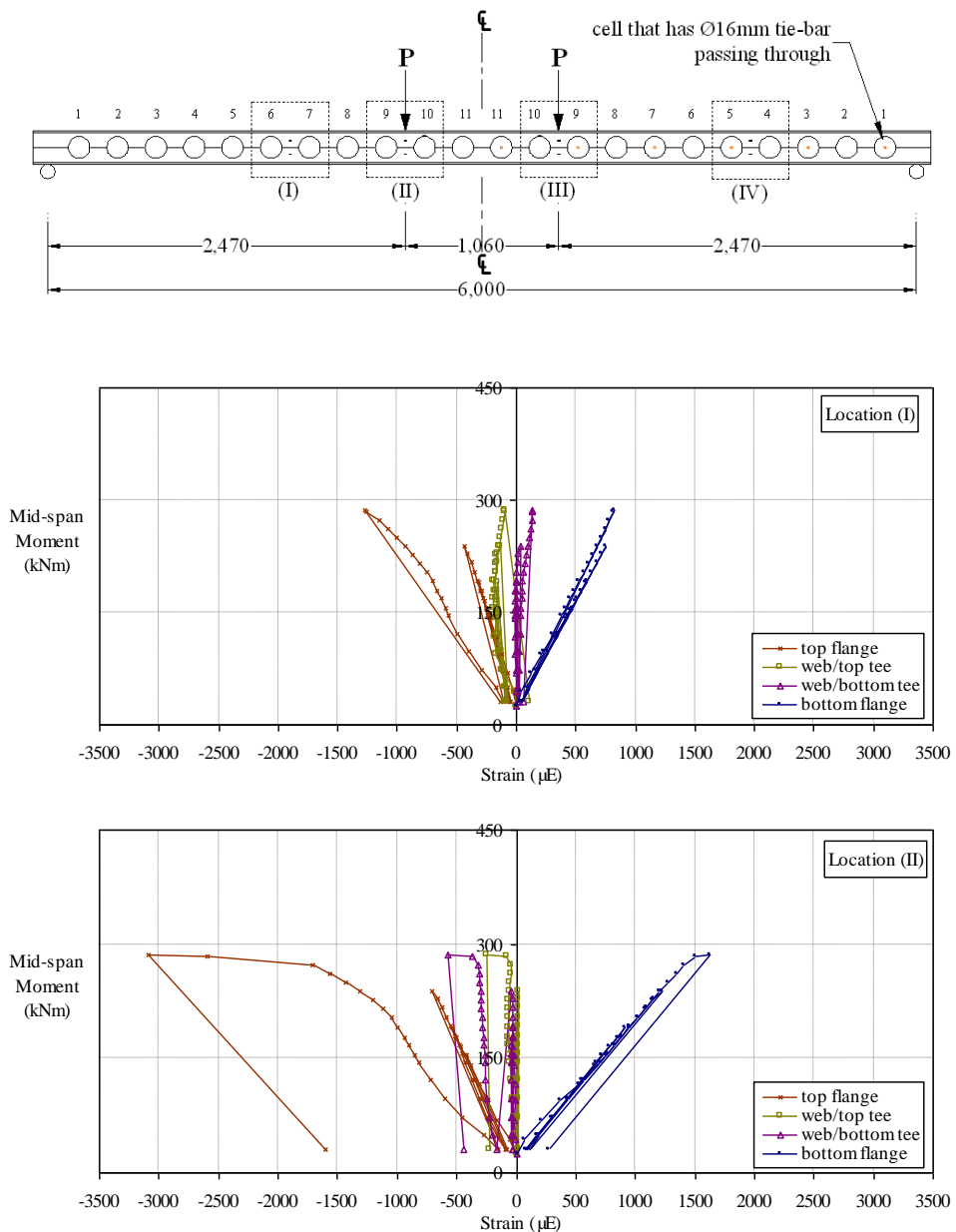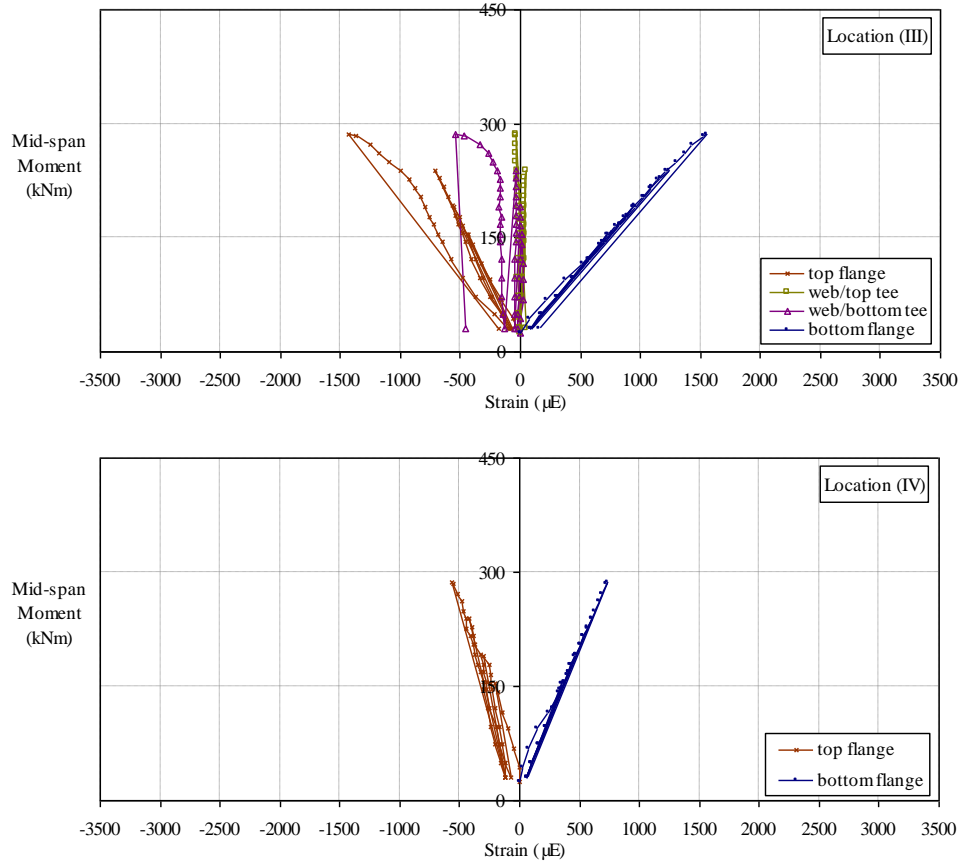
Figure 6.23 Strain curves of the different locations

The strain profiles of the cross section were obtained by taking the strain values at the different loading stages and plotted with the depth of the beam section, as shown in Figure 6.24. The strain profiles illustrated the strain developments of the beam section at the different loading stages, i.e. three loading cycles and the final loading stages. However the strain profile at the location IV was not obtained as the strains gauges on the web posts were not connected to the data logger due to its limited channels, nonetheless the location IV was the least critical location. These strain profiles showed:

- The strains on the web posts were negligible during the three loading cycles, which were the elastic loading. It indicated that elastic neutral axis of the test beam was within the depth of the web opening.

- Overall, the strain profiles were similar at both loading points. Compressive strains on the web posts were developed at the end of the test. The depth of the neutral axis at both loading points shown at the end of the test was the same, 178mm.

- The neutral axis was moved downwards when nonlinear behaviour of the beam specimen was developed.
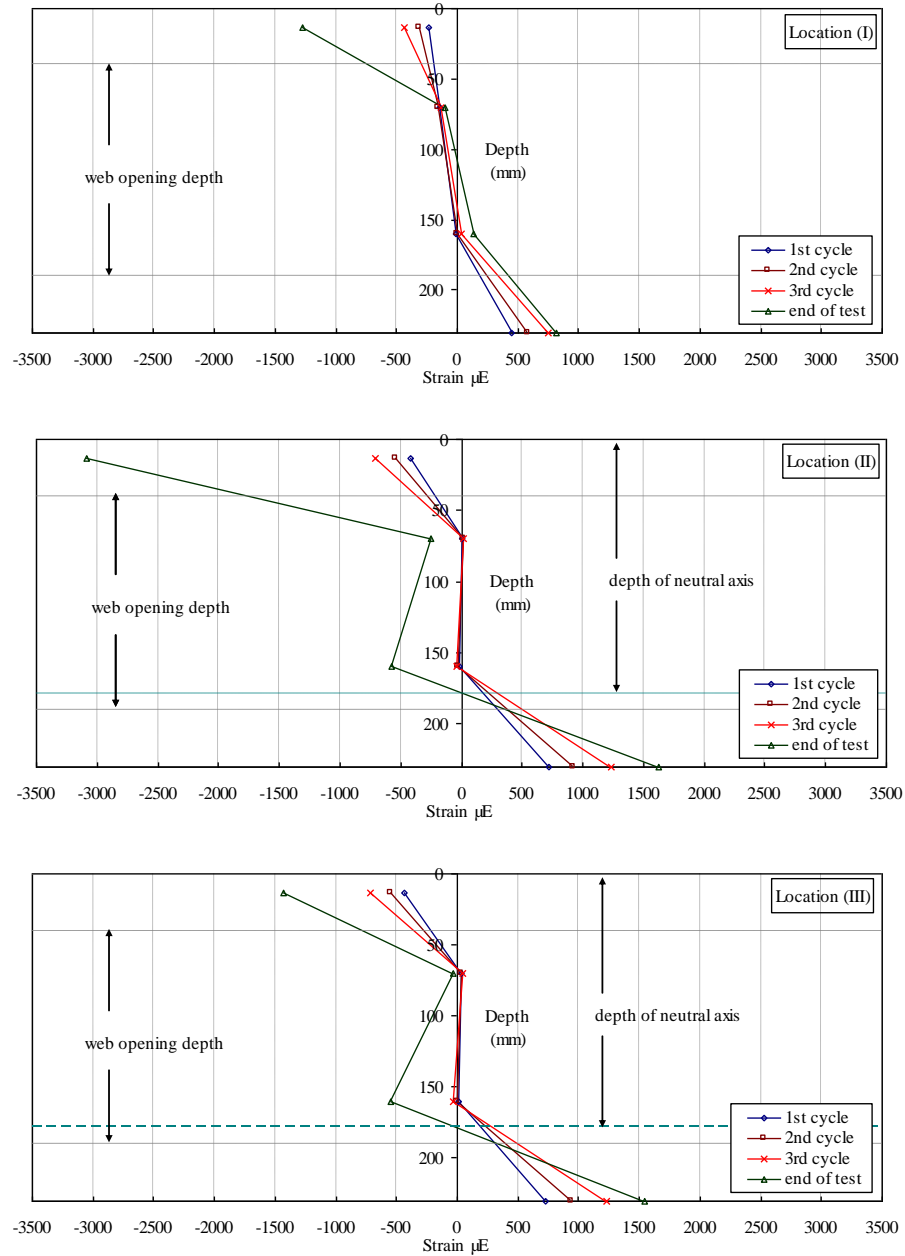
Figure 6.24 Strain profiles of the cross section at different measuring locations

The tensile stresses of the bottom flange at the different loading stages were calculated by using the linear tensile strains with the Young's Modulus of $2e5 \text{N/mm}^2$ as listed in Table 6.3. The small nonlinear tensile strain at the left loading point (location II) at the end of the test was omitted in the calculation; the linear strain value prior to the nonlinear behaviour was used instead.

	Tensile Stress (N/mm^2)			
	1st Loading Cycle	2nd Loading Cycle	3rd Loading Cycle	Final loading
Location (I)	89	116	151	164
Location (II)*	148	184	246	324
Location (III)*	145	187	247	309
Location (IV)	71	92	120	146

* loading points

Table 6.3 Tensile stresses on the steel bottom flange at different loading stages

6.4.1.5 Cracking pattern

The cracks of the concrete slab were vertical tensile cracks. No diagonal shear cracks were observed. The cracks were mainly in the regions of the constant moment and close to the loading points. The cracks were uniformly distributed in the region of constant moment, as depicted in Figure 6.25; these cracks were induced by the pure bending. Only two cracks were shown on the top side of the slab. Several cracks were shown on the bottom side of the slab.

The cracks lose to the left loading point, depicted in Figure 6.26, were longer and wider than those within the pure bending region. These cracks propagated with the increase of load. The cracks lose to the right loading point, depicted in Figure 6.27, were smaller and less concentrated than those close to the left loading point, as the additional tie-bars reduced the development of the cracks. There was an Ø16mm tie-bars passing through every alternative openings in the right half of the beam span.

The first crack occurred at the mid-span deflection of 14mm, which was less than the span/360 of 16.7mm. Hence, the concrete slab cracked before the serviceability limit state was reached. The cracked section was suggested for the deflection analysis, which is carried out in Section 7.2 to develop a design method for deflection check of the composite shallow cellular floor beams.

The transverse separations between the concrete slab and steel section at the end of the left shear span were 2.6mm and 5.2mm, as shown in Figure 6.28. The separation values were the same as that shown in the push-out tests, ranging from 2.3mm to 5.2mm. It further indicated the ultimate failure of the concrete-infill-only shear connection in the left shear span.
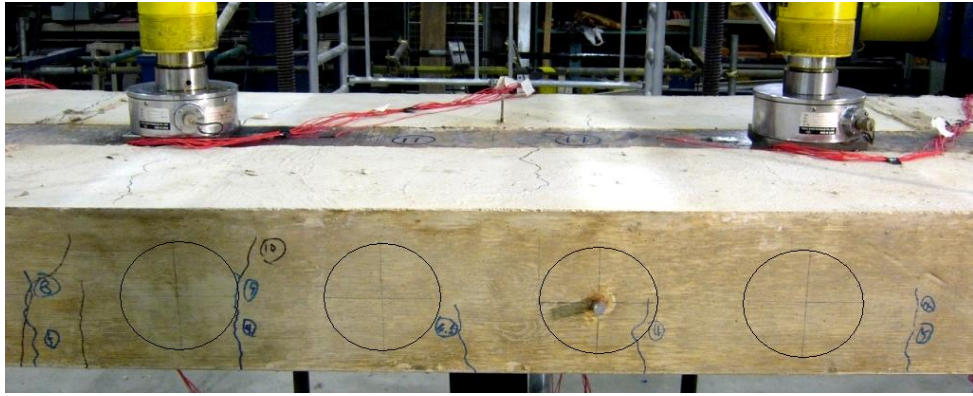
(a)

(b)   (c)

Figure 6.25 Cracking pattern in the pure bending region: (a) vertical tensile cracks,
(b) two cracks on the top of the slab, (c) many cracks on the bottom of the slab
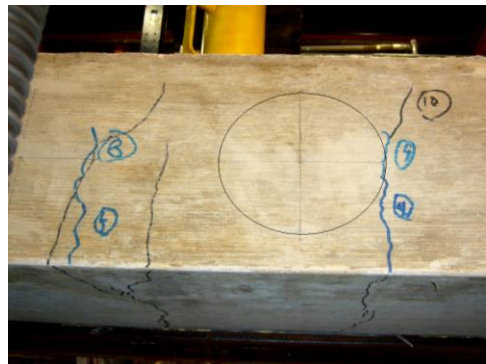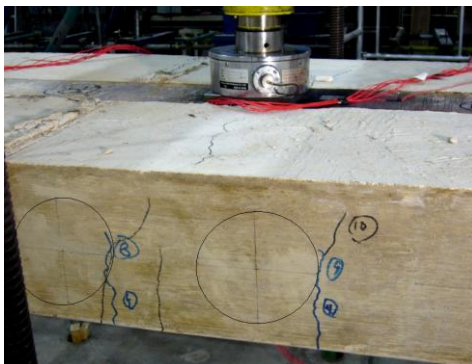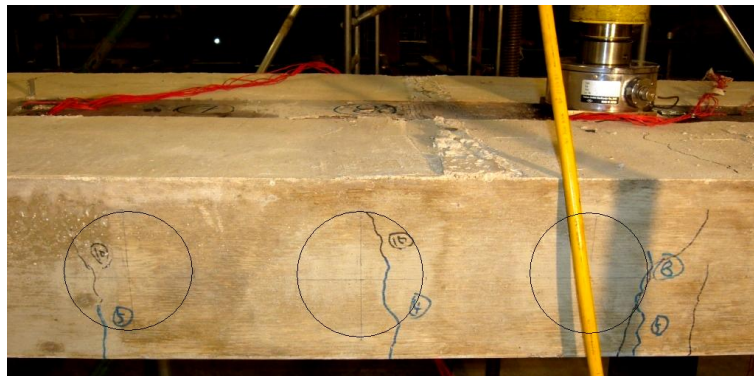
Figure 6.26 Cracking pattern lose to the left loading point
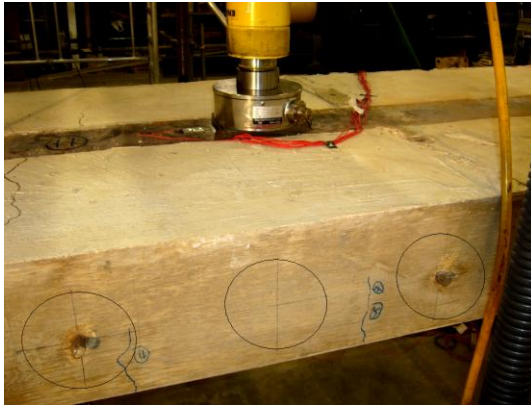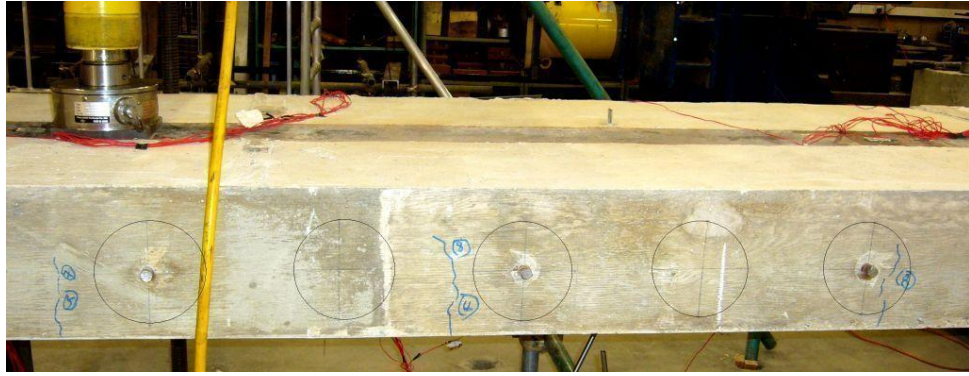
Figure 6.27 Cracking pattern lose to the right loading point

(a)

(b)

(c)

Figure 6.28 Transverse separations at the end of left shear span: (a) prior to the test, (b) separations at the end of test, (c) separation values

6.4.2 Results of three-point asymmetric bending test

The three-point asymmetric bending test created high shear within the shorter shear span, which had the combination of the concrete-infill-only and tie-bar (Ø16mm) shear connection. Two loading cycles were applied before the test beam was tested to the ultimate failure. The test results at the ultimate failure are summarised in Table 6.4. The SF and BM were calculated by including the self weight of the beam specimen. The SF and BM diagrams are shown in Figure 6.29.

Load (kN)	SF* (kN)	BM (kNm)	Deflection at Loading Point (mm)	Deflection at Max-deflection point (mm)	End Slip ˜ (mm)
340	267	-385	65	80	3.82

* SF of the shorter shear span, ˜ end-span slip of the shorter shear span

Table 6.4 Results of the three-point asymmetric bending test
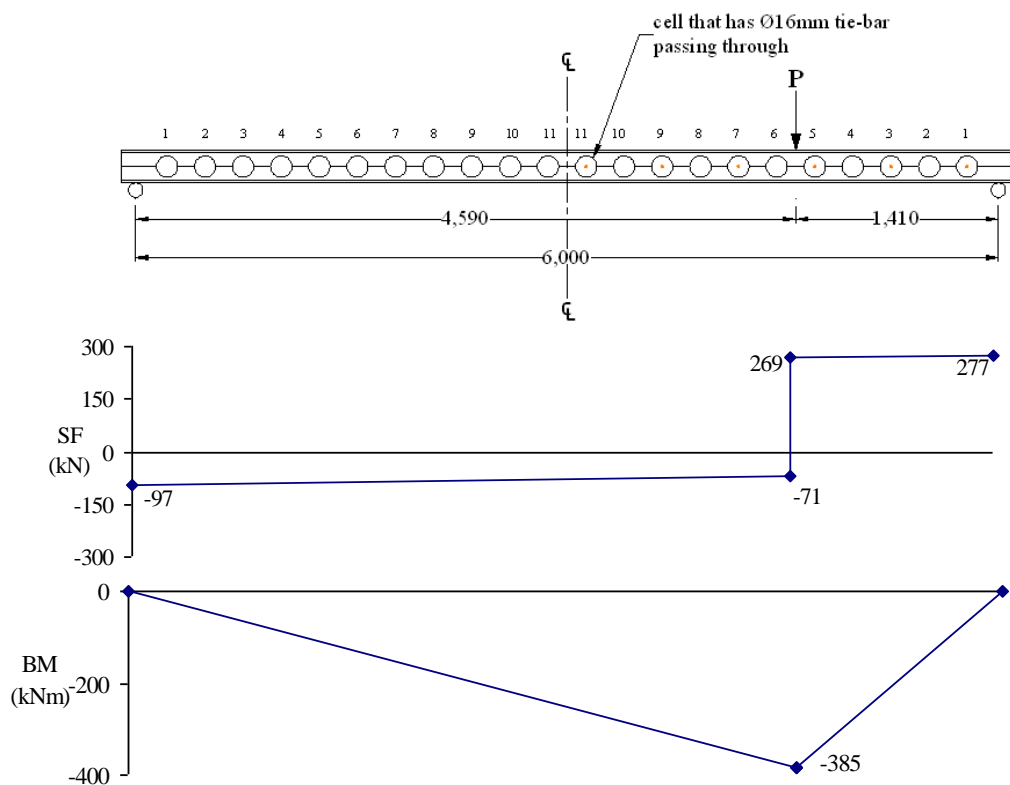
Figure 6.29 SF and BM diagrams of the three-point asymmetric bending test

6.4.2.1 Bending moment

The bending moment of 385kNm was reached at the ultimate failure. The bending moment of the flexural test is compared with the calculated moment resistances in Table 6.5. The moment resistance in full composite action and moment resistance of the steel

section were calculated by using plastic stress block method with measured material properties. The details of the calculation are shown in Appendix J. The comparisons are further illustrated in the deflection curves, Figure 6.30.

It was shown that significant composite action was achieved in the three-point asymmetric bending test. The test moment was 1.5 times the plastic moment resistance of the steel section. The actual degree of shear connection and shear performance of the shear connection were determined in Chapter 7.

Test Moment (kNm)	Full Moment Resistance of the Test Beam (kNm)	Plastic Moment Resistance of the Steel Section (kNm)
385	440	255

Table 6.5 Comparison between the test moment and calculated moment resistances

6.4.2.2 Deflection

The deflections of the three-point asymmetric bending test were measured at the loading point, maximum deflection point and quarter-span, as shown in Figure 6.10a. The deflection curves of the beam specimen are shown in Figure 6.30. The vertical axis was the bending moment at the loading-point, or the applied bending moment calculated by including the self weight of the beam specimen. The plateau region with large residual deflections was clearly shown in the deflection curves. This indicated the plastic flexural failure mode of the beam specimen. The residual deflections of the previous flexural test, four-point symmetric bending test, were not included in the deflection curves, as the deflection analysis was not part of the objectives for the three-point asymmetric bending test. This flexural test was to investigate the flexural behaviour of the beam specimen and shear performance of the shear connection under high shear.

At the ultimate failure (or the maximum load level), the deflections at the loading point and the max-deflection point were 65mm and 80mm respectively. The deflection profiles of the beam specimen are shown in Figure 6.34. The deflected shape of the beam specimen in the flexural test is depicted in Figure 6.35.
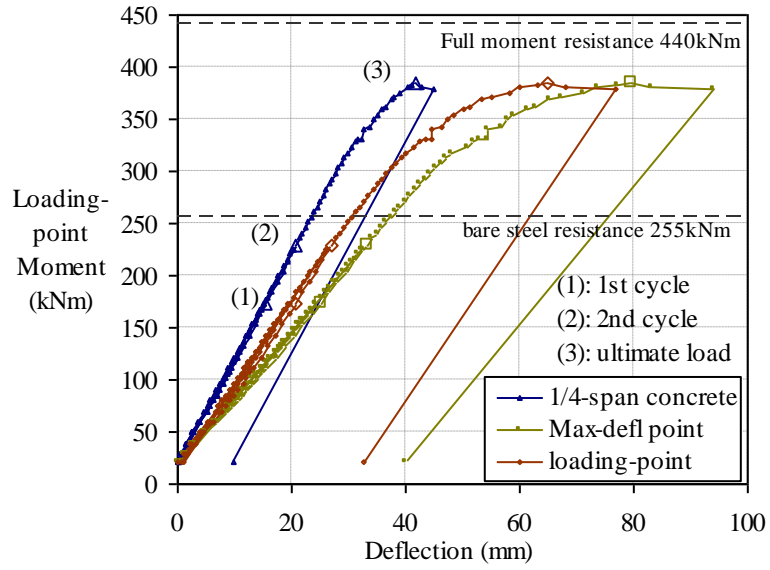
Figure 6.30 Deflections of the three-point asymmetric bending test
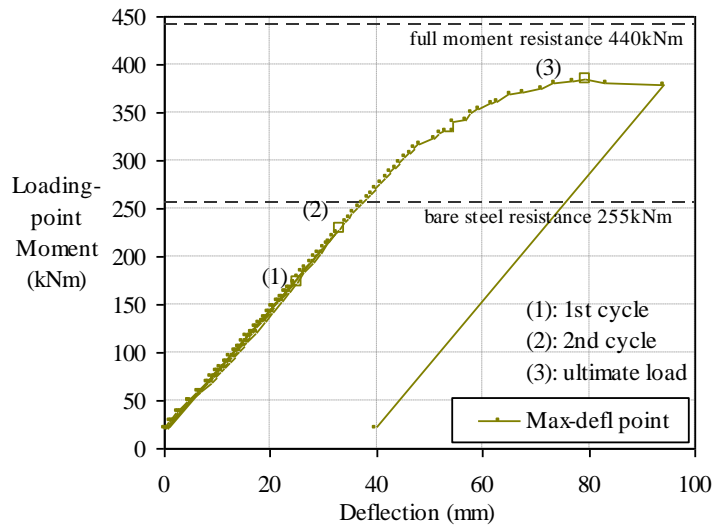
Figure 6.31 Deflections at the maximum deflection point in the three-point bending
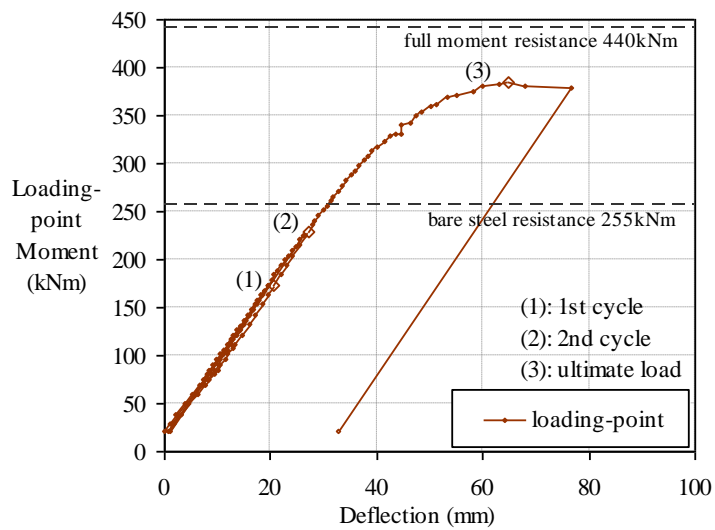
Figure 6.32 Deflections at the loading point in the three-point bending test
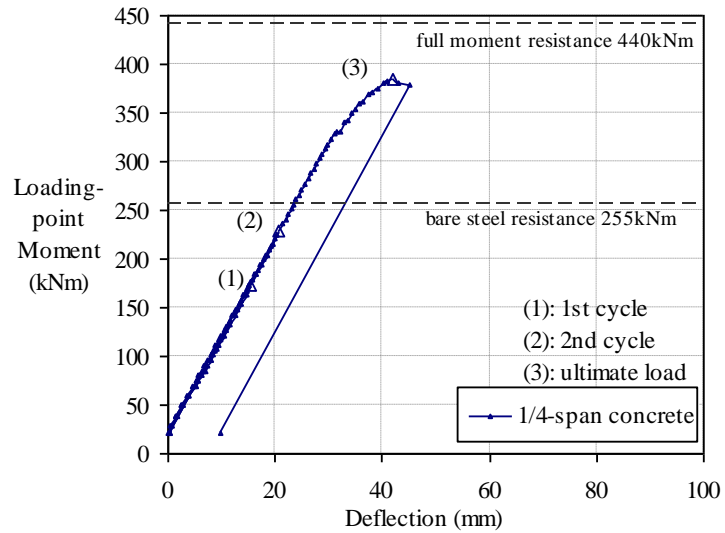
Figure 6.33 Deflections at the quarter-span in the three-point bending test
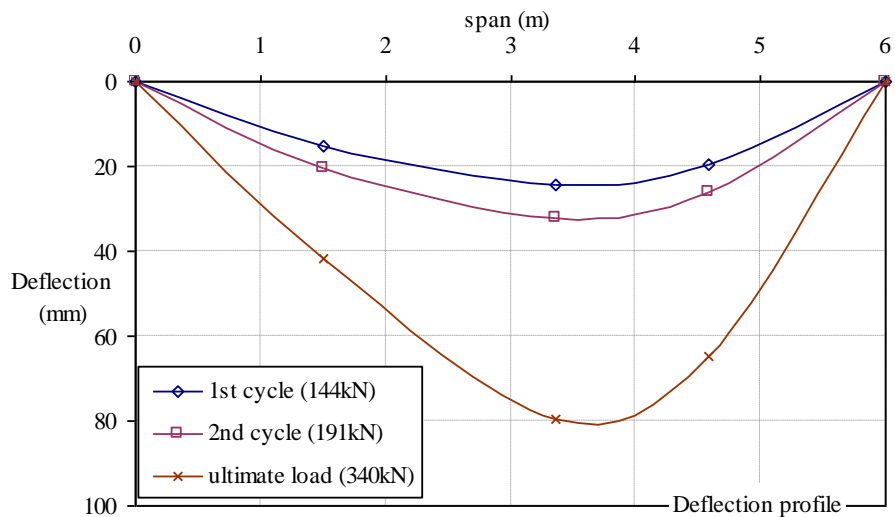
Figure 6.34 Deflection profiles of the three-point asymmetric bending test

Figure 6.35 Deflected shape of the beam specimen in the three-point bending test

6.4.2.3 Slip

There were two concrete-infill-only and three tie-bar (Ø16mm) shear connection within the shorter shear span. The slips between the concrete slab and steel section were measured at various locations, as shown in Figure 6.36. The slips over the span at the different loading stages are shown in Figure 6.37. The residual slip of the shorter shear span in the previous flexural test was 0.1mm (negligible); hence, it was omitted in the slip curves of this test. The residual slip of the long shear span was 3.5mm in the previous flexural test; however it was not included in the slip curves of this test, as the slips of the longer shear span was not part of the investigation for this flexural test.

The slip of the shorter shear span during the first two loading cycles (essentially the elastic loading) was 0.45mm. The overall slip behaviour of the combined shear connection was elastic then followed by plastic deformation with extensive slips, as shown in Figure 6.38a. This ductile slip behaviour and failure mode of the combined shear connection was very similar to that of the tie-bar (Ø16mm) shear connection in the push-out test series-II. It was shown that the additional tie-bars increased the ductility of the shear connection in the flexural test. The slip behaviour and failure mode of the combined shear connection were completely different with those of the concrete-

infill-only shear connection in the four-point symmetric bending test. At the ultimate load, the end slip of the shorter shear span was 4mm, which was similar to the failure slip of the concrete-infill-only shear connection shown in the four-point symmetric bending test.

Uniform behaviour and no-discrete failure (or separate failure) of the two types of shear connection was shown, which had a combined effect towards the composite action. This approved the assumption (made in Section 6.3.2) for the non-discrete failure of the combined shear connection when they were used in combination.

A small amount of ductility was shown by the shear connection in the longer shear span, as illustrated in Figure 6.39. As there were eight un-damaged shear connection in the longer shear span; three of the shear connection had the additional tie-bars which provided the ductility.
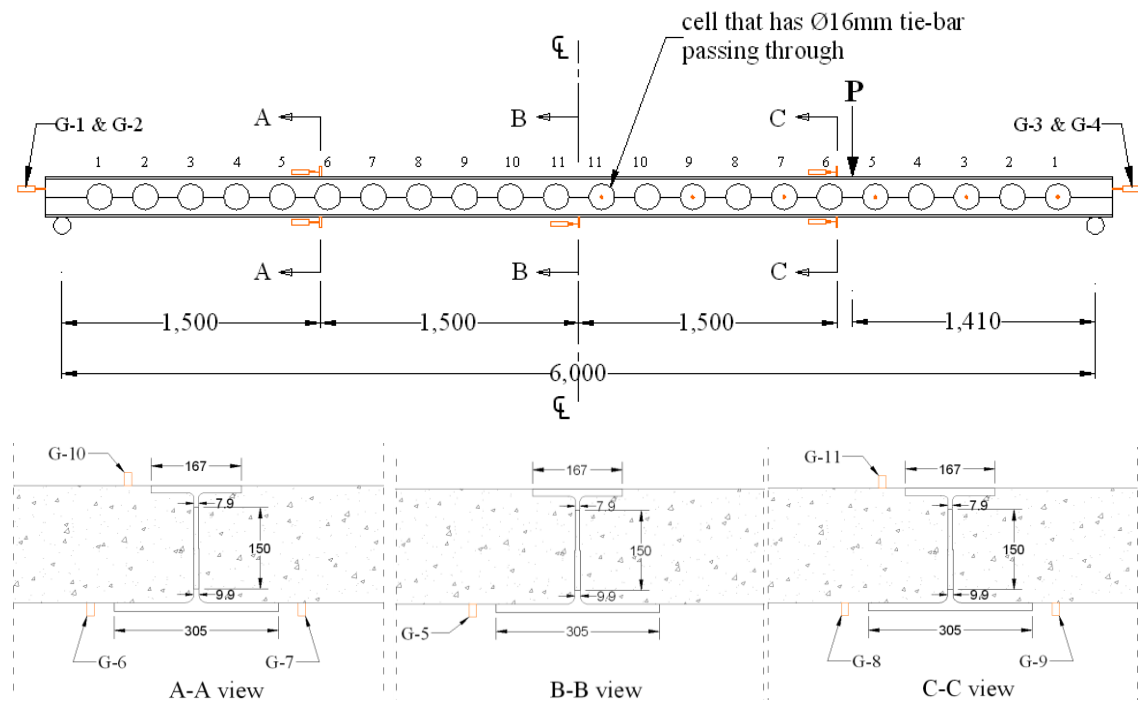
Figure 6.36 Locations of slip instrumentation and labels of the dial gauges
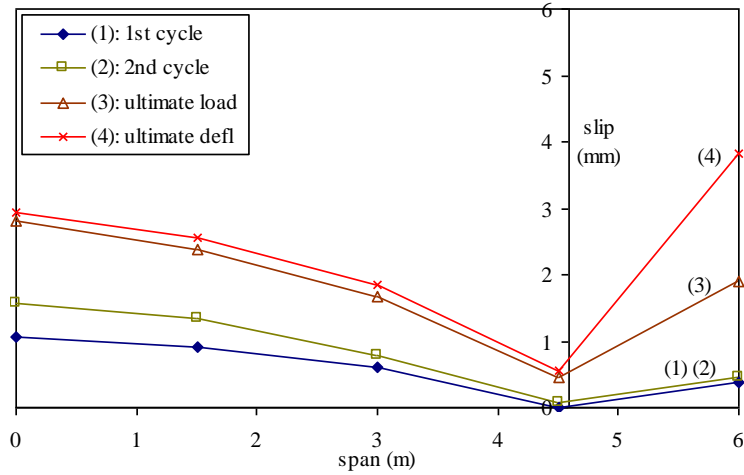
Figure 6.37 Slips over the span at the different loading stages of the three-point asymmetric bending test
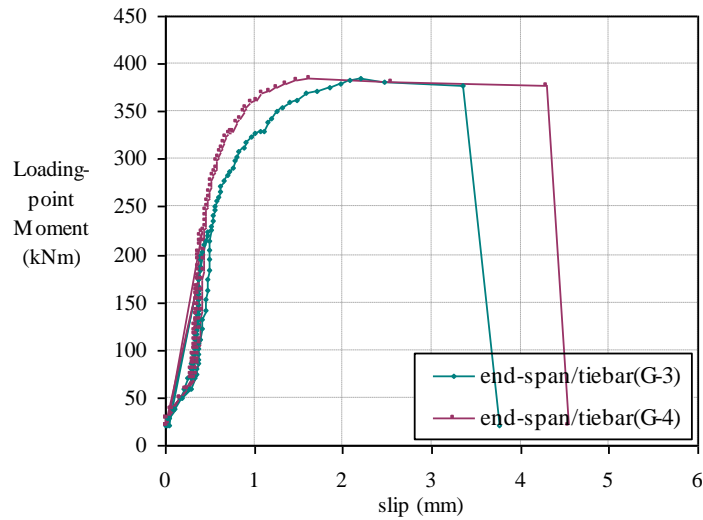
(a)
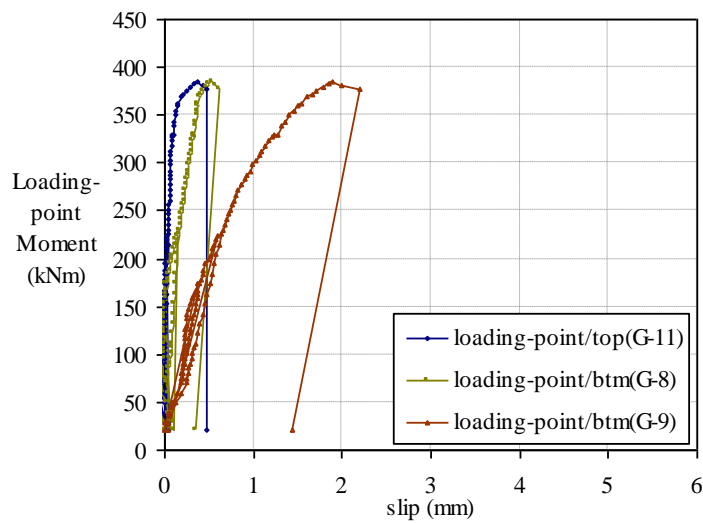
(b)

Figure 6.38 (a) End slips of the shorter shear span with the combined shear connection; (b) Slips at the loading point

(a)

(b)
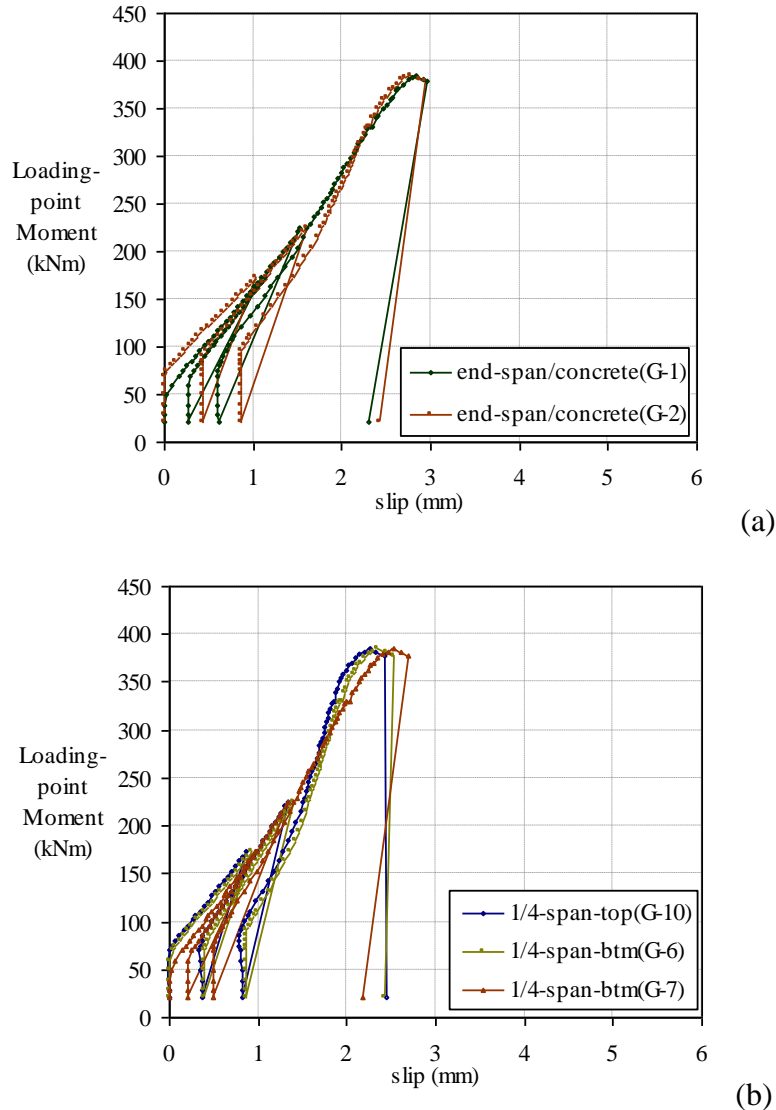
Figure 6.39 Slips of the longer shear span (a) end-span, (b) quarter-span

6.4.2.4 Strain and stress

The strains were measured at various locations, as shown in Figure 6.40. The location IV was the previously planned loading point. The strains under the actual loading point for the three-point asymmetric bending were not obtained. However, the strains at location IV would show the similar strain development to that of the actual loading point. The strain curves at these locations are presented in Figure 6.40. The residual strains of the previous flexural test, four-point symmetric bending test, were not included in these strain curves which were in the aim to demonstrate the strain development for the three-point asymmetric bending test.

The strain patterns shown at locations of I, II and III, apart from IV were the same. Linear strains were developed in the cross section at the location, I, II and III.

Non-linear and chaotic strain pattern was shown at location IV, which was near the loading point. This might be due to the possible disruption of the strain gauges caused by the slips of the concrete slab.

However, the linear strain on the bottom flange was shown at location IV. Its maximum linear tensile strain was 1633με; hence the linear tensile stress was 327N/mm^2. By assuming the tensile strain varied linearly along the shear span, and was proportional to the bending moment, the tensile stress of 400N/mm^2 at the loading point was calculated. This calculated tensile stress was very close to the coupon test yield stress of 414N/mm^2. As the permanent deflections were observed at the end of the test, thus the yield stress of 414N/mm^2 was considered been reached on the bottom flange at the loading point.

The strain profiles of the cross section were also obtained by taking the strain values at the different loading stages and plotted with the depth of the beam section, as shown in Figure 6.41. The strain profile at the location I was not obtained, as the strain gauges on the web posts were not connected with the data logger due to its limited channels; nonetheless, location I was the least critical location in the three-asymmetric bending test. The strain profiles were very similar at the location II and III. However, zigzag strain profile was shown at the location III, as the strain gauges at this location might had been disturbed by the slips of the concrete slab.
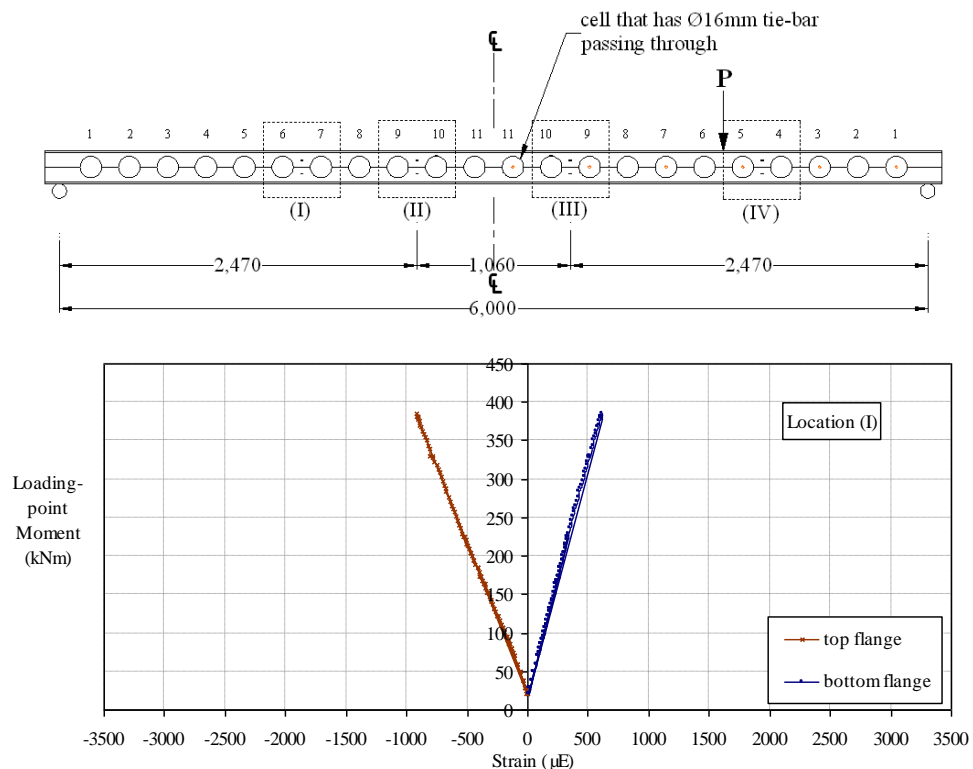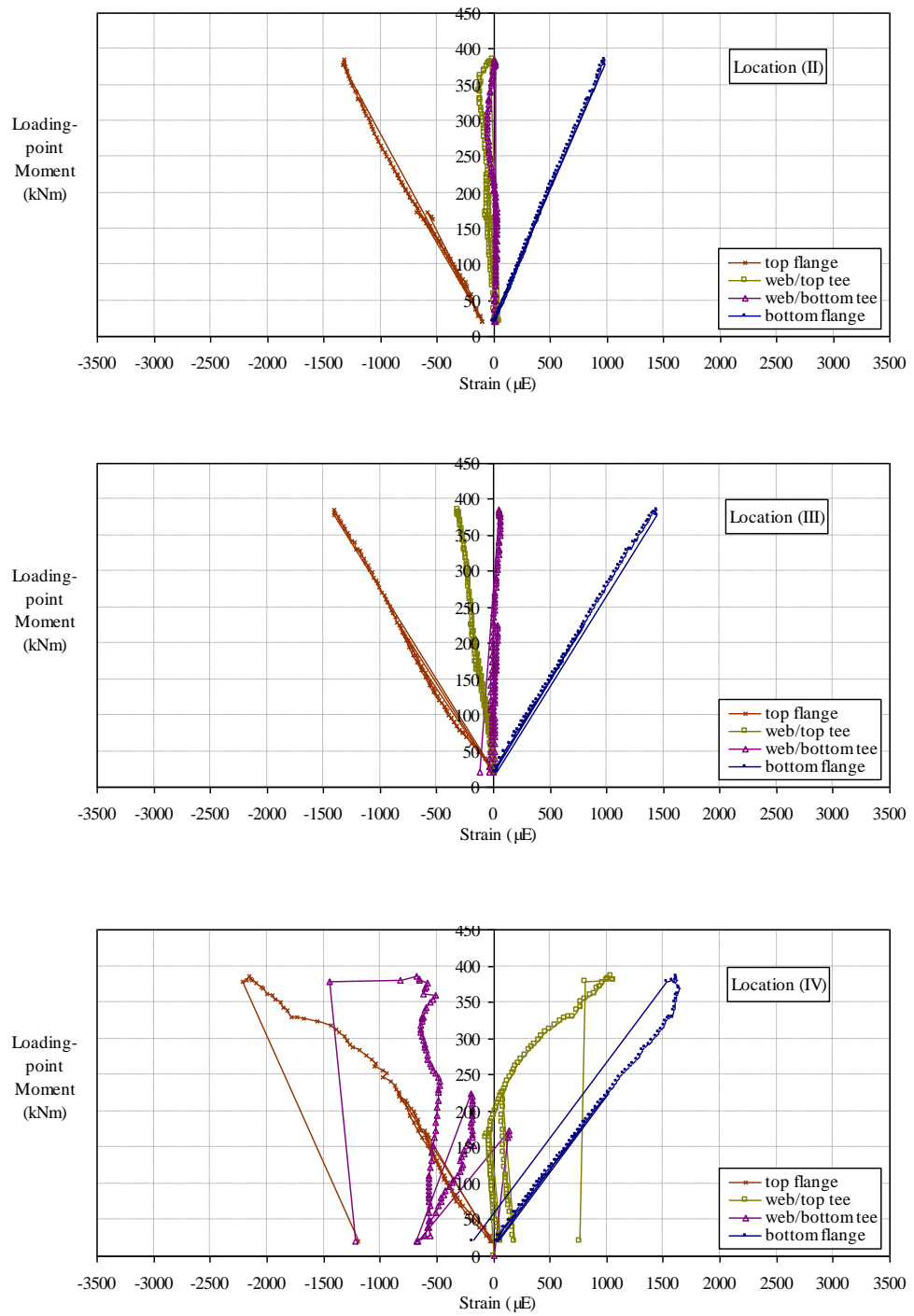
Figure 6.40 Strain curves at the different locations
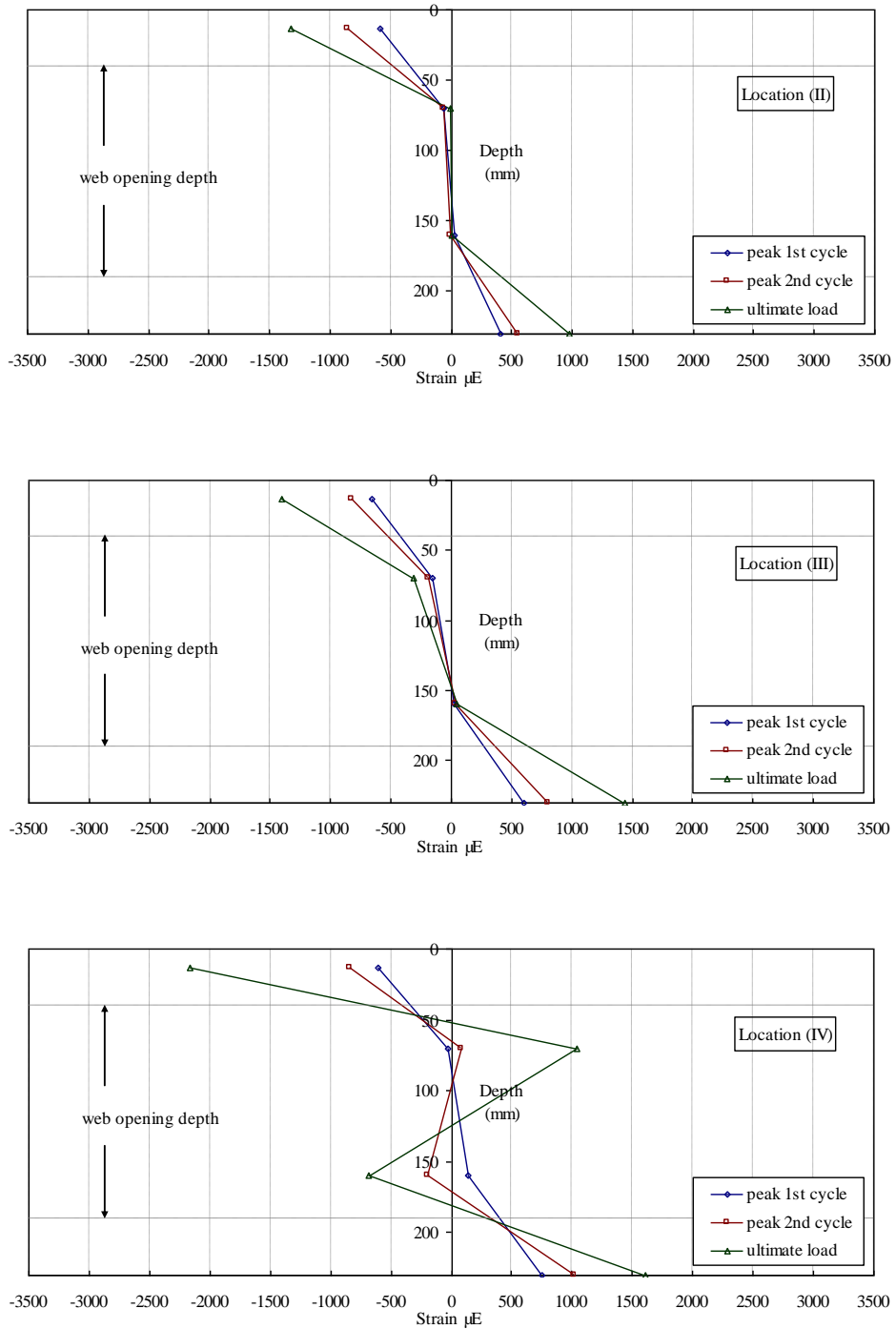
Figure 6.41 Strain profiles of the cross section at the different locations

6.4.2.5 Cracking pattern

Large cracks occurred under the loading point, as depicted in Figure 6.42; the widths of the cracks were 4.0-6.2mm. Small vertical tensile cracks of 0.15mm width were induced in the longer shear span. The overall cracking pattern of the beam specimen in the three-point asymmetric bending is shown in Figure 6.43. The cracks from the previous

flexural test were propagated in the mid-span region, as shown in Figure 6.44. Cracks of width up to 2mm occurred near the support of the short shear span, as depicted in Figure 6.45; they were first induced on the top side of the concrete slab, and then propagated towards the bottom of the slab.
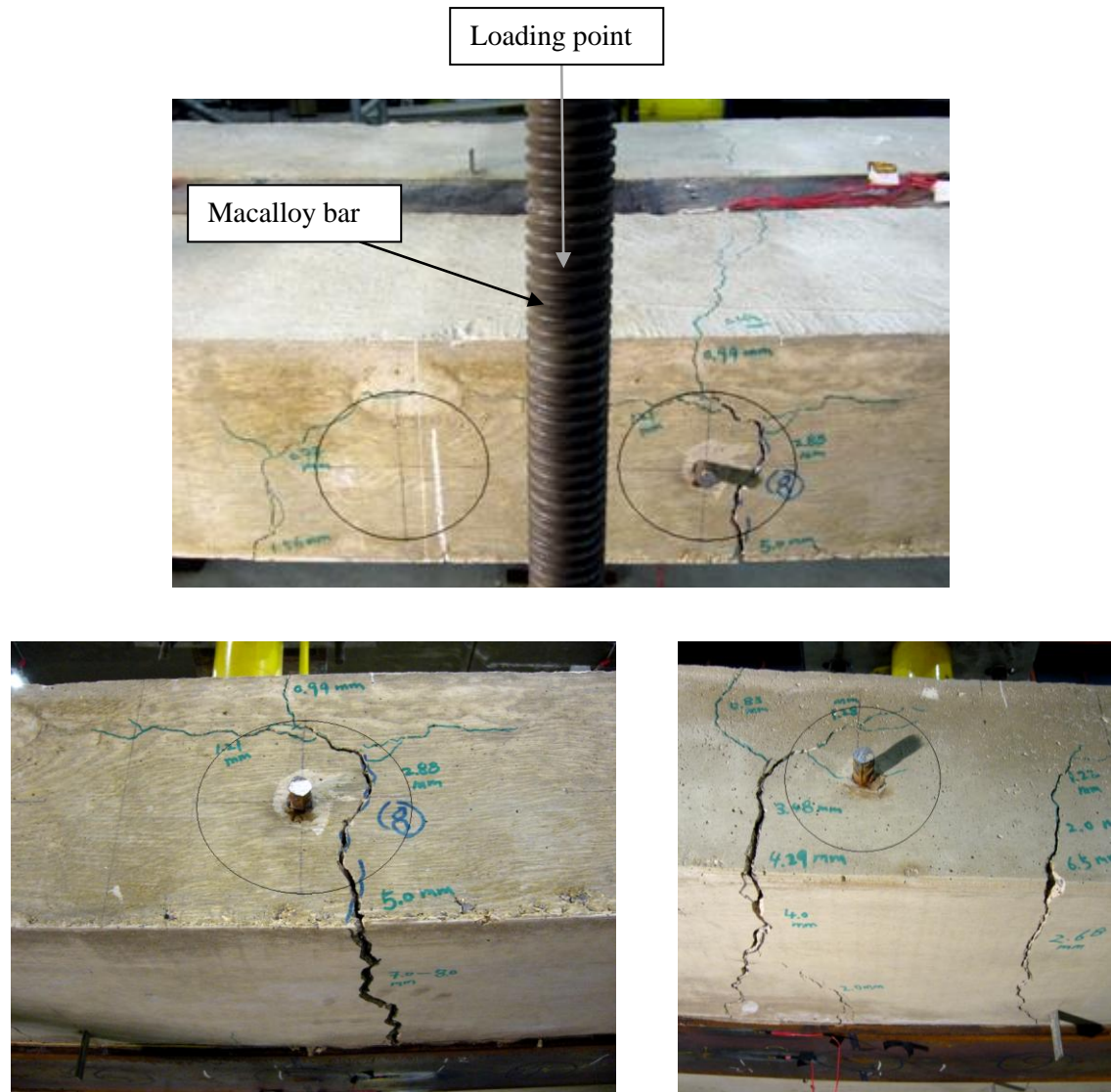
Figure 6.42 Cracks at the loading point in the three-point asymmetric bending test

(a)
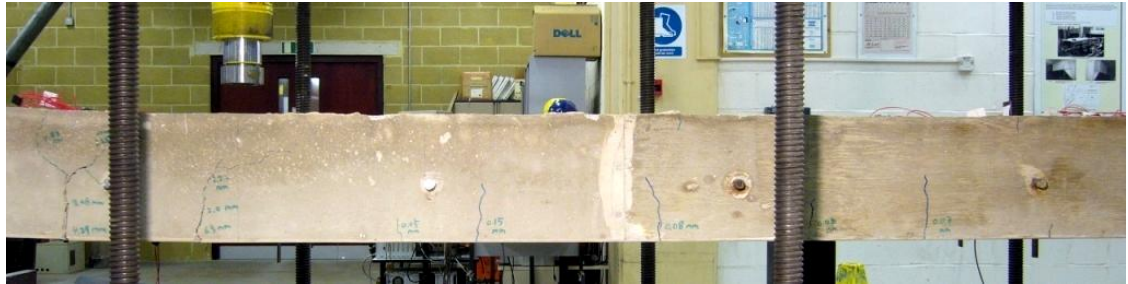
(b)

Figure 6.43 Cracking pattern of the three-point asymmetric bending test
(a) shorter shear span, (b) longer shear span

Figure 6.44 Propagation of the cracks at the mid-span (blue lines are the new cracks)

Figure 6.45 Cracks near the support of the shorter shear span

Figure 6.46 Failure profile of the beam specimen in the three-point bending test

6.4.2.6 Failure mode and failure mechanism

The flexural failure mode of the beam specimen was shown in the three-point asymmetric bending test. It was demonstrated by the permanent deflection profile, as depicted in Figure 6.46. The flexural failure mode confirmed the prediction made in Section 6.3.2. Although, the three-point asymmetric bending test created high shear, which could induce the Vierendeel bending. However, the section was partially encased by solid slab which increased the vertical shear capacity of the composite section, and the web openings were filled with in-situ concrete which enhanced the shear resistance of the web openings and prevented the Vierendeel bending.

The flexural failure mechanism of the beam specimen in the three-point asymmetric bending test was due to the ductile failure of the shear connection. The full plastic moment resistance of the specimen had not been reached, as the plastic strain of the bottom flange was not observed. One of the indications for the full plastic flexural failure of a composite beam was the crushing of the concrete slab. This was not observed in the flexural test. Hence, the beam specimen of the composite shallow cellular floor beam was not failed by the full plastic moment resistance, but due to the failure of the shear connection. The slip curves, Figure 6.38, also demonstrated the ductile failure of the combined shear connection in the three-point asymmetric bending test.

6.4.3 Geometric limits

The test beam specimen was constructed using the steel section with regular spaced circular web openings and solid slab. The web opening diameter was 150mm with 265mm spacing. The size of the steel section represented the actual steel section used for the span of 6m. The concrete slab flushed with the top flange of the steel section and sit on the bottom flange. There was no concrete topping above the steel top flange. The total width of the solid slab was 1m. There was no end plate welded on the steel section, otherwise it would confine the slips of the test beam. The following geometric limits were imposed on the flexural test results, as the configurations of the test beam could not fully represent all aspects of the composite shallow cellular floor beams used in the practice.

- By using solid slab, the test data could not represent the composite beams with ribbed slab, in terms of failure modes, serviceability check (deflection) and composite interaction, as discussed in Section 6.2;

- By greasing the steel section for the test beam, the shear bond strength was eliminated from the flexural tests. Although it was to particularly investigate the shear transferring mechanism of the unique shear connection, but the shear bond resistance was also part of the longitudinal shear resistance of the composite shallow cellular floor beams;

- By having the wide spacing of 265mm, the test beam eliminated the possibility for the failure modes of the web-post buckling and web-post horizontal shear failure, which would be the case especially for the beam with web openings unfilled to represent service integration;

- By having the concrete slab flushed with the steel top flange, the test beam could not represent the use of concrete topping above the steel top flange, which had shown its contribution towards composite action in the ASB flexural tests presented in Lawson et al 1999;

- By having the test beam without the end plated, the test data could only represent the unconfined slip movements.

- Finally, the steel section used for the test beam also imposed geometric limits on the test data, as listed below.

Parameter	Limits
Beam depth/opening diameter	1.5
Spacing/opening diameter	1.8
Beam depth/span	1/26

6.5 Conclusions of the flexural tests

The four-point symmetric bending was first carried out without the failure of the beam specimen, only up to the plastification of the mid-span deflection. This flexural test created a bending moment profile similar to that of the UDL, with a pure bending region. The concrete-infill-only shear connection was particularly investigated in the four-point symmetric bending test. The three-point asymmetric bending test was then carried out up to the ultimate failure of the beam specimen. The test created high shear in the shorter shear span, which had the combination of concrete-infill-only and tie-bar (Ø16mm) shear connection. The following conclusions were made from both flexural tests.

- Both flexural tests showed significant composite action due to the unique shear transferring mechanism. The test moment resistances were 1.5 times the plastic moment resistance of the steel section.

- The brittle failure mode of the concrete-infill-only shear connection was shown in the four-point symmetric bending test. The failure slip and transverse separation of the concrete-infill-only shear connection was the same as that obtained in the push-out tests.

- The four-point symmetric bending test clearly demonstrated the difference between the concrete-infill-only shear connection and combined shear connection (with the tie-bar shear connection), in terms of the slip behaviour and shear resistance. Brittle failure of the concrete-infill-only shear connection was shown in one shear span. The combined shear connection in the other shear span demonstrated complete elastic slip behaviour with negligible slip.

- The ductile failure mode of the combined shear connection was shown in the three-point asymmetric bending test. This failure mode was the same as that of the tie-bar (Ø16mm) shear connection shown in the push-out tests. The additional tie-bar had directly influence on the failure mode of the combined shear connection.

- Overall, the additional tie-bar significantly increased the ductility and shear performance of the shear connection in the flexural test.

- Although the behaviours and shear resistances of the two types of shear connection were complete different in the push-out tests. But, a uniform (non-discrete) behaviour of the combined shear connection was demonstrated in the flexural tests, which showed a combined effect towards the composite action for the test beam. This result confirmed the approach of using a combination of the two types of shear connection as one unit in design calculation.

- The cracked section properties of the beam specimen were suggested for the deflection analysis at the serviceability limit state, as cracks occurred before the serviceability deflection limit of span/360 was reached.

- The flexural failure mode of the beam specimen was shown in both flexural tests. Although the four-point symmetric bending test was not failure test, which was only up to the plastification of the mid-span deflection, but the yielding of

the steel bottom flange was observed as an initial indication for the flexural failure mode.

- The flexural failure mode of the beam specimen was observed under high shear in the three-point asymmetric bending test, which tested to the ultimate failure of the test beam. The failure mechanism of the beam specimen was due to the ductile failure of the shear connection, rather than the plastic moment resistance failure of the beam specimen. The steel bottom flange was yielded with permanent deflected shape and large cracks were shown at the loading point, but crushing of the concrete slab was not observed.

- Although the two shear spans in the four-point symmetric bending test had different shear connection. One shear span had solely the concrete-infill-only shear connection; the other shear span had the additional tie-bar (Ø16mm) passing through every alternative openings. The elastic deflection stiffness of the two shear spans was the same in the flexural test, as the elastic (uncracked) section properties of the two shear spans were the same.

- The same uniform elastic slip was shown for the two shear spans in the four-point symmetric bending test. This was due to that the elastic slip stiffness of the two types of the shear connection was the same, and that the shear force in the two shear spans was the same.

Chapter 7 Analysis of the flexural tests

The results of the flexural tests were analysed to conclude design methods for the composite shallow cellular floor beams at the serviceability limit sate (SLS) and ultimate limit states (ULS). A method for deflection check at the SLS was established in deflection analysis based on elastic theory. A method for moment resistance at the ULS was established in back analysis based on plastic theory. The developed design method for moment resistance of the composite shallow cellular floor beams was compatible with the design methods of BS5950 and Eurocode 4.

7.1 Introduction

The full-scale composite shallow cellular floor beam was investigated in the two flexural tests: four-point symmetric and three-point asymmetric bending tests. Both flexural tests showed significant composite action due to the unique shear transferring mechanism. The flexural tests demonstrated the behaviour of the beam specimen was essentially elastic at the SLS. The effect of partial shear connection (due to slips) was clearly shown when the test deflections compared with calculated deflections using elastic section properties. A method for deflection check of the shallow cellular floor beams was modified based on the principle of the deflection check method specified in BS5950 and EC4, which was the linearly partial interaction method. The modified method for deflection check was then verified with different composite sections.

The result of the flexural tests were back analysed to determine the composite action of the beam specimen and shear performance of the shear connection. The back analysis was carried out by using measured material properties with all partial safety factors set to unity. Based on results of the back analysis and findings of both the flexural tests and push-out tests, a design method for moment resistance of the shallow cellular floor beams was proposed and then verified with the test results. This design method was compatible with the plastic stress block method specified in both BS5950 and EC4 for determining the design moment resistance of the composite shallow cellular floor beams.

7.2 Deflection analysis

The deflections of a composite beam due to unfactored imposed loads were emphasised at the SLS. Deflections of the flexural tests were analysed using cracked and uncracked section properties of the beam specimen, with the aim of developing a design method for deflection check of the composite shallow cellular floor beams at the SLS. Normally, the deflections of a composite beam consisted of two components:

- The deflections of steel section due to self weight of the composite beam;

- The deflections of composite beam due to the imposed loads.

The deflections of the steel section due to self weight of the beam specimen were not investigated in the deflection analysis, as deflections of the steel section could be calculated by using elastic theory with good accuracy. Moreover, the deflection due to self weight of the beam specimen was not measured in the flexural tests, as the deflections had already been induced after the test beam was set up on the supports.

The deflections of the test beam specimen due to the unfactored imposed loads were analysed at the SLS. The deflections were calculated by using both uncracked and cracked section properties of the beam specimen, and then compared with the test deflections. British Standard BS5950-1:2000 specified span/360 was the deflection limit for composite beams carrying brittle or plaster finishes, and span/200 for all other beams. The lower deflection limit of span/360 was used in the deflection analysis of the beam specimen. The procedures of the deflection calculation are outlines below:

1. To convert the cross sectional area of the concrete slab into an equivalent area of steel by dividing a modular ratio of 6.5, which was specified by Eurocode 4 (EN1994-1-1:2004) for short term loading;

2. To calculate the second moment of areas, *I*, of both uncracked and cracked sections using the converted cross sectional areas (the method for determining the depth of concrete slab for the cracked section is explained in Table 7.1);

3. To determine the deflections using elastic theory with *I* and steel Young's Modulus, *E*;

4. To compare the calculated deflections with the test deflections.

7.2.1 Uncracked and cracked sections

Both uncracked and cracked sections of the beam specimen are illustrated in Figure 7.1. The difference in applying the two cross sections for the deflection calculation are summarised in Table 7.1. The calculated depths of the elastic neutral axis (e.n.a) and the second moment of area, *I*, are shown in Table 7.2.
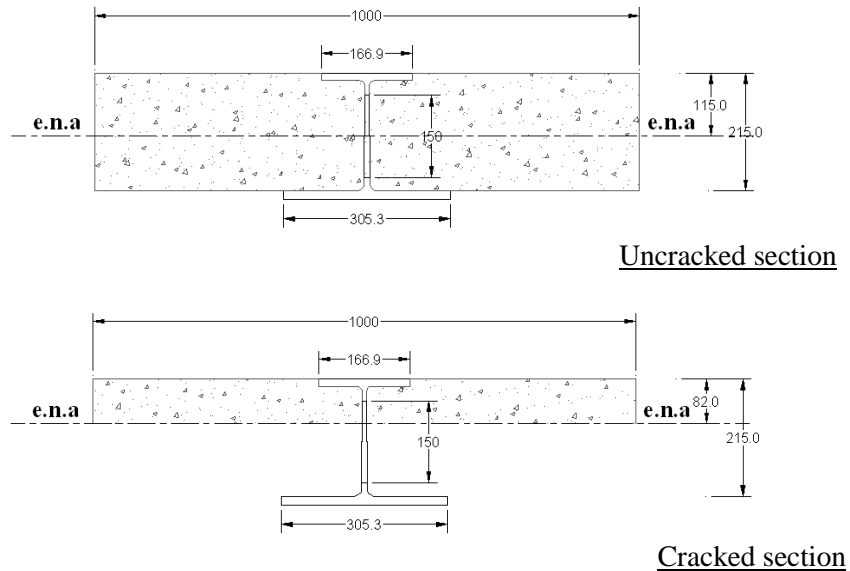
Figure 7.1 Uncracked and cracked sections of the beam specimen

Uncracked section	• By assuming the entire concrete slab was uncracked, the converted cross sectional area was used in the determination for the depth of e.n.a.
Cracked section	• The e.n.a of the cracked section was assumed to be coincided with crack line of the concrete slab, as shown in Figure 7.1; • The concrete below the crack line was neglected; • The converted cross sectional area was also used in the determination for the depth of e.n.a.

Table 7.1 Summary of the uncracked and cracked sections

	The Depth of e.n.a (mm)	The Second Moment of Area, I, (m^4)
Uncracked section	115	2.14E-4
Cracked section	82	1.39E-4

Table 7.2 Section properties of the uncracked and cracked sections

7.2.2 Deflection study

The uncracked section represented the full composite action. By using the uncracked section properties, deflections of the beam specimen was calculated by using load level at the SLS in the flexural test, as span/360 = 16.7mm. The following formula was used in the calculation, where E is the Young's Modulus, I is the second moment of area, v is the deflection, x is the longitudinal distance, and M is the bending moment.

$$-EI\frac{d^2v}{dx^2} = M$$

The load level was 45kN for the test mid-span deflection of 16.7mm in the four-point bending flexural test. By using this load level of 45kN, the calculated deflection for the uncracked section was 9.04mm, which was 54% of the test deflection. This indicated that the slips had affected the stiffness of the beam specimen at the SLS. If the beam specimen had full composite action, then the calculated deflection would be the same or very close to the test deflections. The deflection results further demonstrated the partial shear connection of the test beam specimen.

Furthermore, the test deflection at the end of the flexural test was compared with the calculated deflection using the uncracked section properties. At the end of the test, the load was 106kN with the mid-span deflection of 64.9mm. The calculated deflection was 21.3mm, which was 33% of the test deflection.

	Location	Deflection (mm)		
		Flexural Test (at SLS)	Uncracked Section	Cracked Section
Four-point Bending	Mid-span	16.7	9.0	14.0
	1/4-span	11.1	6.3	9.7
Three-point bending	Max-defl point	16.6	6.8	10.5
	Loading point	13.2	5.3	8.1
	1/4-span	10.1	4.2	6.5

Table 7.3 Comparison between test deflections and calculations

The calculated deflections using both uncracked and cracked section properties were also compared with the test deflections at the SLS, as shown in Table 7.3. The test mid-span deflections were taken as span/360 (16.7mm) at the SLS. The deflections of both uncracked and cracked sections were smaller than the test deflections. Although the cracked section properties yielded better deflections, but it could not represent partial shear connection, which had dominant effect on the deflections. Therefore, the

deflection check for the composite test beam specimen required another method which should include the effect of partial shear connection.

Johnson and May (1975) presented a method for the design of composite beams with partial shear connection. The method assumed that the additional strength and stiffness of the beam due to the composite action varied linearly with degree of shear connection. This method was known as the 'linear partial interaction method'. The relationship for both the moment resistance and stiffness with the degree of shear connection is illustrated in Figure 7.2. The deflections of a simple composite beam under serviceability loads, where the interaction was incomplete, could be determined from Eqn. 7.1. This formula was also documented in both British Standard BS 5950-3.1 and Eurocode 4 EN 1994-1-1 for determining the increased deflections due to partial shear connection.

Eurocode 4, unlike BS 5950, allows this increase in deflection to be ignored in unpropped construction where either degree of shear connection is not less than 0.5, or the forces on the connectors do not exceed $0.7P_{RK}$, where P_{RK} is their characteristic resistance, and for slab with transverse ribs, the height of the ribs does not exceed 80mm. The arbitrary nature of these rules underlines the difficulty of predicting deflections accurately (Johnson 1994).
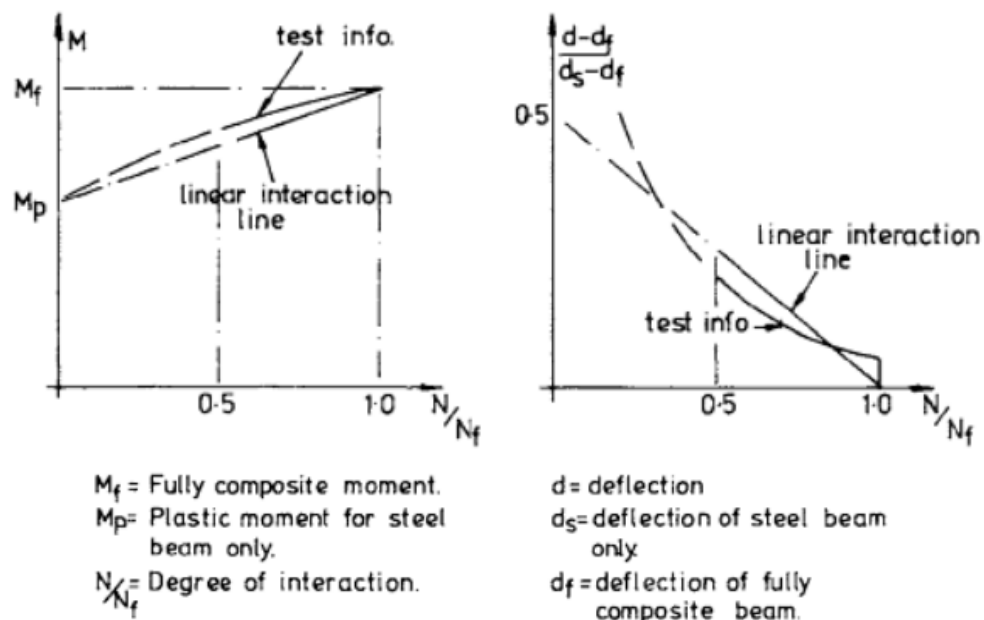
Figure 7.2 Linear interaction concepts (Narayanan 1988)

$$\delta_c^{'} = \delta_c + 0.5(1 - K)(\delta_s - \delta_c) \quad \text{for propped beams}$$

$$\delta_c^{'} = \delta_c + 0.3(1 - K)(\delta_s - \delta_c) \quad \text{for unpropped beams} \qquad (7.1)$$

Where: $\delta_c^{'}$ is the deflection of the composite beam with partial shear connection;

         δ_c is the deflection of the composite beam with full shear connection;

         δ_s is the deflection of the steel beam acting alone;

         K is the degree of shear connection.

The test deflections were back checked with the method presented in Eqn. 7.1 which included the effect of partial shear connection. The deflections of the test beam specimen with full shear connection, δ_c, and deflections of the bare steel section, δ_s, were calculated as listed in Table 7.4. The former term was actually the deflections of the uncracked section. The ratios of $\dfrac{\delta_c^{'} - \delta_c}{\delta_s - \delta_c}$ should readily yield degrees of shear connection. The test deflections at different load levels up to the SLS were used in the back check. The SLS was taken as span/360, 16.7mm, at the mid-span deflection.

It was shown that the calculated degrees of shear connection using Eqn. 7.1 were unrealistic. The back calculated degree of shear connection was 0.07 at the SLS. This could not represent the actual degree of composite action. The slips at the SLS were 0.1mm or 0.2mm, thus the actual degree of interaction would be much higher than 0.07. The calculated results using the method of Eqn. 7.1 could not justify the results of the flexural test, as the method was developed based on the traditional downstand composite beams.

The flexural tests demonstrated the partial shear connection of the beam specimen. A modified method for deflection check should be developed based on the principle of the method presented in Eqn. 7.1, which takes incomplete interaction into account. The method of Eqn. 7.1, or so called linear partial interaction method, simplified the relationship between the ratio of $\dfrac{\delta_c^{'} - \delta_c}{\delta_s - \delta_c}$ and degree of shear connection into a linear function; and this linear relationship was illustrated in Figure 7.2. Based on this simplified relationship, the deflection ratio of the test beam specimen should be in a proportional relationship with its degree of shear connection. It can be expressed as:

$$\frac{\delta_c' - \delta_c}{\delta_s - \delta_c} = aK + b \qquad (7.2)$$

Where: δ_c' is the deflection of the composite beam with partial shear connection;

δ_c is the deflection of the composite beam with full shear connection;

δ_s is the deflection of the steel beam acting alone;

K is the degree of shear connection;

a, b are the coefficients.

The two unknown coefficients of *a* and *b* in Eqn. 7.2 could be determined by using the test data, i.e. test deflections and degrees of shear connection shown in the flexural test. The degree of shear connection was considered as full and taken as 1.0 at the start of the four-point bending test with the load of 8.65kN and 2mm of mid-span deflection. At the end of the test with the plastification of mid-span deflection, the degree of shear connection was taken as 0.46 which calculated in the back analysis in Section 7.3.1.1. This degree of shear connection was determined by using the stress block method with the measured material properties. However it could approximately represent the degree of composite action at that load level. As the flexural test showed major end slips of 6mm at the end of the four-point bending test; hence, the interaction was much reduced at that load level.

By solving the simultaneous equations with the test data at the load level of 8.65kN for full shear connection, and at the load of 106kN for partial shear connection of 0.46, the coefficients of *a* and *b* were obtained, as -1.919 and 2.003, respectively. The *a* and *b* were taken as -2 and 2 respectively to simplify the formula. Hence, Eqn. 7.2 becomes as:

$$\delta_c' = \delta_c + 2(1 - K)(\delta_s - \delta_c) \qquad (7.3)$$

Where: δ_c' is the deflection of the composite beam with partial shear connection;

δ_c is the deflection of the composite beam with full shear connection;

δ_s is the deflection of the steel beam acting alone;

K is the degree of shear connection.

By using the modified method for deflection check, Eqn. 7.3, the degrees of shear connection at different load levels were back calculated, as listed in Table 7.4. It showed that the degree of shear connection was 0.77 at the SLS with the load level of 45kN. This result could approximately represent the actual flexural test, as both slips and cracks were mobilised at the SLS; hence the degree of shear connection would be moderately reduced from the full composite action.

Load (kN)	Deflections (mm)			$\dfrac{\delta_c' - \delta_c}{\delta_s - \delta_c}$	Degree of shear connection, K *	Degree of shear connection, K ^
	Steel section, δ_s	Full composite, δ_c	Test deflection, δ_c'			
8.65	4.92	1.74	2.0	0.083	0.83	1[#]
18.27	10.38	3.67	5.99	0.346	0.31	0.83
28.84	16.39	5.79	10.14	0.410	0.18	0.79
45 [§]	25.58	9.04	16.7	0.463	0.07	0.77
52.88	30.05	10.62	19.61	0.463	0.07	0.77
67.30	38.25	13.51	25.61	0.489	0.02	0.76
85.56	48.63	17.18	34.78	0.560	-0.12	0.72
106 [Δ]	60.25	21.29	64.9	1.119	-1.24	0.46[#]

[§] Load level at the SLS.   * K calculated using Eqn. 7.1 (Johnson).   [#] Test results
[Δ] Load level at the end of test.   ^ K calculated using Eqn. 7.3. (modified)

Table 7.4 Calculated deflections and degrees of shear connection

The modified method for deflection check, Eqn. 7.3, needed to be further verified with different composite sections of the shallow cellular floor beams. The two main procedures of the verifications are:

1. To design different composite sections of the shallow cellular floor beams. The steel sections were designed to have the same depth and web opening diameter as that of the test beam. These steel sections had different second moments of area, *I*, compared with the test beam. The concrete slab was designed as same as that of the test beam: solid slab of 1m width flushed with the top flange and sit on the bottom flange. Overall, these composite sections were designed to have the different stiffness compared with the test beam, but all other parameters were kept same, i.e. depth, web opening diameter and concrete slab.

2. To compute the deflections of these composite sections using both methods of deflection check, i.e. Eqn. 7.1 (Johnson 1975) and Eqn. 7.3

(modified). The calculations were based on the loading configuration of the four-point symmetric flexural test. The mid-span deflections of these composite sections were determined at the different load levels of the flexural test up to the SLS, with the corresponding degrees of shear connection, as listed in Table 7.4. The degrees of shear connection were assumed to be the same for the different composite sections at a load level. Thus the calculated deflections using the two methods were compared with the test deflections for the different composite sections.

The purpose of carrying out these comparisons was to verify whether Eqn. 7.1, the method for deflection check presented in Johnson and May 1975 (also adopted by both BS5950 and EC4), was suitable for the composite shallow cellular floor beams. It was also to further validate the modified method for deflection check, Eqn. 7.3. The comparisons for the deflections are shown in Table 7.5.

A total of five different composite sections were selected for the verification. Two of the composite sections, #1 and #2, had smaller the second moments of area, *I*, compared with that of the test beam. Hence, they had weaker stiffness than the test beam. One of the composite sections, #3, had the similar second moment of area as that of the test beam. The other two composite sections, #4 and #5, had greater the second moments of area than that of the test beam.

By using both methods, Eqn. 7.1 (Johnson) and Eqn. 7.3 (modified), the deflections of these composite sections with partial shear connection were calculated and compared with the test deflections. The comparisons were carried out at the load levels in the flexural test up to the SLS. The degrees of shear connection used in the calculations were assumed the same as that of the test beam at a load level. The comparison results are summarised as:

- For the composite section, #3, which had the similar stiffness as the test beam, the calculated deflections using Eqn. 7.3 (modified) were very close to the test deflections. But the deflections for the composite section, #3, obtained by using the method of Eqn. 7.1 (Johnson) were far off the test deflections and consistently smaller, about 50% less.

- For the composite sections, #1 and #2, which had the weaker stiffness than the test beam, the results of Eqn. 7.3 (modified) correctly showed the increased deflections compared with the test deflections. But the calculated deflections of

Eqn. 7.1 (Johnson) were smaller than the test deflections. This could not demonstrate that the sections of weaker stiffness were to have greater deflections.

- For the comparisons between the test beam and composite sections, #4 and #5, the results of Eqn. 7.3 (modified) accurately showed the trend of reduction in deflections due to the increase in stiffness.

Overall, the calculated deflections using the modified method, Eqn. 7.3, showed good comparison with the test deflections for composite sections of different stiffness. It correctly demonstrated the increase and decrease in deflections due to the variation in stiffness. However, the results obtained by using the method of Eqn. 7.1 (Johnson) could not represent the test deflections of the composite shallow cellular floor beams. Its deflection calculations were impractically lower than the test deflections. This could be due to several factors:

1. Eqn. 7.1, the method for deflection check presented in Johnson and May 1975, was developed for the traditional downstand composite beams. In general, the downstand composite beams were much deeper than the shallow cellular floor beams, as its depth consisted of the depth of steel section with an additional slab depth of 120 - 160mm. Hence, the stiffness of the downstand composite beams was generally greater than that of the composite shallow cellular floor beams. This was one of the reasons that calculated deflections using Eqn. 7.1 (Johnson) were consistently smaller than the test deflections.

2. For a cellular beam with 15 - 20 openings, the total deflections were typically 10% to 15% more than that of the equivalent unperforated downstand composite beams (Lawson et al 2006). The calculated deflections using Eqn. 7.1 (Johnson) with added 15% due to the openings were compared with the test deflections, as shown in Table 7.6. The calculated deflections with the 15% correction were still incomparable with the test deflections, about 30% less. Hence, the use of Eqn. 7.1 with the correction factor of 1.15 was not a suitable method for deflection check of the shallow cellular floor beams. Nevertheless, it was certain that the opening reduced the stiffness for both downstand composite beams and shallow floor beams.

3. The use of the solid slab for the test beam could impose limitations on the results, which could not represent the beam sections with ribbed slab. Further

calculations were carried out to compute the stiffness of the composite section, #1, 2 and 3, with the ribbed slab profile of Multideck 146. The depth of Multideck 146 was 160mm. The width of the slab was kept as 1m. The calculation showed that the composite sections with ribbed slab had much reduced the second moments of area, *I*, as listed in Table 7.7. Hence, the deflections of the composite sections with ribbed slab would be greater than that with solid slab. The calculated deflections are listed in Table 7.7. The composite sections with ribbed slab were assumed to have the same degree of shear connection as the composite sections with solid slab at a load level. Increased deflections were shown by the composite sections with ribbed slab compared with their counterparts. But the increase in deflections was moderate, about 10%.

However, it was shown the reduced differences between the calculated deflections using the method of Eqn. 7.3 (modified) and Eqn. 7.1 (Johnson) with the correction factor of 1.15. The differences were about 15% for the composite sections with ribbed slab, compared with 30% differences for the composite sections with solid slab. This comparison indicated that both methods, i.e. Eqn. 7.3 (modified) and Eqn. 7.1 (Johnson) with the correction factor of 1.15, might be justified for deflection check of the shallow cellular floor beams with ribbed slab. With the lack of experimental data, this conclusion could not be validated; hence further flexural tests on the shallow cellular floor beams with ribbed slab were desired.

7.2.3 Conclusion for deflection check method

The flexural tests on the shallow cellular floor beam showed the effect of partial shear connection on the deflections of the beam specimen. The back check using Eqn. 7.1 the method for deflection check presented in Johnson and May 1975 (also adopted by both BS5950 and EC4) showed about 50% variation between the calculations and test deflections. Based on the principle of the linear partial interaction method, a method for deflection check of the shallow cellular floor beam was modified, as expressed in Eqn. 7.3.

This modified method was then verified with different composite sections of the shallow cellular floor beams. These different composite sections were selected to have different stiffness than that of the test beam, i.e. similar, smaller and greater stiffness.

The calculated deflections using the modified method, Eqn. 7.3, showed the close comparison with the test deflections. It also correctly demonstrated the increase and decrease of deflections due to the variation in stiffness.

The modified method, Eqn. 7.3, was developed based on the principles of the linear partial interaction method and further verified with calculations, but there were limitations imposed by the test data. As the geometry of the test beam only represented the shallow cellular floor beams with solid slab, the modified method needs to be further validated for deflection check of this type of floor beams with ribbed slab. This could be achieved by additional flexural tests and deflection analysis.

Test beam UB305x165/54 UC305x305/97 I (m^4): 2.14E-4			Composite section #1 UB305x165/46 UC254x254/89 I (m^4): 1.94E-4		Composite section #2 UB305x127/48 UC254x254/107 I (m^4): 2.02E-4		Composite section #3 UB356x171/57 UC305x305/118 I (m^4): 2.13E-4		Composite section #4 UB406x178/60 UC356x368/129 I (m^4): 2.22E-4		Composite section #5 UB406x178/74 UC356x368/153 I (m^4): 2.43E-4	
Load (kN)	Degree of shear connection, K	Test deflection (mm)	δ_c' (Eqn. 7.3)	δ_c' (Johnson)	δ_c' (Eqn. 7.3)	δ_c' (Johnson)	δ_c' (Eqn. 7.3)	δ_c' (Johnson)	δ_c' (Eqn. 7.3)	δ_c' (Johnson)	δ_c' (Eqn. 7.3)	δ_c' (Johnson)
8.65	1	2	1.92	1.92	1.84	1.84	1.75	1.75	1.68	1.68	1.53	1.53
18.27	0.83	5.99	6.75	4.73	6.57	4.56	5.80	4.22	5.55	4.05	4.70	3.60
28.84	0.79	10.14	11.45	7.66	11.17	7.40	9.78	6.81	9.35	6.53	7.86	5.79
45	0.77	16.7	18.89	12.21	18.44	11.79	16.06	10.83	15.34	10.38	12.82	9.18

Table 7.5 Deflection check for different composite sections

Test beam UB305x165/54 UC305x305/97 I (m^4): 2.14E-4			Composite section #1 UB305x165/46 UC254x254/89 I (m^4): 1.94E-4			Composite section #2 UB305x127/48 UC254x254/107 I (m^4): 2.02E-4			Composite section #3 UB356x171/57 UC305x305/118 I (m^4): 2.13E-4		
Load (kN)	Degree of shear connection, K	Test deflection (mm)	δ_c' (Eqn. 7.3)	δ_c' (Johnson)	δ_c' + 15% (Johnson)	δ_c' (Eqn. 7.3)	δ_c' (Johnson)	δ_c' + 15% (Johnson)	δ_c' (Eqn. 7.3)	δ_c' (Johnson)	δ_c' + 15% (Johnson)
8.65	1	2	1.92	1.92	2.21	1.84	1.84	2.12	1.75	1.75	2.01
18.27	0.83	5.99	6.75	4.73	5.44	6.57	4.56	5.24	5.80	4.22	4.85
28.84	0.79	10.14	11.45	7.66	8.81	11.17	7.40	8.51	9.78	6.81	7.84
45	0.77	16.7	18.89	12.21	14.04	18.44	11.79	13.56	16.06	10.83	12.46

Table 7.6 Comparison for deflection check using the method of Eqn. 7.1 (Johnson) with added 15% deflections

Load (kN)	K	Test deflection (mm)	Composite section #1 with ribbed slab Multideck 146 UB305x165/46 UC254x254/89 I (m^4): 1.33E-4 (ribbed slab) I (m^4): 1.94E-4 (solid slab)			Composite section #2 with ribbed slab Multideck 146 UB305x127/48 UC254x254/107 I (m^4): 1.46E-4 (ribbed slab) I (m^4): 2.02E-4 (solid slab)			Composite section #3 with ribbed slab Multideck 146 UB356x171/57 UC305x305/118 I (m^4): 1.61E-4 (ribbed slab) I (m^4): 2.13E-4 (solid slab)		
			δ_c' (Eqn. 7.3)	δ_c' (Johnson)	δ_c' + 15% (Johnson)	δ_c' (Eqn. 7.3)	δ_c' (Johnson)	δ_c' + 15% (Johnson)	δ_c' (Eqn. 7.3)	δ_c' (Johnson)	δ_c' + 15% (Johnson)
8.65	1	2	2.80	2.80	3.22	2.55	2.55	2.93	2.31	2.31	2.66
18.27	0.83	5.99	7.97	6.42	7.39	7.55	5.92	6.81	6.58	5.31	6.10
28.84	0.79	10.14	13.18	10.29	11.83	12.56	9.51	10.94	10.89	8.50	9.78
45	0.77	16.7	21.34	16.25	18.69	20.41	15.05	17.30	17.64	13.43	15.44

Test beam
UB305x165/54
UC305x305/97
I (m^4): 2.14E-4

Table 7.7 Deflection check for composite sections with ribbed slab

7.3 Back analysis of four-point symmetric bending test

The results of the four-point symmetric bending test were back analysed to determine the degree of shear connection and shear performance of the shear connection. The back analysis was carried out using measured material properties with all partial safety factors set to unity.

Although the plastic failure of the beam specimen was not reached in the four-point symmetric bending test, plastic theory was used for the back analysis as the concrete-infill-only shear connection within the left shear span failed. Plastic stress block method was used in the back analysis with the assumptions of:

- Concrete tensile strength was neglected;
- The local buckling of the web post was prevented by the concrete encasement;
- The steel section was stressed to a uniform stress in both tension and compression;
- The concrete was stressed to a uniform compression over the depth between the plastic neutral axis (P.N.A) and most compressed fibre of the concrete.

The data used in this back analysis were the tests results and measured material properties obtained at the final loading stage in the four-point symmetric bending test:

- Bending moment at the left loading point of 285kNm,
- Steel tensile stress of 324N/mm^2,
- Concrete cube compressive strength of 30N/mm^2.

7.3.1 Stress block method

In order to verify the accuracy of using the cross section with the full web opening for calculation of moment resistance, the moment resistances of the left shear span of the beam specimen in various degrees of shear connection was first determined. The stress block diagram of the cross section with the full web opening is shown in Figure 7.3. The stress block method was used with the measured material properties. The methodology for determining the moment resistance of the beam specimen in various degrees of shear connection is summarised in the following steps.

1. To determine the compressive resistance of the concrete slab in full shear connection, R_c, using the stress block method with the equilibrium of tension and compression;

2. To determine the longitudinal shear resistance of the shear connection, R_q, using $\eta = R_q/R_c$, where η is the degrees of shear connection;

3. To determine the depth of concrete in compression, d, using the concrete compressive resistance in partial shear connection is equal to R_q;

4. To determine the depth of plastic neutral axis (P.N.A) in partial shear connection using the equilibrium of the tension and compression within the cross section;

5. To determine the moment resistances by taking moments about P.N.A.
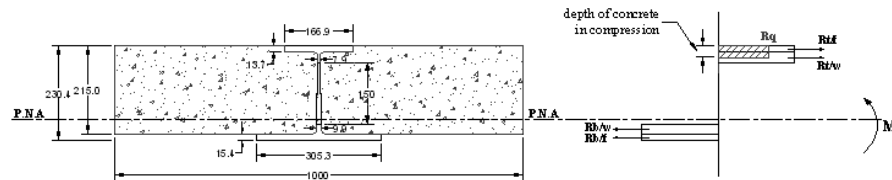
Figure 7.3 Stress block diagram of the cross section with the full web opening

By using the cross section with the full web opening, the calculated moment resistances of the beam specimen in various degrees of shear connection is shown in Figure 7.4. The calculated depths of P.N.A in the various degrees of shear connection are illustrated in Figure 7.5. It was shown that P.N.A was within the bottom flange or below the web opening for all degrees of shear connection. In the other words, the beam specimen should have the full shear connection at the test P.N.A of 178mm in the four-point symmetric bending test. However, the flexural test showed that the full shear connection was not achieved in the left shear span, as the concrete-infill-only shear connection failed. Hence, it was not correct to use the cross section with the full web opening to determine the moment resistance of the beam specimen.
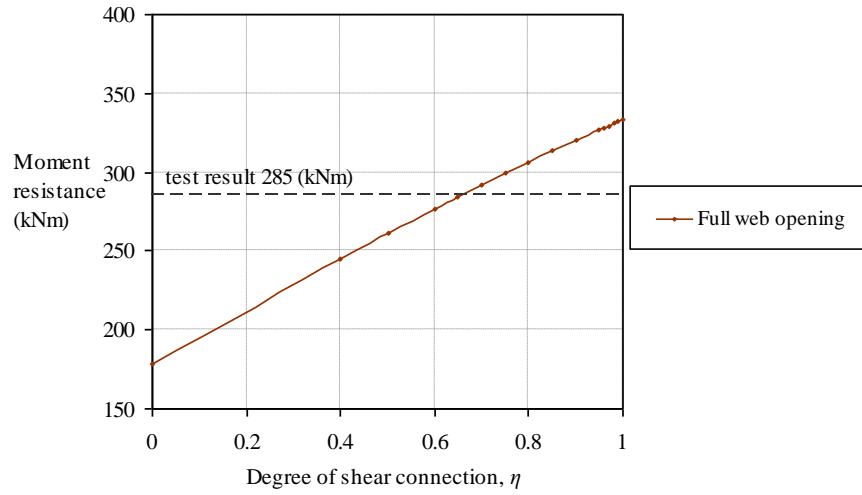
Figure 7.4 Moment resistance of the cross section with the full web opening in various degrees of shear connection
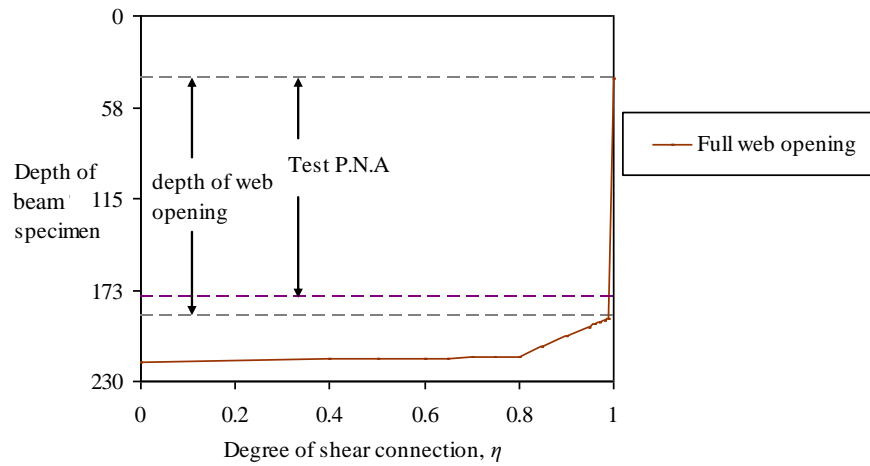
Figure 7.5 Depths of P.N.A for cross section with the full web opening in various degrees of shear connection
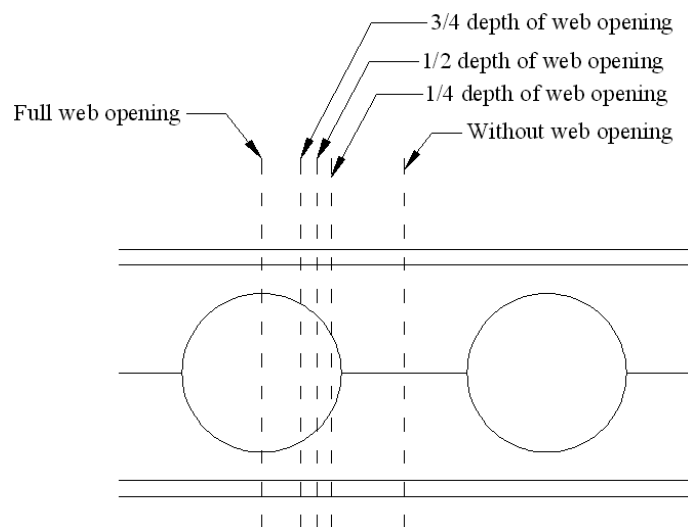
Figure 7.6 Cross sections with different depths of the web opening
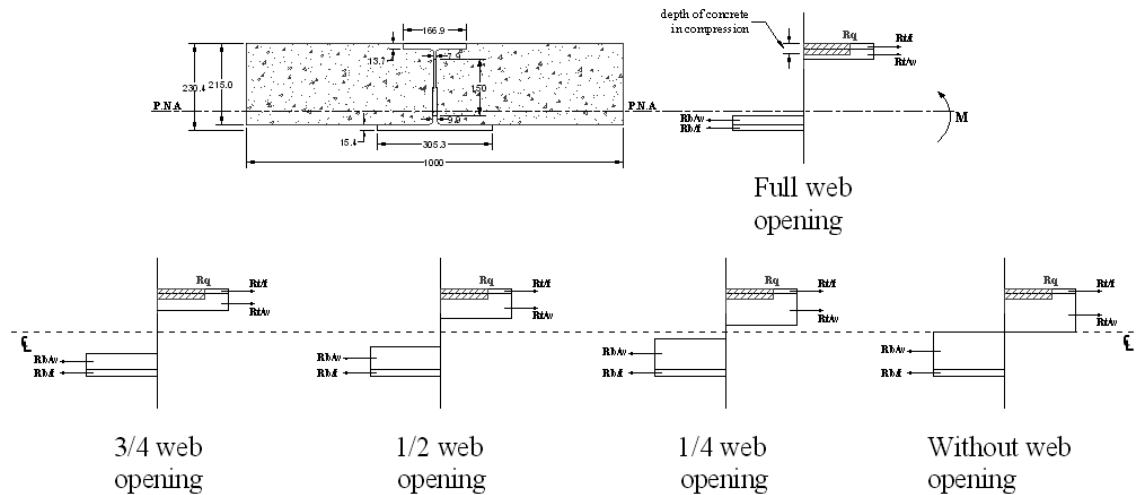
Figure 7.7 Stress block diagrams of the different cross sections

In order to conclude an optimum cross section for determining the moment resistance of the beam specimen, the cross sections at different positions of the web opening, as shown in Figure 7.6, were used to calculate the moment resistance and depth of P.N.A and then to compare with the test results. The stress block diagrams of these different cross sections were illustrated in Figure 7.7.

The calculated moment resistances of these different cross sections in various degrees of shear connection were compared with the test moment of 285kNm, as shown in Figure 7.8. It was shown that the moment resistance was increased with the reduction in the size of the web opening for a degree of shear connection. The calculated depths of P.N.A in the different cross sections were compared with the depth of P.N.A shown in the flexural test, as illustrated in Figure 7.9. It was shown that the P.N.A depths moved upwards with higher degrees of shear connection for a cross section, and that the profile of P.N.A became close to linear for the cross section without the web opening.

The degrees of shear connection of these different cross sections at the test moment of 285kNm and test P.N.A of 178mm are summarised in Table 7.8. The cross section without the web opening showed very low degree of shear connection at the test moment and the P.N.A, which was below the minimum degree of shear connection, 0.4, specified by BS5950 and EC4. Hence, the cross section without the web opening would overestimate the moment resistance by taking into account of the entire web post, and could not represent the actual cross section of the beam specimen.

Among these different cross sections, the cross section with 1/2 depth of the web opening showed the closest comparison for the degrees of shear connection at the test

moment and test P.N.A depth, as listed in Table 7.8. Therefore, the cross section with 1/2 depth of the web opening was the optimum cross section of the beam specimen for determining the moment resistance.

The calculated moment resistances and the depths of P.N.A for the different cross sections in various degrees of shear connection were shown in Appendix H. Calculation details for the moment resistances and P.N.A depth of the cross section with 1/2 depth of the web opening in the degrees of shear connection, 0.5, 0.7 and 1.0, were shown in Appendix G.
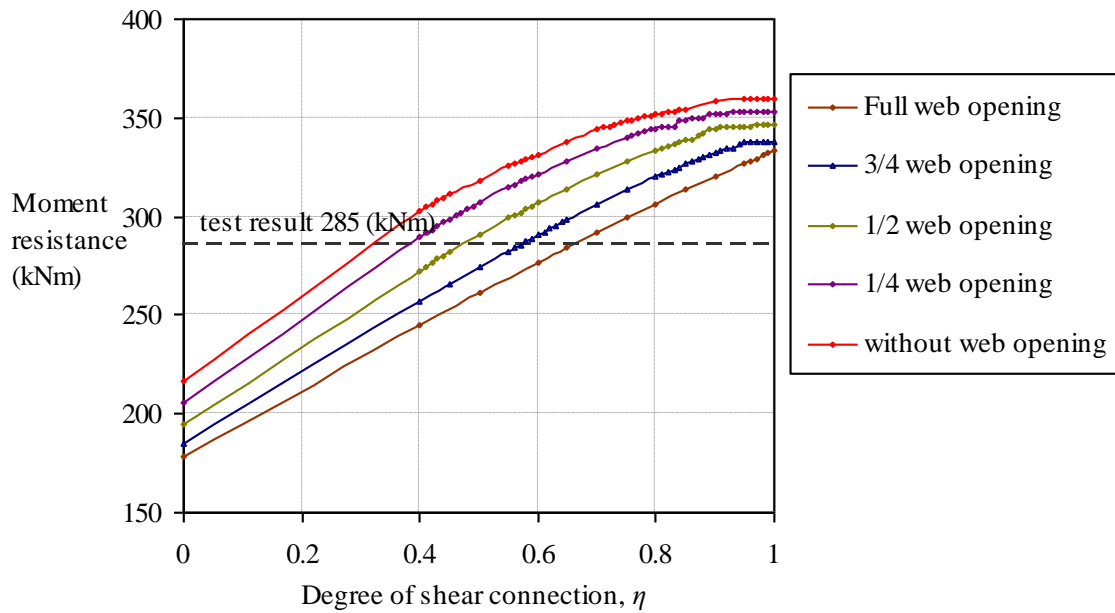
Figure 7.8 Moment resistances of the different cross sections in various degrees of shear connection
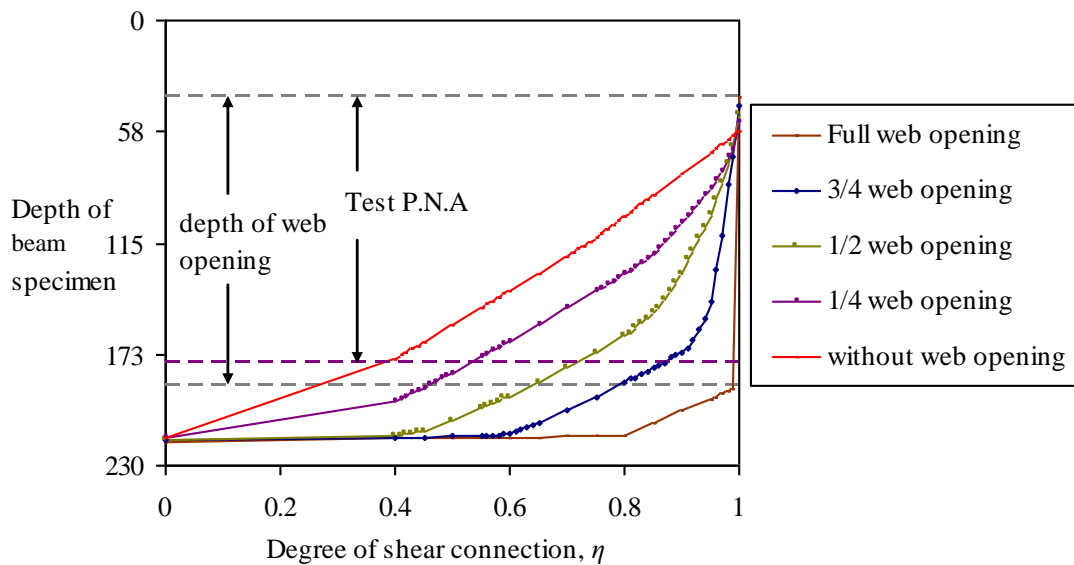
Figure 7.9 Depths of P.N.A for the different cross sections in various degrees of shear connection

Cross Section with Different Depths of the Web Opening	Degree of Shear Connection, η, at Test Moment of 285kNm	Degree of shear Connection, η, at Test P.N.A of 178mm	Ratio of η (at test moment/ at test P.N.A)
Full web opening	0.65	0.99	~~0.65~~
3/4 web opening	0.57	0.88	0.65
1/2 web opening	0.48	0.7	0.69
1/4 web opening	0.35	0.55	0.64
Without web opening	0.3	0.38	~~0.79~~

Table 7.8 Degrees of shear connection for the different cross sections at the test moment and the test P.N.A

7.3.1.1 Determination of degree of shear connection

By using the concluded optimum cross section with 1/2 depth of the web opening, the results of the four-point symmetric bending test were back analysed to determine the degree of shear connection. The plastic stress block diagram of the cross section is illustrated in Figure 7.10. The methodology of the back analysis was summarised in the following steps:

1. To calculate the moment resistance of the steel section, M_s, using the P.N.A depth of 178mm shown in the flexural test. The measured steel stress of 324N/mm^2 at the final loading stage was used as the stress for both tension and compression;

2. To calculate the additional moment resistance due to the composite action, M_{comp}, by subtracting the M_s from test moment of 285kNm;

3. By using the result of the M_{comp}, to calculate the compressive resistance of the concrete slab in partial shear connection, which was also equal to the longitudinal shear resistance of the shear connection, R_q;

4. To determine the degree of shear connection, η, using $\eta = R_q/R_c$, where R_c is compressive resistance of the concrete slab in full shear connection.

The determined degree of shear connection of left shear span in the four-point symmetric bending test was 0.46. The calculation details are shown in Appendix F.
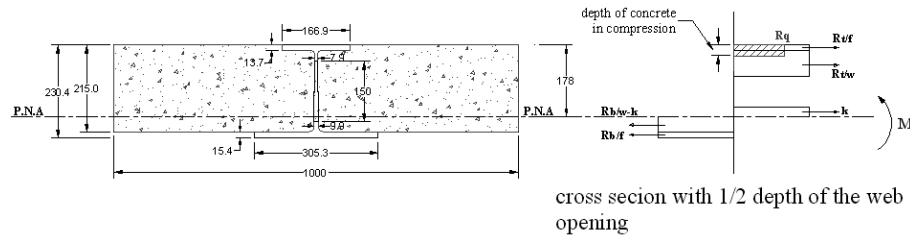
Figure 7.10 Stress block diagram of the optimum cross section at test P.N.A

The calculated moment resistance of the cross sections in various degrees of shear connection, as shown in Figure 7.8, could also be used to check the determined degree of shear connection of 0.46. The moment resistance shown in Figure 7.8 was calculated by using the plastic stress block method with different degrees of shear connection. For the optimum cross section of 1/2 web opening, the degree of shear connection of 0.48 was shown in Figure 7.8 for the test moment of 285kNm. This further confirmed the back calculated degree of shear connection, 0.46, for the four-point symmetric bending test.

7.3.2 Shear performance of the shear connection

The shear performance of the shear connection, α_c, as expressed in Eqn. 7.4, represented the contribution of the shear connection to the composite action in the flexural test.

$$\alpha_c = R_q/ P_u \qquad\qquad (7.4)$$

Where: α_c is the shear performance of the shear connection;

R_q is the longitudinal shear resistance of the shear connection in the flexural test;

P_u is the shear resistance of the shear connection in the push-out tests.

At the degree of shear connection of 0.46 (as determined above), the longitudinal shear resistance of the concrete-infill-only shear connection, R_q, was 446kN, as the compressive resistance of the concrete slab in full shear connection, R_c, was 969kN (obtained in Appendix G), since $R_q = \eta R_c$. There were nine concrete-infill-only shear connection within the left shear span of the four-point symmetric bending test. The longitudinal shear force was uniformly distributed within the shear span, as the constant shear force within the shear span was created by the four-point bending test and uniform slips were shown within the shear span. Hence:

R_q: The longitudinal shear resistance of each concrete-infill-only shear connection in the flexural test was 446/9=50kN.

P_u: The shear resistance of each concrete-infill-only shear connection in the push-out tests was 175kN.

Therefore, the shear performance of the concrete-infill-only shear connection, α_c, in the four-point symmetric bending test was 29%, or approximately 30%.

7.4 Back analysis of three-point asymmetric bending test

The beam specimen was tested to the ultimate failure in the three-point asymmetric bending test. The failure mode of the beam specimen was flexural failure. The slip curves demonstrated the plastic ductile failure of the shear connection in the shear span. The degree of shear connection and the shear performance of the shear connection in the three-point asymmetric bending test were determined in the back analysis based on the plastic theory.

The measured material properties were used in the back analysis with all partial safety factors set to unity. Plastic stress block method was used in the back analysis. The same assumptions made for the back analysis of the four-point symmetric bending test were also applied for this back analysis. The test results and measured material properties obtained at the ultimate failure of the flexural test were:

- Bending moment at the loading point was 385kNm,
- Coupon test yield strength was 414N/mm^2.
- Concrete cube compressive strength was 31N/mm^2.

The coupon test yield strength of 414N/mm^2 was used in the back analysis, as the steel tensile stress at the loading point was not obtained in the three-point asymmetric bending. This was due to the change of loading point after the strain gauges were glued. However, the yield stress was considered reached in the steel bottom flange at the loading point, as the permanent deformations with large residual deflections were observed at the end of the flexural test.

7.4.1 Stress block method

The moment resistances of the beam specimen in various degrees of shear connection were calculated by using the plastic stress block method with the measured material properties obtained at the ultimate failure, as shown in Figure 7.11. The optimum cross section with 1/2 depth of the web opening was used in the calculations. The calculation

results are listed at the end of Appendix J. The calculation details for the moment resistances with degrees of shear connection, 0.5, 0.7 and 1.0, are shown in Appendix J.

The test moment of 385kNm was compared with the calculated moment resistances for various degrees of shear connection, as shown in Figure 7.11. The degree of shear connection in the three-point asymmetric bending test was 0.56.
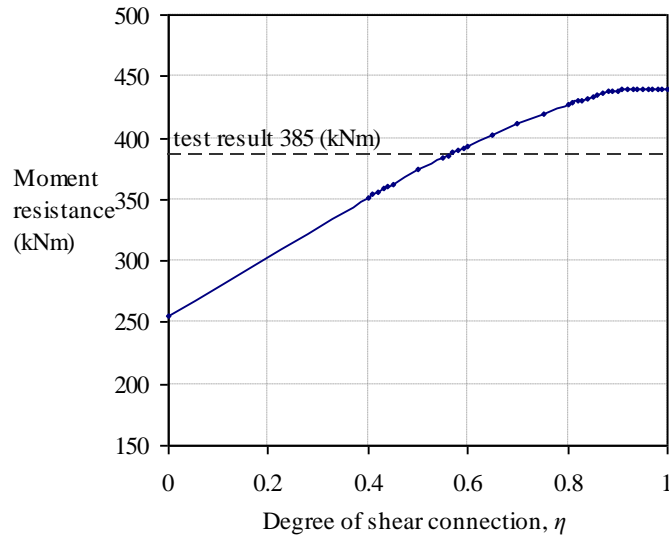
Figure 7.11 Moment resistances for various degrees of shear connection

7.4.2 Shear performance of the shear connection

The shear performance of the shear connection, α_c, in the three-point asymmetric bending test was determined by using Eqn. 7.4. There were three tie-bar (Ø16mm) shear connection and two concrete-infill-only shear connection within the shorter shear span. At degree of shear connection of 0.56 (as determined above), the longitudinal shear resistance of the combined shear connection, R_q, was 662kN, as R_c=1182kN (obtained in Appendix J), since $R_q = \eta R_c$.

The three-point asymmetric bending test showed that the uniform and non-discrete failure behaviour between these two types of shear connection, namely, the concrete-infill-only and tie-bar (Ø16mm) shear connection. The use of the tie-bar prevented the brittle failure of the concrete-infill-only shear connection; so that these two types of shear connection demonstrated the uniform behaviour and combined effect towards the composite action of the beam specimen. It could be considered that the longitudinal shear resistance within the shear span was equally distributed between the shear connection, as the constant shear force was created within the shear span. Hence:

R_q: The longitudinal shear resistance of each shear connection in the flexural test was 132kN.

P_u: The shear resistance of each concrete-infill-only and tie-bar (Ø16mm) shear connection in the push-out tests was 175kN and 369kN respectively.

Therefore, the individual shear performance of the concrete-infill-only and tie-bar (Ø16mm) shear connection in the three-point asymmetric bending test was 75% and 36% respectively. It was shown that the use of the tie-bar not only contributed towards the ductility of the shear connection, also significantly increased the performance of the shear connection. The shear performance of the concrete-infill-only shear connection in the four-point bending test was about 30%, which was much lower then the shear performance of 75% when used in combination with the tie-bar shear connection.

Another way to describe the shear performance of the combined shear connection was to consider the concrete-infill-only and tie-bar shear connection as one unit, as non-discrete failure behaviour and combined effects towards the composite action was shown by the two types of shear connection.

R_q: The longitudinal shear resistance of a combined shear connection in the flexural test was 132 x 2 = 264kN.

P_u: The shear resistance of the concrete-infill-only and tie-bar (Ø16mm) shear connection in the push-out tests was 175kN and 369kN respectively, hence, the combined shear strength was 544kN.

Thus, the shear performance of a combined shear connection in the three-point asymmetric bending test was 49%, or approximately 50%.

7.5 Design method for moment resistance

Based on findings of the push-out tests and flexural tests, a design method for moment resistance of the composite shallow cellular floor beams was proposed. The proposed design method disregarded the case which the composite action was solely provided by the concrete-infill-only shear connection, as brittle failure of the shear connection was shown in both the push-out tests and four-point bending test. The design method considered both the partial and full composite action provided by the combination of the concrete-infill-only and tie-bar shear connection, as ductile failure behaviour of the combined shear connection was shown in the flexural test.

Findings of the push-out tests and flexural tests used for the proposed design method were:

- The developed design method for shear resistance of the shear connection, Eqn. 5.14;

- The concluded optimum cross section, 1/2 depth of the web opening, for determining moment resistance of the composite section using plastic stress block method;

- The shear performance of the combined shear connection (the concrete-infill-only and tie-bar shear connection), 50%, shown in the flexural test.

The design methods specified in both BS5950 and EC4 for moment resistance of a composite beam were implemented into the proposed design method. The steps in using the proposed design method to compute the design moment resistance of the shallow cellular floor beams are summarised as:

1. To calculate the design shear resistance of the shear connection, P_{uc}, using the shear strength design method of Eqn. 5.14;

2. To calculate the longitudinal shear resistance of the combined shear connection in the composite sections, R_q, by using the shear performance of 50%;

3. By using the optimum cross section of 1/2 web opening depth, to determine compressive resistance of the concrete slab in full shear connection, R_c, in accordance with the plastic stress block method specified in BS5950 and EC4;

4. To calculate the degree of shear connection, η, as $\eta=R_q/R_c$;

5. If the composite section is in full shear connection, the design moment resistance, M_{Rd}, is determined by using the plastic stress block method in accordance with BS5950 and EC4;

6. If the composite section is in partial shear connection, the design moment resistance, M_{Rd}, is determined by using the linear interaction method in accordance with BS5950 and EC4.

The moment resistance of the beam specimen in the three-point asymmetric bending test was calculated by using the proposed design method. The calculated design moment resistance was then verified with the flexural test results.

1. P_{uc}=808kN, obtained by using Eqn. 5.14;

2. R_q=404kN, obtained by using the shear performance of the combined shear connection as 50%;

3. R_c=898kN, obtained in accordance with BS5950 and EC4, with the optimum cross section of 1/2 web opening depth (calculation details are shown in Appendix K);

4. η=0.45, which is partial shear connection, as $\eta=R_q/R_c$;

5. M_{Rd}=280kN, obtained by using the linear interaction method in accordance with BS5950 and EC4.

The flow chat of the proposed design method for moment resistance of the composite shallow cellular beams is illustrated in Chart 7.1. The calculated design moment resistance of the beam specimen using the proposed design method was 280kN, which was 27% lower than the test moment of 385kN. Although the proposed design method for moment resistance was verified with the flexural test results, however it would be better to further validate the design method with more flexural tests for different composite sections and various opening diameters. Nevertheless, this type of full-scale tests are time consuming and expensive to carry out. The other approach to further verify the design method is the Finite Element Analysis (FEA), again the accurate FEA models of the large scale tests are also time consuming to develop, as the concrete behaviour is difficult to predict. For the future research, the FEA for the flexural behaviour of different composite sections would be desirable.

```
┌─────────────────────────────────┐
│   Design method for shear resistance │
│       of the shear connection,      │
│              Eqn. 5.14              │
└─────────────────────────────────┘
                 │
                 ▼
┌─────────────────────────────┐   ┌─────────────────────────────┐
│   Shear resistance of the shear │   │     Shear performance of the    │
│      connection, $P_{uc}$       │   │  combined shear connection, $\alpha$, │
│                                 │   │             as 50%              │
└─────────────────────────────┘   └─────────────────────────────┘
                 │                                 │
                 └─────────────┬───────────────────┘
                               ▼
        ┌─────────────────────────────┐   ┌─────────────────────────────────┐
        │   Longitudinal shear        │   │  Compressive resistance of the  │
        │  resistance of the shear    │   │  concrete slab in full shear    │
        │     connection, $R_q$,      │   │  connection, $R_c$, calculated in │
        │    as ($R_q = \alpha P_u$)  │   │   accordance with BS5950 &      │
        │                             │   │             EC4                 │
        └─────────────────────────────┘   └─────────────────────────────────┘
                     │                                 │
                     └─────────────┬───────────────────┘
                                   ▼
                    ┌─────────────────────────────┐
                    │    Degree of shear          │
                    │   connection, $\eta$, as    │
                    │     $\eta = R_q/R_c$        │
                    └─────────────────────────────┘
                         │                    │
                ┌────────┘                    └────────┐
                ▼                                      ▼
          ◇ Full shear ◇                        ◇ Partial shear ◇
          ◇ connection ◇                        ◇  connection   ◇
                │                                      │
                ▼                                      ▼
┌─────────────────────────────┐        ┌─────────────────────────────┐
│  Design moment resistance in│        │  Design moment resistance in│
│  full shear connection,     │        │  partial shear connection,  │
│  $M_{pl,Rd}$, using stress  │        │  $M_{Rd}$, using linear     │
│  block method in accordance │        │  interaction method in      │
│  with BS5950 or EC4         │        │  accordance with BS5950 or  │
│                             │        │  EC4                        │
└─────────────────────────────┘        └─────────────────────────────┘
```

Chart 7.1 Flow chart of the design method for moment resistance of the composite shallow cellular floor beams

7.6 Conclusions

The flexural tests on the composite shallow cellular beams demonstrated that significant composite action due to the unique shear transferring mechanism. The behaviour of the test beam was essentially elastic at the SLS, but the deflection calculations based on the uncracked or cracked section properties showed the effects of partial shear connection on the deflections. The calculated deflections using the method for deflection check presented in Johnson and May 1975, also adopted in both BS5950 and EC4, were consistently lower than the test deflections, about 50% lower. Based on the principle of this established method, or so called the 'linear partial interaction method', a modified method for deflection check of the shallow cellular floor beams was developed and verified with the deflection calculations of different composite sections.

The degree of composite interaction and shear performance of the shear connection were determined in the back analysis in the aims to develop a design method for moment resistance of the shallow cellular floor beams. The calculated moment resistance and depth of P.N.A using the cross section with the full web opening did not compare well with the flexural test results. An optimum cross section with 1/2 depth of the web opening was concluded for determining the moment resistance of the shallow cellular floor beams using the plastic stress block method.

The use of the tie-bar demonstrated the significant increase in shear performance for the shear connection. The shear performance of the concrete-infill-only shear connection in the four-point bending test was about 30%, which was much lower than the shear performance of 75% when used in combination with the tie-bar shear connection. Another way to describe the shear performance of the combined shear connection was to consider the concrete-infill-only and tie-bar shear connection as one unit. The shear performance of the combined shear connection shown in the flexural test was 50%, which was adopted in the design calculation for moment resistance of the shallow cellular floor beams. Also, the concluded design method for shear resistance of the shear connection was used in the design method for the moment resistance; the flow chat was shown in Chat 7.1.

The calculations using both developed design methods, i.e. deflection check and moment resistance, were verified with the test results. But there was limitation imposed on the test data. As the test beam only represented the shallow cellular floor beams with solid slab; hence for future research, it would be desirable to investigate the flexural performance of the composite beams with ribbed slab.

	Test Moment (kNm)	Degree of Shear Connection, η	Shear Performance of Shear Connection, α
Four-point bending test	285	0.46	30% [*]
Three-point bending test	385	0.56	50% [~]

[*] shear performance of the concrete-infill-only shear connection
[~] shear performance of the combined shear connection

Table 7.9 Results of the flexural tests and back analysis

Chapter 8 Conclusions and recommendations

The shear transferring mechanism for composite shallow cellular floor beams is different from those systems with the conventional headed shear studs and has not been studied previously. The experimental and analytical studies carried out in this research provide comprehensive information on the behaviour and shear resisting properties of the unique shear transferring mechanism and has achieved better understanding of the failure mechanism of the shear connection. Overall this research has advanced the method of shear connection in shallow floor beam construction.

8.1 Conclusions

The unique shear transferring mechanism is formed by the web opening features of the composite shallow cellular floor beams. The steel sections of the composite beams are fabricated by welding two asymmetric cellular tees along the web. There are regularly spaced openings on the web post. The in-situ concrete fills the opening with or without the additional element of tie-bar, resisting longitudinal shear force.

Two series of push-out tests were carried out to investigate the shear connection under the direct longitudinal shear force. Two flexural tests were carried out to investigate the composite shallow cellular floor beams and its shear connection under the bending load. Analytical studies were performed to establish design methods for both shear connection and composite shallow cellular floor beams. The conclusions from the experimental and analytical studies are presented in two sections as:

Section 8.1.1 Experimental studies	• Behaviour and failure mechanism of the shear connection in both push-out tests and flexural tests; • Flexural behaviour and composite action of the composite shallow cellular floor beam in the flexural tests;
Section 8.1.2 Analytical studies	• Design methods for the shear connection and composite shallow cellular floor beams.

8.1.1 Conclusions of experimental studies

Two types of tests were carried out to investigate the unique shear transferring mechanism, namely the push-out tests and flexural tests. The push-out tests applied the direct longitudinal shear force to the shear connection. The load-slip behaviour and shear resisting properties of the shear connection were obtained in the push-out tests. The specimens of the push-out tests were designed to represent the actual configurations of the shear connection used for the composite shallow cellular floor beams, and to create the desired loading conditions for the shear connection.

There were two series of push-out test. The push-out test series-I investigated the four types of the shear connection, i.e. concrete-infill-only, tie-bar (Ø12mm), ducting and web-welded stud shear connection. Comprehensive information was obtained from the push-out tests; however there were aspects of the tests could be improved, i.e. avoiding local bond failure, minimum three identical specimens for a type of shear connection and preventing the shear failure for the tie-bar. In the light of the push-out test series-I, the second groups of push-out tests, series-II, were designed and carried out to further investigate the concrete-infill-only and tie-bar (Ø16mm) shear connection. The conclusions of both push-out test series are presented in the following section.

8.1.1.1 Push-out tests

The conclusions for the shear connection are presented in the areas of behaviour and failure mechanism. The findings of both push-out test series were also summarised.

Concrete-infill-only shear connection

- Behaviour: In both push-out test series, the concrete-infill-only shear connection showed a distinctive brittle failure mode, as the rupture failure occurred without any plastic deformations. This brittle failure mode was due to the fact that the concrete-infill-only shear connection consisted of solely the concrete infill element, and that concrete was a brittle material.

- Failure mechanism:

    The top section of the concrete infill element was crushed by the web in the longitudinal shear direction, and the other part of the

concrete infill element was ruptured by the tensile splitting in the transverse direction.

Tie-bar shear connection

- Behaviour: Both Ø12mm and Ø16mm tie-bar shear connection showed the ductile load-slip behaviour and failure mode. Large slips occurred before and after the ultimate loads. The tie-bar (Ø16mm) shear connection demonstrated a mechanism of sustaining the ultimate load while large slips were induced. It was shown that the tensile strength of the Ø16mm tie-bar was more effective.

- Failure mechanism:

  The Ø12mm tie-bars were positioned close to the perimeter of the web opening. One of the tie-bars was sheared off, as it was in direct contact with the movement of the web post (or slips) while the other tie-bar remained intact.

  The tie-bar did not fail in the tie-bar (Ø16mm) shear connection. The shear resisting mechanism of the tie-bar would be the tensile strength, as the ductile slip behaviour and significantly gained strength were shown by the additional tie-bar. Anchorage failure was not seen in the tie-bar.

  The failure mechanism of the concrete infill element in both tie-bar shear connection was the same as that of the concrete-infill-only shear connection.

Ducting shear connection

- Behaviour: The ducting shear connection showed brittle failure mode, similar to that of the concrete-infill-only shear connection. The ducting deformed extensively. Large slips occurred after the ultimate loads were reached. The ducting itself had little shear resistance due to its geometry and thickness. Nonetheless, the presence of the ducting reduced the tendency of brittle failure mode.

- Failure mechanism:

  Crushing of the concrete infill element led to the deformations of the ducting. Concrete infill element was crushed together with tensile splitting.

<u>Web-welded stud shear connection</u>

- Behaviour: The web-welded stud shear connection showed ductile load-slip behaviour and failure mode. Plastic deformations with large slips occurred before and after the ultimate loads. The headed studs demonstrated great influence on the behaviour of the web-welded studs shear connection, whose behaviour was the same as that of the headed studs in the standard push-out tests.

- Failure mechanism:

  The headed studs were sheared off with bending near the root; concrete around the studs was crushed. The failure mechanism of the concrete infill element was the same as those of the concrete-infill-only shear connection.

<u>Findings of both push-out test series are summarised below.</u>

- The additional elements of the tie-bars and studs used in combination with the concrete infill element had significantly increased the ductility, slip capacity and shear resisting capacity of the shear connection.

- Strong tie resistance was shown by all four types of the shear connection, as very little separation was shown in the push-out tests.

- The push-out tests showed that the shear resistance of the shear connection increased with increase of the web opening diameter and concrete strength.

- The concrete-infill-only shear connection showed the distinctive brittle failure mode with the slip capacity of 4-5mm. The brittle failure mode was due to that the shear connection consisted of solely the concrete infill element, and that concrete was a brittle material.

- In contrast, the tie-bar (Ø16mm) shear connection showed the ductile failure mode with the slip capacity of 12-14mm. It was shown that the

tensile resistance of the tie-bar became effective in the tie-bar shear connection, and that the 1m length provided adequate anchorage resistance to the Ø16mm tie-bar.

- The additional tie-bars of Ø16mm increased the shear resistance of the shear connection by twofold. The comparison was base on the shear connection of Ø150mm web opening with 30N/mm^2 concrete strength.

- The shear resistance of a concrete-infill-only shear connection with Ø150mm web opening was 1.75 times the shear resistance of a headed stud of Ø19mm and 100mm height. This comparison was base on the concrete strength of 30N/mm^2.

- Similarly, the shear resistance of a tie-bar (Ø16mm) shear connection with Ø150mm web opening was 3.7 times the shear resistance of a headed stud of Ø19mm and 100mm height. This comparison was base on the concrete strength of 30N/mm^2.

- This tie-bar (Ø16mm) shear connection showed both desired shear resistance and ductility. This type of shear connection required no additional welding which was required for the web-welded stud shear connection. Hence, the tie-bar (Ø16mm) shear connection was the optimum shear connection for the composite shallow cellular floor beams.

8.1.1.2 Flexural tests

The full-scale flexural test beam specimen was designed to represent the actual composite shallow cellular floor beams of a common span range with solid concrete slab. Two flexural tests were carried out on the test beam, i.e. the four-point symmetric and three-point asymmetric bending tests. The test beam was designed to further investigate the concrete-infill-only and tie-bar (Ø16mm) shear connection. The four-point symmetric bending was first carried out without the failure of the beam specimen, only up to the plastification of the mid-span deflection. The test created a bending moment profile similar to that of the UDL. The concrete-infill-only shear connection was particularly investigated in the four-point symmetric bending test. The three-point asymmetric bending test was then carried out up to the ultimate failure of the beam specimen. The test created high shear in the shorter shear span, which had the

combination of concrete-infill-only and tie-bar (Ø16mm) shear connection. The conclusions made from both flexural tests were:

- Significant composite action due to the unique shear transferring mechanism was demonstrated in both flexural tests. The test moment resistances were 1.5 times the plastic moment resistance of the steel section only.

- Partial shear connection was shown before the yielding of the steel section. The behaviour of the beam specimen was essentially elastic when the serviceability limit state was reached.

- The flexural failure mode of the beam specimen was shown in both flexural tests. Although the four-point symmetric bending test was not failure test, but the yielding of the steel bottom flange was observed as an initial indication for the flexural failure mode. The failure mechanism of the beam specimen in the three-point asymmetric bending test was due to the ductile failure of the shear connection, rather than the plastic moment resistance. The steel bottom flange had yielded with permanent deflected shape, and large cracks were shown at the loading point but crushing of the concrete slab was not observed.

- The brittle failure mode of the concrete-infill-only shear connection was shown in the four-point symmetric bending test. The failure slip and transverse separation of the shear connection was the same as that shown in the push-out tests.

- The four-point symmetric bending test clearly demonstrated the difference between the concrete-infill-only shear connection and combined shear connection (with the tie-bar shear connection), in terms of the slip behaviour and shear resistance. Brittle failure of the concrete-infill-only shear connection was shown in one shear span. The combined shear connection in the other shear span demonstrated complete elastic slip behaviour with negligible slips.

- The ductile failure mode of the combined shear connection was shown in the three-point asymmetric bending test. This failure mode was the same as that of the tie-bar (Ø16mm) shear connection in the push-out tests. The

additional tie-bar had direct influence on the failure mode of the combined shear connection.

- Overall, the additional tie-bar significantly increased the ductility and shear performance of the shear connection in the flexural tests.

- The behaviours and shear resistance of the two types of shear connection were different in the push-out tests. However, a uniform (non-discrete) behaviour of the combined shear connection was demonstrated in the flexural tests, which showed a combined effect towards the composite action for the test beam.

8.1.2 Conclusions of analytical studies

The results of the push-out tests and flexural tests were analysed. Design methods for the shear connection and shallow cellular floor beams were developed, as listed in the table below. The details of the design methods are presented in the next two sections.

Design methods	
Push-out tests	• Design method for shear resistance of the shear connection
Flexural tests	• Design method for deflection check at the serviceability limit state (SLS) • Design method for moment resistance at the ultimate limit state (ULS)

8.1.2.1 Analytical studies of push-out test results

The mathematical analysis on the results of the push-out tests was carried out in the aims of developing a design method for shear resistance of the unique shear connection. Base on the failure mechanism shown in the push-out tests, a method was proposed first by combining the shear resistance of the concrete infill element with resistance of the additional elements, i.e. tie-bar or studs, to calculate the total shear resistance of the shear connection. The empirical formula of the method was resulted from the mathematical analysis. The calculated shear resistance using the concluded formula compared well with the results of the push-out tests. The ratio for the shear resistance of the calculation to test results was 0.935.

Because of the complex three-dimensional stress-strain state of the concrete infill element, it was difficult to analyse it by using the mathematical model rather than the empirical formula. The FEA of the concrete-infill-only shear connection was carried out

to further verify the formula obtained from the mathematical analysis. Firstly, a calibrated FEA model of the concrete-infill-only shear connection was developed. Then a parametric study was performed by using the calibrated FEA model to investigate the variables of concrete strength and diameter of web opening. Finally, the results of the FEA parametric study were compared with the calculated shear resistance using the developed formula.

The calculated results were very close to the results of the FEA parametric study, as the average ratios of the calculated shear resistance to results of the FEA were 0.935, 0.703 and 0.863 for web opening diameters of 100, 150 and 200mm, respectively. In order to develop a design method for the shear resistance of the shear connection, a partial safety factor was added into the mathematical formula as expressed below. The shear resistance obtained from the design method with the partial safety factor of 1.5 were compared with the results of the push-out tests. The ratio of the design shear resistance (P_{uc}) to test results was 0.624 for the partial safety factors of 1.5.

$$P_{uc} = \frac{1.6758\left(f_{cu}A_c\right) + 1.4355\left(f_{ct}A_t\right) + R_{add}}{\gamma}$$

Where: $A_c = tD$

$$A_t = \frac{\pi D^2}{4}$$

P_{uc} is the design shear resistance of the shear connection;

f_{cu} is the concrete cube compressive strength in N/mm^2;

f_{ct} is the concrete tensile splitting strength in N/mm^2;

A_c is the area of concrete in the compression;

A_t is the area of concrete in the tensile splitting;

t is the thickness of the web;

D is the diameter of the web opening;

R_{add} is the shear resistance of the additional elements i.e. tie-bar or shear studs;

γ is the partial safety factor.

8.1.2.2 Analytical studies of flexural test results

The results of the flexural tests were analysed to develop design methods for the composite shallow cellular floor beams at the serviceability limit sate (SLS) and ultimate limit states (ULS). A method for deflection check at the SLS was established in

a deflection analysis based on elastic theory. A method for moment resistance at the ULS was established in back analysis based on plastic theory.

Design method for deflection check

The flexural tests on the composite shallow cellular beams demonstrated significant composite action due to unique shear transferring mechanism. The behaviour of the test beam was essentially elastic at the SLS, but the deflection calculations based on the uncracked or cracked section properties showed the effects of partial shear connection on the deflections. The calculated deflections using the method for deflection check presented in Johnson and May 1975, also adopted in both BS5950 and EC4, were 50% lower than the test deflections. Based on the principle of this established method, or so called 'linear partial interaction method', a modified method for deflection check of the shallow cellular floor beams was developed as shown below.

$$\delta_c^{'} = \delta_c + 2(1 - K)(\delta_s - \delta_c)$$

Where: $\delta_c^{'}$ is the deflection of the composite beam with partial shear connection;

δ_c is the deflection of the composite beam with full shear connection;

δ_s is the deflection of the steel beam acting alone;

K is the degree of shear connection.

This modified method was then verified with different composite sections of the shallow cellular floor beams. These different composite sections were selected to have different stiffness than that of the test beam. The calculated deflections using the modified method showed close comparison with the test deflections. It also correctly demonstrated the increase and decrease of deflections due to the variation in stiffness.

Design method for moment resistance

The degree of shear connection and shear performance of the shear connection were determined in the back analysis in the aims to develop a design method for moment resistance of the shallow cellular floor beams. The calculated moment resistance and depth of P.N.A using the cross section with the full web opening did not compare well with the flexural test results. An optimum cross section with 1/2 depth of

web opening was calculated for determining the moment resistance of the shallow cellular floor beams using the plastic stress block method.

The use of the tie-bar demonstrated a significant increase in shear performance for the shear connection. The shear performance of the concrete-infill-only shear connection in the four-point bending test was about 30%, which was much lower than the shear performance of 75% when used in combination with the tie-bar shear connection. The uniform (non-discrete) behaviour of the combined shear connection was demonstrated in the flexural tests and another way to describe the shear performance of the combined shear connection was to consider the concrete-infill-only and tie-bar shear connection as one unit.

The shear performance of the combined shear connection shown in the flexural test was 50%, which was adopted in the design calculation for moment resistance of the shallow cellular floor beams. The resulting shear resistance design method for the shear connection was implemented in developing the design method for the moment resistance. The design model was compatible with the conventional design methods of BS5950 and EC4. The flow chat of the design method is shown below.

259
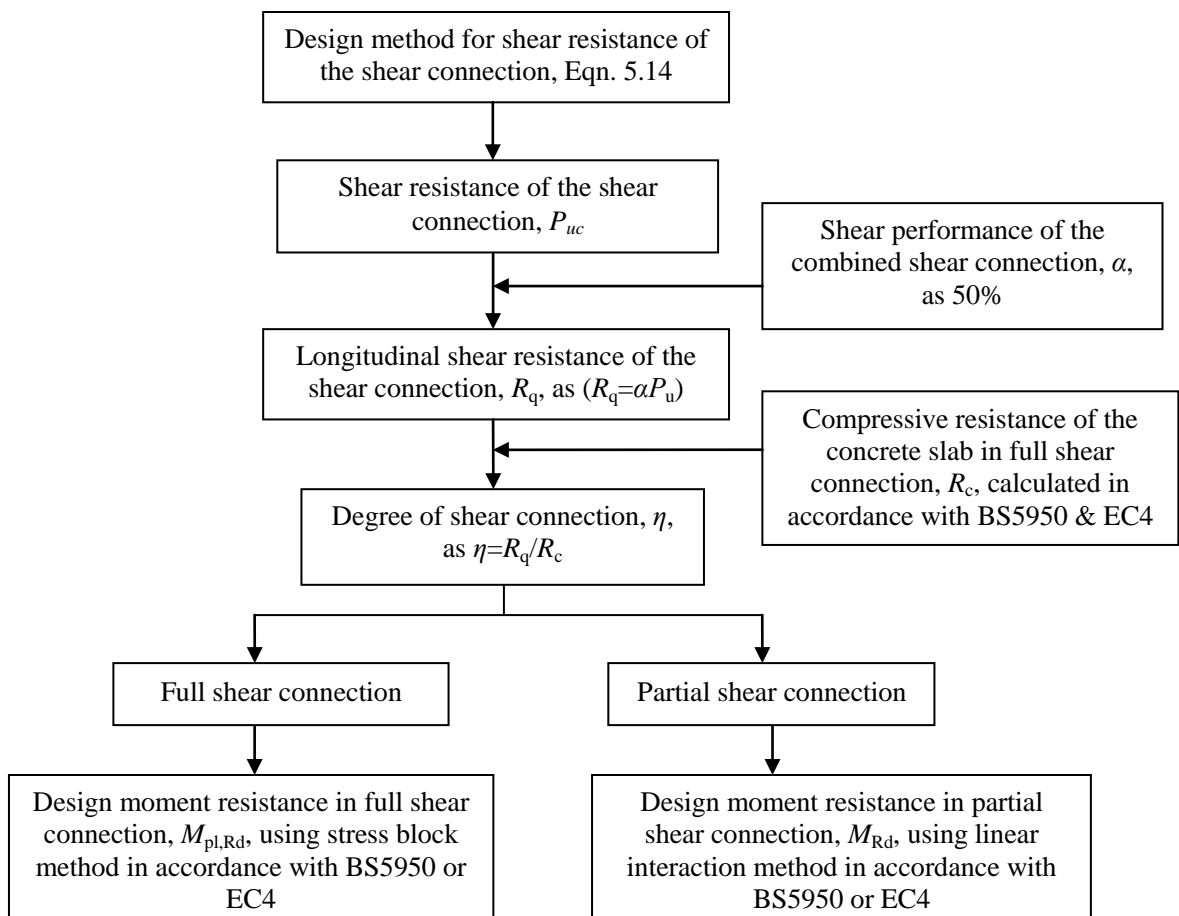
8.2 Recommendations

The recommendations made in this research were discussed in the areas of: improvement of the shear connection and future research topics.

8.2.1 Recommendations for the shear connection

The results of the push-out tests provided comprehensive information on the behaviour and shear resisting properties of the shear connection. However the design details for some of the shear connection could be improved. The following recommendations were made.

(6) It is recommended that the concrete-infill-only shear connection should not be used as the sole mean to provide shear connection to the composite shallow cellular floor beams, as the brittle failure mode of the shear connection was shown in the push-out tests. The concrete-infill-only shear connection should be used in combination with other additional elements, i.e. tie-bars or studs, to provide the necessary ductility.

(7) The shear failure of the tie-bar (Ø12mm) was shown in the push-out tests, as the tie-bars were positioned close to the perimeter of the web openings. It was recommended that the tie-bars should be positioned away from the perimeter of the web openings with a minimum distance of 20mm. This recommended minimum distance is based on the maximum slip capacity of the tie-bar shear connection shown in the push-out tests.

(8) It is recommended that the ducting shear connection should be used only in the region of low shear, as low shear resistance of the ducting shear connection was shown in the push-out tests. Also, it is recommended that the ducting shear connection should not be used in the region where large slips are expected, as buckling of the ducting occurred at the slip value of 1.5-3.5mm.

8.2.2 Recommendations for future research

(1) The behaviour and shear resistance of the shear connection used for the composite shallow cellular floor beams under direct static shear force were extensively investigated in the two push-out test series. The fatigue properties of the shear connection had not been investigated previously. Push-out tests with dynamic loading on the shear connection is recommended as a future research topic. The findings of the dynamic loading test will provide specific

information for design calculation where the composite shallow cellular floor beams might subject to repeated loading. The results of the dynamic loading test could also be used to compare with those of the push-out tests with static loading performed in this research.

(2) It was recommended that FEA of the composite shallow cellular floor beams should be carried out in order to further verify the developed design methods for both deflection check and moment resistance. The FEA should investigate the composite beams with ribbed slab and variations in the size of the beam section and web opening diameter.

Appendix A

Synthetic fibre reinforcement and superplasticizer

The synthetic fibre, STRUX 90/40, was used for the fibre-reinforced concrete of specimens of the push-out test series-I. This synthetic fibre reinforcement was a product of Grace Construction Products Limited. The fibres were 40mm in length with an aspect ratio of 90, as depicted in Figure A-1. The synthetic fibre was a replacement of the traditional welded wire mesh or steel fibre reinforcement in flooring and formwork applications. Its benefits for construction process were: ease of use, rapid dispersion, good finishing and improved pumpability. The advantages for performance of the concrete were: non-corrosive, ductility and durability.
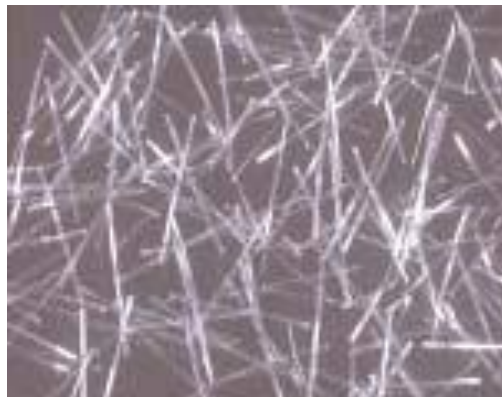
Figure A-1 Synthetic fibres, STRUX 90/40
(courtesy of Grace Construction Products Limited)

The fundamental mechanism of this synthetic fibre was a mechanical action, not a chemical reaction between the fibres and cement paste. Therefore, it had no effect on the hydration process of the cement. Although, the Grace Construction Limited stated the synthetic fibres only improves the cracking control, not compressive or flexural strengths of the concrete. The concrete strength tests carried out in this research showed the tensile strength of the fibre-reinforced concrete was higher than that of the normal concrete with the same compressive strength, as shown in the table below.

	Compressive strength (MPa)	Tensile strength (MPa)
Fibre-reinforced concrete	35	4.06
Normal concrete	35	3.26

Table A-1 Strength comparison between the normal and fibre-reinforced concrete

The normal dosage rate of the STRUX®90/40 was 1.8-7.0kg/m^3 of concrete volume. This is dependent on the specifications of the application. The dosage rate used for the push-out test series-I specimens was 5.3kg/m^3. The material properties of the synthetic fibres are:

Specific gravity	0.92
Absorption	None
Modulus of elasticity	9.5GPa
Tensile strength	540MPa
Melting point	160^{0}C
Alkali, Acid and Salt resistance	High

The superplasticizer, ADVA Flow 410, was used for the fibre-reinforced concrete of the push-out test series-I specimens to improve its workability. The ADVA Flow 410 was also a product of Grace Construction Products Limited. The dosage rate of 650ml per 100kg cement mass was used for the fibre-reinforced concrete of the push-out test series-I specimens. The slump of the fibre-reinforced concrete was increased from 50mm to 120mm, which was the designed workability.

Appendix B

Concrete strength of push-out test series-I

The concrete strength of all push-out test series-I specimens was determined at 7-day, 28-day and on-the-day of the push-out tests. The concrete compressive cube tests were carried out in accordance with British Standard, BS1881:116: 1983. The concrete cylinder tensile splitting tests were carried out in accordance with British Standard, BS1881:117: 1983. The results of the concrete strength are shown in table below.

Specimen No.	Cube compressive strength, f_{cu}, (MPa)			Tensile splitting strength, f_{ct}, (MPa)		
	7-day	28-day	On-the-day of the test	7-day	28-day	On-the-day of the test
T1-A-N	36.2	45.2	56.5	2.89	3.62	4.53
T1-A-F	37.2	46.5	58.1	3.10	3.88	4.85
T1-B-N	36.2	45.2	56.5	2.89	3.62	4.53
T1-B-F	37.2	46.5	58.1	3.10	3.88	4.85
T2-A-N	34.9	43.6	54.5	2.89	3.62	4.54
T2-A-F	33.2	41.5	51.9	2.60	3.26	4.07
T2-B-N	34.9	43.6	54.5	2.89	3.62	4.54
T2-B-F	33.2	41.5	51.9	2.60	3.26	4.07
T3-A-N	35.3	44.2	55.2	2.50	3.13	3.91
T3-A-F	32.9	41.2	51.5	2.49	3.11	3.89
T3-B-N	35.3	44.2	55.2	2.50	3.13	3.91
T3-B-F	32.9	41.2	51.5	2.49	3.11	3.89
T4-A-N	42.9	53.6	67.0	2.98	3.73	4.66
T4-A-F	32.1	40.2	50.2	2.61	3.26	4.08
T4-B-N	42.9	53.6	67.0	2.98	3.73	4.66
T4-B-F	32.1	40.2	50.2	2.61	3.26	4.08

Concrete strength of push-out test series-II

The concrete strength of all push-out test series-II specimens was determined at 7-day, 28-day and on-the-day of the push-out tests. The concrete compressive cube tests were carried out in accordance with BS1881:116: 1983. The concrete cylinder tensile splitting tests were carried out in accordance with, BS1881:117: 1983. The results of the concrete strength are shown in table below.

Specimen No.	Cube compressive strength, f_{cu}, (MPa)			Tensile splitting strength, f_{ct}, (MPa)		
	7-day	28-day	On-the-day of the test	7-day	28-day	On-the-day of the test
T5-1	24	30	35	2.00	2.49	3.21
T5-2	25	33	35	2.11	2.79	3.21
T5-3	22	31	32	2.31	3.26	2.90
T5-4	23	29	30	1.99	2.51	3.02
T6-1	21	27	29	2.06	2.65	2.85
T6-2	21	29	32	1.92	2.65	2.92
T6-3	18	24	28	1.60	2.13	2.49
T6-4	15	23	27	1.43	2.19	2.57

Concrete strength of flexural tests

Concrete strength of the flexural test specimen was determined at 7-day, 14-day, 28-day and on-the-day of the flexural tests. The concrete cube compressive tests were carried out in accordance with BS1881:116: 1983. The concrete cylinder tensile splitting tests were carried out in accordance with BS1881:117: 1983. The results are list in the table below.

	Compressive Cube Strength, f_{cu}, (MPa)	Cylinder Tensile Splitting Strength, f_{ct}, (MPa)
7-day	21	2.2
14-day	24	2.6
28-day	28	2.7
Four-point bending test (on-the-day)	30	2.9
Three-point bending test (on-the-day)	31	2.9

Appendix C

Coupon test results of Ø16mm & Ø12mm tie-bars

Ø16mm tie-bar coupon test	
Diameter	7.95 (mm)
Cross-sectional area	49.64 (mm^2)
Failure load	26.9 (kN)
Yield strength (MPa)	441.7
Tensile strength (MPa)	542.2

Ø12mm tie-bar coupon test	
Diameter	6.33 (mm)
Cross-sectional area	31.47 (mm^2)
Failure load	13.85 (kN)
Yield strength (MPa)	440.1
Tensile strength (MPa)	525.6
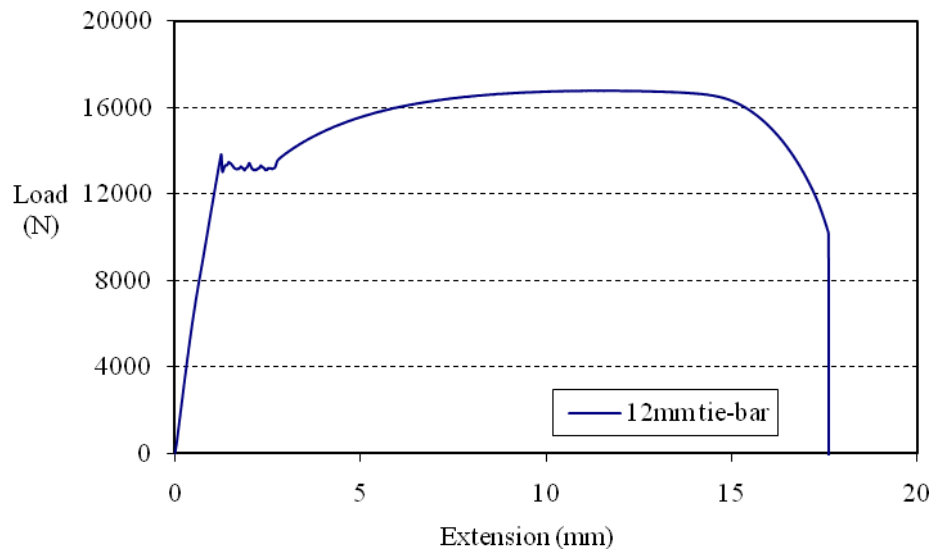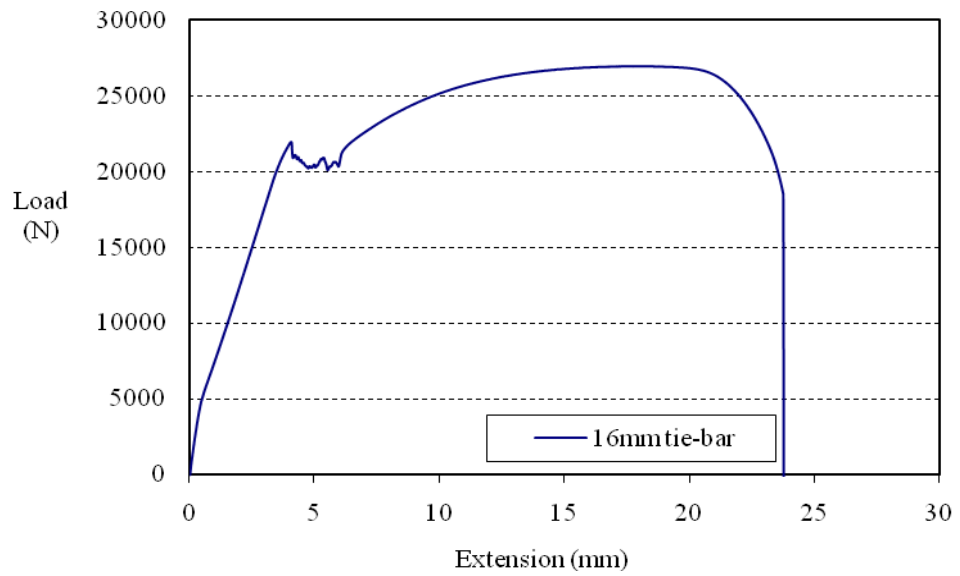
Coupon test results of headed studs

Ø19mm headed stud coupon test	
Diameter	6.6 (mm)
Cross-sectional area	34.22 (mm^2)
Failure load	18.14 (kN)
Yield strength (MPa)	452.1
Tensile strength (MPa)	530.2
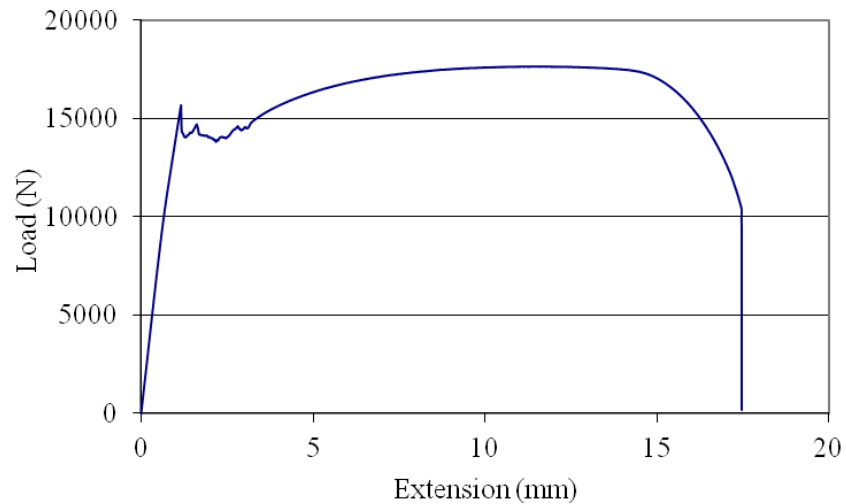
Steel section of the push-out test series-II

Six coupons were machined from the steel section of the push-out test series-II. Four of the coupons were cut from the flanges and two were cut from web post. Overall average strengths were:

- Yield strength, 420MPa
- Ultimate strength, 530MPa

267
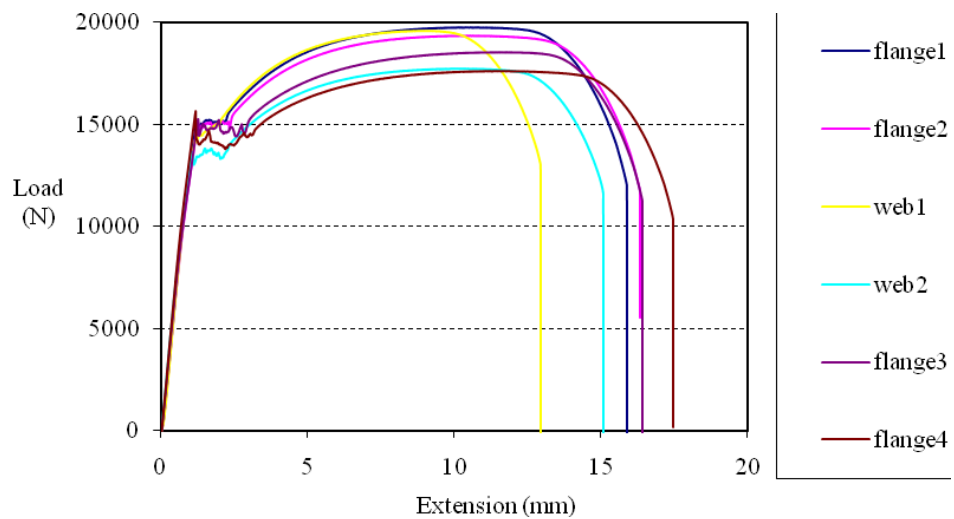
Steel section of the flexural test beam specimen

Six coupons were machined from the steel section. Two coupons were cut from either the top or bottom flange. One coupon was cut from either the top or bottom web post. Overall average strengths were:

- Yield strength,   414MPa
- Ultimate strength,   527MPa
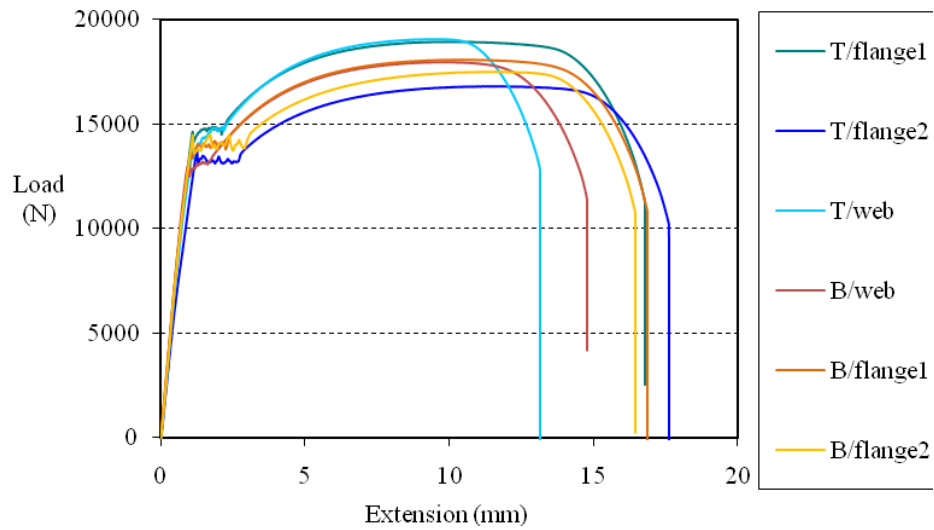
Appendix D

FEA element size analysis

A concrete cube of 100 x 100mm was used to carry out the element size analysis. Only a quarter of the cube was modelled using the symmetric boundary conditions. The concrete element Solid65 was used with the same concrete material properties as those of the calibration model of the push-out tests. The meshed model of the 1/4 concrete cube is shown in Figure D-1. Four different element sizes were used in order to determine the optimum size of the concrete element for the FEA push-out tests. These four element sizes were 20, 15, 10 and 5mm.

The concrete strength for the cube model was 32MPa. Pressure of 31MPa was applied to the cube model. Vertical displacements at the centre of the cube top face were compared between the models of different element sizes, as shown in Figure D-2. Element stresses at the centre of the cube bottom face were compared with the models of different element sizes, as shown in Figure D-3. The results of the models with the four element sizes were listed in Tables D-1, D-2, D-3 and D-1.

The results of vertical displacement and element stresses were almost identical between the models of different elements. Hence, all four element sizes could be used to model the FEA push-out tests. The computational cost was increased using the fine element size, i.e. 5mm and 10mm. On the other hand, the element of 20mm would be too coarse for the modelling the concrete infill. Therefore, element size of 15mm was chosen as the optimum element size for the FEA push-out tests.
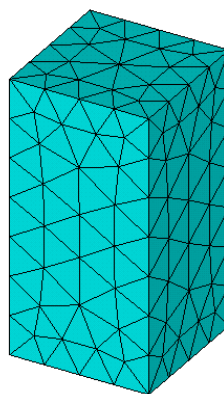
Figure D-1 Meshed model of a 1/4 concrete cube with 15mm elements
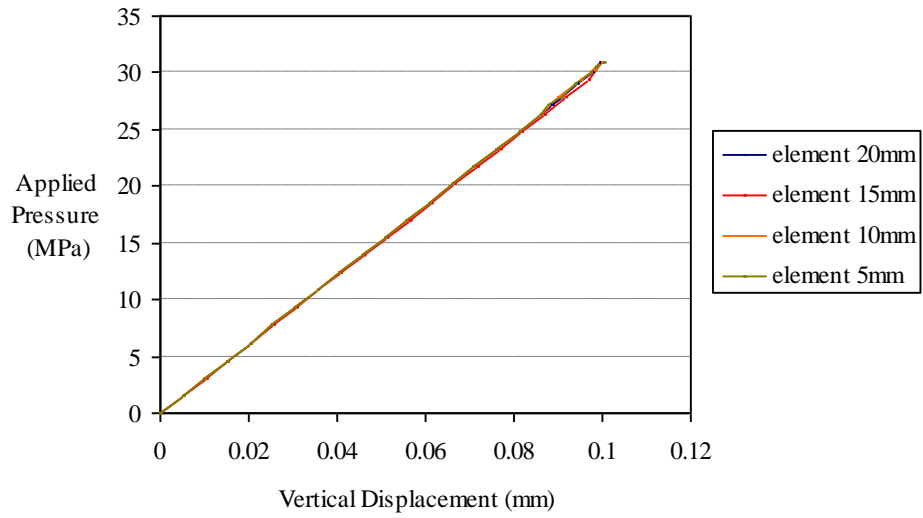
Figure D-2 Vertical displacements of models with different element sizes
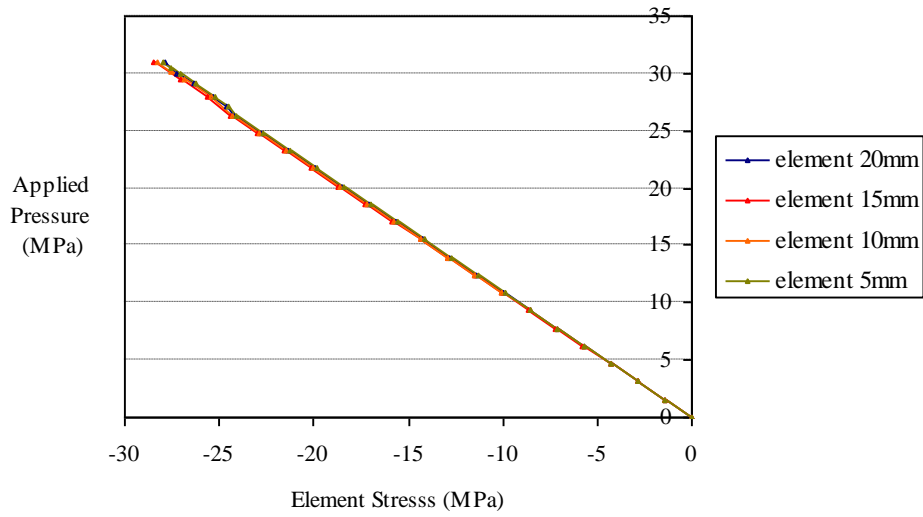
Figure D-3 Elemental stresses of models with different element sizes

Applied Pressure (MPa)	Vertical Displacement (mm)	Elemental Stress (MPa)
1.6	0.0051	-1.42
6.2	0.0203	-5.70
12.4	0.0406	-11.39
15.5	0.0507	-14.24
20.2	0.0660	-18.51
29.1	0.0942	-26.37
31.0	0.0995	-27.89

Table D-1 Results of the FE model with element size of 20mm

Applied Pressure (MPa)	Vertical Displacement (mm)	Elemental Stress (MPa)
1.6	0.0051	-1.44
6.2	0.0205	-5.75
12.4	0.0410	-11.51
15.5	0.0512	-14.39
20.2	0.0666	-18.70
29.5	0.0968	-27.05
31.0	0.0998	-28.47

Table D-2 Results of the FE model with element size of 15mm

Applied Pressure (MPa)	Vertical Displacement (mm)	Elemental Stress (MPa)
1.6	0.0051	-1.43
6.2	0.0203	-5.72
12.4	0.0405	-11.45
15.5	0.0507	-14.31
20.2	0.0659	-18.60
29.5	0.0953	-26.86
31.0	0.0999	-28.22

Table D-3 Results of the FE model with element size of 10mm

Applied Pressure (MPa)	Vertical Displacement (mm)	Elemental Stress (MPa)
1.6	0.0051	-1.42
6.2	0.0203	-5.66
12.4	0.0406	-11.33
15.5	0.0508	-14.16
20.2	0.0660	-18.41
29.1	0.0941	-26.23
31.0	0.1003	-27.92

Table D-4 Results of the FE model with element size of 5mm

Appendix E

Contour plots of the calibration model with concrete strength, f_c, of 32MPa

(b)   (b)
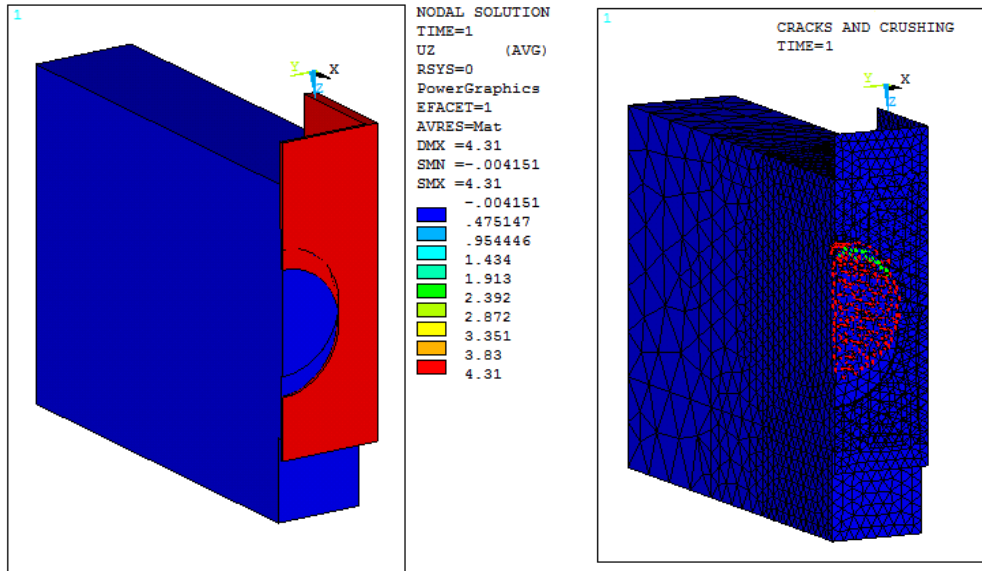
(a) Contour plot of vertical displacement (slips); (b) Contour plot of cracks

Contour plots of the calibration model with concrete strength, f_c, of 35MPa

(a)   (b)
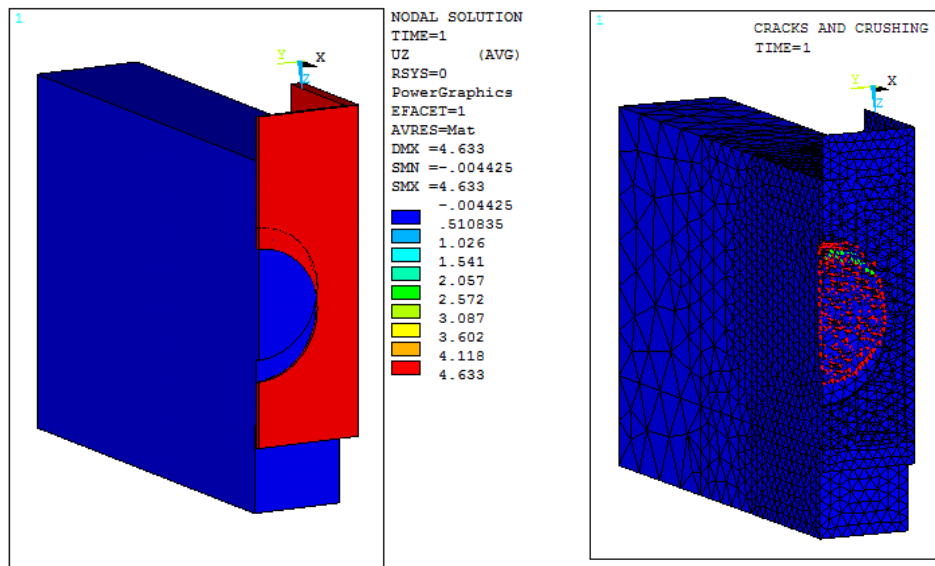
(a) Contour plot of vertical displacement (slips); (b) Contour plot of cracks

Stress contour plots of the concrete and steel for calibration model with f_c, of 32MPa
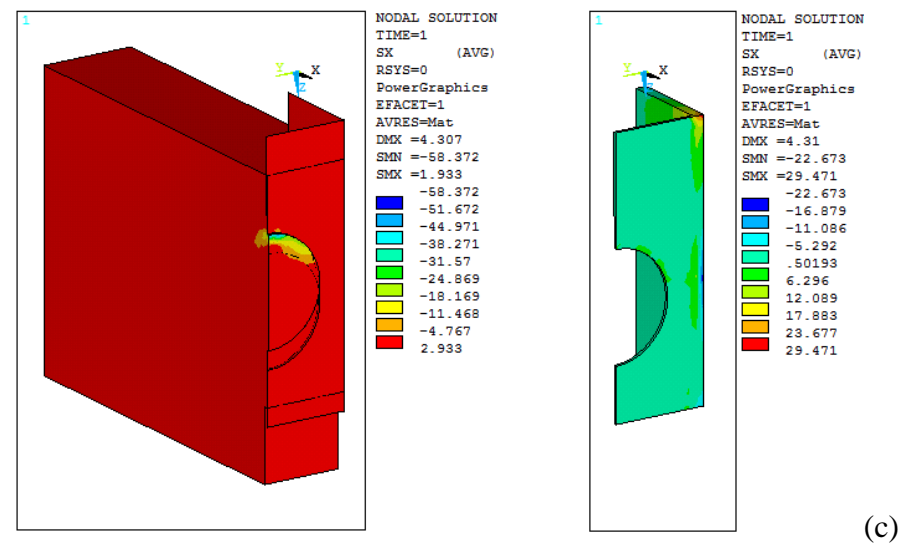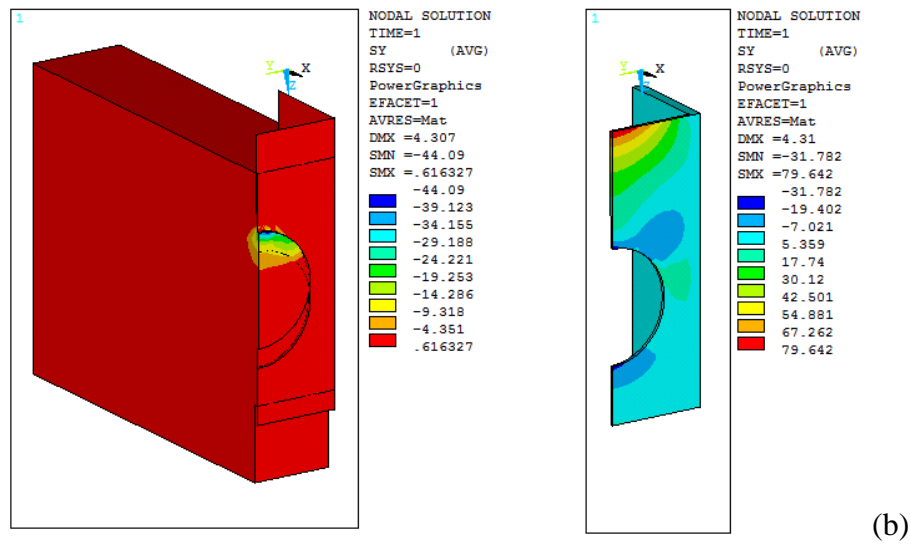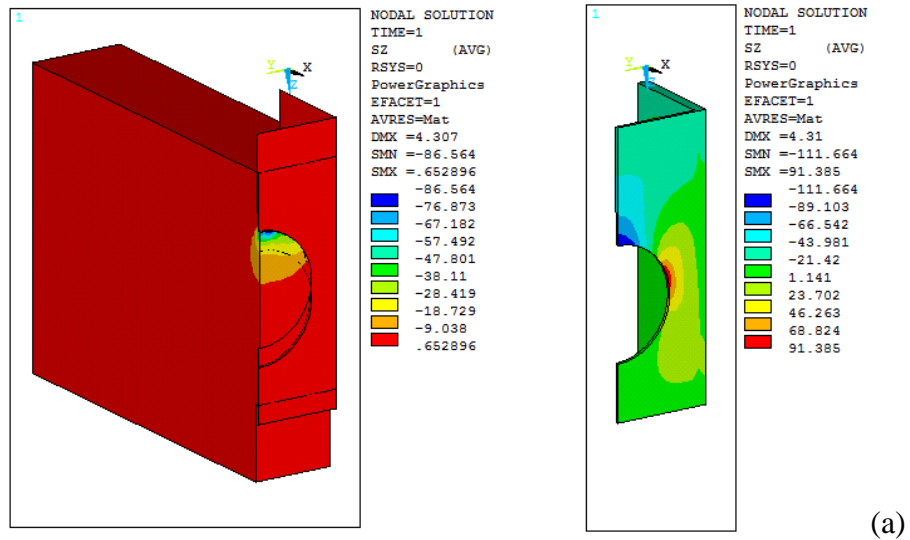
(a)

(b)

(c)

(a) Compression (vertical direction), (b) y-direction stress in line with web post,
(c) Separation (x-direction)

Stress contour plots of the concrete and steel for calibration model with f_c, of 35MPa
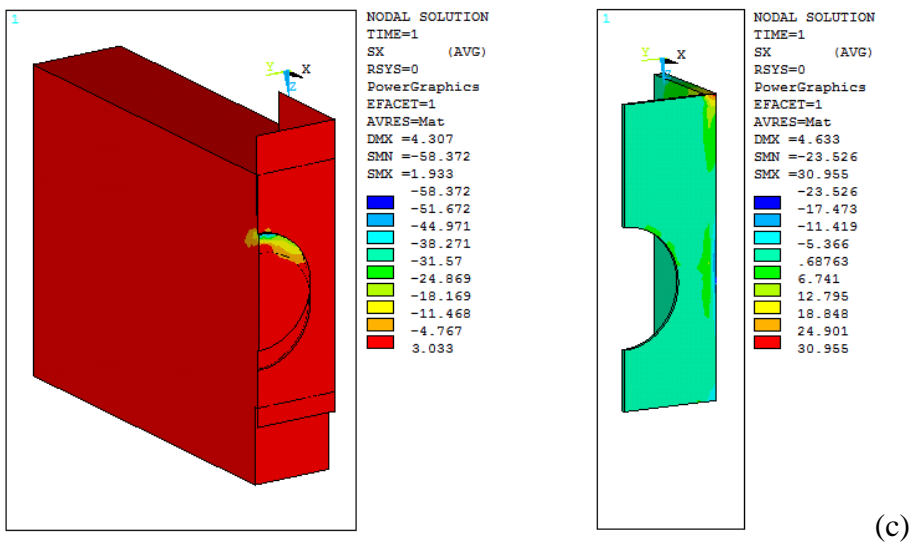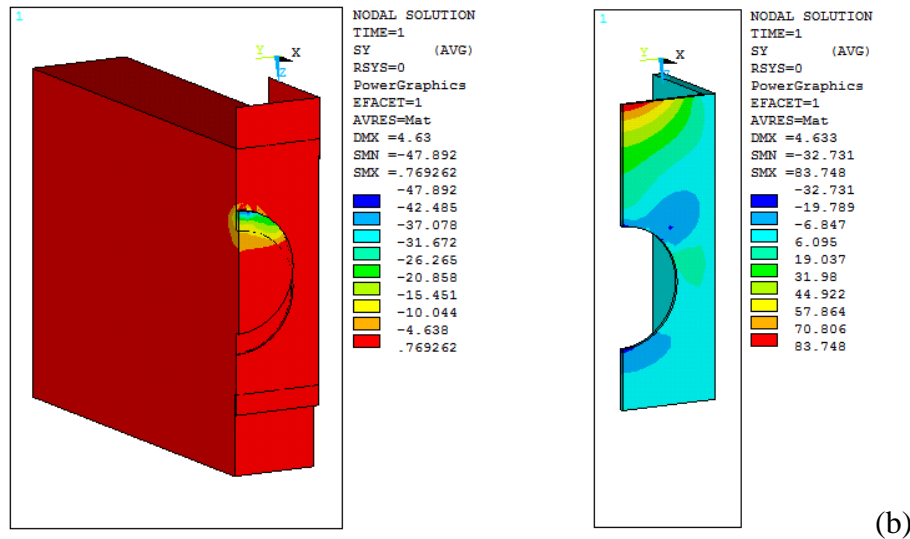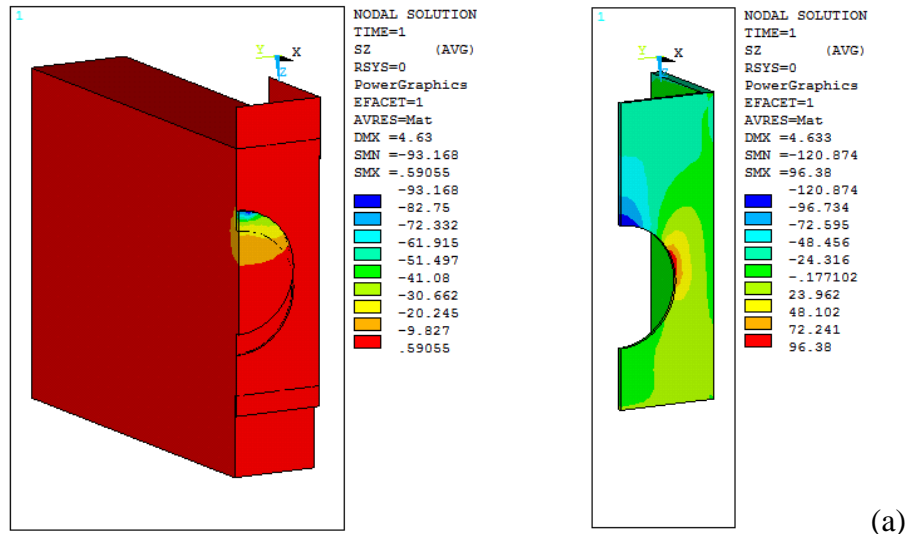
(a)

(b)

(c)

(a) Compression (vertical direction), (b) y-direction stress in line with web post,
(c) Separation (x-direction)

Contour plot of the FEA model with Ø200mm web opening and concrete strength of 38MPa

         (a)   (b)
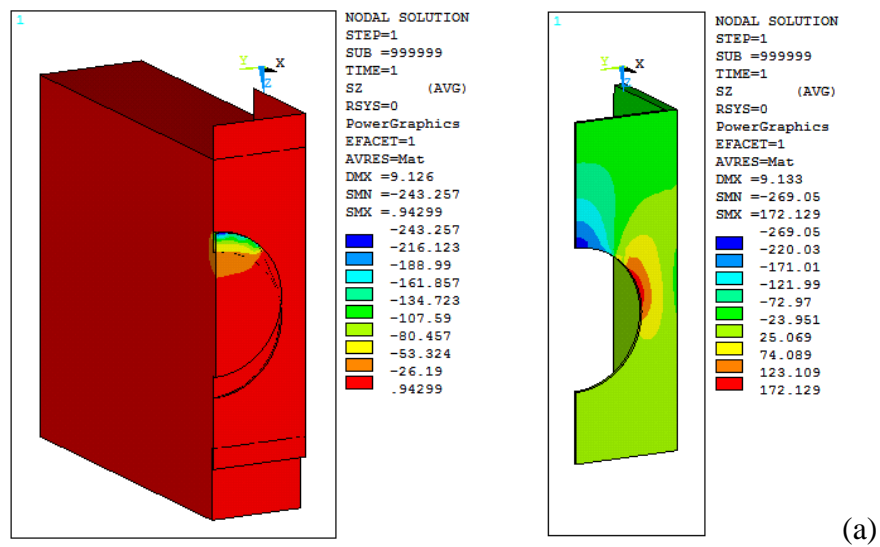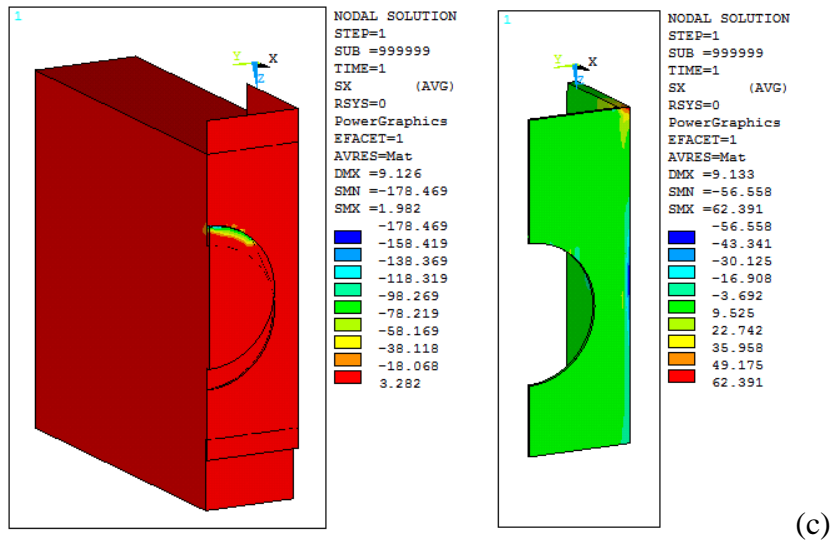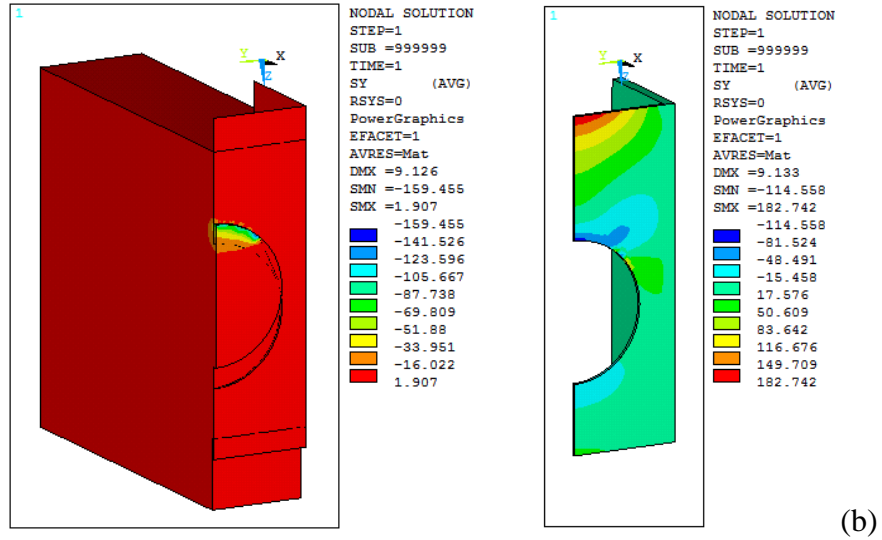
(a) Contour plot of vertical displacement (slips); (b) Contour plot of cracks

                                                (a)

(b)

(c)

Stress contour plot of the concrete and steel volumes: (a) Compression (vertical direction), (b) y-direction stress in line with web post, (c) Separation (x-direction)

Contour plot of the FEA model with Ø100mm web opening and concrete strength of 30MPa

(a)   (b)
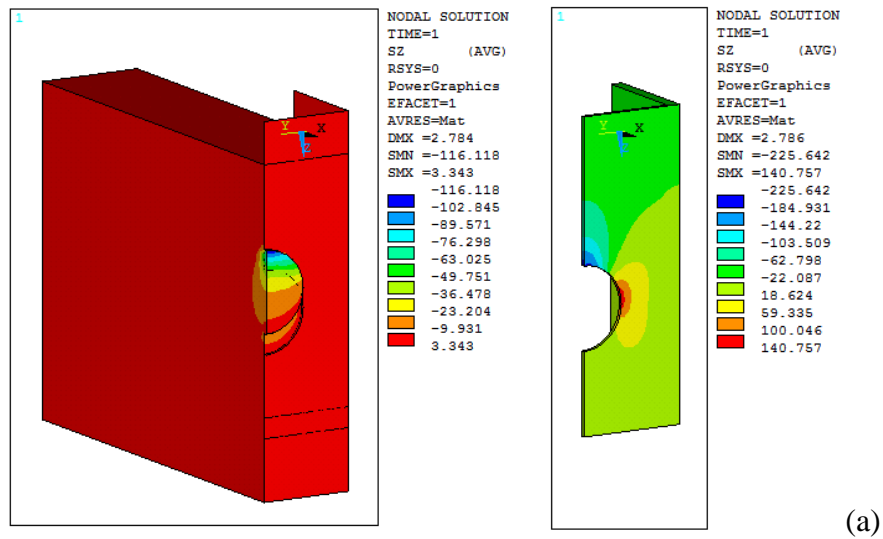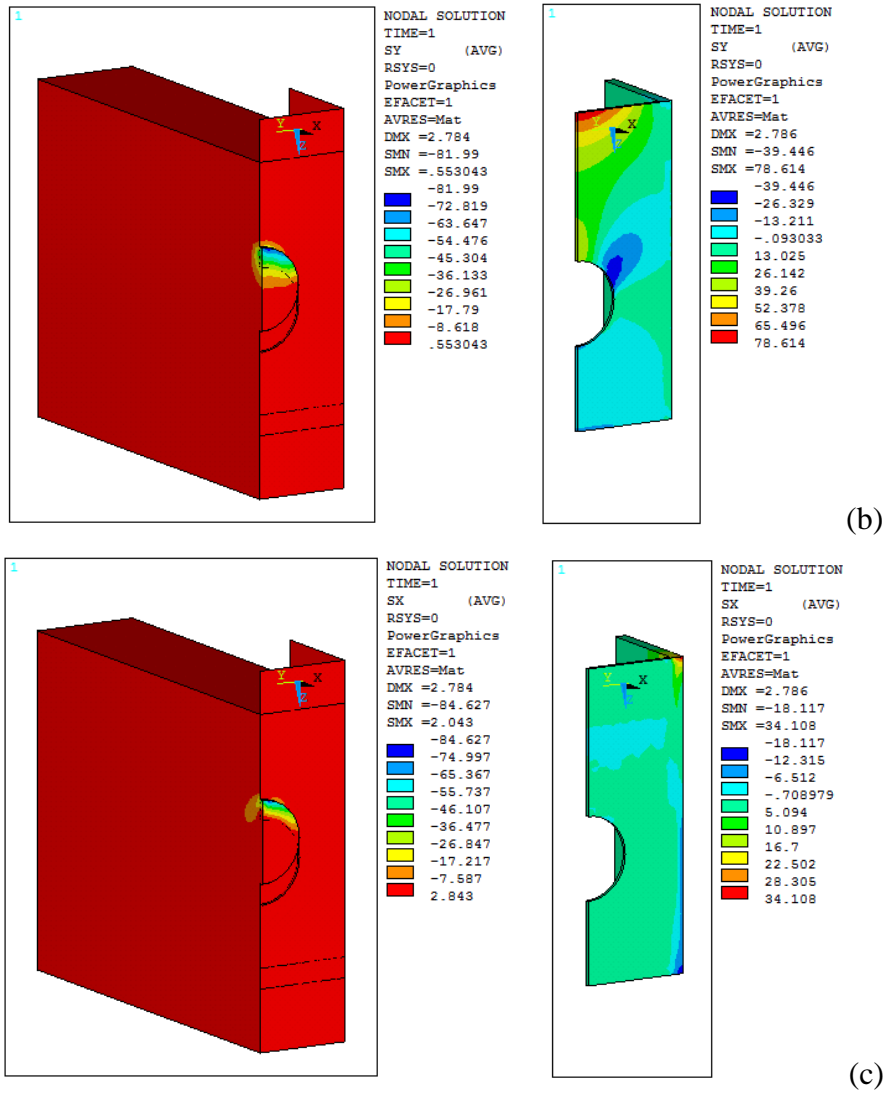
(a) Contour plot of vertical displacement (slips); (b) Contour plot of cracks

(a)

(b)

(c)

Stress contour plot of the concrete and steel volumes: (a) Compression (vertical direction), (b) y-direction stress in line with web post, (c) Separation (x-direction)

Appendix F

Back analysis of the four-point bending test using the stress block method

Step 1 Moment resistance of the steel section

The moment resistance of the steel section, M_s, was calculated using the test P.N.A of 178mm. The optimum cross section, with 1/2 depth of the web opening, was used in the calculation. The measured steel stress of 324N/mm^2, at the final loading stage, was used as the stress for both tension and compression. The stress block diagram of the steel section was shown in Figure F-1. The moment resistance of the steel section, M_s, was 210kNm, determined by taking moments about P.N.A.
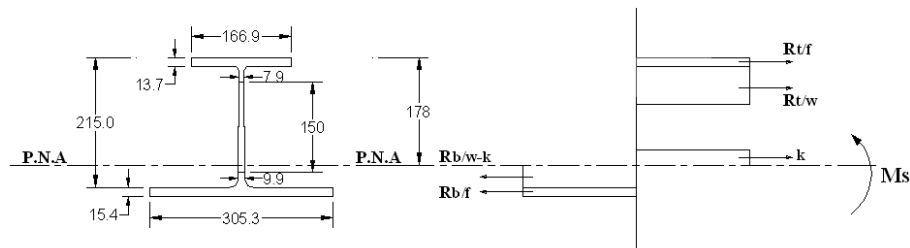
Figure F-1 Stress block diagram of the steel cross section at the test P.N.A

Step 2 Additional moment resistance due to composite action

The additional moment resistance due to the composite action, M_{comp}, was 75kNm determined by subtracting M_s of 210kNm from the test moment of 285kNm.

Step 3 Longitudinal shear resistance of the shear connections

The longitudinal shear resistance of the shear connections, R_q, was equal to the compressive resistance of the concrete slabs in partial shear connection. Hence, the $R_q=1000(0.67f_{cu})d$, where d is the depth of concrete in compression. Based on $M_{comp}=R_q(178 - d/2)$, the R_q of 450kN was obtained. The $0.67f_{cu}$ was the concrete compressive strength in bending. The depth of concrete in compression, d, was 22.3mm.

Step 4 Degree of shear connection

The degree of shear connection, η, was determined using $\eta = R_q/R_c$, where R_c was the compressive resistance of the concrete slabs in full shear connection. The R_c was 969kN determined in Appendix G. Hence, the degree of shear connection was 0.46.

Appendix G

Calculated moment resistance of the beam specimen in four-point bending test

The moment resistance of the beam specimen in the four-point symmetric bending test was calculated in the degrees of shear connection, 0, 0.5, 0.7 and 1.0. The stress block method was used in the calculation with the measure material properties at the final loading stage and the concluded optimum cross section (with the 1/2 depth of the web opening). The moment resistance in zero degree of shear connection was the moment resistance of the steel section alone. The results of the calculation are summarised in the table below. The calculation details are shown in the following sections.

Degree of Shear Connection, η	Shear Resistance of Shear Connections, R_q (kN)	Depth of Concrete in Compression, d (mm)	Depth of P.N.A (mm)	Moment Resistance, (kNm)
0	--	--	217.1	196.3
0.5	485	24.1	207.6	290.7
0.7	679	33.8	179.6	321.2
1.0	969	48.3	48.3	347.6

G.1 Moment resistance of the steel section (M_s)

The plastic stress block method was used to determine moment resistance of the steel section. The stress block diagram is illustrated in Figure G-1. The measured tensile stress of 324N/mm^2 at the final loading stage was used as both tension and compression.
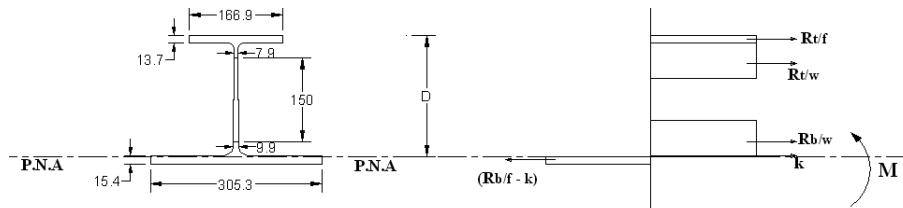
Figure G-1 Stress block diagram of the steel section

Step 1 Determine the depth of plastic neutral axis (P.N.A)

The equilibrium of tension and compression, expressed in Eqn. G.1, was used to determine the depth of P.N.A, D.

$$R_{t/f} + R_{t/w} + R_{b/w} + K = R_{b/f} - K \tag{G.1}$$

Where: $R_{t/f}$ is the resistance of the top flange ($A_{t/f}P_y$);

$R_{t/w}$ is the resistance of the web post of the top tee ($A_{t/w}P_y$);

$R_{b/w}$ is the resistance of the web post of the bottom tee

($A_{b/w}P_y$)

$R_{b/f}$ is the resistance of the bottom flange ($A_{b/f}P_y$)

K is the bottom flange in compression [$305.3P_y$ (D-215)].

By substituting the steel stress and the cross sectional areas of the steel elements into Eqn. G.1, hence D = 217.1mm, which was within the bottom flange.

Step 2 Determine plastic moment capacity

Taking moments about P.N.A,

$$M_s = R_{t/f}D_{t/f} + R_{t/w}D_{t/w} + R_{b/w}D_{b/w} + K(D-215)/2 + (R_{b/f} - K)(230-D)/2$$

$$(G.2)$$

Where: M_s is the plastic moment resistance of the steel section

$D_{t/f}$ is the distance between the $R_{t/f}$ and P.N.A,

$D_{t/w}$ is the distance between the $R_{t/w}$ and P.N.A,

$D_{b/w}$ is the distance between the $R_{b/w}$ and P.N.A,

$D_{b/f}$ is the distance between the $R_{b/f}$ and P.N.A.

By substituting the resistance of the steel elements and their distances to P.N.A into Eqn. G.2, hence, $M_s = 196.3$kNm.

G.2 Moment resistance of the cross section in full shear connection (M_{pc})

The plastic stress block diagram of the cross section is illustrated in Figure G-2. The moment resistance of the cross section was determined using the measured material properties at the final loading stage, i.e. steel stress of 324N/mm^2 and concrete strength of 30N/mm^2. The shear strength of the shear connections was assumed unaffected by the depth of P.N.A. The results of the push-out tests were used in the calculation.
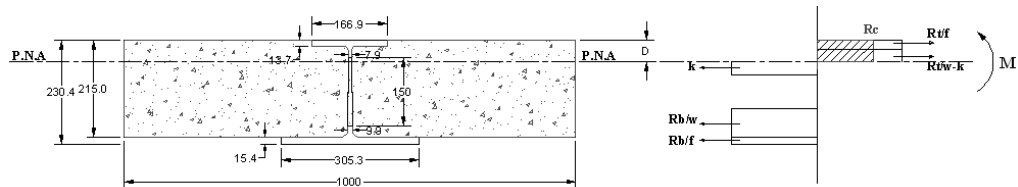
Figure G-2 Stress block diagram of the cross section in full shear connection

Step 1 Determine the depth of P.N.A

The equilibrium of tension and compression, expressed in Eqn. G.3, was used to determine the depth of P.N.A, D.

$$R_{t/f} + (R_{t/w} - K) + R_c = K + R_{b/w} + R_{b/f} \tag{G.3}$$

Where: $R_{t/f}$ is the resistance of the top flange $(A_{t/f}P_y)$;

               $R_{t/w}$ is the resistance of the web post of the top tee $(A_{t/w}P_y)$;

               R_c is the compressive resistance of the concrete slab in full shear connection $(1000*0.67f_{cu}D)$

               $R_{b/w}$ is the resistance of the web post of the bottom tee $(A_{b/w}P_y)$;

               $R_{b/f}$ is the resistance of the bottom flange $(A_{b/f}P_y)$;

               K is the web post of the top tee in tension $[7.9(77.5-D)P_y]$

By substituting the cross sectional areas of the steel elements, $P_y = 324\text{N/mm}^2$ and $f_{cu} = 30\text{N/mm}^2$ into the Eqn. G.3, hence, D = 48.3mm

Also, the compressive resistance of the concrete slab in full shear connection, R_c, of 969kN was obtained.

Step 2 Determine the plastic moment capacity

Taking moments about P.N.A,

$$M_{pc} = R_{t/f}D_{t/f} + (R_{t/w} - K)(D - D_{t/f})/2 + R_cD_c + K(77.5 - D)/2 + R_{b/w}D_{b/w} + R_{b/f}D_{b/f}$$

$$\tag{G.4}$$

Where: M_{pc} is the full plastic moment of the composite section

               $D_{t/f}$ is the distance between the $R_{t/f}$ and P.N.A,

               $D_{t/w}$ is the distance between the $R_{t/w}$ and P.N.A,

               D_c is the distance between the R_c and P.N.A,

               $D_{b/w}$ is the distance between the $R_{b/w}$ and P.N.A,

               $D_{b/f}$ is the distance between the $R_{b/f}$ and P.N.A.

By substituting the resistance of the steel elements, their distance to P.N.A and R_c, into Eqn. G.4, hence, $M_{pc} = 347.6\text{kNm}$.

G.3 Moment resistance of the cross section in degree of shear connection of 0.5

The stress block diagram of the cross section in degree of shear connection of 0.5 is illustrated below.
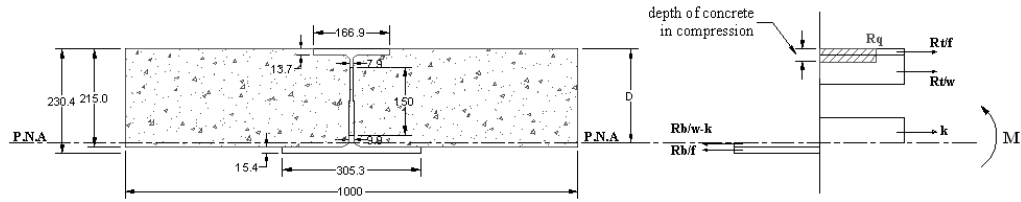
Figure G-3 Stress block diagram of the cross section in degree of shear connection of 0.5

Step 1 Determine the depth of P.N.A

The longitudinal shear resistance of the shear connections, R_q, was calculated first using the compressive resistance of the concrete slabs, R_c, and degree of shear connection, η, as $\eta = R_q/R_c$.

- R_c=969kN,
- $\eta = 0.5$,
- Hence $R_q = 485$kN.

The depth of P.N.A, D, was determined using the equilibrium of tension and compression, expressed in Eqn. G.5.

$$R_{t/f} + R_{t/w} + R_q + K = R_{b/w} - K + R_{b/f} \qquad (G.5)$$

Where: $R_{t/f}$ is the resistance of the top flange ($A_{t/f}P_y$);

$R_{t/w}$ is the resistance of the web post of the top tee ($A_{t/w}P_y$);

R_q is the longitudinal shear resistance of shear connections;

$R_{b/w}$ is the resistance of the web post of the bottom tee ($A_{b/w}P_y$)

$R_{b/f}$ is the resistance of the bottom flange ($A_{b/f}P_y$)

K is the bottom web in compression.

By substituting the R_q and the cross sectional areas of the steel elements into Eqn. G.5, hence D = 207.6mm.

The depth of concrete in compression, d, was determined using the R_q of 485kN, as the longitudinal shear resistance of the shear connections, R_q, was equal to the compressive resistance of the concrete slabs in partial shear connection. The d of 24.1mm was obtained.

Step 2 Determine the plastic moment capacity

Taking moments about P.N.A

$$M = R_{t/f}D_{t/f} + R_{t/w}D_{t/f} + R_qD_q + KD_k + (R_{b/w}\text{-}k)(215\text{-}D) + R_{b/f}D_{b/f}$$

(G.6)

<div style="margin-left:3em">

Where: M is the moment resistance of the composite section

     $D_{t/f}$ is the distance between the $R_{t/f}$ and P.N.A,

     $D_{t/w}$ is the distance between the $R_{t/w}$ and P.N.A,

     D_q is the distance between the R_q and P.N.A,

     D_k is the distance between the K and P.N.A,

     $D_{b/w}$ is the distance between the $R_{b/w}$ and P.N.A,

     $D_{b/f}$ is the distance between the $R_{b/f}$ and P.N.A.

</div>

By substituting the resistance of the steel elements, their distance to P.N.A and the R_q into Eqn. G.6, hence, $M = 290.7$kNm.

G.4 Moment resistance of the cross section in degree of shear connection, 0.7

The stress block diagram of the cross section in degree of shear connection of 0.7 is illustrated below.

Figure G-4 Stress block diagram of the cross section in degree of shear connection of 0.7

Step 1 Determine the depth of P.N.A

The longitudinal shear resistance of the shear connections, R_q, was calculated first using the compressive resistance of the concrete slabs, R_c, and the degree of shear connection, η, as $\eta = R_q/R_c$.

- R_c=969kN,
- $\eta = 0.7$,
- Hence $R_q = 679$kN.

The depth of P.N.A, D, was determined using the equilibrium of tension and compression, expressed in Eqn. G.7.

$$R_{t/f} + R_{t/w} + R_q + K = R_{b/w} - K + R_{b/f}$$

(G.7)

Where: $R_{t/f}$ is the resistance of the top flange ($A_{t/f}P_y$);

$R_{t/w}$ is the resistance of the web post of the top tee ($A_{t/w}P_y$);

R_q is the longitudinal shear resistance of shear connections;

$R_{b/w}$ is the resistance of the web post of the bottom tee ($A_{b/w}P_y$)

$R_{b/f}$ is the resistance of the bottom flange ($A_{b/f}P_y$)

K is the bottom web in compression.

By substituting the R_q and the cross sectional areas of the steel elements into Eqn. G.7, hence D = 179.6mm.

The depth of concrete in compression, d, was determined using R_q of 679kN, as the longitudinal shear resistance of the shear connections, R_q, was equal to the compressive resistance of the concrete slabs in partial shear connection. The d of 33.8mm was obtained.

Step 2 Determine the plastic moment capacity

Taking moments about P.N.A

$$M = R_{t/f}D_{t/f} + R_{t/w}D_{t/f} + R_qD_q + KD_k + (R_{b/w}\text{-k})(215\text{-D}) + R_{b/f}D_{b/f}$$

(G.8)

Where: M is the moment resistance of the composite section

$D_{t/f}$ is the distance between the $R_{t/f}$ and P.N.A,

$D_{t/w}$ is the distance between the $R_{t/w}$ and P.N.A,

D_q is the distance between the R_q and P.N.A,

D_k is the distance between the K and P.N.A,

$D_{b/w}$ is the distance between the $R_{b/w}$ and P.N.A,

$D_{b/f}$ is the distance between the $R_{b/f}$ and P.N.A.

By substituting the resistance of the steel elements, their distance to P.N.A and the R_q into Eqn. G.8, hence, $M = 321.2$kNm.

Appendix H

Moment resistance of the different cross sections
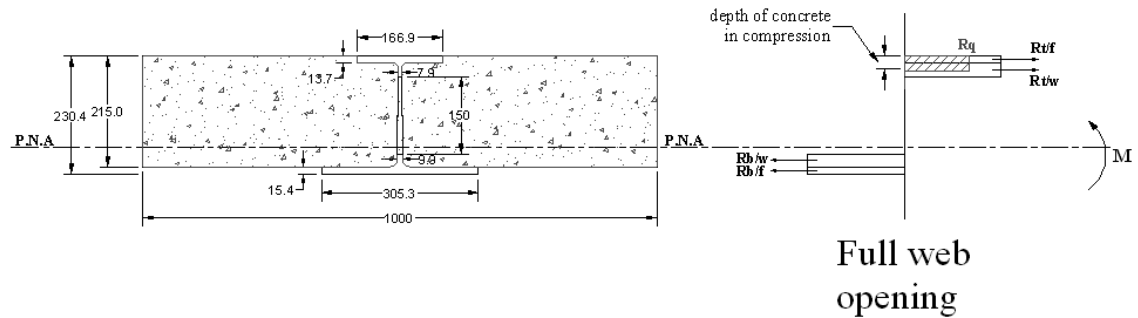
Full web opening

Degree of Shear Connection, η	Shear Resistance of the Shear Connectors, R_q (kN)	Depth of Concrete in Compression, d (mm)	Depth of P.N.A (mm)	Moment Resistance, (kNm)
0	--	--	218.2	178.6
0.4	319	15.9	216.6	245.4
0.5	399	19.8	216.2	261.2
0.6	478	23.8	215.8	276.7
0.65	518	25.8	215.6	284.3
0.7	558	27.8	215.4	291.8
0.75	598	29.7	215.2	299.2
0.8	638	31.7	214.6	306.6
0.85	678	33.7	208.4	313.7
0.9	717	35.7	202.2	320.5
0.95	757	37.7	195.9	327.0
0.96	765	38.1	194.7	328.2
0.97	773	38.5	193.5	329.5

Table H-1 Results of the cross section with full web opening
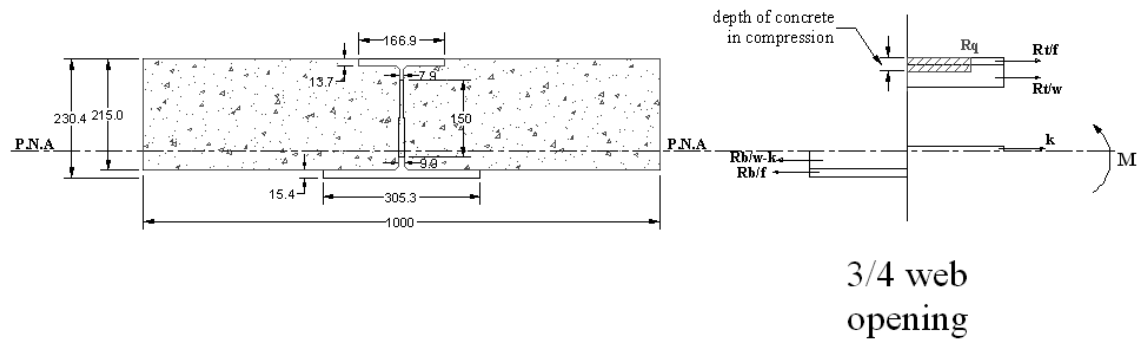
3/4 web
opening

Degree of Shear Connection, η	Shear Resistance of the Shear Connectors, R_q (kN)	Depth of Concrete in Compression, d (mm)	Depth of P.N.A (mm)	Moment Resistance, (kNm)
0	--	--	217.7	185.1
0.4	353	17.6	215.9	257.2
0.45	397	19.8	215.7	265.7
0.5	442	22.0	215.4	274.1
0.55	486	24.2	215.2	282.4
0.56	495	24.6	215.1	284.1
0.58	512	25.5	215.0	287.4
0.6	530	26.4	213.9	290.6
0.61	539	26.8	212.3	292.3
0.62	548	27.3	211.5	293.9
0.63	556	27.7	210.1	295.5
0.64	565	28.1	209.2	297.0
0.65	574	28.6	207.9	298.6
0.7	618	30.8	202.1	306.1
0.75	662	33.0	195.2	313.3
0.8	707	35.2	187.0	320.1
0.82	724	36.0	184.9	322.7
0.84	742	36.9	181.5	325.2
0.86	760	37.8	178.7	327.7
0.88	777	38.7	174.7	330.1
0.9	795	39.6	172.2	332.4
0.91	804	40.0	169.6	333.6
0.93	821	40.9	159.6	334.9
0.95	839	41.8	145.0	337.6

Table H-2 Results of the cross section with 3/4 depth of the web opening

1/2 web
opening

Degree of Shear Connection, η	Shear Resistance of the Shear Connectors, R_q (kN)	Depth of Concrete in Compression, d (mm)	Depth of P.N.A (mm)	Moment Resistance, (kNm)
0	--	--	217.1	196.3
0.4	388	19.3	215.2	272.8
0.45	436	21.7	212.5	282.0
0.5	485	24.1	207.6	290.7
0.55	533	26.5	200.8	299.1
0.56	543	27.0	199.8	300.7
0.57	553	27.5	198.6	302.2
0.58	562	28.0	197.0	303.8
0.59	572	28.5	195.6	305.4
0.6	582	28.9	194.8	306.9
0.65	630	31.4	187.5	314.3
0.7	679	33.8	179.6	321.2
0.75	727	36.2	171.8	327.6
0.8	776	38.6	163.3	333.5
0.81	785	39.1	161.8	334.7
0.82	795	39.6	158.7	335.8
0.83	805	40.0	156.8	336.9
0.84	814	40.5	154.6	337.9
0.86	834	41.5	149.3	339.0
0.88	853	42.5	140.5	341.6
0.9	873	43.4	130.8	344.1
0.91	882	43.9	123.6	345.2
0.93	902	44.9	112.8	345.5
0.95	921	45.8	100.3	345.8

Table H-3 Results of the cross section with 1/2 depth of the web opening
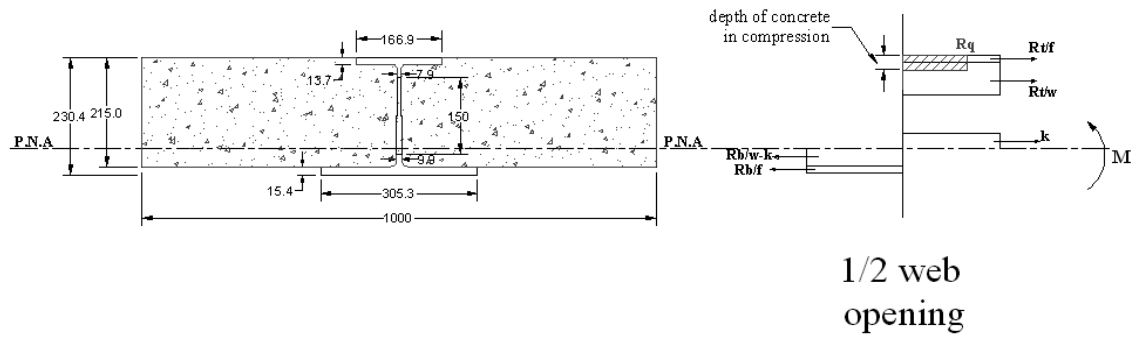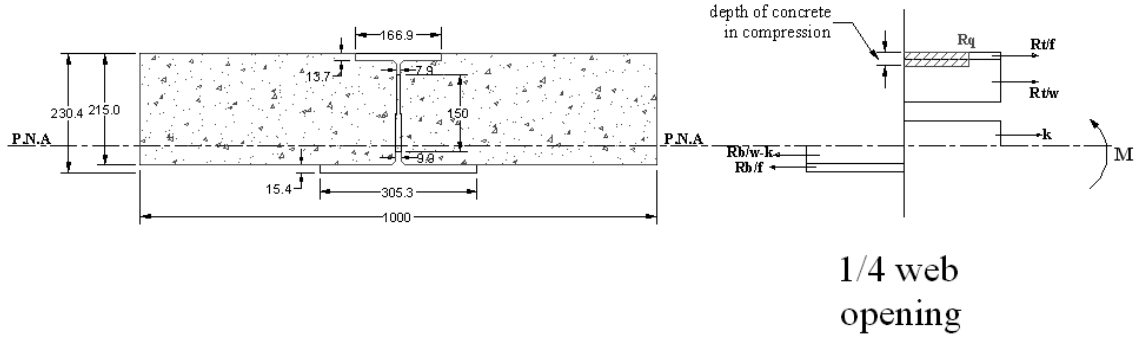
288

1/4 web opening

Degree of Shear Connection, η	Shear Resistance of the Shear Connectors, R_q (kN)	Depth of Concrete in Compression, d (mm)	Depth of P.N.A (mm)	Moment Resistance, (kNm)
0	--	--	216.6	205.9
0.4	422	21.0	197.6	289.8
0.42	443	22.1	194.6	293.4
0.44	464	23.1	192.2	296.9
0.45	475	23.6	191.2	298.7
0.46	486	24.2	188.3	300.4
0.48	507	25.2	185.6	303.7
0.5	528	26.3	182.6	306.9
0.56	591	29.4	172.6	316.2
0.58	612	30.5	169.3	319.0
0.6	633	31.5	166.9	321.8
0.65	686	34.1	158.1	328.5
0.7	739	36.8	148.5	334.5
0.76	802	39.9	138.5	341.0
0.78	823	41.0	135.8	343.0
0.8	845	42.0	130.8	344.4
0.82	866	43.1	127.5	345.5
0.84	887	44.1	123.3	348.5
0.86	908	45.2	117.7	349.3
0.88	929	46.2	111.7	350.0
0.9	950	47.3	105.2	352.0
0.91	961	47.8	101.4	352.3
0.93	982	48.8	94.6	352.7
0.95	1003	49.9	86.7	353.0

Table H-4 Results of the cross section with 1/4 depth of the web opening
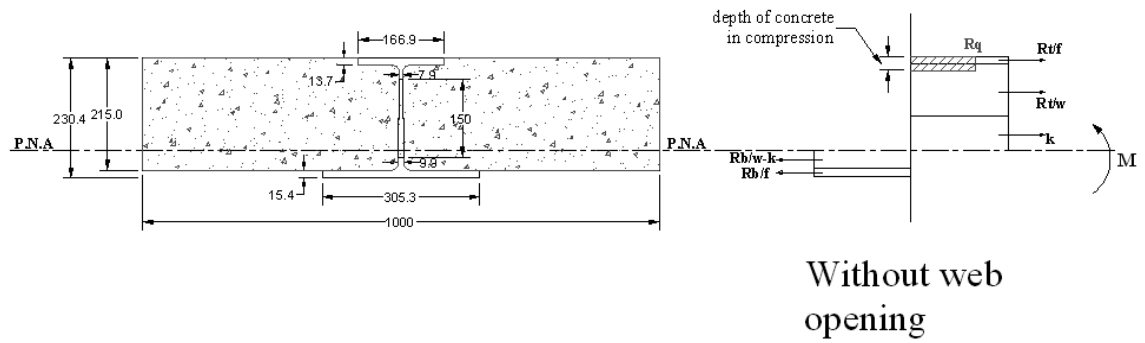
289

Without web opening

Degree of Shear Connection, η	Shear Resistance of the Shear Connectors, R_q (kN)	Depth of Concrete in Compression, d (mm)	Depth of P.N.A (mm)	Moment Resistance, (kNm)
0	--	--	216.0	216.5
0.4	457	22.7	175.4	302.8
0.42	480	23.9	171.8	306.2
0.44	502	25.0	168.2	309.4
0.45	514	25.6	166.5	311.0
0.5	571	28.4	157.6	318.6
0.55	628	31.2	148.7	325.5
0.56	639	31.8	146.9	326.8
0.58	662	33.0	143.3	329.3
0.6	685	34.1	139.8	331.7
0.65	742	36.9	130.9	337.3
0.7	799	39.8	122.0	344.0
0.72	822	40.9	118.4	345.8
0.73	834	41.5	116.6	346.6
0.74	845	42.0	114.8	347.5
0.75	856	42.6	112.6	348.3
0.76	868	43.2	110.3	349.0
0.78	891	44.3	105.9	350.5
0.8	913	45.5	101.4	351.8
0.82	936	46.6	97.0	353.0
0.84	959	47.7	92.5	354.1
0.85	971	48.3	90.3	354.6
0.9	1028	51.1	79.1	358.3
0.95	1085	54.0	68.0	359.5

Table H-5 Results of the cross section without web opening

Appendix J

Calculated moment resistance of the beam specimen in three-point asymmetric bending test

The moment resistance of the beam specimen was determined using the cross section with 1/2 depth of the actual web opening in the degrees of shear connection, 0, 0.5, 0.7 and 1.0. The measured material properties, i.e. steel stress of 414N/mm^2 and concrete strength of 31N/mm^2 were used in the calculation. The moment resistance in zero degree of shear connection was the moment resistance of the steel section alone. The calculation details are shown in the following sections.

J1 Moment resistance of the steel section (M_s)

The stress block method was used to determine the moment capacity of the steel section. The stress block diagram is illustrated in Figure J-1. The measured tensile stress of 414N/mm^2 was used as both tension and compression.
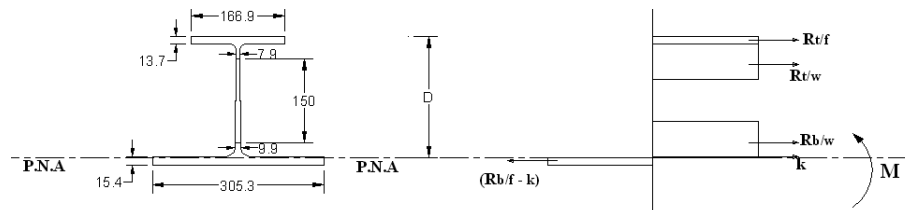
Figure J-1 Stress block diagram of the steel section

Step 1 Determine the depth of plastic neutral axis (P.N.A)

The equilibrium of tension and compression, expressed in Eqn. J.1, was used to determine the depth of the P.N.A, D.

$$R_{t/f} + R_{t/w} + R_{b/w} + K = R_{b/f} - K \qquad (J.1)$$

Where:　　$R_{t/f}$　is the resistance of the top flange ($A_{t/f}P_y$);

　　　　　　$R_{t/w}$　is the resistance of the web post of the top tee ($A_{t/w}P_y$);

　　　　　　$R_{b/w}$　is the resistance of the web post of the bottom tee

　　　　　　　　　　($A_{b/w}P_y$)

　　　　　　$R_{b/f}$　is the resistance of the bottom flange ($A_{b/f}P_y$)

　　　　　　K　　is the bottom flange in compression [$305P_y$ (D-215)].

By substituting the cross sectional areas of the steel elements and steel yield strength of 414N/mm^2 into Eqn. J.1, hence D = 217.1mm, which was within the bottom flange.

Step 2 Determine the plastic moment capacity

Taking moments about the P.N.A,

$$M_s = R_{t/f}D_{t/f} + R_{t/w}D_{t/w} + R_{b/w}D_{b/w} + K (D\text{-}215)/2 + (R_{b/f} - K) (230\text{-}D)/2$$

(J.2)

Where: M_s is the plastic moment of the steel section

$D_{t/f}$ is the distance between the $R_{t/f}$ and the P.N.A,

$D_{t/w}$ is the distance between the $R_{t/w}$ and the P.N.A,

$D_{b/w}$ is the distance between the $R_{b/w}$ and the P.N.A,

$D_{b/f}$ is the distance between the $R_{b/f}$ and the P.N.A.

By substituting the resistance of the steel elements and their distances to the P.N.A into Eqn. J.2, hence, M_s = 254.8kNm.

J2 Moment resistance of the cross section in full shear connection (M_{pc})

The stress block diagram of the cross section is illustrated in Figure J-2. The moment resistance of the cross section was determined using the measured material properties, i.e. steel stress of 324N/mm^2 and concrete strength of 31N/mm^2. The shear resistance strength of the shear connectors was assumed unaffected by the depth of the P.N.A. The results of the push-out tests were used in the calculation.
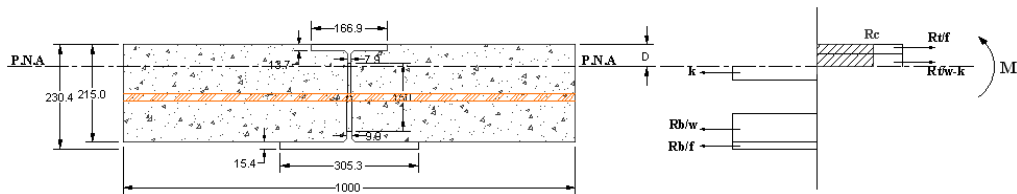
Figure J-2 Stress block diagram of the cross section in full shear connection

Step 1 Determine the depth of P.N.A

The equilibrium of tension and compression, expressed in Eqn. J.3, was used to determine the depth of the P.N.A, D.

$$R_{t/f} + (R_{t/w} - K) + R_c = K + R_{b/w} + R_{b/f}$$ (J.3)

Where: $R_{t/f}$ is the resistance of the top flange ($A_{t/f}P_y$);

$R_{t/w}$ is the resistance of the web post of the top tee ($A_{t/w}P_y$);

R_c is the compressive resistance of the concrete slab in full shear connection ($1000*0.67f_{cu}D$)

$R_{b/w}$ is the resistance of the web post of the bottom tee ($A_{b/w}P_y$);

$R_{b/f}$ is the resistance of the bottom flange ($A_{b/f}P_y$);

K is the web post of the top tee in tension [$7.9(77.5-D)P_y$]

By substituting the cross sectional areas of the steel elements, $P_y = 414N/mm^2$ and $f_{cu} = 31N/mm^2$ the Eqn. J.3, hence, D = 56.9mm

Also, the compressive resistance of the concrete slab in full shear connection, R_c, of 1182kN was obtained.

Step 2 Determine the plastic moment capacity

Taking moments about the P.N.A,

$$M_{pc}=R_{t/f}D_{t/f}+(R_{t/w}-K)(D-D_{t/f})/2 + R_cD_c + K(77.5-D)/2 + R_{b/w}D_{b/w} + R_{b/f}D_{b/f}$$

(J.4)

Where: M_{pc} is the full plastic moment of the composite section

$D_{t/f}$ is the distance between the $R_{t/f}$ and the P.N.A,

$D_{t/w}$ is the distance between the $R_{t/w}$ and the P.N.A,

D_c is the distance between the R_c and the P.N.A,

$D_{b/w}$ is the distance between the $R_{b/w}$ and the P.N.A,

$D_{b/f}$ is the distance between the $R_{b/f}$ and the P.N.A.

By substituting the R_c, the resistance of the steel elements and their distance to the P.N.A into Eqn. J.4, hence, $M_{pc} = 440kNm$

J.3 Moment resistance of the cross section in the degree of shear connection of 0.5

The stress block diagram of the cross section in the degree of shear connection of 0.5 is illustrated below.
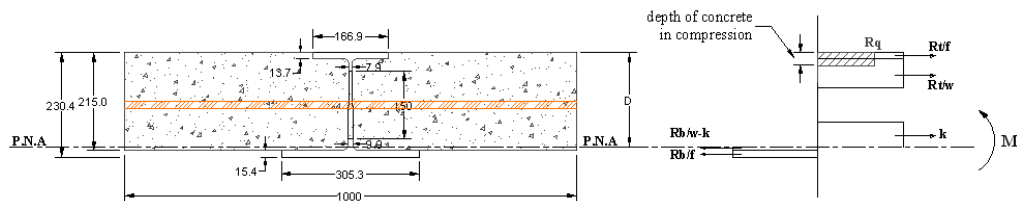

Figure J-3 Stress block diagram of the cross section in degree of shear connection of 0.5

Step 1 Determine the depth of P.N.A

The longitudinal shear resistance of the shear connectors, R_q, was calculated first using the compressive resistance of the concrete slabs, R_c, and the degree of shear connection, η, as $\eta = R_q/R_c$.

- R_c=1182kN,
- $\eta = 0.5$,
- Hence $R_q = 591$kN.

The depth of the P.N.A, D, was determined using the equilibrium of the tension and compression, as expressed in Eqn. J.5.

$$R_{t/f} + R_{t/w} + R_q + K = R_{b/w} - K + R_{b/f} \tag{J.5}$$

Where: $R_{t/f}$ is the resistance of the top flange ($A_{t/f}P_y$);

                $R_{t/w}$ is the resistance of the web post of the top tee ($A_{t/w}P_y$);

                R_q is the longitudinal shear resistance of shear connectors;

                $R_{b/w}$ is the resistance of the web post of the bottom tee

                      ($A_{b/w}P_y$)

                $R_{b/f}$ is the resistance of the bottom flange ($A_{b/f}P_y$)

                K is the bottom web in compression.

By substituting the R_q and the cross sectional areas of the steel elements into Eqn. J.5, hence D = 211.3mm.

The depth of concrete in compression, *d*, was determined using the R_q of 591kN, as the longitudinal shear resistance of the shear connectors, R_q, was equal to the compressive resistance of the concrete slabs in partial shear connection. The *d* of 28.5mm was obtained.

Step 2 Determine the plastic moment capacity

Taking moments about the P.N.A

$$M = R_{t/f}D_{t/f} + R_{t/w}D_{t/f} + R_qD_q + KD_k + (R_{b/w}\text{-k})(215\text{-D}) + R_{b/f}D_{b/f}$$

$$\tag{J.6}$$

Where: M is the moment resistance of the composite section

                $D_{t/f}$ is the distance between the $R_{t/f}$ and the P.N.A,

                $D_{t/w}$ is the distance between the $R_{t/w}$ and the P.N.A,

                D_q is the distance between the R_q and the P.N.A,

                D_k is the distance between the *K* and the P.N.A,

$D_{b/w}$ is the distance between the $R_{b/w}$ and the P.N.A,

$D_{b/f}$ is the distance between the $R_{b/f}$ and the P.N.A.

By substituting the R_q, the resistance of the steel elements and their distance to the P.N.A into Eqn. J.6, hence, $M = 373.8$kNm.

J.4 Moment resistance of the cross section in the degree of shear connection of 0.7

The stress block diagram of the cross section in the degree of shear connection of 0.7 is illustrated below.
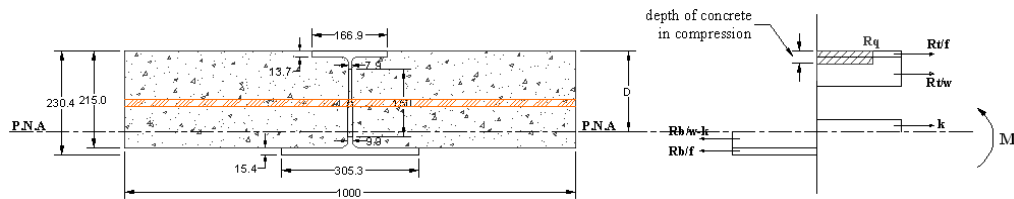
Figure J-4 Stress block diagram of the cross section in degree of shear connection of 0.7

Step 1 Determine the depth of P.N.A

The longitudinal shear resistance of the shear connectors, R_q, was calculated first using the compressive resistance of the concrete slabs, R_c, and the degree of shear connection, η, as $\eta = R_q/R_c$.

- $R_c = 1182$kN,

- $\eta = 0.7$,

- Hence $R_q = 827$kN.

The depth of the P.N.A, D, was determined using the equilibrium of the tension and compression, as expressed in Eqn. J.7.

$$R_{t/f} + R_{t/w} + R_q + K = R_{b/w} - K + R_{b/f} \qquad (J.7)$$

Where: $R_{t/f}$ is the resistance of the top flange ($A_{t/f}P_y$);

$R_{t/w}$ is the resistance of the web post of the top tee ($A_{t/w}P_y$);

R_q is the longitudinal shear resistance of shear connectors;

$R_{b/w}$ is the resistance of the web post of the bottom tee

($A_{b/w}P_y$)

$R_{b/f}$ is the resistance of the bottom flange ($A_{b/f}P_y$)

K is the bottom web in compression.

By substituting the R_q and the cross sectional areas of the steel elements into Eqn. J.7, hence D = 182.0mm.

The depth of concrete in compression, *d*, was determined using the R_q of 827kN, as the longitudinal shear resistance of the shear connectors, R_q, was equal to the compressive resistance of the concrete slabs in partial shear connection. The *d* of 39.8mm was obtained.

Step 2 Determine the plastic moment capacity

Taking moments about the P.N.A

$$M = R_{t/f}D_{t/f} + R_{t/w}D_{t/f} + R_qD_q + KD_k + (R_{b/w}\text{-k})(215\text{-D}) + R_{b/f}D_{b/f}$$

(J.8)

Where: *M*   is the moment resistance of the composite section

                       $D_{t/f}$ is the distance between the $R_{t/f}$ and the P.N.A,

                       $D_{t/w}$ is the distance between the $R_{t/w}$ and the P.N.A,

                       D_q is the distance between the R_q and the P.N.A,

                       D_k is the distance between the *K* and the P.N.A,

                       $D_{b/w}$ is the distance between the $R_{b/w}$ and the P.N.A,

                       $D_{b/f}$ is the distance between the $R_{b/f}$ and the P.N.A.

By substituting the R_q, the resistance of the steel elements and their distance to the P.N.A into Eqn. J.8, hence, *M* = 411.6kNm.

Degree of Shear Connection, η	Shear Resistance of the Shear Connectors, R_q (kN)	Depth of Concrete in Compression, d (mm)	Depth of P.N.A (mm)	Moment Resistance, (kNm)
0	--	--	217.1	254.8
0.4	473	22.8	215.2	351.6
0.42	496	23.9	215.2	356.2
0.44	520	25.0	215.1	360.7
0.45	532	25.6	215.0	362.9
0.5	591	28.5	211.3	373.8
0.55	650	31.3	204.0	384.2
0.57	674	32.4	201.0	388.1
0.58	686	33.0	199.6	390.1
0.59	697	33.6	198.1	392.0
0.6	709	34.2	196.7	393.9
0.65	768	37.0	189.3	403.0
0.7	827	39.8	182.0	411.6
0.75	887	42.7	174.7	419.5
0.8	946	45.5	165.9	426.9
0.82	969	46.7	163.0	429.7
0.84	993	47.8	159.1	432.3
0.88	1040	50.1	150.0	437.4
0.9	1064	51.2	143.5	438.6
0.91	1076	51.8	139.8	438.8
0.93	1099	52.9	129.3	439.3
0.95	1123	54.1	114.8	439.6

Table J-1 Results of the partial shear connection in three-point bending test

Appendix K

Design moment capacity of the flexural test beam specimen using BS5950 and EC4

British Standard (BS5950-3.1:1990) and Eurocode 4 (EN1994-1-1:2004) determine the design moment capacity of a composite section by using both stress block and linear interaction methods. These two methods are based on plastic theory, which assumes the stresses within the cross section reach a constant value in both tension and compression. The methodologies of the two methods are summarised in the following sections.

K.1 Stress block method

The assumptions specified by the BS5950 and EC4 in applying the stress block methods are:

- The structural steel is stressed to a uniform yield stress in both tension and compression;

- The concrete tensile strength is neglected;

- In full shear connection, the concrete is stressed to a uniform compression over the depth above the plastic neutral axis (P.N.A);

- In partial shear connection, the concrete is stressed to a uniform compression up to the depth that concrete can develop the compressive resistance equals to the longitudinal shear resistance of the shear connectors.

The BS5950 specifies that the yield stress of 355N/mm^2 should be used as the steel stress of both tension and compression. The different formulas of the concrete compressive stress, $\sigma_{c,Rd}$, are specified in the BS5950 and EC4, as shown in Table K-1.

BS5950	$\sigma_{c,Rd}=0.45f_{cu}$	f_{cu} is the concrete characteristic cube strength (N/mm^2)
EC4	$\sigma_{c,Rd}=0.85f_{cd}$	f_{cd} is the concrete design compressive cylinder strength (N/mm^2)

Table K-1 Concrete compressive stress, $\sigma_{c,Rd}$, specified by BS5950 and EC4

The stress block diagrams of a typical downstand composite beam are shown in Figure K-1. The forces within the cross sections are in equilibrium state. The moment capacity of the cross sections is calculated by taking moments about the plastic neutral

axis (P.N.A). The stress block diagrams of the flexural test beam specimen are shown in Figure K-2. The optimum cross section with 1/2 depth of the actual web opening is used to determine the design moment resistance of the flexural test beam specimen.
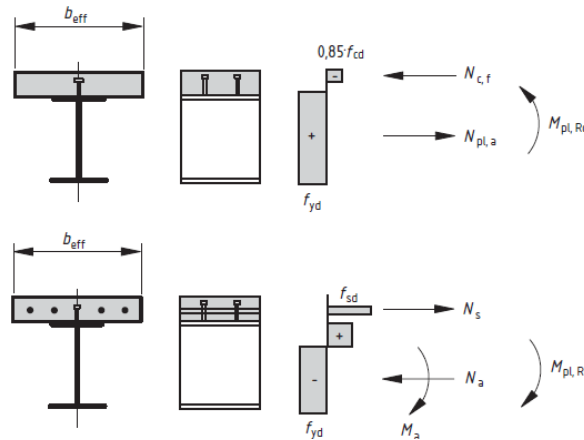

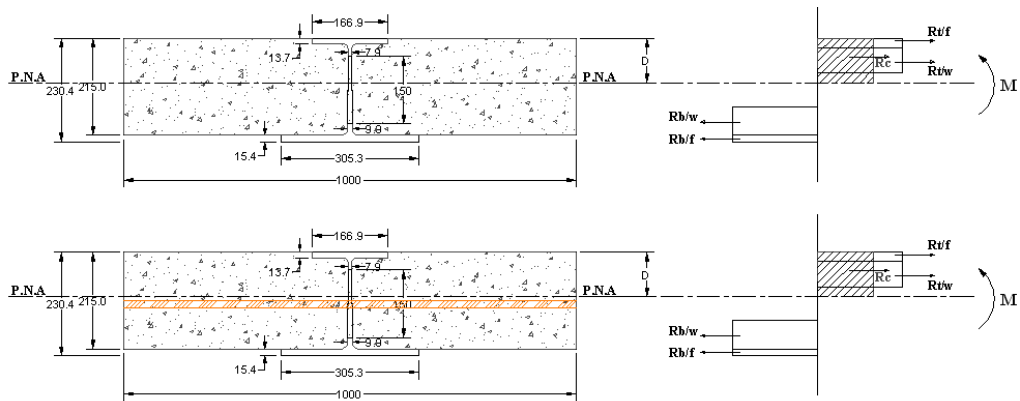Figure K-1 Stress block diagrams of downstand composite beam (EN1994-1-1:2004)

Figure K-2 Stress block diagram of the optimum cross sections of the flexural test beam specimen in full shear connection

K.2 Linear interaction method

The linear interaction method, as expressed in Eqn. K-1, is a simplified relationship of the moment resistance and the degree of shear connection. The comparison between the linear interaction and stress block methods is illustrated in Figure K-3. It is shown that the linear interactive method yields conservative results.

$$M_{Rd} = M_{pl,a,Rd} + \eta(M_{pl,Rd} - M_{pl,a,Rd}) \qquad (K-1)$$

Where: M_{Rd} is the design moment resistance of the composite section in partial shear connection;

$M_{pl,a,Rd}$ is the plastic moment resistance of the steel section;

η is the degree of shear connection;

$M_{pl,Rd}$ is the design moment resistance of the composite section in full shear connection.

1: Stress Block Method
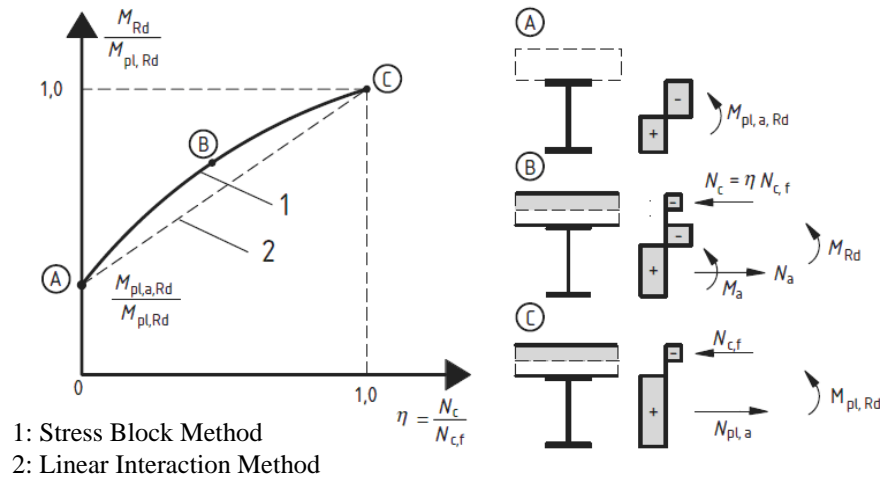2: Linear Interaction Method

Figure K-3 Comparisons between the stress block and linear interaction methods (EN1994-1-1:2004)

K.3 Design moment capacity

The design moment capacity of the flexural test beam specimen in full and partial shear connections is calculated, in accordance with the BS5950 and Eurocode 4. The stress block method is used to calculate the design moment capacities of the both full and partial shear connections. The linear interactive method is used to calculate the design moment capacities of the partial shear connection. The concrete mean compressive cube strength of 30N/mm^2 is used to calculate the concrete compressive stress, $\sigma_{c,Rd}$. The steel yield stress of 355N/mm^2 is used as both tension and compression.

K.3.1 Full shear connection

The criterion of the full shear connection is that the longitudinal shear resistance of the shear connectors, R_q, is greater than or equal to the full compressive resistance of the concrete slabs due to the full composite action, R_c, as $R_q \geq R_c$. The assumptions made in applying the full shear connection for the design moment capacity calculation of the flexural test beam specimen are:

- Concrete tensile strength is neglected;
- Local web post buckling of the steel section is prevented by the partially concrete encasement;
- The structural steel is stressed to a uniform yield stress in both tension and compression;

- The concrete is stressed to a uniform compression over the depth above the P.N.A;

- The shear resisting capacities of the shear connectors are not affected by the position of the P.N.A;

The steps in applying the stress block method for determining the design moment capacities of the flexural test beam specimen in full shear connection are:

1. To calculate the compressive resistance of the concrete slabs in full composite action, R_c, by using the equilibrium of the forces within the cross section;

2. To determine the depth of the P.N.A;

3. To calculate the design moment capacity in full shear connection, $M_{pl,Rd}$, by taking moments about the P.N.A.

There are two types of cross sections in the flexural test beam specimen: cross sections with concrete-infill-only and tie-bar shear connectors, as shown in Figure K-2. The full compressive resistance, R_c, between the both cross sections are the same, because the steel section of the both cross sections are the same. This leads to the same depths of the P.N.A for the both cross sections. Furthermore, the design moment capacities in full shear connection, $M_{pl,Rd}$, between the both cross sections are the same, as the moment capacities are calculated by taking moment about the P.N.A. The details of the calculation are shown below.

Step 1, Full compressive resistance of the concrete slabs, R_c

The equilibrium of the forces within the cross section, expressed in Eqn. K-2, is used to determine the full compressive resistance of the concrete slabs, R_c.

$$R_{t/f} + R_{t/w} + R_c = R_{b/w} + R_{b/f} \tag{K-2}$$

Where: $R_{t/f}$ is the resistance of the top flange ($A_{t/f}P_y$);

$R_{t/w}$ is the resistance of the web post of the top tee ($A_{t/w}P_y$);

R_c is the full compressive resistance of the concrete slabs due to full composite action;

$R_{b/w}$ is the resistance of the web post of the bottom tee, ($A_{b/w}P_y$);

$R_{b/f}$ is the resistance of the bottom flange ($A_{b/f}P_y$)

By substituting the cross sectional areas of the steel elements and steel stress, $P_y = 355\text{N/mm}^2$, into Eqn. K-2, Hence, $R_c=898\text{kN}$.

Step 2, Depth of the P.N.A, D

The depth of the P.N.A is calculated using the full compressive resistance of the concrete slabs, R_c, and the concrete compressive stress, $\sigma_{c,Rd}$.

$$R_c= \sigma_{c,Rd}\, B_e\, D \qquad\qquad\qquad\qquad (\text{K-3})$$

Where: R_c is the full compressive resistance of the concrete slabs due to full composite action;

$\sigma_{c,Rd}$ is the concrete compressive stress;

B_e is the effective width of the concrete slab;

D is the depth of the P.N.A.

The concrete compressive stress, $\sigma_{c,Rd}$, is converted using the mean compressive cube strength of 30N/mm^2, in accordance with the BS5950 and EC4. The same result of the $\sigma_{c,Rd}$ is obtained, as shown in Table K-2. This shows the consistency between the BS5950 and EC4. The effective width of the flexural test beam specimen is 1m. The full compressive resistance of the concrete slabs, R_c, is 898kN. The results of the depth of the P.N.A are listed in Table K-2.

	Mean Compressive Cube Strength (N/mm^2)	$\sigma_{c,Rd}$ (N/mm^2)	R_c (kN)	D (mm)
BS5950 ($\sigma_{c,Rd}=0.45f_{cu}$)	30	9	898	99.8
EC4 ($\sigma_{c,Rd}=0.85f_{cd}$)	30	9	898	99.8

Table K-2 Depths of the P.N.A of the flexural test beam specimen in full shear connection

Step 3, Design moment capacities of full shear connection, $M_{pl,Rd}$

The design moment capacities of the flexural test beam specimen in full shear connection, $M_{pl,Rd}$, are determined by taking moments about the P.N.A. The results are shown in Table K-3. The design moment capacity, $M_{pl,Rd}$, obtained using the BS5950 and EC4 are the same.

	Concrete Cube Strength (N/mm^2)	P_y (N/mm^2)	R_c (kN)	Depth of P.N.A (mm)	$M_{pl,Rd}$ (kNm)
BS5950	30	355	898	99.8	354
EC4	30	355	898	99.8	354

Table K-3 Design moment capacities of the beam specimen in full shear connection

K.3.2 Partial shear connection

The criterion of the partial shear connection is that the longitudinal shear resistance of the shear connectors, R_q, is less than the compressive resistance of slabs due in full composite action, R_c, as $R_q < R_c$. The ratio of the R_q to the R_c is defined as the degree of shear connection, η ($\eta = R_q/R_c$). The limits of the degree of shear connection specified by both BS5950 and EC4 are $0.4 \le \eta \le 1.0$.

The design moment capacity in partial shear connection is determined using both stress block and linear interaction methods. The concrete compressive resistance developed in partial shear connection equals to the longitudinal shear resistance of the shear connector, R_q. The stress block diagrams of the flexural test beam cross sections in partial shear connection are illustrated in Figure K-4. The optimum cross section with 1/2 depth of the web opening is used to determine the design moment capacities of the flexural test beam specimen in partial shear connection. The steps in applying the stress block method are:

1. To calculate the longitudinal shear resistance of the connectors, R_q, at a degree of shear connection, η, as $\eta = R_q/R_c$, where R_c is the full compressive resistance of the concrete slabs;
2. To calculate the depth of concrete in compression, d;
3. To calculate the depth of the P.N.A using the equilibrium of the forces within the cross section;
4. To determine the design moment capacities in partial shear connection, M_{Rd}, by taking moments about the P.N.A.
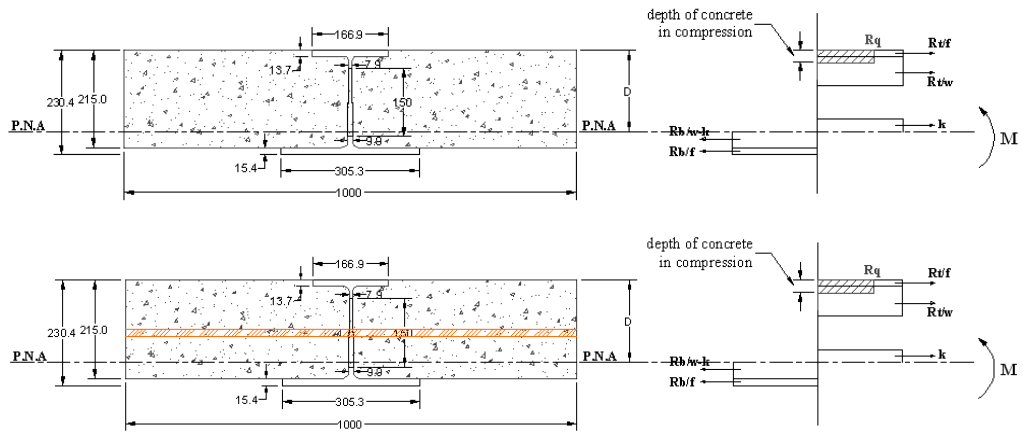
Figure K-4 Stress block diagrams of the cross sections of the beam specimen in partial shear connection

The previous section showed that the compressive resistance of the concrete slabs in full shear connection, R_c, between the two cross sections (with or without tie-bar) is the same. Hence, for a given degree of shear connection, the longitudinal shear resistance of the shear connectors, R_q, between the both cross sections is the same, as $\eta=R_q/R_c$. This leads to the same depths of the P.N.A. Furthermore, for a given degree of shear connection, the design moment capacities in partial shear connection, M_{Rd}, between the both cross sections are the same, as the moment capacities are determined by taking moments about the P.N.A. The design moment capacities of the flexural test beam specimen in various degrees of shear connection are shown in Figure K-5.
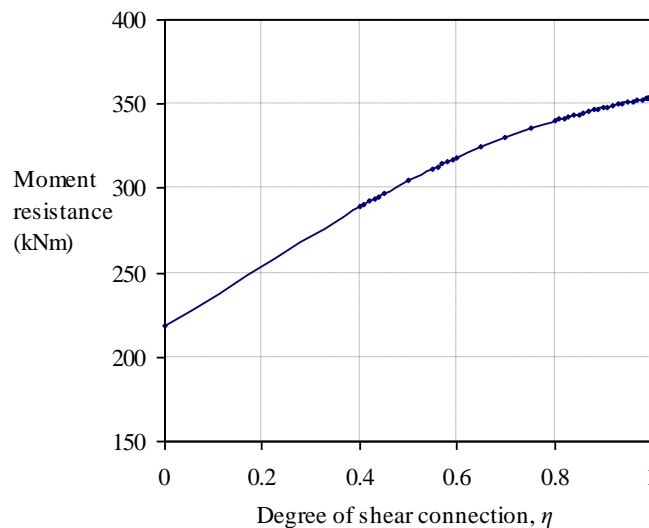

Figure K-5 Design moment capacities of the beam specimen over various degrees of shear connection

304

K.3.2.1 Linear interaction method

The linear interaction method, as expressed in Eqn. K.1, is a simplified method to determine the design moment capacity in partial shear connection. The optimum cross section with 1/2 depth of the web opening and the measured material properties of the flexural test beam specimen are used in the linear interaction method. The plastic moment capacity of the steel section, $M_{pl,a,Rd}$, of 219kNm is calculated using the stress block method, with the design yield stress of 355N/mm^2 as both tension and compression. The design moment capacity in full shear connection, $M_{pl,Rd}$, is 354kNm, which is determined in Table K-3.

The results of the linear interaction method are compared with that of the stress block and linear interaction is Figure K-6. The conservative design moment capacities are obtained by using the linear interaction method; however, the maximum difference at the region of 0.5-0.6 degrees of shear connection is quite small, 6%.
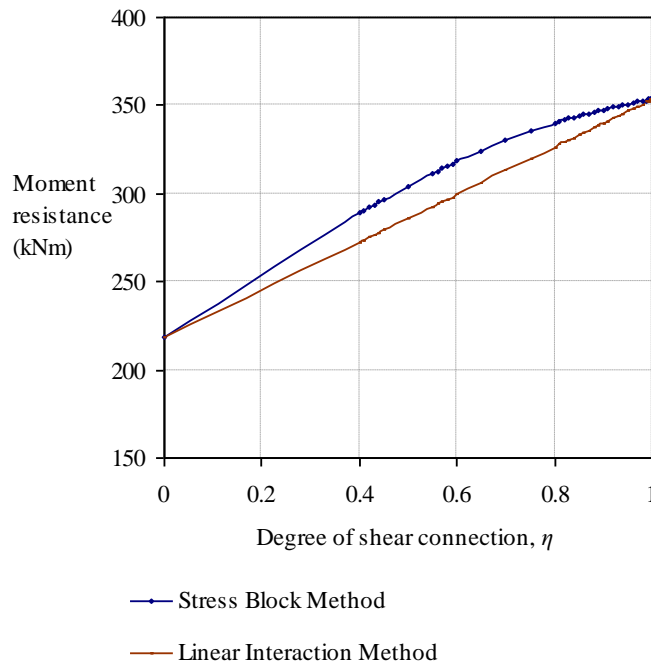

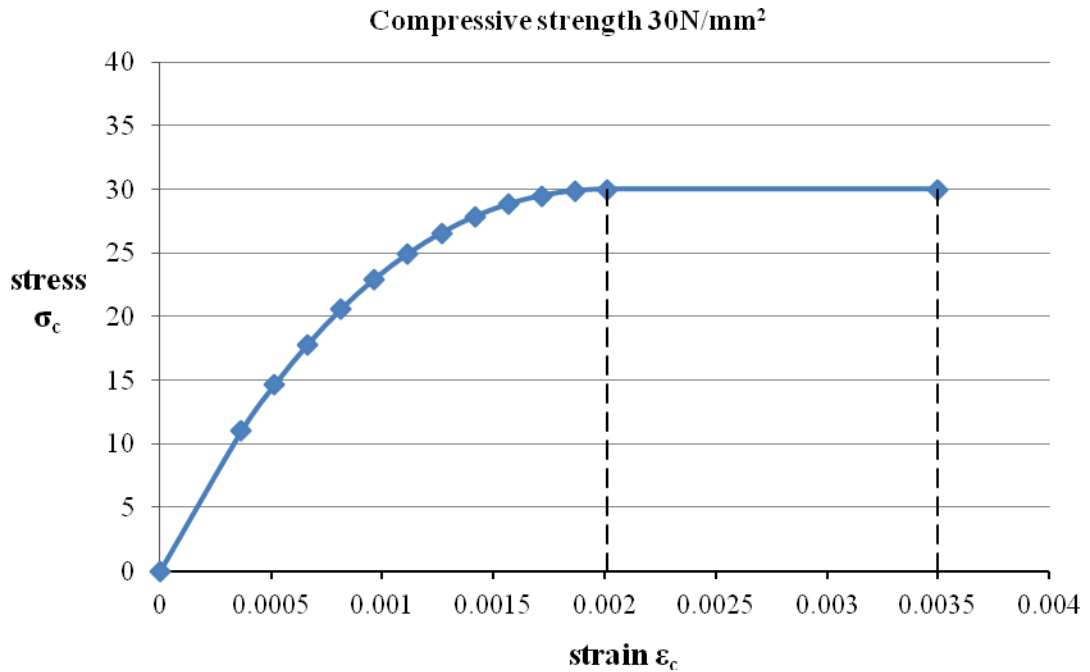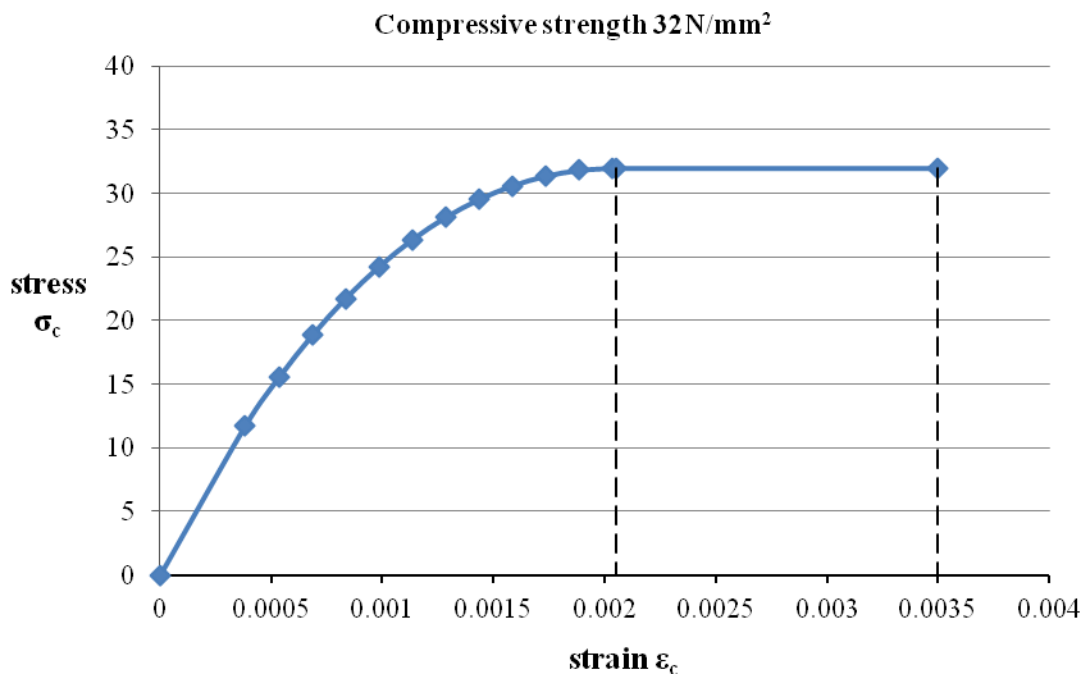Figure K-6 Comparison between the stress block method and linear interaction method

Appendix L

Stress-strain curves of concrete material for FEA

Figure L1 Stress-strain curve for concrete compressive strength of 30N/mm^2

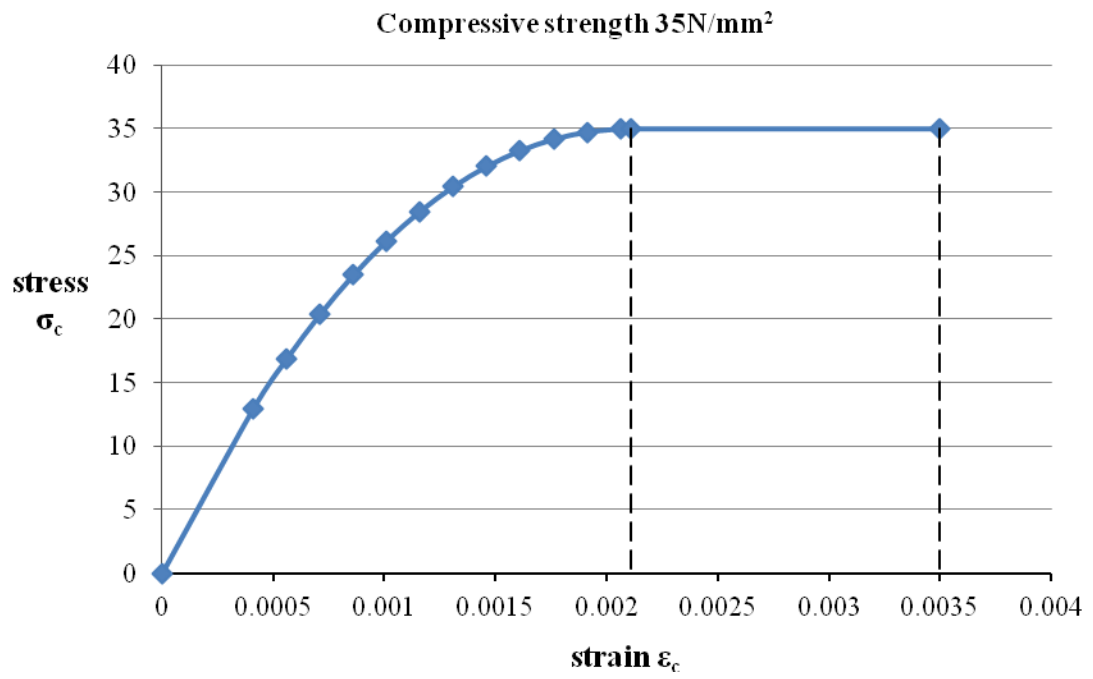Figure L2 Stress-strain curve for concrete compressive strength of 32N/mm^2

Figure L3 Stress-strain curve for concrete compressive strength of 35N/mm^2

Bibliography

American Institute of Steel Construction, AISC 1994, "Manual of Steel Construction-Load and Resistance Factor Design", Second Edition, 1994, Chicago.

American Institute of Steel Construction, ANSI/AISC 360-05, "Specification for Structural Steel Buildings", March 2005, Chicago.

ANSYS, "Release 11.0 Documentation for ANSYS", ANSYS Inc., Pennsylvania.

Ahn, J.-H., Kim, S.-H. and Jeong, Y.-J., "Shear Behaviour of Perfobond Rib Shear Connector under Static and Cyclic Loadings", Magazine of Concrete Research, V60, n5, 2008, pp. 347-357, ISSN: 0024-9831.

Bode, H., Dorka, U.E., Stengel, J., Sedlacek, G. and Feldmann, M., "Composite Action in Slim Floor System", Proceedings of Conference: Composite Construction in Steel and Concrete III, ASCE, Germany, June 1996, pp. 472-485, ISBN: 9780784402566.

Bode, H., Stengel, J. and Zhou, D., "Composite Beam Test for a New High-rise Building in Frankfurt", Proceedings of Conference: Composite Construction in Steel and Concrete III, ASCE, Germany, June 1996, pp. 448-461, ISBN: 9780784402566.

Bradford, M.A., Filonov, A., Hogan, T.J., Ranzi, G. and Uy, B., "Strength and Ductility of Shear Connection in Composite T-Beams", Proceedings of the 8th International Conference, Steel, Space and Composite Structures, Kuala Lumpur, 2006, pp. 15-26.

British Standard, BS5950-3.1: 1990, "Structural Use of Steel Work in Building, Part 3: Design in Composite Construction, Section 3.1 Code of Practice for Design of Simple and Continuous Composite Beams".

Chen, Q., Shi, Y.J., Wang, Y.Q., Chen, H. and Zhang, Y., "Structural Analysis on Light Steel Frame with Steel-Concrete Composite Slim Beam", Journal of Building Structures, V32, n2, 2002, pp. 17-20, ISSN: 10006869.

Chinn, J., "Push-out Tests on Lightweight Composite Slabs", AISC Engineering Journal, American Institute of Steel Construction (AISC), V2, n4, 1965, pp. 129-134, ISSN: 0013-8029.

Clawson, W.C. and Darwin, D., "Tests on Composite Beams with Web Openings", Journal of the Structural Division, ASCE, V108, n1, 1982, pp. 145-162, ISSN: 0044-8001.

Davies, C., "Small-Scale Push-out Tests on Welded Stud Shear Connectors", Concrete, Sep 1967, pp. 311-316.

Davies, C., "Steel-Concrete Composite Beams for Buildings", George Godwin, 1975, ISBN: 0711449066.

Dowling, P., Owens, G. and Burgan, B., "Developments in European Steel Construction", Journal of Steel Structures, V1, 2001, pp. 75-90, ISSN: 1598-2351.

Easterling, W.S., Gibbings, D.R. and Murray, T.M., "Strength of Shear Studs in Steel Deck on Composite Beams and Joists", AISC Engineering Journal, AISC, V30, n2, 1993, pp. 44-55, ISSN: 0013-8029.

Eurocode 4, EN1994-1-1: 2004, "Design of Composite Steel and Concrete Structures, Part 1-1: General Rules and Rules for Buildings", December 2004.

Eurocode 2, EN1992-1-1: 2004, "Design of Concrete Structures, Part 1-1: General Rules and Rules for buildings", December 2004.

Goble, G.G., "Shear Strength of Thin Flange composite Specimens", AISC Engineering Journal, AISC, V5, n2, 1968, pp. 62-65, ISSN: 0013-8029.

Grant, J.A., Fisher, J.W. and Slutter, R.G., "Composite Beams with Formed Steel Deck", AISC Engineering Journal, AISC, V14, n1, 1977, pp. 24-43, ISSN: 0013-8029.

Hawkins, N.M., "Strength of Stud Shear Connectors", Institute of Engineering, Australia, Civil Engineering Transactions, 1973, pp 46-52.

Hegger, J., Roggendorf, T. and Kerkeni, N., "Shear Capacity of Prestressed Hollow Core Slabs in Slim Floor Constructions", Journal of Engineering Structures, V31, n2, Feb 2009, pp. 551-559, ISSN: 0141-0296.

Hicks, S., "Current Trend in Modern Floor Construction", The Magazine of British Constructional Steelwork Association (BCSA), Vol. 11, No.1, 2003, pp. 32-33.

Huo, B.Y., Tsavdaridis, K.D. and D'Mello, C., "Experimental and Analytical Study of Push-out Shear Tests in Ultra Shallow Floor Beams", Proceedings of the 34th International Symposium on Bridge and Structural Engineering, IABSE, Venice, Italy, 2010, pp. 174 (abstract) full paper in CD, ISBN. 978385748122.

Johnson, R. P. and May, I. M., "Partial-Interaction Design of Composite Beams" Structural Engineer, Vol. 53, No. 8, August 1975, PP. 305-311, ISSN: 00392553.

Johnson, R.P., "Composite Structures of Steel and Concrete, Volume 1: Beams, Slabs, Columns, and Frames for Buildings", Second Edition, Blackwell Scientific Publications, 1994, ISBN: 0632025077.

Johnson, R.P., "Prediction of Shear Resistance of Headed Studs in Troughs of Profiled Sheeting", Proceedings of Conference: Composite Construction in Steel and Concrete VI, ASCE, Colorado USA, 2008, ISBN: 9780784411421.

Johnson, R.P. and Oehlers, D.J., "Analysis and Design for Longitudinal Shear in Composite T-Beams", Proceedings of Institute of Civil Engineering, Part 2, V71, n4, 1981, pp. 989-1021, ISSN: 03078361.

Ju, Y.K., Chun, S.C., Kim, S.E., Kim, D.H., Kim, S.D. and Chung, K.R., " Structural Performance of I-TECH Composite Beam Steel with Web Openings", Proceedings of the CIB-CTBUH International Conference on Tall Buildings, Kuala Lumpur, 2003, pp. 411-418, ISBN: 9834128304.

Ju, Y.K., Lee, C.H., Chun, S.C. and Kim, S.D., "Structural Behaviour of Reinforced Concrete Column to ITECH Composite Beam Joint", Proceedings of the 13th World Conference on Earthquake Engineering, Vancouver, 2004.

Ju, Y.K., Kim, D.H. and Kim, S.D., "Experimental Assessment of the Shear Strength of an Asymmetric Steel Composite Beam with Web Openings", Canadian Journal of Civil Engineering, V32, n2, 2005, pp. 314-328, ISSN: 1208-6029.

Ju, Y.K., Chun, S.C. and Kim, S.E., "Flexural Test of a Composite Beam using Asymmetric Steel Section with Web Openings", Journal of Structural Engineering, ASCE, V135, n4, 2009, pp. 448-458, ISSN: 0733-9445.

Jurkiewiez, B. and Hottier, J.M., "Static Behaviour of a Steel–Concrete Composite Beam with an Innovative Horizontal Connection", Journal of Constructional Steel Research, V61, n9, Sep 2005, pp. 1286-1300, ISSN: 0143974X.

Kuhlmann, U. and Breuninger, U., "Behaviour of Horizontally Lying Studs with Longitudinal Shear Force", Proceedings of Conference: Composite Construction in Steel and Concrete IV, ASCE, Alberta, 2000, pp. 438-449, ISBN-13: 9780784406168.

Kuhlmann, U. and Kürschner, K., "Structural Behaviour of Horizontally Lying Shear Studs", Proceedings of Conference: Composite Construction in Steel and Concrete V, ASCE, South Africa, 2004, pp. 534-543, ISBN-13: 9780784408261.

Lawson, R.M., Lim, J., Hicks, S.J. and Simms, W.I., "Design of Composite Asymmetric Cellular Beams and Beams with Large Web Openings", Journal of Constructional Steel Research, V62, n6, June 2006, pp. 614-629, ISSN: 0143974X.

Lawson, R.M., Mullett, D.L. and Rackham, J.W., "Design of Asymmetric Slimflor Beams Using Deep Composite Decking", The Steel Construction Institute, SCI Publication P175, 1997, ISBN: 1859420443.

Lawson, R.M., Bode, H., Brekelmans, J.W.P.M., Wright, P.J. and Mullett, D.L., "'Slimflor' and 'Slimdek' Construction: European Developments", Journal of Structural Engineer, V77, n8, 1999, pp. 22-30, ISSN: 00392553.

Leonhardt, E.F., Andra, W., Andra, H-P. and Harre, W., "New Improved Shear Connector with High Fatigue Strength for Composite Structures (Neues, vorteilhaftes Verbundmittel für Stahlverbund-Tragwerke mit hoher Dauerfestigkeit)", Beton-Und Stahlbetonbau, V12, 1987, pp.325-331, ISSN: 1437-1006.

Lu, X. and Makelainen, P., "Strength and Stiffness of Composite Slim Floor Beams", Proceedings of the 4th Pacific Structural Steel Conference, Singapore, 1995, pp. 93-100, ISBN-10: 0080422659.

Mangerig, I. and Zapfe, C., "Concrete Dowels in Composite Construction", Proceedings of the 5th Japanese-German Joint Symposium on Steel and Composite Bridge, Osaka, 2003.

Mullett, D.L., "Slim Floor Design and Construction", The Steel Construction Institute, SCI Publication P110, 1992, ISBN: 9781870004695.

Mullett, D.L., "Composite Floor System", Blackwell Science Ltd, 1998, ISBN: 0632041439.

Mullett, D.L. and Lawson, R.M., "Slim Floor Construction Using Deep Decking", The Steel Construction Institute, SCI Publication P127, 1993, ISBN: 9781870004893.

Narayanan, R., "Steel-Concrete Composite Structures: Stability and Strength", Elsevier Applied Science Publishers, 1988, ISBN: 1851661344.

Oehlers, D.J. and Bradford, M.A., "Composite Steel and Concrete Structural Members: Fundamental Behaviour", Pergamon Press, 1995, ISBN: 0080419194.

Oguejiofor, E.C. and Hosain, M.U., "Behaviour of Perfobond Rib Shear Connectors in Composite Beams: Full Size Tests", Canadian Journal of Civil Engineering, V19, n2, 1992, pp. 224-235, ISSN: 1208-6029.

Oguejiofor, E.C. and Hosain, M.U., "Perfobond Rib Shear Connectors for Composite Beams", Proceedings of Engineering Foundation Conference: Composite Construction in Steel and Concrete II, ASCE, Potosi, 1992, pp. 883-898, ISBN-13: 9780872629806.

Oguejiofor, E.C. and Hosain, M.U., "A Parametric Study of Perfobond Rib Shear Connectors", Canadian Journal of Civil Engineering, V21, n4, 1994, pp. 614-625, ISSN: 1208-6029.

Oguejiofor, E.C. and Hosain, M.U., "Numerical Analysis of Push-out Specimens with Perfobond Rib Shear Connectors", Computers and Structures, V62, n4, 1997, pp. 617-624, ISSN: 0045-7949.

Ollgaard, J.G., Slutter, R.G. and Fisher, J.W., "Shear Strength of Stud Connectors in Lightweight and Normal-Weight Concrete", AISC Engineering Journal, AISC, V8, n2, 1971, pp. 55-64, ISSN: 0013-8029.

Peltonen, S. and Leskelä, M.V., "Connection Behaviour of a Concrete Dowel in a Circular Web Hole of a Steel Beam", Proceedings of Conference: Composite Construction in Steel and Concrete V, ASCE, South Africa, 2004, pp. 544-552, ISBN-13: 9780784408261.

Queiroz, G., Pimenta, R.J., Calixto, J.M. and Da Mata, L.A.C., "New Type of Slim Floor", Journal of Constructional Steel Research, V46, n1, April 1998, pp. 213-214, ISSN: 0143974X.

Rackham, J.W., Hicks, S. and Newman, G.M., "Design of Asymmetric Slimflor Beams with Precast Concrete Slabs", The Steel Construction Institute, SCI Publication P342, 2006, ISBN: 9781859421680.

Redwood, R.G. and Wong, P.K., "Web Holes in Composite Beams with Steel Deck", Proceedings of Canadian Structural Engineering Conference, Canadian Steel Construction Council, Montreal, 1982, ISBN-13: 9780888110503.

Slutter, R.G. and Driscoll, G.C., "Flexural Strength of Steel-Concrete Composite Beams", Journal of Structural Engineering, ASCE, V91, n2, 1965, pp. 71-99, ISSN: 0733-9445.

Tsavdaridis, K.D., D'Mello, C. and Huo B.Y., "Computational Study Modelling the Experimental Work Conducted on the Shear Capacity of Perforated Concrete-Steel Ultra Shallow Floor Beams (USFB)", Proceedings of 16th Hellenic Concrete Conference, Paphos, Cyprus, 2009, pp. 159 (abstract) full paper in CD.

Wang, Y., Yang, L., Shi, Y. and Zhang, R., "Loading Capacity of Composite Slim Frame Beams", Journal of Constructional Steel Research, V65, 2009, pp. 650-661, ISSN: 0143974X.

Willam, K.J. and Warnke, E.D., "Constitutive Model for the Triaxial Behaviour of Concrete", Proceeding of International Association for Bridge and Structural Engineering (IABSE), V19, ISMES, Bergamo, Italy, 1974, pp. 174.

Valente, I. and Cruz, P.J.S., "Experimental Analysis of Perfobond Shear Connection between Steel and Lightweight Concrete", Journal of Constructional Steel Research, V60, 2004, pp. 465-479, ISSN: 0143974X.

Veldanda, M.R. and Hosain, M.U., "Behaviour of Perfobond Rib Shear Connectors in Composite Beams: Push-out Tests", Canadian Journal of Civil Engineering, V19, n1, 1992, pp. 1-10, ISSN: 1208-6029.

Veríssimo, G.S., Paes, J.L.R, Valente, I., Cruz, P.J.S. and Fakury, R.H., "Design and Experimental Analysis of a New Shear Connector for Steel and Concrete Composite Structures", Proceedings of the 3rd International Conference on Bridge Maintenance, Safety and Management, IABMAS, Porto, July 2006.

Viest, I.M., "Investigation of Stud Shear Connectors for Composite Concrete and Steel T-Beams", Journal of the American Concrete Institute, V52, n8, April 1956, pp 875-892.

Yang, L., Wang, Y.Q. and Shi, Y.J., "Loading Capacity of Simply Supported Steel-concrete Composite Slim Beams", Journal of Advanced Materials Research, V163-167, Dec 2010, pp 2185-2193, ISSN: 1662-8985.